A structure-function analysis of a Rho GTPase Exchange Factor (GEF) – GTPase Activating Protein (GAP) interaction

A thesis submitted for the degree of Doctor of Philosophy of

The Australian National University

by

Hamilton Fraval, B. Biotech (Hons)

March 2011

Molecular Genetics and Evolution

Research School of Biological Sciences

Australian National University

Canberra ACT

Australia

Statement

This work contains no material which has been accepted for the award of any other degree or diploma in any university or other tertiary institution and contains no material published or written by another person, except where due reference has been made in the text.

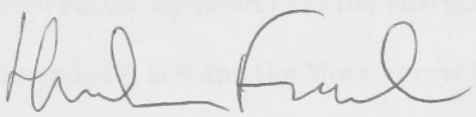

Hamilton Fraval, March 2011

Acknowledgements

Firstly I would like to thank Professor Robert Saint for giving me the opportunity to follow my interest in the wonderful world of molecular biology. I appreciate that, despite a busy schedule, you always made time to talk about and help me with matters both great and small.

Many thanks to all past and present members of the Saint lab who made my time in the lab an enjoyable experience. Special thanks go to Peter, for his wisdom in the early years, Vicki, for being the oracle, and more recently Mike.

I would also like to thank all the Fraval and more recently Henderson clans for their continued support and encouragement over the years. A special thanks to Big T for providing much needed R & R and the Morris crew for putting up with me.

Finally, extra special thanks must go to the lovely Missy Chrissy. You were there through thick and thin and I'm pretty sure I wouldn't have made it through without your unyielding love and support. But no, you cannot be co-author of this thesis. Big ups also to Tip Top Thomas for bringing me such joy and providing continuous entertainment.

Abstract

Cytokinesis is the final stage of cell division where major rearrangements of the cytoskeleton occur that result in the formation and constriction of a contractile ring at the equator of the cell. The GTPase Rho is essential for cytokinesis and it is the role of the Rho GTPase Exchange Factor (GEF) Pbl to stimulate the accumulation of an equatorial band of active Rho. Accumulation of Pbl at the midzone requires an interaction with the GTPase Activating Protein (GAP) Tum, which forms a heterotetrameric complex with the microtubule motor protein Pavarotti (Pav). It is the motor activity of Pav that localizes Pbl and Tum to the equator where they activate downstream cytokinetic effectors and thereby induce contractile ring formation and constriction. However, the mechanism/s that regulate the Pbl-Tum interaction during cytokinesis are unknown.

This thesis describes two strategies that probe the Pbl-Tum interaction using a structure-function analysis. The first strategy details attempts to over-express and purify Pbl and Tum in an effort to obtain enough pure protein with which to perform structural studies. The second strategy compares the effect of wild-type and mutant transgenes to identify phosphorylation events that mediate the Pbl-Tum interaction. Through this work I identified a previously uncharacterized phosphorylation event in Tum that is required to bind and localize Pbl to the equator in vivo in *Drosophila*.

Abbreviations

AP: Alkaline phosphatase
ATP: Adenosine triphosphate
BAC: Bacterial artificial chromosome
bp: base pairs
BCIP: 5-bromo-4-cloro-3-indolyl-phosphate
C. elegans: *Caenorhabditis elegans*
DMF: Dimethylformamide
DNA: Deoxyribonucleic acid
dNTP: Deoxyribonucleoside triphosphate
DTT: Dithiothreitol
E. coli: *Escherischia coli*
EDTA: Ethylenediaminetetraacetic acid
FBS: Fetal bovine serum
FPLC: Fast Protein Liquid Chromatography
GAP: GTPase activating protein
GDI: Guanine nucleotide dissociation inhibitor
GEF: Guanine nucleotide exchange factor
GFP: Green fluorescence protein
His: Histidine amino acid
HRP: Horse-radish peroxide
IPTG: Isopropyl β-D-thiogalactopyranoside
kb: kilobase pairs
MAP: Microtubule-associated protein
MAPK: Mitogen activated protein kinase
mAU: milli Absorbance Units
MBP: Maltose binding protein
NBT: 4-nitro blue tetrazolium chloride
P[acman]: P/ΦC31 artificial chromosome for manipulation
PBS: Phosphate buffered saline
PBST: PBS with 0.1% Tween 20
PCR: Polymerase chain reaction
pi: post infection
RNAi: RNA interference
rpm: revolutions per minute
SDS: Sodium dodecyl sulfate
TAE: Tris-acetate-EDTA
TE: Tris-EDTA
TEV: Tobacco etch virus
Tris: Tris (hydroxymethyl) aminoethane
U: Units
X-gal: 5-bromo-4-chloro-3-indolyl-β-D-galactopyranoside

Chapter One – Introduction

Cytokinesis is the term for the division of one cell into two. In animal cells, it begins during anaphase and involves the pinching of the cell membrane between the separating chromosomes, resulting in the division of one cell into two. The onset of cytokinesis is tightly regulated so that it occurs only after sister chromatid separation, thereby ensuring faithful transmission of one copy of the genome to each daughter cell. The progression of the division furrow is dependant on the formation of an actin filament and myosin-based structure known as the contractile ring (Pollard, 2009). The actomyosin contractile ring is a feature of all animal cells and provides the mechanical force to drive membrane constriction.

A network of anti-parallel interdigitating microtubules at the midzone between the separating chromosomes delivers a stimulatory signal that specifies the position of the cleavage site (Alsop and Zhang, 2003; Devore et al., 1989; Rappaport, 1985). Although the exact nature of the stimulatory signal is unknown, it appears to involve the coordinated activities of a number of proteins, which activate the RhoA small GTPase, a key activator of contractile ring formation, at the cortical midzone of the cell (Narumiya and Yasuda, 2006). In *Drosophila melanogaster*, the Rho GTP Exchange Factor (RhoGEF) Pebble (Pbl) and the Rho GTPase Activating Protein (RhoGAP) Tumbleweed (Tum, also known as RacGAP50C) are known to be required for cytokinesis (Hime and Saint, 1992; Lehner, 1992; Somma et al., 2002), as are their mammalian orthologues,

Ect2 and HsCyk-4 (also known as RacGAP1 or MgcRacGAP) (Piekny et al., 2005). Furthermore, Pbl and Tum seem to function at the apex of the events that drive cytokinesis and specify the position of contractile ring formation. Although cytokinesis has been studied for over a century, the signalling pathways and interactions that initiate cytokinesis remain poorly characterized. The studies reported in this thesis used a structure function approach to better understand the way in which Pbl and Tum dictate cytokinesis. In this introduction, I first give an overview of the animal cell cycle, focussing primarily on and using gene and protein names for *D. melanogaster*, before discussing in detail the function of Pbl, Tum and other key players in the initiation of cytokinesis and positioning of the contractile ring.

1.1 The cell cycle

The cell cycle is the process by which a cell duplicates its contents and divides to produce two cells. It can be broken up into four main stages; Gap phase one (G1), Synthesis (S) phase, Gap phase two (G2) and Mitotic (M) phase. Together G1, G2 and S phase constitute the period between cell divisions known as interphase. Cell mass often increases in the G1 and G2 phases, with new organelles and proteins being synthesised in preparation for cell division. The genome is replicated in S phase and mitosis occurs at M phase of the cell cycle. Mitosis involves segregation of the replicated chromosomes to opposing poles, following which cytokinesis creates two daughter cells.

In *Drosophila*, this basic pattern of G1/S/G2/M/cytokinesis is modified at different life-cycle stages. For example, the earliest divisions do not actually

involve growth phases or cytokinesis. The first 13 division cycles occur in a syncytial blastoderm where dividing nuclei are contained within a common cytoplasm. At cycle 7 nuclei begin to migrate from the interior of the embryo to the periphery and the last three syncytial cycles occur just beneath the cortex. Cellularisation, a process in which the plasma membrane extends inwards and encloses each cortical nucleus, occurs following the completion of cycle 13. Thus in a developing *Drosophila* embryo, cycle 14 is the first division cycle to exhibit cytokinesis.

1.2 Mitosis

Mitosis can be divided into four main sub-phases; prophase, metaphase, anaphase and telophase. In prophase the chromatin condenses to reveal discrete pairs of sister chromatids and the nuclear membrane breaks down. Metaphase is characterised by the attachment of mitotic spindle fibres to kinetochores that then position the sister chromatids at the equator of the cell. During anaphase the sister chromatids disjoin and separate to opposite poles of the cell. Cytokinesis initiates during this phase. Telophase sees the reformation of the nuclear envelope and the continued ingression of the equatorial furrow.

1.3 Cytokinesis

In animal cells, cytokinesis is highly conserved and, as noted above, involves the formation of a contractile ring whose position is specified at the onset of anaphase by the microtubule spindle. Cortical microtubules are arranged so that their plus ends are positioned at the equatorial cortex of the cell and it is here

that the contractile ring forms. The contractile ring constricts until the cortex surrounds a thick bundle of microtubules and other associated proteins known as the midbody. This structure and the cell membrane bridging the daughter cells is eventually resolved through abscission to create two separate cells (Steigemann and Gerlich, 2009).

The molecular pathways that regulate cytokinesis are relatively well established. Briefly, formation of the contractile ring involves F-Actin polymerising factors such as Diaphanous (Castrillon and Wasserman, 1994) and Chickadee (Giansanti et al., 1998) as well as myosin regulators such as the kinases ROK and Citron (discussed below). These proteins are, in turn, regulated by the small GTPase Rho1, which is itself regulated by the RhoGEF Pebble and RhoGAP Tum. Tum forms a complex with the kinesin-like microtubule motor protein Pavarotti (Pav) (Adams et al., 1998; Mishima et al., 2002; Somers and Saint, 2003), providing a critical link between the contractile ring and the microtubule-based spindle. Finally the temporal coordination of constriction, with respect to mitosis, involves a number of key mitotic kinases such as Cdk1, Aurora B, and Polo Kinase, which are discussed in more detail below. The final stage of cytokinesis, abscission, is a poorly understood process but is known to require midbody-targeted vesicle secretion, disassembly of the microtubules within the midbody, plasma membrane fission and the enrichment of phosphatidylinisitol 4,5 bisphosphate at the membrane surrounding the midbody (Guizetti and Gerlich, 2010).

These molecular structures and pathways regulating cytokinesis are detailed in the following sections.

1.4 The Contractile ring

The contractile ring is formed primarily from filamentous actin (F-actin) and non-muscle myosin II (Figure 1.1). It is a highly dynamic structure that has a rapid turnover of both actin and myosin (Murthy and Wadsworth, 2005; Yumura, 2001). Furrow ingression is achieved through the combined actions of non-muscle myosin II and F-actin. However, it is unclear exactly how the force is generated to stimulate constriction. The predominant 'purse string' model suggests that myosin slides F-actin to shorten the ring where the ingression force comes from the component of the sliding force that is directed inward (Schroeder, 1972). However, the evidence for the alignment of contractile fibres in this orientation is limited.

1.4.1 Non-muscle myosin II

The first indication that non muscle myosin may be involved in cytokinesis came from the observation that it accumulated at the equatorial cell cortex in dividing HeLa cells (Fujiwara and Pollard, 1976). Myosin was later demonstrated to be required for cytokinesis, by showing that the injection of anti-myosin antibodies into starfish blastoderms inhibited subsequent cleavages (Mabuchi and Okuno, 1977). This crucial cytokinetic role has since been demonstrated in many other organisms including *Drosophila*, *Dictyostelium*, budding yeast and fission yeast

(Bezanilla et al., 1997; Bi et al., 1998; De Lozanne and Spudich, 1987; Karess et al., 1991).

A myosin monomer consists of two myosin heavy chains (MHCs), two essential light chains and two regulatory light chains (MRLCs). The MHC is referred to as the motor domain and is responsible for binding to actin, and for ATP binding and hydrolysis. The activity of myosin is regulated through the phosphorylation of activation and inhibition sites on MRLC. Phosphorylation of MRLC at Ser19 has been shown to promote filament assembly and enhance myosin's contraction ability (Adelstein and Conti, 1975; Scholey et al., 1980; Somlyo and Somlyo, 1994). Furthermore, an additional phosphorylation site at Thr18 has also been shown to enhance the activity of myosin (Ikebe, 1989).

Citron kinase, Rho kinase (ROK) and myosin light chain kinase (MLCK) have all been shown to be capable of phosphorylating MRLC at Ser19/Thr18 (Kosako et al., 2000; Madaule et al., 1998; Poperechnaya et al., 2000). However, it is unclear which kinase/s actually phosphorylate MRLC during cytokinesis. On the other hand, phosphorylation of MRLC on its inhibition sites is thought to reduce MHC's affinity for actin (Ikebe et al., 1987; Nishikawa et al., 1984). An in vitro kinase assay implicated Cdc2 as the responsible kinase for phosphorylation of this inhibitory site, but this is yet to be demonstrated in vivo (Satterwhite et al., 1992).

Myosin phosphatase acts antagonistically to MRLC activation. In mammals, the targeting subunit of myosin phosphatase, MYTP1, is

Figure 1.1 The structure of the contractile ring

A simple drawing of the predicted structure of a contractile ring. The ring is arranged so that antiparallel actin filaments interact with myosin molecules. The attachment of barbed actin ends to the plasma membrane via a formin is hypothetical. As myosin molecules move to the barbed end of an associated actin filament tension is applied to the plasma membrane and constriction is achieved. Image taken from Pollard T. D. 2010. Mechanics of Cytokinesis in Eukaryotes Curr Opin Cell Biol *22*, 50–56.

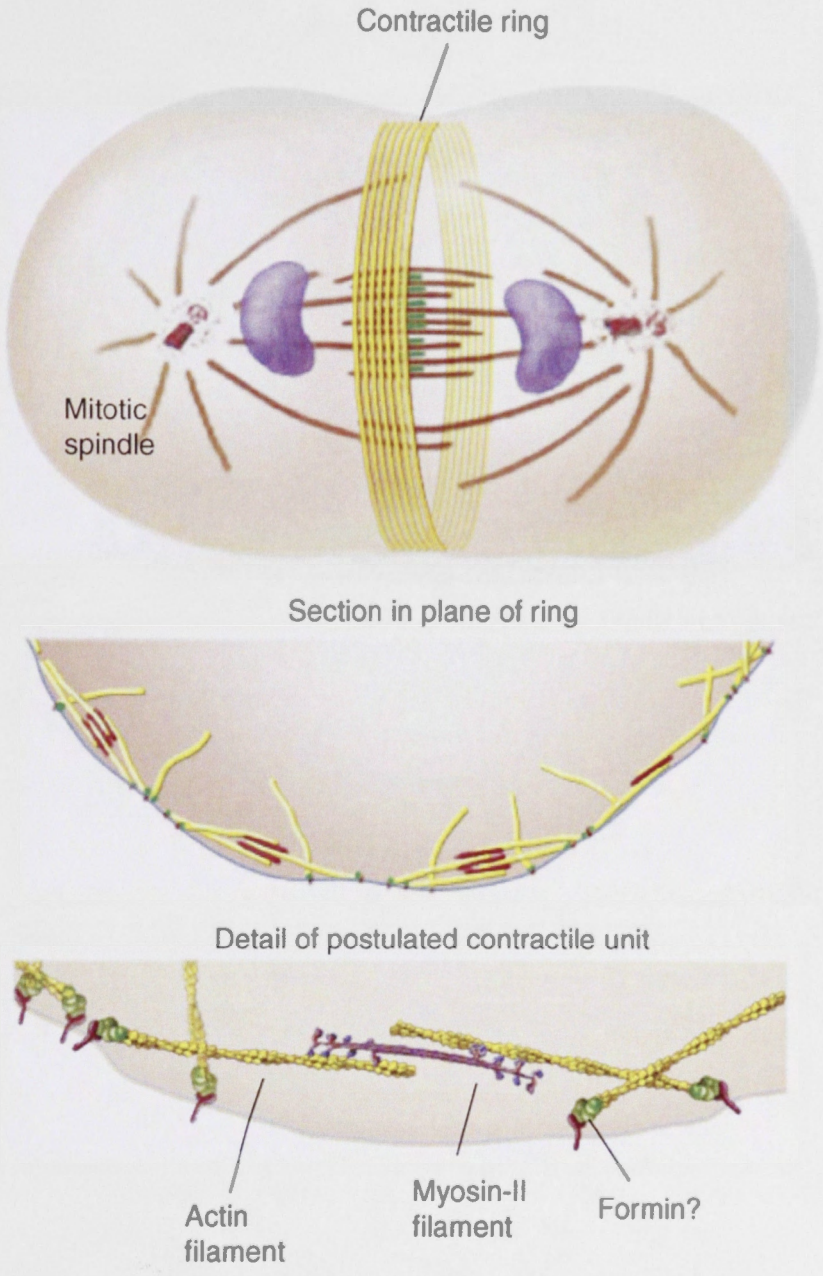
Contractile ring
Mitotic spindle
Section in plane of ring
Detail of postulated contractile unit
Actin filament
Myosin-II filament
Formin?

phosphorylated during metaphase, which increases its phosphatase activity (Totsukawa et al., 1999). These activating phosphorylations disappear during cytokinesis, and ROK phosphorylates Thr695 in MYPT1 to inhibit myosin phosphatase activity at the cleavage furrow (Kimura et al., 1996). Furthermore, ROK phosphorylation of Thr850 induces myosin dissociation from myosin phosphatase (Velasco et al., 2002). Thus ROK inhibits myosin phosphatase during cytokinesis in mammals to promote the active form of MRLC and stimulate actomyosin contractility.

Studies in other organisms also indicate a role for MYTP in cytokinesis. In *C. elegans*, mutations in MYTP cause defects in cytokinesis and morphogenesis (Piekny and Mains, 2002). MYTP is required for dorsal closure and eye morphogenesis in *Drosophila*, where it acts as a negative regulator of the Rho GTPase (Mizuno et al., 2002; Tan et al., 2003). Furthermore, a recent study demonstrated that mutations in MYTP caused the over constriction of ring canals in *Drosophila* germ cells (Ong et al., 2010). Ring canals are derived from contractile rings that undergo an incomplete cytokinesis. Therefore myosin phosphatase seems to have a conserved role in cytokinesis.

1.4.2 F-actin

Actin is a highly conserved eukaryotic protein that polymerizes to form filamentous actin (F-actin) structures. In animal cells and fission yeast actin filaments at the contractile ring have mixed polarities. They are orientated in both directions around the ring with the barbed ends attaching to various sites around the equatorial plasma membrane (Kamasaki et al., 2007; Sanger and

Sanger, 1980; Schroeder, 1973). The actin network is extremely dynamic during cytokinesis with filaments constantly polymerizing and depolymerizing (Pelham and Chang, 2002). Several proteins have been shown to bind and regulate actin dynamics during cytokinesis.

1.4.3 Actin binding proteins

1.4.3.1 Profilin and Cofilin

Profilin is a small protein that binds to polymerisation-ready ATP bound actin monomers. Profilin acts as a polymerisation catalyst to promote filament growth by ushering actin onto growing barbed end filaments (Kang et al., 1999). The *Drosophila* gene *chickadee* encodes the fly orthologue of *profilin* and has been shown to be essential for cytokinesis (Giansanti et al., 1998). Depletion of Profilin in *C. elegans* and over-expression of a dominant-negative form of Profilin in mammals both inhibit contractile ring formation (Severson et al., 2002; Suetsugu et al., 1999). These results emphasise the crucial role Profilin plays in actin filament assembly during cytokinesis.

By contrast, Cofilin plays an important role in cytokinesis through its ability to disassemble actin filaments (Gunsalus et al., 1995). Interfering with Cofilin function through the introduction of mutations or by RNAi results in cytokinesis defects in mammals, *Xenopus*, *Drosophila*, *C. elegans* and fission yeast (Abe et al., 1996; Gunsalus et al., 1995; Hotulainen et al., 2005; Nakano and Mabuchi, 2006; Ono et al., 2003). Cofilin is required not only for the reorganisation of interphase actin filaments into the contractile ring, but also for the maintenance and constriction of the ring (Nakano and Mabuchi, 2006).

Phosphorylation regulates the activity of Cofilin by directing its recruitment to and the progression of the cleavage furrow (Abe et al., 1996; Tanaka et al., 2005). Thus Cofilin plays an important role in contractile ring dynamics during cytokinesis.

1.4.3.2 Formins

The first link between formins and cytokinesis came from a study in *Drosophila* that found that the mutation of the formin protein Diaphanous (Dia) led to a failure in spermatid cell division (Castrillon and Wasserman, 1994). Dia and other diaphanous related formins (DRFs) have subsequently been found to be essential for the formation and maintenance of the actin cytokinesis network in many animal and fungal species (Chang et al., 1997; Imamura et al., 1997; Peng et al., 2003; Severson et al., 2002; Swan et al., 1998; Tolliday et al., 2002; Tominaga et al., 2000). The activity of DRFs are regulated by an autoinhibitory interaction that is relieved upon Rho GTPase binding (Alberts, 2001). In their active conformation, DRFs nucleate linear unbranched actin filaments and remain associated with the rapidly growing barbed end. This association prevents filament capping that would otherwise inhibit further growth. Due to the extended lifetime of formins on the barbed ends of actin filaments, DRFs are attractive but as yet unproven candidates to anchor actin filaments to the plasma membrane.

1.4.3.3 Anillin

Anillin (also known as Scraps) was first identified in *Drosophila* through its affinity for F-actin (Miller et al., 1989). Related proteins have since been

discovered in all eukaryotes. The accumulation of Anillin at the cleavage furrow during embryonic divisions indicated a role in cytokinesis (Field and Alberts, 1995). Anillin has since been found to play a pivotal role in the organization of the cytoskeletal scaffolding that is required for cytokinesis. This role is fulfilled through interactions with a number of key cytokinetic proteins including myosin, septins, Rho and the RhoGAP protein Tum (D'avino et al., 2008; Gregory et al., 2008; Kinoshita et al., 2002; Piekny and Glotzer, 2008; Straight et al., 2005). The equatorial localisation of Anillin has been shown to require Rho activation in mammals and *Drosophila* (Hickson and O'Farrell, 2008; Piekny and Glotzer, 2008; Somma et al., 2002). Moreover, while Anillin is not required for the initial formation of the contractile ring or equatorial F-actin accumulation, *anillin* knockdown by RNAi results in aberrant F-actin accumulation and cells ultimately fail to divide (Echard et al., 2004; Somma et al., 2002). Similarly, although equatorial myosin recruitment is not dependent on Anillin, maintaining the localisation of myosin at the furrow as ingression proceeds requires Anillin in both *Drosophila* and mammals (Hickson and O'Farrell, 2008; Straight et al., 2005; Zhao and Fang, 2005a). Thus Anillin is indispensable for maintaining the integrity of the contractile ring.

An important function of Anillin is to act as a direct link between the actin and microtubule networks. This is achieved through an interaction between Anillin and Tum. The two proteins co-localise at the plus ends of cortical central spindle microtubules and have been shown to interact both in vitro and in vivo (D'avino et al., 2008; Gregory et al., 2008). Tum itself binds to the microtubule bundling motor protein Pavarotti (Pav), which is responsible for its furrow

localisation (Somers and Saint, 2003). Therefore, by interacting with Tum, which in turn binds Pav, Anillin provides a stable connection between the spindle microtubules and the contractile ring as the furrow ingresses.

1.4.3.4 Septins

Septins were first identified in a *Saccharomyces cerevisiae* screen for mutants that arrest at cytokinesis (Hartwell, 1971). They have since been found to be important for cytokinesis in a diverse range of organisms (Field and Kellogg, 1999; Kinoshita, 2003; Trimble, 1999). Septins contain a central GTPase domain and are able to bind both actin and microtubules. Immunoprecipitation experiments in *Drosophila* and *S. cerevisiae* have demonstrated that septins can form long filaments (Field et al., 1996; Frazier et al., 1998), where the presence of several different septin proteins within these structures seems to be a conserved feature (Surka et al., 2002).

Studies in *S. cerevisiae* have shown that septins contribute to cytokinesis completion by acting as scaffolds to concentrate essential signaling proteins, acting as diffusion barriers and in controlling the timing of mitotic exit (Barral et al., 2000; Castillon et al., 2003; Moffat and Andrews, 2003; Takizawa et al., 2000). Although septins are thought to act as a scaffold for contractile ring assembly in other animal cells, their precise role in cytokinesis is unknown. *Drosophila* have five septins, Peanut (Pnut), Sep1, Sep2, Sep4 and Sep5 (Adam et al., 2000). Pnut, Sep1 and Sep2 can form stable filaments in vitro consisting of two subunits of each septin in a heteromeric six subunit complex (Field et al., 1996). Pnut and Sep1 colocalise to the cleavage furrow of dividing cells, eventually becoming

restricted to the midbody, and mutations in *pnut* result in cytokinesis failure (Neufeld and Rubin, 1994). Mammals possess twelve septin genes, Sept1-Sept12 (Field and Kellogg, 1999). Inhibition of SEPT 2 and SEPT 9 through siRNA knockdown or antibody microinjection results in impaired cell division (Kinoshita et al., 1997; Surka et al., 2002). These studies observed the accumulation of binucleate cells and daughter cells interconnected by stable midbody bridges. This suggests a role for septins in late cytokinesis or abscission. However, a clearly defined role for septins during cytokinesis in higher eukaryotes remains elusive.

1.5 The Ras superfamily of GTPases

As should already be clear from the above discussion, the Rho GTPase is central to the formation of the contractile ring. Rho is a member of the Ras superfamily of small GTPases, which act as molecular switches in a wide range of biological pathways. The activity of all Ras members is regulated by their ability to bind and hydrolyse guanine nucleotides. Five subfamilies exist within the Ras superfamily; Ras, Ran, Arf, Rab and Rho. Each subfamily regulates distinct signalling pathways. The Ras subfamily are involved in cellular proliferation and differentiation (Lowy and Willumsen, 1993), while Ran members are involved in nuclear protein transport (Moore and Blobel, 1993). The Arf and Rab subfamilies are implicated in vesicular transport (Balch, 1990) while the Rho GTPases modulate the cytoskeleton (Kozma et al., 1995; Ridley and Hall, 1992; Ridley et al., 1992). Moreover, the cytoskeletal rearrangements induced by Rho, the founding member of this subfamily of GTPases, have been found to be crucial for the completion of cytokinesis. To achieve the rapid responses required for these

rearrangements, several types of regulators are involved in modulating GTPase activity.

1.5.1 The GTPase cycle

Small GTPases oscillate between two states, an active GTP-bound state and an inactive GDP-bound state (Figure 1.2). Three types of regulators are involved in modifying GTPase activity.

i) GTPase exchange factors (GEFs). These factors catalyse the conversion of inactive small GTPases to their active state (Figure 1.2). This is achieved by a GEF-GTPase interaction that dissociates bound GDP and stabilises a nucleotide free intermediate structure (Whitehead et al., 1997). Due to the prevalence of GTP compared with GDP within the cytoplasm, the nucleotide free GTPase is more likely to bind a GTP molecule leading to the displacement of the GEF (Lenzen et al., 1998) and activation of the GTPase. The exchange of GDP with GTP induces a conformational change in the GTPase that enables interactions with downstream effectors (Bourne et al., 1990).

ii) GTPase Activating Proteins (GAPs) (Figure 1.2). These proteins enhance the relatively low intrinsic GTPase activity of small GTPases and thereby help inactivate Rho GTPases and rapidly shut off their associated signalling pathways.

iii) Guanine nucleotide Dissociation Inhibitors (GDIs). GDIs provide a further level of regulation by binding and maintaining GTPases in their GDP-bound inactive form. Although Rho GDIs may also regulate GTPases during cytokinesis, their involvement has so far only been demonstrated in *Dictyostelium* (Imai et al., 2002; Rivero et al., 2002).

1.5.2 The Rho family of GTPases

The Rho family of GTPases regulate, directly or indirectly, numerous processes such as actin and microtubule dynamics, gene expression, the cell cycle, cell polarity and membrane transport. The most highly conserved and extensively studied Rho GTPases are Rho (RhoA/Rho1), Rac (Rac1) and Cdc42, which have well described roles in the modification of the actin cytoskeleton. Early studies in mammalian cultured cells demonstrated that the activation of each of these Rho family members stimulated the formation of unique actin structures. While Rho activation in Swiss 3T3 fibroblasts results in contractile actin filament formation (Ridley and Hall, 1992), microinjection of Rac1 leads to the formation of broad membrane ruffles or lamellipodia (Ridley et al., 1992), and activation of Cdc42 produces thin finger-like projections termed filopodia (Kozma et al., 1995). Furthermore, in mammalian cultured cells there seems to be hierarchical co-operativity between Rho family members where Cdc42 activates Rac, which in turn activates Rho (Nobes and Hall, 1995). However, antagonistic cross-talk has also been observed where Rho and Rac have opposing effects on MRLC phosphorylation (Sanders et al., 1999). It is tempting to speculate that such a relationship might contribute to contractile ring actomyosin dynamics during cytokinesis. Indeed Rho GTPases play a number of pivotal roles during mitosis, including cytokinesis, many of which revolve around their ability to direct cytoskeletal changes. In particular, Rho is critical for the formation, constriction and stability of the contractile ring.

Figure 1.2 The Rho GTPase cycle

Rho GTPases can exist in an inactive GDP-bound form or an active GTP-bound form. Guanine nucleotide exchange factors (GEFs) catalyze the conversion of inactive Rho to its active form. GTPase activating proteins (GAPs) inactivate Rho GTPases by stimulating their intrinsic GTPase activity resulting in GTP hydrolysis. In their active form Rho GTPases interact with their downstream effectors to modulate the actin cytoskeleton.

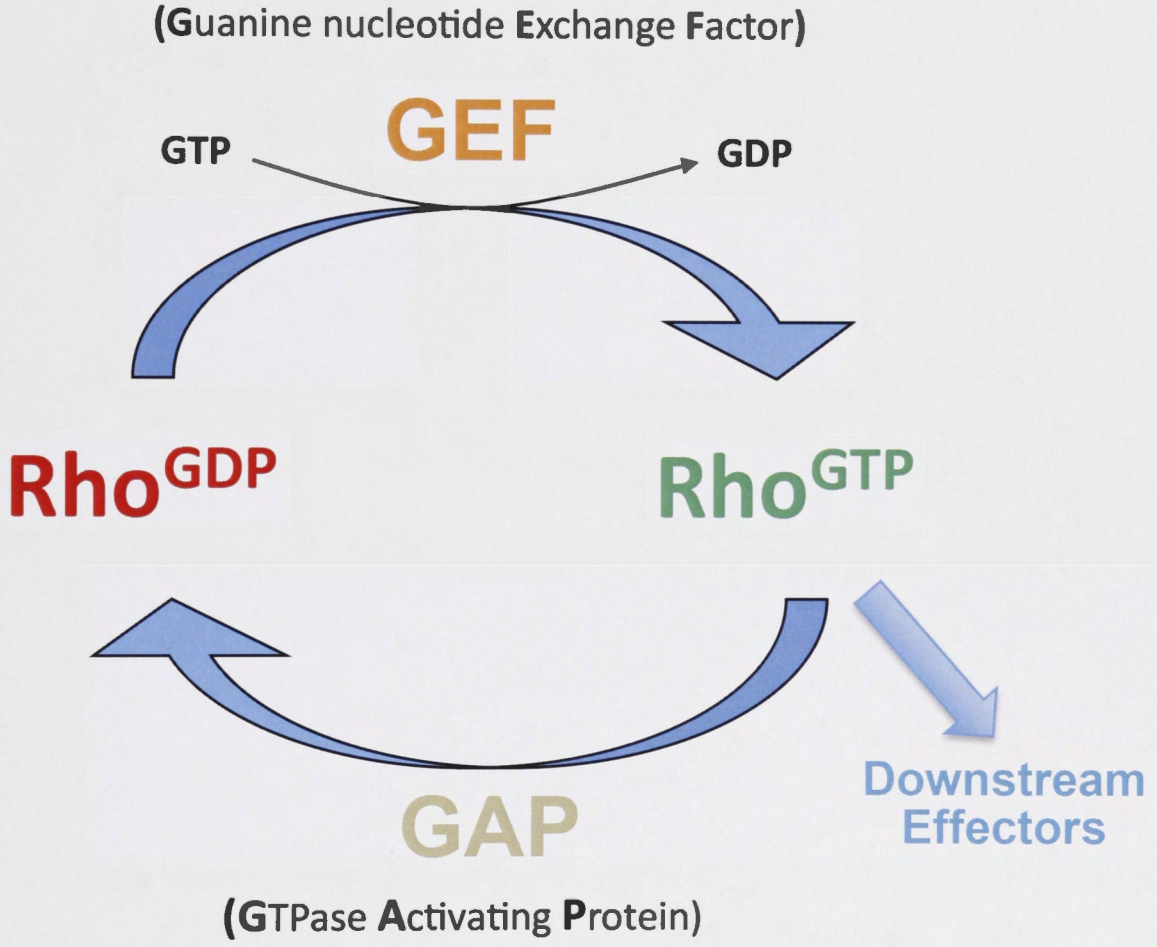
(Guanine nucleotide Exchange Factor)
GEF
GTP
GDP
Rho^GDP
Rho^GTP
GAP
Downstream Effectors
(GTPase Activating Protein)

1.5.3 The role of Rho GTPases in cytokinesis

Cytokinesis requires major cytoskeletal rearrangements to enable the membrane furrowing that is required for the separation of the two daughter cells, and Rho GTPases have been identified as key regulators of this process.

The key GTPase driving cytokinesis is Rho1. This was first identified in sea urchin embryos with the use of the C3 exoenzyme from *Clostridium botulinum* that specifically inactivates Rho1 (Mabuchi et al., 1993). Subsequent studies have shown that Rho1 is essential for cytokinesis in mammalian cell culture (O'Connell et al., 1999), *Drosophila* (Prokopenko et al., 1999), *Xenopus* (Drechsel et al., 1997; Kishi et al., 1993), and *C. elegans* (Jantsch-Plunger et al., 2000). Cells in which Rho has been depleted or inhibited fail to construct a contractile ring and are unable to constrict. Several different probes that detect active GTP-bound Rho have been used to demonstrate that a narrow band of Rho accumulates at the equator of cells undergoing cytokinesis (Bement et al., 2005; Yoshizaki et al., 2003). Localisation of Rho to the equator occurs prior to furrow ingression and is independent of myosin and actin recruitment (Bement et al., 2005; Yüce et al., 2005). Rather, the equatorial localisation and activation of Rho requires the RhoGEF protein Pbl/Ect2 (Glotzer, 2005).

The mechanisms by which active Rho leads to the formation and constriction of the contractile ring have been the subject of intense investigation. It has become clear that Rho effectors are fundamental to the actomyosin

contractile network. As mentioned earlier, formins such as Dia require Rho binding to relieve their autoinhibitory conformation and thus enable them to promote actin filament assembly (Alberts, 2001). Rho is also involved in stimulating myosin. Cleavage furrow localisation and activation of Citron kinase and ROK, two kinases that phosphorylate and activate myosin contractility (Kosako et al., 2000; Madaule et al., 1998), are dependent on Rho1 (Di Cunto et al., 1998; Eda et al., 2001; Kosako et al., 1999; Matsui et al., 1996; Shandala et al., 2004). Citron kinase recruitment promotes contractile ring stability during late cytokinesis by maintaining Anillin and actin at the furrow (D'Avino et al., 2004; Echard et al., 2004; Naim et al., 2004). ROK also contributes to myosin activation through the inhibition of myosin phosphatase (Kimura et al., 1996). However, ROK appears to act earlier than Citron kinase, as mammalian, *Drosophila* and *C. elegans* cells depleted of ROK form furrows but either fail to ingress or exhibit delayed constriction whereas constriction occurs normally but abscission fails upon depletion of Citron kinase (Kosako et al., 2000; Naim et al., 2004; Piekny and Mains, 2002; Royou et al., 2002). Thus active Rho1 promotes contractile ring formation, constriction and stability by localising and activating important furrow components (Figure 1.3).

It is thought that Rho1 inactivation may be required at the end of cytokinesis to permit cleavage furrow disassembly (Chalamalasetty et al., 2006). This may be achieved, at least partly, through ubiquitin mediated degradation of Rho1 by Cul3-BACURD ubiquitin ligase complexes (Chen et al., 2009). An activation or enhancement of the GAP activity of Tum towards Rho1 may also contribute to Rho inactivation. Indeed, a late Aurora B-mediated

Figure 1.3 ***Rho activation and possible pathways of action of the downstream effectors involved in the formation and constriction of the contractile ring***

Rho can exist in an inactive GDP-bound form or an active GTP-bound form. In its active state Rho interacts with formins to relieve their autoinhibitory conformation and thereby promote actin filament formation. Citron kinase and ROK are also activated by Rho and induce contractility of the contractile ring by phosphorylating and activating RMLC. ROK also contributes to myosin activation by inhibiting myosin phosphatase.

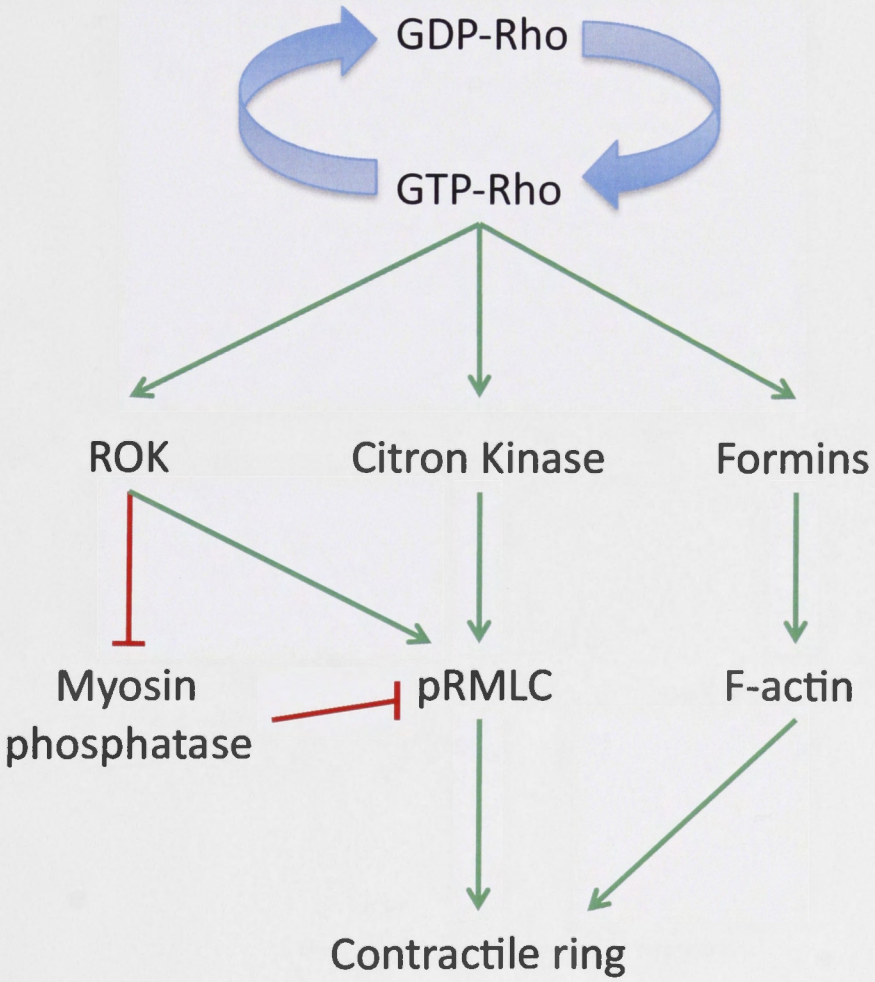
GDP-Rho
GTP-Rho
ROK
Citron Kinase
Formins
Myosin phosphatase
pRMLC
F-actin
Contractile ring

phosphorylation of HsCyk-4, the mammalian orthologue of Tum, was proposed to increase its GAP activity towards Rho (Minoshima et al., 2003).

In addition to its role in actomyosin dynamics, Rho1 may also participate in the maintenance of the anaphase microtubule spindle. Studies in mammalian cell culture have observed defects in microtubule stabilisation and organisation upon injection of the C3 exoenzyme (Kanada et al., 2009; O'Connell et al., 1999). Furthermore, equatorial localisation of Rho depends on spindle position and displacement of the spindle leads to a repositioning of the active Rho zone (Bement et al., 2005). Thus a positive feedback mechanism may exist between Rho and spindle microtubules. As will be discussed in the next section, the microtubules perform an indispensable role in cytokinesis by specifying the site of cleavage furrow formation.

Although Rho is clearly the key GTPase involved in cytokinesis recent studies have also suggested a role for Rac in facilitating contractile ring constriction. Fluorescence resonance energy transfer (FRET) imaging revealed that Rac-GTP localises cortically at the cell poles during cytokinesis (Yoshizaki et al., 2003). The conspicuous absence of active Rac at the equator was recently given some functional significance. In *C. elegans* zygotes, inactivation of Rac by the Tum orthologue Cyk-4 is required for the completion of furrow ingression (Canman et al., 2008). A similar mechanism may occur in *Drosophila*, since genetic experiments have demonstrated that Tum is able to inhibit Rac activity (D'Avino et al., 2004) and its GAP activity is known to be required for the completion of cytokinesis (Zavortink et al., 2005). Furthermore, Canman and

colleagues went on to establish that Rac inhibition contributes to furrowing by preventing the activation of the Arp2/3 complex, which promotes branching of actomyosin filaments. It was proposed that Rac inactivation prevents the formation of branched actomyosin networks in the furrow region that may otherwise prevent contractile ring constriction. However, further work is required to fully dissect the role of Rac in contractile ring dynamics.

There is little evidence to suggest that Cdc42 fulfils a cytokinetic function. Although activated and dominant negative forms of Cdc42 cause cytokinetic defects (Drechsel et al., 1997; Dutartre et al., 1996), embryonic fibroblasts isolated from *cdc42* knockout mice are able to divide normally (Chen et al., 2000). Cdc42 has been shown to play a role in metaphase spindle formation and kinetochore microtubule attachment (Ban et al., 2004; Oceguera-Yanez et al., 2005; Yasuda et al., 2004), but a defined function for Cdc42 in cytokinesis is yet to be described.

1.6 Microtubules

Microtubules are cylindrical polymers composed of dimers of α-tubulin and β-tubulin. They possess polarity with a fast growing plus end and a slow growing minus end that is often capped by the ring shaped γ-tubulin microtubule nucleator complex (Desai and Mitchison, 1997). Microtubules facilitate many essential cellular functions including vesicle and organelle transport, cell migration, chromosome separation, and cytokinesis. During cytokinesis the cleavage site must be carefully positioned to ensure that the segregated chromosomes are correctly separated into two daughter cells. The midzone

microtubules constructed during anaphase are important for this process as they coordinate the position of the contractile ring (De Lozanne and Spudich, 1987; Knecht and Loomis, 1987; Mabuchi and Okuno, 1977; Straight et al., 2003). Thus it is no surprise that great efforts have been made to determine how the microtubule spindle dictates the cleavage site and stimulates furrowing.

1.6.1 Microtubule organisation

Organisation of the cellular microtubule network begins with the centrosome, an organelle composed of two centrioles arranged perpendicular to one another, which can nucleate microtubule filaments. Prior to entry into mitosis the centrioles split, move to opposite poles of the cell and replicate giving rise to two new centrosomes. As cells enter mitosis an array of microtubules emanates from each centrosome. Upon breakdown of the nuclear membrane, microtubules from each centrosome eventually attach to each kinetochore and position the chromosomes at the metaphase plate. This metaphase microtubule spindle is commonly referred to as the mitotic spindle (Figure 1.4). During anaphase chromosomes are segregated to opposing poles and a similar but distinct microtubule spindle, known as the central spindle, emerges from the mitotic spindle (Figure 1.4). The mitotic and central spindles share a similar organisation where overlapping interdigitating anti-parallel bundled microtubules are aligned so that the plus ends terminate at the equator (Mastronarde et al., 1993). Other microtubules, referred to here as astral microtubules, radiate out from the centrosome and contact the cell cortex (Figure 1.4). Furrow ingression proceeds into telophase until the microtubules

are compacted into the dense midbody structure. These microtubules are ultimately disassembled to permit abscission.

Although the mitotic and central spindle structures appear to have a similar overall organisation, evidence suggests that the central spindle arises independently from the mitotic spindle. Central spindle functional equivalents can form in the absence of important mitotic spindle components such as chromosomes and centromeres. For example, anucleate cells are able to construct a central spindle that contains central spindle components (Bucciarelli et al., 2003) as do regions of overlap between neighbouring spindles (Savoian et al., 1999). Furthermore, cells depleted of chromosomes and centrosomes or cells treated with microtubule depolymerising drugs during metaphase are able to bundle microtubules and induce furrowing (Alsop and Zhang, 2003; Canman et al., 2000). This evidence suggests that the central spindle arises independently of the pre-existing bipolar metaphase mitotic spindle.

While both the mitotic and central spindles are dynamic the stability of the microtubules within each structure seems to differ. Using Fluorescence Recovery After Photobleaching (FRAP) the mitotic spindle microtubules were found to turn over faster ($t_{1/2}$ = 10-20 secs) than central spindle microtubules ($t_{1/2}$ = > 2 mins) (Salmon et al., 1984; Saxton and McIntosh, 1987; Saxton et al., 1984). Furthermore, it has been shown that central spindle microtubules, unlike astral microtubules, are selectively stabilised as they are largely resistant to depolymerising drugs (Murthy and Wadsworth, 2008). However central spindle microtubules are not completely inert as polymerisation and markers of plus end

Figure 1.4 Microtubule structures present during cell division

Schematic representation of the microtubule structures present from metaphase through to the end of telophase. The mitotic spindle constructed during metaphase originates from the centrosomes. Microtubules attach to kinetochores and align sister chromatids along the equator. Several distinct sets of microtubules exist in anaphase. Astral polar microtubules radiate out from the centrosome and eventually contact the polar cortex. Equatorial microtubules contact the cortex at the equator and contribute to concentrating cytokinesis components to the region of furrow formation. The central spindle consists of interpolar interdigitating microtubles whose plus ends terminate at the equator. The spindle midzone is comprised of both central spindle and equatorial microtubules. Furrowing eventually compacts equatorial and central spindle microtubules into a dense midbody structure at telophase. Image adapted from Glotzer M. 2009. The 3Ms of central spindle assembly: microtubules, motors and MAPs Nat Rev Mol Cell Biol *10*, 9-20.

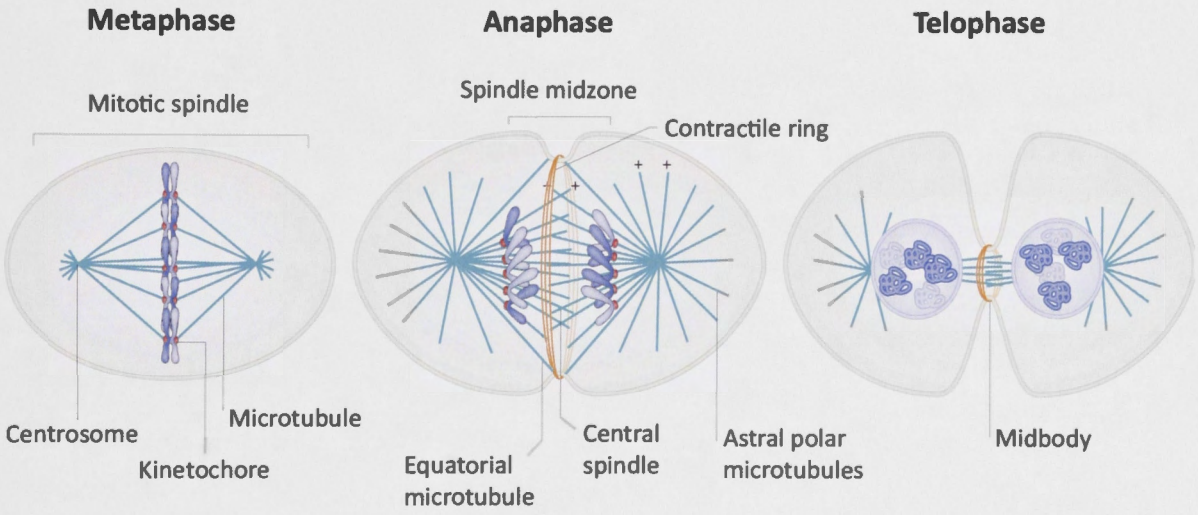
Metaphase
Anaphase
Telophase
Mitotic spindle
Spindle midzone
Contractile ring
Centrosome
Microtubule
Kinetochore
Equatorial microtubule
Central spindle
Astral polar microtubules
Midbody

microtubule growth can be detected (Rosa et al., 2006; Saxton and McIntosh, 1987; Shelden and Wadsworth, 1990). Thus the mitotic and central spindles are not only formed independently but the nature of the microtubule structures appears to be different.

1.6.2 Microtubules specify the cleavage furrow site

Although it is acknowledged that microtubules dictate the position of contractile ring formation, exactly which microtubules specify the furrow site remains a contentious issue. An early study showed that micromanipulation of the anaphase microtubule spindle results in the regression of the existing furrow and the formation of a new cleavage site at the midpoint of the spindle (Rappaport, 1985). This and numerous other studies demonstrated that the microtubule spindle determines the cleavage plane position. To identify whether the furrowing signal/s were sent to the poles or equator, cells were perforated or had oil droplets inserted to try and block signals from astral or equatorial microtubules. While blocks at the poles had little effect, inhibiting equatorial signals prevented cleavage (Rappaport, 1968; Rappaport and Rappaport, 1983). This led to the proposal of an 'equatorial stimulation' model, where microtubules that terminate at the equator impart a positive signal to the cortex to induce furrow formation and ingression (Rappaport, 1996). In support of this, microsurgery in grasshopper spermatocytes to remove components of the microtubule spindle showed that bundled overlapping anti-parallel microtubules could induce furrowing at the expected position of the overlapping plus ends (Alsop and Zhang, 2003, 2004). Subsequent studies have tried to confirm and

extend these findings. Studies in some organisms have shown that preventing central spindle assembly can result in cytokinesis failure (Glotzer, 2005).

However, recent work has indicated that a separate population of equatorial microtubules contributes to furrow induction. A study in *Drosophila* spermatocytes suggests initial furrow ingression can also be initiated by a subset of stable astral microtubules that contact the equatorial cortex (Inoue et al., 2004), referred to here as equatorial microtubules (Figure 1.4). In this model, the central spindle microtubules were proposed to play a role in stabilizing and propagating furrow ingression. In support of this, a subpopulation of stable equatorial microtubules have also been observed at the furrow site in mammalian cultured cells and also in sea urchin eggs where only half the bipolar spindle is present (Canman et al., 2003; Foe and von Dassow, 2008). Moreover, single taxol-stabilized microtubules can produce 'furrowlets' in mammalian cultured cells (Shannon et al., 2005). Furthermore, computational modelling has indicated that stable microtubules are more effective concentrators than dynamic microtubules (Odell and Foe, 2008). However, microtubule stains in fixed cells of some species appear to contradict the equatorial model as microtubules are less dense at the equator compared with the polar cortex (Asnes and Schroeder, 1979; Dechant and Glotzer, 2003; White and Borisy, 1983; Yoshigaki, 2003). Nevertheless, fixed cell analysis may not give an accurate representation of the actual microtubule network within a cell, as fixation is unlikely to preserve all microtubules. Alternatively, extensive cortical microtubule contacts at the cleavage site might not be required due to the advantages that stable microtubules may impart. Thus experimental data would

suggest that stable equatorial microtubules act to concentrate essential furrow components to induce furrowing and the central spindle subsequently stabilises and propagates furrow ingression, although other mechanisms may exist in certain cell types.

A variation on this model suggests that polar astral microtubules provide some spatial cue to position the furrow at the equator. This was first suggested by examining torus-shaped cells where opposing asters were shown to be able to direct cytokinesis in the absence of an intervening central spindle (Rappaport, 1961). The ability of juxtaposed asters to direct furrowing has also been demonstrated in multipolar mammalian cultured cells (Rieder et al., 1997; Sanger et al., 1998). However, a study that tried to replicate the torus-shaped cell experiment in cultured mammalian somatic cells produced a different outcome. Although numerous astral microtubules penetrated the region beyond the perforation where furrowing would normally occur, it was the side of the perforation immediately adjacent to the central spindle that exhibited furrowing (Cao and Wang, 1996). This suggests that the central spindle is primarily responsible for initiating furrowing in mammalian cells. Similar experiments in *C. elegans* gave an intermediate result where furrows were observed at opposing asters in addition to the central spindle midline (Baruni et al., 2008). Moreover, several studies suggest that the central spindle signal supersedes the astral signals as aster furrows abdicate in favour of a central spindle midzone furrow (Baruni et al., 2008; Bringmann and Hyman, 2005). In support of this, studies in *Drosophila* have indicated that asters are not strictly required for cleavage furrow formation and cytokinesis (Basto et al., 2006; Bonaccorsi et al., 1998).

Although the role that different microtubule populations play in furrow positioning continues to be debated, it is clear that microtubules impart some sort of signal to position the cleavage furrow. The extent to which polar astral, equatorial or central spindle microtubules dictate this process may depend on the cell type or organism under investigation. This may be due to varying distances between the cortex and anaphase microtubule structures in different cell types. For example, the central spindle of a *Drosophila* embryo epidermal cell is in close proximity to the cortex whereas the central spindle is some distance from the cortex in sea urchin embryos. One possible explanation for the ability of adjacent asters to induce furrowing is that they are able to generate enough anti-parallel bundled microtubules to initiate furrowing. However, astral furrows frequently do not fully ingress highlighting the role the central spindle plays in propagating furrow ingression. It is likely that signals from astral, equatorial and central spindle microtubules combine to coordinate cleavage furrow positioning where the equatorial stimulus signal is able to override contributory messages at the poles. Irrespective of the relative contributions, the evidence for a furrow-inducing microtubule signal is compelling, at least in many cell types. The next sections examine microtubule associated proteins and molecular motors that function in spindle assembly and delivery of the furrow-inducing signal.

1.6.3 MAPs and motor proteins are required for spindle assembly

Microtubule associated proteins (MAPs) and motor proteins play a crucial role in cytokinesis by contributing to central spindle organisation and localising key cytokinetic proteins to the equator. Despite the ability of many MAPs and motors to bundle microtubules in vitro, no single component is sufficient for central spindle construction in vivo. Thus central spindle assembly relies on a complex relationship between many MAPs and motor proteins.

Relatively few proteins that bind to microtubule minus ends and contribute to central spindle organisation have been identified. The kinesin-14 minus end directed motor protein, known as Ncd in *Drosophila*, has been shown to have a conserved role in spindle organisation during both meiosis and mitosis in a wide range of organisms (Hatsumi and Endow, 1992; Kimble and Church, 1983; Matthies et al., 1996; Mountain et al., 1999; Saunders and Hoyt, 1992; Segbert et al., 2003). Ncd is not only enriched at the spindle poles but can also be detected all over the central spindle microtubules (Goshima et al., 2005; Mountain et al., 1999; Walczak et al., 1997). Recent in vitro studies in *Drosophila* and yeast have demonstrated that Ncd preferentially slide anti-parallel microtubules relative to each other and can stabilise parallel microtubules (Braun et al., 2009; Fink et al., 2009). Thus Ncd and its orthologues may participate in spindle organisation by stabilising parallel microtubules at the poles while assisting in the formation of the anti-parallel central spindle microtubule array. The *Drosophila* protein Asp binds to and stabilises

microtubule minus ends and facilitates central spindle organisation and microtubule nucleation (do Carmo Avides et al., 2001; Wakefield et al., 2001). However the human orthologue, called ASPM, seems largely redundant in most tissues except in the brain (Bond et al., 2002).

By contrast, many plus end directed MAPs and motor proteins have been shown to be involved in the formation and maintenance of the central spindle. For example, the MAP Feo/PRC1/Ase1p is involved in cell division in every organism so far examined (Jiang et al., 1998; Loiodice et al., 2005; Schuyler et al., 2003; Vernì et al., 2004; Yamashita et al., 2005) and is able to bundle microtubules both in vitro and in vivo (Mollinari et al., 2002; Zhu and Jiang, 2005). PRC1 is localised to the central spindle midzone by the kinesin 4 motor protein Kif4 (Zhu and Jiang, 2005). Indeed many motor proteins, in addition to participating in spindle organisation, also concentrate key furrow components. The plus end directed motor protein Subito (Sub) in *Drosophila* and its mammalian orthologue MKLP2 not only contribute to central spindle assembly but also localise the Aurora B and Polo kinases to the equator (Cesario et al., 2006; Gruneberg et al., 2004; Neef et al., 2007; Neef et al., 2003). Here I will focus on an essential plus end directed motor protein, known in *Drosophila* as Pavarotti (Pav), which has received significant attention due to its role in the formation of the central spindle and the localisation of key cytokinesis factors.

1.6.4 Pavarotti - a plus end directed motor protein essential for cytokinesis

The *Drosophila* plus-end directed kinesin 6 motor protein, Pav, accumulates at the centrosomes and spindle midzone in anaphase, becomes restricted to the midbody at telophase and is sequestered within the nucleus during interphase (Adams et al., 1998). Disruption of Pav or its mammalian and *C. elegans* orthologues (MKLP1 and Zen-4 respectively), results in cytokinesis failure (Adams et al., 1998; Kuriyama et al., 2002; Raich et al., 1998). However, the point at which cytokinesis fails appears to differ somewhat among organisms. While *pav* mutants do not localise contractile ring components or induce furrowing, one cell *zen-4* mutant embryos can construct a contractile ring and exhibit cortical furrowing before regression occurs and cytokinesis fails (Adams et al., 1998; Raich et al., 1998; Zavortink et al., 2005). However, *zen-4* mutants do not show any signs of furrowing if other proteins required for spindle elongation are depleted (Dechant and Glotzer, 2003; Verbrugghe and White, 2007). Results from studies using mammalian cell lines concur with results observed in *Drosophila*, where little or no furrowing is detected upon MKLP1 depletion (Nishimura and Yonemura, 2006; Yüce et al., 2005). This may indicate that there are different furrowing mechanisms used in higher organisms.

The Pav protein consists of an N-terminal motor domain, a central neck linker, and a C-terminal tail containing a nuclear localisation signal (NLS) (Figure 1.5A). Mutant and truncated versions of MKLP1 have been used to demonstrate that the N-terminal motor domain is responsible for its localisation to the spindle

midzone (Matuliene and Kuriyama, 2002). The motor activity and microtubule binding ability of MKLP1 is negatively regulated during metaphase by Cyclin dependant kinase 1 (Cdk1) phosphorylation (Mishima et al., 2004). Preventing Cdk1 phosphorylation perturbs metaphase spindle assembly and results in chromosome segregation defects. Thus Cdk1 ensures that the anaphase spindle is assembled at the correct time. Furthermore, while Aurora B is not required to stimulate early MKLP1/Zen-4 functions such as spindle assembly and localisation, it is required for cytokinesis completion (Guse et al., 2005). This is partly due to Aurora B phosphorylating a NLS in MKLP1 and thereby preventing premature importation into the nucleus (Neef et al., 2006).

As mentioned above, Pav interacts with the RhoGAP Tum to form an evolutionarily conserved complex termed centralspindlin (Mishima et al., 2002; Somers and Saint, 2003). In *C. elegans*, disruption of either of the centralspindlin components, Zen-4 and Cyk-4, results in a disorganized spindle and cytokinesis failure (Jantsch-Plunger et al., 2000; Raich et al., 1998). Moreover, Zen-4 and Cyk-4 are interdependent for their proper localisation to the equator (Jantsch-Plunger et al., 2000). The Cyk-4 interacting region in Zen-4 was mapped to the neck linker region, C-terminal to the motor domain (Figure 1.5A) (Mishima et al., 2002). Further biochemical analysis revealed that centralspindlin can bundle microtubules in vitro and exists as a heterotetramer in vivo (Mishima et al., 2002). Although both Pav and Zen-4 can form dimers in the absence of Tum/Cyk-4, the motor and microtubule bundling functions of centralspindlin are not activated until a heterotetrameric complex is formed (Mishima et al., 2002; Pavicic-Kaltenbrunner et al., 2007; Sommi et al., 2010). Moreover, a distinct

Figure 1.5 Schematic structures of Pav, Tum and Pbl proteins

Schematic representations of the domains of the Pav (**A**), Tum (**B**) and Pbl (**C**) proteins. The regions identified to interact with various protein partners are indicated above or below each protein in coloured text.

A. Pav

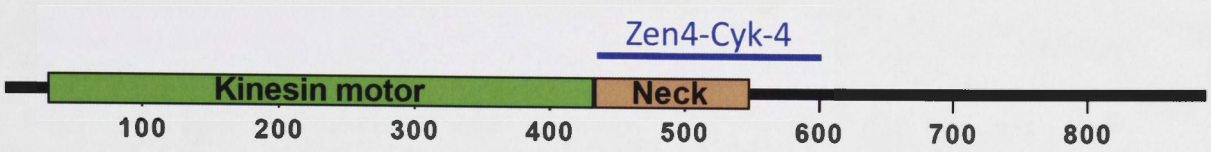

B. Tum

C. Pbl

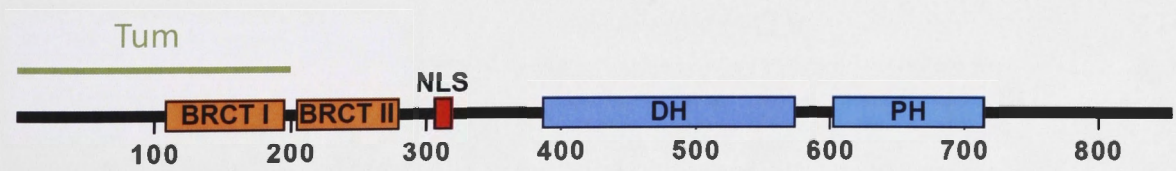

region of MKLP1 is important for clustering centralspindlin complexes together, which stimulates microtubule bundling, translocation and stable midzone accumulation (Hutterer et al., 2009). Furthermore, Aurora B promotes centralspindlin clustering by directly phosphorylating MKLP1 and preventing an inhibitory interaction with 14-3-3 (Douglas et al., 2010).

Not only does centralspindlin contribute to central spindle organization, but it also ensures the correct localisation of Tum. This is important, as Tum interacts with and controls the function of a number of key cytokinesis components.

1.7 Tum plays a central role in cytokinesis

The Drosophila gene *tum* (also known as *racGAP50C*) encodes a protein with an N-terminal coiled-coil domain, a central C1 phorbol ester/diacylglycerol binding motif followed by a C-terminal GAP domain (Figure 1.5B). The importance of Tum for central spindle and contractile ring assembly in *Drosophila* was first identified using RNAi in S2 cells (Somma et al., 2002). Disruption of the *C. elegans* and mammalian orthologues, Cyk-4 and HsCyk-4 (also known as MgcRacGAP) respectively, also perturbs central spindle assembly and prevents the completion of cytokinesis (Jantsch-Plunger et al., 2000; Mishima et al., 2002; Nishimura and Yonemura, 2006). Tum and its orthologues share a conserved localisation pattern during mitosis; they accumulate on the spindle during metaphase, localise to a discrete band around the equator at anaphase and become restricted to the midbody at telophase (Hirose et al., 2001; Jantsch-Plunger et al., 2000; Somers and Saint, 2003).

As mentioned previously, Tum interacts with Pav, resulting in its recruitment to the equator. Yeast two hybrid experiments identified the Pav binding region to be N-terminal to the coiled-coil domain (Somers and Saint, 2003). Several other interacting partners of Tum have also been identified. The interaction of Tum with Anillin acts as a link between the microtubule spindle and the contractile ring (D'avino et al., 2008; Gregory et al., 2008). Tum also interacts with the RhoGEF protein Pbl (Somers and Saint, 2003) and specifically disrupting this interaction prevents contractile ring assembly resulting in cytokinesis failure (Zavortink et al., 2005). This association also occurs between the mammalian orthologues Ect2 and HsCyk-4 and is proposed to contribute to activation of the RhoGEF (Kamijo et al., 2006; Nishimura and Yonemura, 2006; Zhao and Fang, 2005b). The Ect2-HsCyk-4 interaction was suggested to be phosphorylation dependent as phosphatase treatment of mitotic lysates significantly decreased the amount of HsCyk-4 detected in an Ect2 pull-down assay (Yüce et al., 2005). Indeed recent work has identified that Polo like kinase 1 (Plk1) activity induces the Ect2-HsCyk-4 interaction in vivo (see 1.9.1) (Burkard et al., 2007; Petronczki et al., 2007). Thus the Pbl-Tum interaction ensures equatorial accumulation of Pbl which in turn leads to Rho activation (see 1.8) and contractile ring formation. More recently, FRET and yeast two hybrid assays were used to demonstrate an interaction between Tum and Polo kinase during cytokinesis (Ebrahimi et al., 2010). In summary, Tum interacts with a number of proteins (Figure 1.5B) that mediate central spindle construction, induce contractile ring formation and promote its stabilization during furrow ingression.

Several studies have tried to identify whether the GAP domain contributes to cytokinesis regulation. Various mutations or deletions of the GAP domain have revealed that it is required for the completion of cytokinesis in *Drosophila*, *C. elegans* and mammals (Canman et al., 2008; Hirose et al., 2001; Miller and Bement, 2009; Zavortink et al., 2005). In vitro assays demonstrated that Cyk-4 and HsCyk-4 exhibit significantly more GAP activity towards Cdc42 and Rac than Rho (Jantsch-Plunger et al., 2000; Toure et al., 1998) and that this GAP activity was required for completion of cytokinesis through the inactivation of Rac (Canman et al., 2008). Similarly, genetic experiments in *Drosophila* indicated that Tum was also able to inhibit the activity of Rac (D'Avino et al., 2004). However, a role in Rho regulation late in cytokinesis cannot be excluded, as Aurora B phosphorylation of HsCyk-4 has been suggested to activate its GAP activity towards Rho (Minoshima et al., 2003). Cdk1 and the phosphatase PP2A have also been implicated in HsCyk-4 phosphoregulation (Touré et al., 2008), although the exact effect this has on the cytokinetic functions of Tum requires further clarification. Furthermore, a recent study in *Xenopus laevis* demonstrated that the expression of Cyk-4 GAP-dead or GAP-deleted versions in cells depleted of the endogenous protein led to a broadening of the active Rho zone at the equator (Miller and Bement, 2009). Thus the GAP activity of Tum and its orthologues appears to contribute to both Rac and Rho inactivation during cytokinesis. Perhaps phosphorylation events may alter GAP specificity at particular stages of cytokinesis. Therefore although Tum/HsCyk-4/Cyk-4 appear to regulate GTPase activity during cytokinesis, further work is required to confirm the targets and mechanism/s by which specificity is achieved.

1.8 Pebble is required for the construction of the contractile ring

The *Drosophila* gene *pbl* encodes a multi-domain RhoGEF consisting of two tandem N-terminal BRCT domains, a NLS signal, and tandem C-terminal Dbl homology (DH) and Pleckstrin homology (PH) domains (Figure 1.5C). Analysis of *pbl* mutant embryos revealed a failure of the first post-blastoderm cytokineses, which occur at cycle 14, resulting, in large multinucleate cells (Hime and Saint, 1992; Lehner, 1992) and a failure to form a contractile ring (Prokopenko et al., 1999). Genetic interactions and yeast two hybrid assays established Rho as the target of Pbl (Prokopenko et al., 1999). Moreover, in vitro GEF assays have confirmed that Pbl can activate Rho (van Impel et al., 2009). The *C. elegans* and mammalian Pbl orthologues, Let-21 and Ect2 respectively, have also been shown to be required for the completion of cytokinesis through the activation of Rho (Morita et al., 2005; Tatsumoto et al., 1999). Thus recruitment of a Rho activator appears to be a conserved mechanism by which cleavage is initiated. Apart from its ability to bind and activate GTPases, the only other known binding partner of Pbl is Tum. The N-terminus containing the first BRCT domain was identified by a yeast two hybrid assay as the region interacting with Tum (Figure 1.5C) (Somers and Saint, 2003). This interaction ensures Pbl accumulates at the equator of the cell and may contribute to GEF activation.

Many studies have focused on the mechanisms that regulate the activity of Ect2. These have revealed that the BRCT and DH/PH domains of Ect2 can associate and that this intra-molecular interaction inhibits GEF activity (Kim et al., 2005; Saito et al., 2004). Furthermore, Ect2 can oligomerise, which may

provide a further level of regulation (Kim et al., 2005) since oligomerisation is known to regulate the GEF activity of several Dbl family members including RasGRF, Dbl, Lsc, and p115RhoGEF (Anborgh et al., 1999; Chikumi et al., 2004; Eisenhaure et al., 2003; Zhu et al., 2001). Phosphoregulation of Pbl/Ect2 has also been demonstrated to regulate its interactions and activity. The kinase Cdk1 was first implicated as an important negative regulator of Pbl. It was shown that by prolonging the activity of Cdk1 by the expression of stable forms of cyclin B, the cytokinetic activities of Pbl were inhibited (Echard and O'Farrell, 2003). Furthermore, inhibiting Cdk1 activity at metaphase induced premature cytokinesis, in an Ect2 and HsCyk-4 dependent manner (Niiya et al., 2005). Subsequent studies attempted to provide molecular detail as to how Cdk1 regulated Pbl/Ect2. Phosphorylation of Ect2 at T341 was shown to relieve its intra-molecular inhibitory conformation, and activate its GEF activity (Hara et al., 2006). Furthermore, phosphorylation of the same residue inhibits Ect2-HsCyk-4 binding (Yüce et al., 2005). This finding was supported by results showing that phospho-Ect2 interacts weakly with HsCyk-4 in co-immunoprecipitation assays while unphosphorylated Ect2 interacts more strongly (Touré et al., 2008). Furthermore, the phosphatase PP2A has been suggested to relieve Cdk1 phosphorylations on Ect2 to enable it to interact with HsCyk-4 (Touré et al., 2008). Thus, during metaphase Cdk1 appears to prime Ect2 for its cytokinesis activities by inducing an open conformation, while at the same time preventing its premature association with HsCyk-4.

Cdk1 phosphorylation of Ect2 at a different residue (T412) appears to contribute to Rho activation (Niiya et al., 2006). In fact, early biochemical data

has shown that phosphorylation of Ect2 occurs in vitro, and is required for GEF activity (Tatsumoto et al., 1999). Furthermore, T412 phosphorylation is proposed to mediate an interaction between Ect2 and the Polo-like kinase 1 (Plk1) (Niiya et al., 2006). This may promote Plk1-dependent phosphorylation of Ect2, which has also been demonstrated to occur in vitro (Hara et al., 2006; Niiya et al., 2006; Wolfe et al., 2009). However, whether Plk1 phosphorylates Ect2 in vivo, and what function this may serve, is unknown.

From these data we can conclude that relieving the autoinhibitory conformation through phosphorylation appears to be one way in which GEF activity is stimulated. It is possible that other phosphorylation events, perhaps within the GEF domain itself, also modulate GEF function and/or specificity. Furthermore, it is possible that the Pbl-Tum interaction also contributes to GEF activation although this is yet to be demonstrated.

1.9 The role of kinases during cell division

As cells progress from one phase of mitosis to another, the activity and interactions of many proteins must be rapidly modified. Kinases play a central role in the progression of mitosis by stimulating or inhibiting interactions, activating specific functions of target proteins or inducing protein degradation. As outlined previously, Aurora B and Cdk1 are important for cytokinesis as they regulate the activities of Pav, Tum and Pbl.

Aurora B localisation and activation itself requires three regulatory proteins, INCENP, Survivin and Borealin/Dasra B that together constitute the

Chromosome Passenger Complex (CPC) (Adams et al., 2000; Cooke et al., 1987; Gassmann et al., 2004; Sampath et al., 2004; Terada et al., 1998; Uren et al., 2000; Wheatley et al., 2001). Aurora B is localised to the midzone at anaphase and is required for the completion of cytokinesis (Guse et al., 2005). It is also known to be essential for centralspindlin assembly and localisation (Kaitna et al., 2000; Mishima et al., 2002), for promoting the clustering of centralspindlin complexes (Douglas et al., 2010) and preventing the premature import of MKLP1 into the nucleus (Neef et al., 2006). Aurora B is also suggested to activate/switch the GAP activity of HsCyk-4 towards Rho late during cytokinesis (Minoshima et al., 2003), although this is disputed due to structural considerations (Mishima and Glotzer, 2003). Thus although the late mitotic roles of Aurora B are beginning to be uncovered, further investigation is warranted particularly with respect to its effect on Tum/HsCyk-4.

Cdk1 is arguably the most important kinase involved in cell division. Although compensatory mechanisms exist between different Cdks in mammals, it was recently shown that Cdk1 alone can drive the cell cycle (Santamaria et al., 2007). The activity of Cdk1 is modulated by the presence of regulatory cyclin subunits. Cyclin B is critical for Cdk1 activity during mitosis. In *Xenopus* egg extracts Cdk1 is activated once a threshold concentration of cyclin B is reached (Solomon et al., 1990). The level of cyclin B peaks prior to the onset of mitosis, leading to Cdk1 activation, and is quickly degraded at the onset of anaphase leading to inactivation of Cdk1. During the early stages of mitosis, Cdk1 inhibits the function and interactions of numerous proteins. One of the outcomes of Cdk1 activity is the inhibition of anaphase spindle formation, since cells that express

non-degradable cyclin B fail to form a spindle midzone (Wheatley et al., 1997). This is at least partly achieved by phosphorylating MKLP1 during metaphase (Mishima et al., 2004), which inhibits its motor activity and thereby prevents the untimely formation of the central spindle. Similarly, PRC1 recruitment to the midzone is inhibited by Cdk1 phosphorylation (Zhu et al., 2006). Cdk1 also prevents the premature association of cytokinesis binding partners such as PRC1-Plk1 (Neef et al., 2007) and Ect2-HsCyk-4 (Yüce et al., 2005). As cells transition from metaphase to anaphase, cyclin B is degraded and Cdk1 activity concomitantly falls. As a result, the inhibitory Cdk1 phosphorylations outlined above are lost enabling cytokinetic activities and interactions to occur. Therefore, Cdk1 plays a crucial role in regulating the initiation of cytokinesis.

1.9.1 Uncovering the cytokinetic role of Polo kinase

A role for Polo kinase in cell division was first discovered in *Drosophila*. (Sunkel and Glover, 1988) showed that mutations in *polo* caused centrosome and spindle defects in mitosis and meiosis. Polo kinase is now known to have numerous mitotic roles including the regulation of mitotic entry, chromosome segregation, centrosome maturation and bipolar spindle formation (Archambault and Glover, 2009). A cytokinetic role for Polo was suggested by its localisation, which mimicked that of many other cytokinesis components; i.e. midzone accumulation at anaphase before becoming restricted to the midbody at telophase (Logarinho and Sunkel, 1998). Equatorial localisation of Polo/Plk1 during anaphase has since been found to rely on interactions with several different motor proteins and MAPs including Sub/MKLP2 (Cesario et al., 2006; Neef et al., 2003), Pav/MKLP1 (Adams et al., 1998; Lee et al., 1995) and Feo/PRC1 (D'avino et al.,

2007; Neef et al., 2007). Perturbing any of these interactions disrupts Polo/Plk1 accumulation at the midzone. Furthermore, the recruitment of Polo appears to be largely mediated by the Polo-box domain (PBD), which constitutes a phosphopeptide-binding motif (Elia et al., 2003a; Elia et al., 2003b). For example, Plk1 phosphorylates PRC1 to create a PBD docking site for itself, which results in its recruitment to the equator (Neef et al., 2007). Furthermore, Plk1 may also interact with Ect2 and MKLP1 as the PBD of Plk1 can coimmunoprecipitate with Ect2 from mitotic lysates (Liu et al., 2004; Niiya et al., 2006).

The early mitotic roles of Polo hindered efforts to determine if it also contributed to cytokinesis. A role for Polo in contractile ring formation was first suggested by the use of a *polo* hypomorph in *Drosophila*, where defects in contractile ring formation were observed (Carmena et al., 1998). However, it was not until almost a decade later that tangible evidence for a cytokinetic function was established. Two separate studies employed different techniques to inhibit Plk1 kinase activity; one used a Plk1 specific inhibitor and the other an ATP analogue sensitive Plk1 mutant (Burkard et al., 2007; Petronczki et al., 2007). Mammalian cell lines were blocked at metaphase and the Plk1 specific inhibitor or ATP analogue added after the cells were released. Using these approaches, Plk1 inhibition was found to disrupt equatorial localisation of Ect2 but not HsCyk-4 or MKLP1. Thus Plk1 activity was proven to be crucial for the Ect2-HsCyk-4 interaction. However, describing the mechanism by which Plk1 induced the Ect2- HsCyk-4 interaction required further investigation.

1.10 Aims of this study

Although it is clear that Tum and Pbl play an essential role in spindle and contractile ring formation, the events regulating the Pbl-Tum interaction remain poorly characterised. The experimental work presented here was aimed at gaining further insight into the processes that dictate the interaction and function of both Pbl and Tum. The initial approach utilised protein over-expression and purification strategies in an effort to isolate significant amounts of pure Pbl and Tum for structural studies. Such structural data could be used to precisely define residues that interact with binding partners, mediate regulatory conformations or function as kinase targets. The subsequent chapter details attempts to identify, by site directed mutagenesis-mediated generation of specific mutant alleles, potential phosphorylation sites in Pbl, Tum and Pav that might alter their activities and/or interacting partners during cytokinesis.

Chapter Two - Materials and Methods

2.1 Materials

2.1.1 Chemicals

All reagents were of analytical grade, or the highest grade obtainable.

2.1.2 Antibiotics

Ampicillin: 100μg/ml working concentration (Sigma-Aldrich)

Chloramphenicol: 12.5μg/ml working concentration (Roche)

Tetracycline: 10μg/ml working concentration (Sigma-Aldrich)

Gentamicin: 7μg/ml working concentration (Sigma-Aldrich)

Kanamycin: 50μg/ml working concentration (Roche)

2.1.3 Enzymes

Restriction endonucleases: New England Biolabs

T4 DNA ligase: New England Biolabs

Pfu TURBO™ DNA polymerase: Stratagene

Taq polymerase: Promega, Roche, New England Biolabs

Proteinase K: Sigma-Aldrich

Ampligase thermostable DNA ligase: Epicentre Biotechnologies

2.1.4 Antibodies

Primary Antibodies:

anti-GFP (Rabbit): Invitrogen, Molecular Probes, used at 1/200 dilution on tissues

anti-α-tubulin (Mouse): Sigma-Aldrich, used at 1/100 dilution on tissues

anti-βGal – 40-1a (Mouse): Developmental Studies Hybridoma Bank, used at 1/100 dilution on tissues

anti-Myc (Rat): Abcam, used at 1/500 dilution in Western blots and 1/100 dilutions on tissues

anti-Pbl R9 (Rabbit): a gift from Hugo Bellen, used at 1:2000 in Western blots

anti-Pav (Rabbit): a gift from David Glover, used at 1:100 on tissues

anti-Anillin (Rabbit): a gift from Julie Brill used at 1:200 on tissues

anti-Tum (Rat): a gift from Greg Somers used at 1:100 on tissues

Secondary Antibodies:

Goat anti-mouse Alexa 488: Jackson ImmunoResearch Laboratories, used at 1/100 dilution on tissues

Goat anti-rabbit Alexa 488: Jackson ImmunoResearch Laboratories, used at 1/100 dilution on tissues

Goat anti-mouse Alexa 568: Jackson ImmunoResearch Laboratories, used at 1/100 dilution on tissues

Goat anti-mouse Cy5: Jackson ImmunoResearch Laboratories, used at 1/50 dilution on tissues

Goat anti-mouse AP: Jackson ImmunoResearch Laboratories, used at 1/500

dilution on tissues

Goat anti-mouse HRP: Jackson ImmunoResearch Laboratories, used at 1/2000 dilution on western blots

Goat anti-rabbit HRP: Jackson ImmunoResearch Laboratories, used at 1/2000 dilution on western blots

Goat anti-rat HRP: Jackson ImmunoResearch Laboratories, used at 1/2000 dilution on western blots

2.1.5 DNA and actin stains

To stain DNA, tissues were incubated in 1μg/ml Hoechst 33258 (Sigma-Aldrich) in PBST for 10 minutes and then washed three times in PBST before mounting on slides. To stain filamentous actin, tissues were incubated in 80μm rhodamine phalloidin (Molecular Probes) in PBST for three hours.

2.1.6 Genotype of *E. coli* bacterial strains

DH5α: F- f80, *lacZ*ΔM15, *rec*A1, *end*A1, *gyr*A96, *thi*-1, *hsd*R17, (r_K-, M_K+), *sup*E44, *rel*A1, *deo*R, Δ(*lacZ*YA-*argF*) U169

DH10B: F- *mcrA Δ(mrr-hsdRMS-mcrBC) ΔlacX74 deoR endA1 araD139 Δ(ara, leu) 7697 rpsL recA1 nupG φ80dlacZΔM15 galU galK*

DH10Bac: F- *mcrA Δ(mrr-hsdRMS-mcrBC) ϕ80lacZΔM15 ΔlacX74 recA1 endA1 araD139 Δ(ara,leu)7697 galU galK λ- rpsL nupG/bMON14272/pMON7124*

SW102: F- *mcrA Δ(mrr-hsdRMS-mcrBC) ΔlacX74 deoR endA1 araD139 Δ(ara, leu) 7697 rpsL recA1 nupG φ80dlacZΔM15 galU galK [λc1857 (cro-bioA)<>Tet] ΔgalK gal490*

EPI300: F- *mcrA Δ(mmr-hsdRMS-mcrBC) ϕ80dlacZΔM15 ΔlacX74 recA1 endA1 araD139 Δ(ara, leu)7697 galU galK λ-rpsL nupG trfA dhfr*

2.1.7 BACs and cosmids

pbl: Cosmid cos34 (a gift from G. Hime)

pav: BAC 39011 (BACPAC Resources)

tum: BAC 6M19 (BACPAC Resources)

2.1.8 Insect cell lines

Generation and amplification of baculoviral stocks: *Spodoptera frugiperda* Sf9 cells (Invitrogen)

Protein over-expression: *Trichoplusia ni* High Five cells (BTI-TN-5B1-4) (Invitrogen)

2.1.9 Molecular weight markers

1kb DNA ladder: New England Biolabs

Prestained molecular weight protein marker (Broad range 6-175kDa): New England Biolabs

2.1.10 Kits

QIAquick Gel Extraction Kit (Qiagen)

QIAprep Spin Miniprep Kit (Qiagen)

QIAfilter Plasmid Midi Kit (Qiagen)

QuikChange Site-Directed Mutagenesis kit (Stratagene)

2.1.11 Oligonucleotides

Oligonucleotide primers were obtained from Geneworks: Thebarton, SA or Invitrogen: Mount Waverley, VIC.

Construction of P[acman] vectors	
Pbl LAF	catgctcgagggcgcgccgcactctccaccaccttcagc
Pbl LAR	gcctactcaagcaaaatcgttgagggatcccgcttgataacaacgagttgaccg
Pbl RAF	cggtcaactcgttgttatcaagcgggatccctcaacgattttgcttgagtaggc
Pbl RAR	gctctagagcggccgcctattacagcggtttggactgcc
PblLAGFP	ccactttcggtgcaacccacgcggaaaaacaaggccgttgtgggccgcattatgagtaaag gagaagaacttttcactgg
PblRAGFP	caaaatggaatacacaatttgactgtggagtcatcatcatcatcagctctatttgtatagttc atccatgccatgtg
PblLAGalK	ccactttcggtgcaacccacgcggaaaaacaaggccgttgtgggccgcattcctgttgaca attaatcatcggca
PblRAGalK	caaaatggaatacacaatttgactgtggagtcatcatcatcatcagctctatcagcactgtcc tgctccttgtg
Tum LAF	catgctcgagggcgcgccccgtcctcctcatatcgcagc
Tum LAR	cgtgctttagtttataatcgaacgcatggatcctgtctgtccactcacccaatcc
Tum RAF	ggattgggtgagtggacagacaggatccatgcgttcgattataaactaaagcacg
Tum RAR	gctctagagcggccgcagcaaatggtgacggctaagg
TumLA5xmyc	attaagaagcggaagttttacggcacaccgccggcatctgcgcacaagaaaatggagcaa aagctcatttgtgaag
TumRA5xmyc	agtaaacttaagtaacacgtcaaatgctttccaacaaggaaagtctcgttaagtcaggtcgc

	ccaaggtctc
TumLAGalK	attaagaagcggaagttttacggcacaccgccggcatctgcgcacaagaaacctgttgaca attaatcatcggca
TumRAGalK	agtaaacttaagtaacacgtcaaatgctttccaacaaggaaagtctcgttatcagcactgtc ctgctccttgtg
TumLA4myctag	attaagaagcggaagttttacggcacaccgccggcatctgcgcacaagaaa
TumRA4myctag	agtaaacttaagtaacacgtcaaatgctttccaacaaggaaagtctcgtta
Pav LAF	catgctcgagggcgcgcccggtaagtgctggtcaattaattgg
Pav LAR	gtcgtgtgaacctgagagagcggatcccattagtgccggtccgttcc
Pav RAF	ggaacggaccggcactaatgggatccgctctctcaggttcacacgac
Pav RAR	gctctagagcggccgcgcgttgtgtggcggattagg
Amplification of *pbl*, *tum* and *pav* regions for mutagenesis	
PblphosflankF1	cagccgttgagcgcaattc
PblphosflankR1	cgcctcagttgttgttgttgttc
Pblmutflank5R1	gaattgcgctcaacggctgcgcgtcggaatcacaaatca
Pblmutflank3R1	cctttcttttttactctcacaacagttagggcgcctcagttgttgttgttgttc
Pblmut5F1	tgatttgtgattccgacgcg
Pblmut3R1	cctttcttttttactctcacaacagttaggg
TumphosflankF	cgagtgaaaaccgattcgtagaactac
TumphosflankR	ctcatcagtggacggtgctgc
Tummutflank5R	gtagttctacgaatcggttttcactcgcagggactgcctgcacactg
Tummutflank3R	atgtcttctgactgaaggtgtggttcctcatcagtggacggtgctgc
Tummut5F	cagtgtgcaggcagtccctg
Tummut3R	atgtcttctgactgaaggtgtggttc
PavphosflankF	tatttttctgacaacaatgtactctggtcc
PavphosflankR	tgtccctcaatgccgagattg
Pavmutflank5R	ggaccagagtacattgttgtcagaaaaatagtttaccatattctcatcatagtcctcaattc
Pavmutflank3R	ttagattttcgacttcttgctgctgtgtccctcaatgccgagattg
Pavmut5F	gaattgaggactatgatgagaatatggtaaac
Pavmut3R	ttagattttcgacttcttgctgctg
***galk* primers for insertion of *pbl*, *pav* and *tum* mutated sequences**	
PblGalKF1	cagccgttgagcgcaattcgcttacattgttgatcattttgttggttaaatcctgttgacaatta

	atcatcggca
PblGalKF2	gaaacattcataaatcacaaatattttaaataagcggaaaaatactgtattcctgttgacaat taatcatcggca
PblGalKF3	cgagatgaaacagacactgggccagaactcgcggcccatttacaattacgccctgttgaca attaatcatcggca
PblGalKR1	cgcctcagttgttgttgttcttgctgtcggtacagtgtcgccgaagagtcagcactgtcct gctccttgtg
PblGalKR2	ggctcttggagcgaagataggtagtatactcgtgcgtgtgtctcgatttcaatcagcactgtc ctgctccttgtg
PblGalKR3	ccgtattgggcatcacctggaagacacacgtattaggattttgtgggtaagtcagcactgtc ctgctccttgtg
TumGalKF	cgagtgaaaaccgattcgtagaactaccgagacaagcaaaaatggcgctctccgcacctgt tgacaattaatcatcggca
TumGalKR	ctcatcagtggacggtgctgcagtggcgttccggattcagcgacaacgtgaggtcagcact gtcctgctccttgtg
PavGalKF	tatttttctgacaacaatgtactctggtccctaaaatttatttatcccgtttagcacctgttgac aattaatcatcggca
PavGalKR	tgtccctcaatgccgagattgcagcgggaggctacgtcctgggctgaggtgacctcagcac tgtcctgctccttgtg
Primers for mutagenesis	
PblPoloAA5+10F	gaagatccatggaaatggaggccattgaagagcaagcgaagtgcggtgagtactgaaag
PblPoloAA5+10R	ctttcagtactcaccgcacttcgcttgctcttcaatggcctccatttccatggatcttc
PblPoloAA51F	ctgcccatcgttacgtcggacgccggtctggacattctcggagag
PblPoloAA51R	ctctccgagaatgtccagaccggcgtccgacgtaacgatgggcag
PblPoloAA75F	cgagggtgccgccttcgaggcgatac
PblPoloAA75R	gtatcgcctcgaaggcggcaccctcg
PblPoloAA190+196F	ccgcttgggcggatcgtaatgcgctggagttcgatgccgcgcaagagaatttcaccaagac
PblPoloAA190+196R	gtcttggtgaaattctcttgcgcggcatcgaactccagcgcattacgatccgcccaagcgg
TumProAA23F	atgcaagtgcttaccgatggagctcctgaggagggtgagtaaaactg
TumProAA23R	cagttttactcaccctcctcaggagctccatcggtaagcacttgcat
TumPoloAA59F	gatacaaaacgagctggacaaggccttgaccaaaatgggcgacctg
TumPoloAA59R	caggtcgcccattttggtcaaggccttgtccagctcgttttgtatc

TumPoloAA142F	gaatgccgtgcgggaggacaaggcatatggcgacatcaactccacc
TumPoloAA142R	ggtggagttgatgtcgccatatgccttgtcctcccgcacggcattc
TumPoloAA157F	ggatcgttgctgtcggatttggccattacacactccgaggacgac
TumPoloAA157R	gtcgtcctcggagtgtgtaatggccaaatccgacagcaacgatcc
TumProAA208F	gaatggcagtatgtccgggactgcaccaaccactggcaaatcgcgg
TumProAA208R	ccgcgatttgccagtggttggtgcagtcccggacatactgccattc
TumPoloAA258F	ggcgtgattcgtgcagagtcggccattgagtcgctgcctgtaattg
TumPoloAA258R	caattacaggcagcgactcaatggccgactctgcacgaatcacgcc
TumProAA278F	gatcggcgacggactatcctcggcgccacggcgatcggtgcttaaag
TumProAA278R	ctttaagcaccgatcgccgtggcgccgaggatagtccgtcgccgatc
TumPoloAA288F	cgatcggtgcttaaagaggccgcggcaccgccgctgacgccggtaaatg
TumPoloAA288R	catttaccggcgtcagcggcggtgccgcggcctctttaagcaccgatcg
TumProAA293F	gaggccaccgcaccgccgctggcgccggtaaatgctatggcacctc
TumProAA293R	gaggtgccatagcatttaccggcgccagcggcggtgcggtggcctc
TumProAA308F	cacgttgtcgctgaatccggagctccactgcagcaccgtccactg
TumProAA308R	cagtggacggtgctgcagtggagctccggattcagcgacaacgtg
PavPoloAA449F	gtgatgaagttcgccgagatggcccaggaggtgcaaattgctcgg
PavPoloAA449R	ccgagcaatttgcacctcctgggccatctcggcgaacttcatcac
PavProAA458+467F	gctcgggcggcgcctatgaagcaagatttgggtctggcgcccggccgtcg
PavProAA458+467R	cgacggccgggcgccagacccaaatcttgcttcataggcgccgcccgagc
PavProAA516F	gattttcccgcctacgaaatggacgctcccgaggcacagatcaaaatc
PavProAA516R	gattttgatctgtgcctcgggagcgtccatttcgtaggcgggaaaatc
PavPoloAA583+595F	gtttacaagcaggagcgcgatcgcgccgcggcactcgagaagaaggttcgcatccacgag gcctccattgacgtgcttaacaatac
PavPoloAA583+595R	gtattgttaagcacgtcaatggaggcctcgtggatgcgaaccttcttctcgagtgccgcggc gcgatcgcgctcctgcttgtaaac
PavPoloAA615F	gaacggcagattgaagagctggctttcaagctgaacgagaaggag
PavPoloAA615R	ctccttctcgttcagcttgaaagccagctcttcaatctgccgttc
PavProAA728F	ctacacgaacagatatatatgcagcgccacgtcatgtaagtgtatgattaatc
PavProAA728R	gattaatcatacacttacatgacgtggcgctgcatatatatctgttcgtgtag
PavProAA836+840F	gtggagtgcctcaagcagaaggcgccggttcacgcgcccacgcgaaagcgacccagc
PavProAA836+840R	gctgggtcgctttcgcgtgggcgcgtgaaccggcgccttctgcttgaggcactccac

Primers to clone *tum* into pTriExMBPSfiI	
TumSfiIFwd	ataggccattatggccttatggcgctctccgcattggc
TumSfiIRev	ataggccgaggcggcctttcttgtgcgctgatgccggcgg
Primers to clone *tum* and *MBPtum* into pFastBacDual	
TumXhofwd	tctcgagatggcgctctccgcattggcg
TumHisKpnR	taggtaccttaatggtgatgatggtgatg
MBPTumF	tctcgagatggaaataaaaacaggtgc
MBPTumR	taggtaccttagtgatggtgatggtgatggtggtg
Primers to clone *pbl*^{fl} into bacPAK8 and pFastBacDual	
PblBamfwd	aggatccatggaaatggagaccattgaag
Pblecorev2	cgaattcttaatggtgatgatggtgatgtccgccaatgcggcccacaacggcc
Primers to clone *pbl*$^{N\text{-}term}$ and *pbl*$^{C\text{-}term}$ into pFastBac HT A	
PblNtermF	atggatccatggaaatggagaccattgaagagc
PblNtermR	atctcgagctaagacaatagaccggcatccg
PblCtermF	atggatccgtctcaaatagtttattcgattgtaccacc
PblCtermR	atctcgagctaaatgcggcccacaacg
Primers to sequence *pbl, tum and MBPtum*	
3Pbl4	cactccggatcatcgagc
5Pbl5	gcctgaaggcattcgagg
5Pbl9	gctgttgcatgccgagcc
5Pbl10	tgacactgcacatcaacg
5Pbl11	aatgtcagcacgctcagc
RacGapSph	gaccagcatgcgatctacacgg
RGDOWN1	acgaattgcccagtgcccag
RG1445-68	ccaaaacagcccaggatatgttgg
RGPstup	gccactgcagcaccgtccactg
RG21up	tcggaattcaccatgctggagggcaaactc
RacGAPCUT3endBam-5'	cgggatcccctcgatgtgcgcacatcaaaatc
RGDAGBam-5'	cgggatccttgtgccaccaccaaggtcaccatac
RGR84AR	cgtgttccgcctggcgggccgccttgatctccatgtcg
RacGAPXba5'	cgtgttccgcctggcgggccgccttgatctccatgtcg
MBPTumF	tctcgagatggaaataaaaacaggtgc

MBPTumR	taggtaccttagtgatggtgatggtgatggtggtg
General sequencing primers	
M13F	gttttcccagtcacgac
M13R	cacaggaaacagctatgac

2.1.12 Media

2.1.12.1 *Drosophila* Media

Harvard fly food:

47.4g Agar, 165g Torula yeast and 312g maize meal was dissolved in 1.3 liters of water, and added to 3.3 liters of boiled water, stirred and combined with 660g glucose. The mixture was boiled, before being allowed to cool to 80°C. 54ml Tegosept was added.

Apple juice agar plates:

2% agar, 25% apple juice, 1.25% sucrose.

2.1.12.2 Bacterial media

All media was prepared with distilled and deionised water and sterilized by autoclaving. Heat labile reagents were filter sterilized through 0.22µm filters. Antibiotics were added from filter sterilized stock solutions to the media after it had been autoclaved. For both liquid and solid media cultures the following antibiotic concentrations were used: Ampicillin, 100µg/ml; Chloramphenicol, 12.5µg/ml; and Tetracycline, 10µg/ml.

Liquid media:

Luria-Bertani (LB) broth: 1% (w/v) tryptone, 0.5% yeast extract, 1% NaCl, pH 7.0.

SOC: 2% bactotryptone, 0.5% yeast extract, 10mM NaCl, 2.5mM KCl, 10mM $MgCl_2$, 10mM $MgSO_4$, 20mM glucose (glucose filter sterilized and added after autoclaving).

Solid Media:

Plates: LB with 1.5% (w/v) agar were supplemented with antibiotics where appropriate.

Gal+ selection: M63 + 1.5%(w/v) bacto-agar, 0.2% D-galactose, 1mg/l D-biotin, 45mg/l L-leucine, 12.5µg/ml chloramphenicol.

Gal- selection: M63 + 1.5%(w/v) bacto-agar, 0.2% D-glycerol, 1mg/l D-biotin, 45mg/l L-leucine, 0.2% 2-deoxy-galactose (DOG), 12.5µg/ml chloramphenicol.

Gal indicator plates: 1.5% MacConkey agar, 0.2% D-galactose, 12.5µg/ml chloramphenicol.

2.1.12.3 Insect cell media

Sf9 cell media: Grace's insect cell media, supplemented (1x) (Invitrogen). Supplemented with 10% FBS.

High Five cell media: EX-CELL 405 Serum-Free Medium for Insect cells (Sigma-Aldrich). Supplemented with 10% FBS.

2.1.13 Buffers and Solutions

Agarose gel loading buffer: 2.5ml glycerol, 2.0ml 50X TAE, 0.025g bromophenol (10X) blue (Sigma-Aldrich), 0.025g xylene cyanol (Sigma-Aldrich), 5.5ml H_2O.

AP staining buffer: 100mM Tris-HCl (pH 9.0), 100mM NaCl, 50mM $MgCl_2$, 0.1% Tween-20, 8.24ml MilliQ H_2O.

BCIP: 50mg/ml in 100% dimethylformamide (DMF).

Coomassie Blue R-250 (Biomatik).

dNTPs (mix): 10mM solution (New England Biolabs).

ECL Solution A: 5ml 100mM Tris-HCl (pH 8.5), 22µl 90mM para-coumaric acid, 50µl 250mM luminol.

ECL Solution B: 5ml 100mM Tris-HCl (pH 8.5), 3µl hydrogen peroxide.

Elution Buffer: 50mM NaH_2PO_4, 300mM NaCl, 250mM imidazole, pH 8.

Embryo injecting buffer: 5mM KCl, 0.1mM $NaPO_4$ pH 6.8.

Fetal Bovine Serum (FBS) (Invitrogen), heat inactivated.

IPTG: 0.5M in MilliQ H_2O.

PBS: 7.5mM Na_2HPO_4, 2.5mM NaH_2PO_4, 145mM NaCl.

PBST: 1 x PBS, 0.1% Tween 20.

Phenol/chloroform: 50% phenol, 48% chloroform, 2% isoamyl alcohol (stored under TE in the dark).

Protein gel running buffer: 1.5% Tris Base, 7.2% Glycine, 0.5% SDS.

Protein sample buffer (3X): 3% SDS, 30% glycerol, 0.15 M Tris-HCl (pH 6.8), 3% β-mercaptoethanol added fresh. Bromophenol Blue added to color.

Protein gel stain solution: 10% acetic acid, 1:1 v/v (methanol:MilliQ H_2O), 0.25%

Protein gel destain solution: 10% acetic acid, 1:1 v/v (methanol:MilliQ H_2O).

Proteinase K: 10mg/ml in MilliQ H_2O.

Lysis Buffer: 50mM NaH_2PO_4, 300mM NaCl, 10mM imidazole, 1% Igepal CA-360, pH 8. All protease inhibitors added fresh from 100x stock solutions except for EDTA, which was added immediately after His tag purification.

M63 media: 2g $(NH_4)_2SO_4$, 13.6g KH_2PO_4, 0.5mg $FeSO_4.7H2O$, adjust pH to 7 with KOH.

M9 washing solution: 6g Na_2HPO_4, 3g KH_2PO_4, 1g NH_4Cl and 0.5g NaCl.

MMR buffer: 20mM Tris-HCl [pH 8.5], 3mM $MgCl_2$, 50 mMKCl, 0.4 mg/ml bovine serum albumin, and 0.5mM NAD^+.

NBT: 50mg/ml in 70% DMF.

Squishing Buffer: 10mM Tris-Cl pH 8.2, 1mM EDTA, 25mM NaCl, 200μg/ml Proteinase K.

TAE: 40mM Tris-acetate, 20mM sodium acetate, 1mM EDTA, pH 8.2.

TE: 10mM Tris-HCl pH 7.4, 1mM EDTA.

Tegosept (fungal inhibitor): 23.8g p-Hydroxy-benzoic acid methyl ester dissolved in 91.8ml ethanol.

Wash Buffer: 50mM NaH_2PO_4, 300mM NaCl, 10mM imidazole, pH 8.

Western Blot transfer buffer: 50mM Tris, 0.3% glycine, 0.04% SDS, 20% methanol.

X-gal: 40μg/μl in DMF.

2.1.14 Protease inhibitors

trans-epoxysuccinyl-L-leucylamido-(4-guanidino)butane (E-64): 100x stock made up in MilliQ H_2O, used at a final concentration of 10μM in buffers (Sigma-Aldrich).

Ethylenediaminetetraacetic acid (EDTA): 100x stock made up in MilliQ H_2O, final concentration of 2μM used in buffers (Sigma-Aldrich).

4-(2-Aminoethyl) benzenesulfonyl fluoride hydrochloride (AEBSF): 100x stock made up in MilliQ H_2O, final concentration of 2μM used in buffers (Sigma-Aldrich).

Pepstatin A: 100x stock made up in methanol, final concentration of 10μM used in buffers (Sigma-Aldrich).

2.1.15 *D. melanogaster* strains

Wild-type

A w^{1118} strain that had recently been isogenised for chromosomes 2 and 3 was used as the wild-type control for phenotypic analysis.

ΦC31 stocks

A fly strain of the genotype *y¹ M{vas-int.Dm}ZH-2A w*; PBac{y⁺-attP-3B}VK00037* was used to generate transgenic lines containing *tum-myc* constructs. Here, the constructs were inserted at the cytogenetic position 22A on the 2nd chromosome. A fly strain of the genotype *y¹ w^67c23 ; ; P{y⁺t7.7=CaryP}attP154* was crossed to a fly strain of the genotype *y¹ M{3xP3-RFP.attP}ZH-2A w*; M{vas-int.Dm}ZH-102D* and the progeny used to generate transgenic lines containing *pav* or *pbl-GFP* constructs (see Figure 2.1B).

Deficiency stocks

The deficiency stocks *w^1118; Df(3L)Exel9000/TM6B, Tb¹, w^1118; Df(3L)BSC370/TM6C, Sb¹ cu¹, w^1118 ; Df(3L)Exel8098/TM6B, Tb¹, w^1118 ; Df(2R)Exel7128/CyO* and *w^1118; Df(2R)BSC383/CyO* were acquired from the Bloomington stock center.

pbl alleles

The *pbl²* and *pbl³* alleles corresponding to nonsense mutations that result in truncated protein products of 37 and 185 amino acids respectively were used in this study (Prokopenko et al., 1999).

tum alleles

The *tum^AR2* allele, corresponding to a nonsense mutation that produces a truncated protein of 470 amino acids (Jones and Bejsovec, 2005), was used in this study.

pav alleles

The pav^{B200} and pav^{963} allele, the exact mutations of which have not been molecularly defined, were used in this study (Collins and Cohen, 2005; Salzberg et al., 1994).

2.1.16 Protein purification equipment

2.1.16.1 Cell lysate syringe filters

Acrodisc PSF syringe filter with GxF prefilter / 0.45um Supor membrane (Pall life sciences)

2.1.16.2 Protein concentrating devices

Amicon Ultra 30K and 100K NMWL centrifugal filter devices (Millipore)

2.1.16.3 Protein Purification columns

HiTrap Desalting, 5ml- GE Healthcare

HiTrap Q FF (strong anion exchanger), 1ml - GE Healthcare

HisTrap HP, 1ml - GE Healthcare

Ni-NTA Superflow cartridge, 5ml - Qiagen

HiPrep 16/60 Sephacryl S-300 HR, 120ml - GE Healthcare

Superdex 200 10/300 GL - GE Healthcare

2.1.17 Crystallization trial screening kits

Hampton Crystal Screen (Hampton Research)

Hampton Crystal Screen 2 (Hampton Research)

Hampton Index HT (Hampton Research)

2.2 Methods

Standard molecular genetic techniques were performed as described in (Ausubel, 1994) or (Sambrook, 1989).

2.2.1 PCR amplification of DNA

2.2.1.1 PCR for cloning

Pfu Turbo DNA polymerase (Stratagene) was used in all of the reactions to produce products for cloning according to the manufacturers instructions. PCR conditions were using 0.5U Pfu polymerase, 10pg - 1ng template DNA, 0.2mM primers and 0.2mM dNTPs in Pfu PCR buffer (20mM Tris-HCl (pH 8.8), 10mM KCl, 10mM $(NH_4)_2SO_4$, 2mM $MgSO_4$, 0.1% Triton X-100, 0.1 mg/ml BSA). Reactions were performed using a MJ Research, PTC-200 peltier, thermal cycler, or a Corbett Research Palm Cycler with the following conditions: Initial denaturation of 95°C for 5 minutes followed by 35 cycles of 95°C for 30 sec, 55°C for 30 second and 72°C for 1 minute per kb of product.

2.2.1.2 Diagnostic PCR

PCR reactions to generate products that were not subsequently cloned were performed with *Taq* polymerase according to the manufacturers instructions. PCR conditions were: 0.5U *Taq* polymerase, 1µl template DNA, 0.2mM primers and 0.2mM dNTPs in 1X *Taq* PCR buffer (20mM Tris-HCl (pH 8.8), 10mM KCl, 10mM $(NH_4)_2SO_4$, 2mM $MgSO_4$, 0.1% Triton X-100, 0.1 mg/ml BSA). Reactions

were performed using a MJ Research, PTC-200 peltier, thermal cycler, or a Corbett Research Palm Cycler with the following conditions: initial denaturation of 95°C for 5 minutes followed by 35 cycles of 95°C for 30 sec, 55°C for 30 second and 72°C for 1 minute per kb of product. For PCRs involving allele-specific oligonucleotides, the annealing temperature was increased to 60°C.

2.2.2 A-tailing of PCR products for cloning into pGEM-T vector

Following PCR with a high fidelity proofreading polymerase, the product was column purified using a QIAquick Gel Extraction Kit (Qiagen) and 200ng was incubated with 0.2mM dATP and 0.2U Taq polymerase in 1X PCR buffer at 72°C for 30 minutes. 2µl of this product was then used directly for cloning into pGEM-T (Promega).

2.2.3 Automated sequencing

DNA was sequenced using the BigDye Terminator v3.1 Cycle Sequencing Kit (Applied Biosystems), as described in the manufacturer's protocol with the modification of using an eighth of the described amount of the reaction mix. Here, double-stranded DNA was used as a template and, in general, primers were de-salted. Temperature cycling was: 25 cycles of 96°C for 10 seconds, 50°C for 5 seconds and 60°C for 4 minutes with a temperature ramp setting of 2. Running and analysis of the BigDye Terminator reactions was conducted by the Australian Genome Research Facility (Brisbane, Australia).

2.2.4 Multiple site-directed mutagenesis strategy

Multiple site-directed mutagenesis PCR reactions were carried out according to (Hames et al., 2005). Briefly, mutagenesis reactions were performed with 2.5 units *Pfu Turbo* DNA polymerase, 15 units of Ampligase (Epicentre), with 10 picomoles of each primer, 100ng template DNA, 0.5mM dNTPs in MMR buffer in a total volume of 50µl. The PCR conditions were; initial DNA denaturation for 5 min at 95°C followed by 35 cycles of denaturation at 95°C for 30 sec, primer annealing at 57°C for 30 sec, and elongation at 65°C for 6 min. The PCR products were then A-tailed, ligated into pGEM-T (Promega) and the presence of the mutations verified by sequence analysis. If one or two mutations were not incorporated a single site-directed mutagenesis approach was taken.

2.2.5 Single Site-directed mutagenesis

Site-directed mutagenesis to incorporate a single change was carried out as detailed in Stratagene's QuikChange Site-Directed Mutagenesis manual. Briefly, reaction conditions were 1X supplied *Pfu TURBO* reaction buffer, 50ng template plasmid, 125ng each of the forward and reverse mutagenesis primers, 0.5mM dNTPs and 2.5U of *Pfu TURBO* polymerase in a total volume of 50µl. The reaction was cycled according to the manufacturers instructions in a MJ Research, PTC-200 peltier, thermal cycler. Parental DNA was digested with *DpnI*, which specifically cleaves methylated (non-mutagenised) DNA. 1µl of the reaction was then transformed into chemically competent *DH5α*. The presence of the introduced mutation was confirmed by sequence analysis.

2.2.6 Restriction endonuclease digestion of DNA

Restriction digestions were performed using the buffers recommended by the manufacturer at a 1X concentration. For complete digestion, 3-5 units of enzyme were added per μg of DNA and incubated at 37°C for 3 hours.

2.2.7 Purification of DNA from agarose gels

Agarose gels were stained with ethidium bromide and bands were viewed and excised from the gel under illumination by long wave ultra-violet light to minimize damage to the DNA. The QIAquick gel extraction kit was used to purify DNA bands from agarose gels. The procedure was as per the manufacturers protocol, except MilliQ water heated to 65°C was substituted for the elution step rather than the supplied elution buffer.

2.2.8 Ligation of DNA fragments

DNA fragments to be ligated were placed in a mix (total volume 20μl) containing 1U of T4 DNA ligase, and 1X ligation buffer and incubated at room temperature overnight. Usually, a molar ratio of between 3:1 and 6:1 insert : vector was used. For transformation by electroporation, the ligation was phenol/chloroform extracted, precipitated by adding 1μl glycogen, 1/10 volume 3M Sodium Acetate pH 5.2 and 2.5 volumes ethanol, then washed in 70% ethanol prior to resuspension in 5-7μl MilliQ water.

2.2.9 Preparation of electrocompetent cells

500ml of L-broth was inoculated with 5ml of an overnight culture of *E. coli DH5α*,

DH10B, DH10Bac, SW102 or *EPI300* cells and grown to an OD_{A600} of 0.4-0.5. The culture was then chilled on ice for 15 to 30 minutes and the cells harvested by centrifugation at 3000g for 15 minutes. The cells were then resuspended in 500ml of ice-cold MilliQ H2O, pelleted at 4 000g, resuspended in 250ml of ice-cold MilliQ H2O, pelleted at 5000g, resuspended in 10ml of ice-cold 10% glycerol, re-pelleted at 3000g and finally resuspended in 1ml of ice-cold 10% glycerol. The cells were then snap frozen as 45ml aliquots by pipetting into a microcentrifuge tube sitting in liquid nitrogen. These aliquots were stored at -80°C.

2.2.10 Transformation of bacteria

To transform electrocompetent bacteria with DNA, bacterial cells were thawed on ice. 1-10ng of the DNA to be transformed was added to the cells, mixed and incubated on ice for 5 minutes. Cells and DNA were transferred to ice-cold 2mm electroporation cuvettes and electroporated in a Bio-Rad *E. coli* Pulser set to 2.5 kV and 25μF capacitance. The cuvette was immediately washed out with 1ml of room temperature SOC, and the suspension incubated at 37°C for 40 minutes. Cells were pelleted for 5 minutes at 3000rpm, then 800μl of the supernatant was removed, and the cells gently resuspended in the remaining 200μl SOC. The cell suspension was plated onto LB-agar plates supplemented with appropriate antibiotics and incubated at 37°C overnight. If selection for β-Galactosidase activity (blue/white color selection) was required, 20μl of 0.5M IPTG and 40μl of 40μg/μl X-GAL were spread onto LB agar plates along with the bacterial suspension.

2.2.11 Constructs generated

2.2.11.1 Generation of baculovirus over-expression constructs

pBacPAK8 pbl^{fl} construct

The entire CDS of pbl was PCR amplified from pUAS::pbl-GFP (Somers and Saint, 2003) and cloned into pBacPAK8 (Clontech) using BamHI (5') and EcoRI (3') restriction sites. The 3' primer incorporated a 6xHis tag sequence at the end of the *pbl* coding sequence. The absence of PCR induced mutations within the sequence was verified by sequence analysis.

pFastBac HT A $pbl^{N\text{-}term}$ and $pbl^{C\text{-}term}$ constructs

The first 906 and last 1698 nucleotides of pbl were amplified off pUAS::pbl-GFP and cloned into pFastBac HT B (Invitrogen) using BamHI (5') and XhoI (3') restriction sites for the $pbl^{N\text{-}term}$ and $pbl^{C\text{-}term}$ pFastBac HT B constructs respectively. Cloning into the pFastBac HT B construct resulted in a fusion proteins containing an N-terminal 6xHis tag. The absence of PCR induced mutations within the sequences was verified by sequence analysis.

pFastBacDual tum and MBPtum constructs

To create a construct that would over-express *tum*, the CDS of *tum* was amplified off pVP16 RG#28 (Somers and Saint, 2003) and cloned into pFastBacDual (Invitrogen) using the XhoI (5') and KpnI (3') restriction sites. To create a construct that would over-express an MBPTum fusion protein, the CDS of *tum* was amplified off pVP16 RG#28 and cloned into pTriExMBPSfi using two distinct SfiI restriction sites (Pengelley et al., 2006). The resulting vector was then used

to amplify the *MBPtum* sequence that was subsequently cloned into pFastBacDual using XhoI (5') and KpnI (3') restriction sites. The absence of PCR induced mutations within the sequence was verified by sequence analysis.

pFastBacDual pbl^{fl} MBPtum construct

To create an over-expression vector that would express both pbl^{fl} and MBPtum, pbl^{fl} was amplified off pUAS::pbl-GFP cloned into the previously constructed pFastBacDual MBPtum vector using BamHI (5') and EcoRI (3') restriction sites. The absence of PCR induced mutations within the sequences was verified by sequence analysis.

2.2.11.2 Generation of *pbl*, *tum* and *pav* P[acman] constructs by Recombineering

2.2.11.2.1 Recombineering mediated Gap repair

Recombineering mediated gap repair was conducted according to (Venken et al., 2006). Briefly, BACs containing *tum* or *pav* were identified using the Release 3 or Release 4.3 annotated *Drosophila* genome sequence in the Flybase Genome Browser (http://www.flybase.org) and obtained from BacPac Resources (http://bacpac.chori.org). A previously acquired cosmid was used for *pbl*. The region selected for gap repair included the target gene as well as the flanking genomic DNA that extended to the neighboring transcripts. The rational behind the inclusion of regions flanking each gene was to ensure that all the essential genetic regulatory elements would be included thus maintaining endogenous expression levels. Two sets of primers were designed to amplify two homology

arms of ~500bp each at the 5' and 3' ends of the selected region. The 5' homology arm is referred to as the left arm (LA) and the 3' homology arm is referred to as the right arm (RA). The homology arms were amplified so that the LA contained a 5' *AscI* and 3' *BamHI* site while the RA contained a 5' *BamHI* and 3' *NotI* site. The LA and RA were knitted together in a secondary PCR and digested with *AscI* and *NotI*. The digested LA-RA product was then ligated into *AscI-NotI* digested and PCR purified P[acman] vector. Ligation products were electroporated into *EPI300* cells and induced to high copy number. Correct clones were isolated using restriction analysis and sequencing. In order to perform gap repair, 1 μg of P[acman]- LA-RA construct was linearised with *BamHI* and PCR purified. Approximately 30ng of this was electroporated to competent *SW102* cells containing the appropriate BAC/cosmid that had been heat shocked at 42°C for 15 minutes to induce the λ-Red function just prior to making them competent. As a negative control 30ng of the linearised vector was also electroporated into competent *SW102* cells containing the appropriate BAC/cosmid that had been kept at 30°C, where λ-Red is not induced. After recombineering, gap repaired P[acman]-pbl construct DNA was isolated and electroporated into *EPI300* cells and plasmid copy number induced. The DNA was then isolated and confirmed by restriction digest analysis and sequencing. These constructs were then modified using the *galK* selection method to insert tags and the desired mutations.

2.2.11.2.2 Construction of *pbl*, *pav* and *tum* sequences mutated for putative Polo and proline-directed phosphorylation sites.

A region of *pbl*, *tum* or *pav* that contained the nucleotides to be mutated and at

least 50 bp flanking sequence were subcloned into pGEM-T (Promega) and mutagenesis strategies employed to introduce the desired mutations (see 2.2.4 and 2.2.5). The resulting mutated sequences were then amplified off these vectors and used to replace the corresponding regions of the cloned wild type genes in the *P[acman]* vectors by homologous recombination to thereby create the Polo and proline-directed phosphorylation mutant versions. Due to the presence of large introns within *pbl*, three different regions, each containing some of the mutations to be incorporated, were subcloned into pGEM-T and subsequently recombineered sequentially into *pbl-GFP P[acman]*.

2.2.11.2.3 *galK* positive and negative selection recombineering to modify genomic fragments in P[acman]

Recombineering using *galK* selection was conducted according to (Warming et al., 2005). Briefly, two sets of primers were designed to span 50bp flanking the region of *pbl, tum* or *pav* where a tag (e.g. GFP) was to be inserted or the wild type sequence was to be replaced with a mutated sequence. The first set of primers contained sequences that would enable the amplification of the *galK* open reading frame within the homology arms. The second primer set contained sequences that would enable the amplification of the tag or mutated *pbl, tum* or *pav* sequences within the homology arms. Using the first primer set, a PCR product containing the *galK* open reading frame with flanking homology regions was created. Using the second primer set, a PCR product containing the *pbl, tum* or *pav* mutated sequence or the tag of interest with flanking homology regions were created. The PCR products were *DpnI* digested and gel purified. The following process describes the recombineering procedure for inserting a GFP

tag into *P[acman]-pbl*, but the same process was undertaken for inserting other tags or mutated sequences into any of the *pbl*, *pav* or *tum P[acman]* constructs. The *P[acman]-pbl* genomic construct was transformed into *SW102* cells. Two separate SW102 *P[acman]-pbl* cultures were made where the λ-Red function was induced in one but not the other culture. Both the induced and uninduced cultures were then made electrocompetent as detailed in 2.2.10. The competent cells were electroporated with 10-30ng of the *galK* PCR product, allowed to recover in LB at 32°C for 1 hr, harvested, washed in M9 washing solution twice and plated on M63 minimal medium containing galactose as the sole carbon source. The plates were grown at 30°C for 3 days. Six to ten of the many resulting colonies were streaked on MacConkey indicator plates. DNA was extracted from a culture grown from a single dark red *Gal+* colony and restriction digest verification carried out to confirm *galK* insertion. *Gal+ SW102* cells containing *P[acman]-pbl(galK)* were made competent with or without the induction of λ-Red function. This time 10-30ng of the GFP PCR product was electroporated into the competent cells, which were allowed to recover in LB at 32°C for 4.5hr. Cells were then harvested and washed in M9 washing solution twice and plated on M63 minimal medium containing glycerol as the sole carbon source and 2-deoxy-galacose-1-phosphate (DOG) for selection against *galK*. Plates were grown at 30°C for 3 days. A few of the many resulting colonies were streaked for single white/colorless (*Gal-)* colonies on MacConkey indicator plates. Following this, the construct was isolated from *SW102* cells, transformed into *EPI300* cells, induced to high copy number and plasmids isolated either by Qiagen Mini or Midi preps. The correct construct was confirmed by restriction enzyme digestion analysis and sequencing. The final construct was then used to transform

Drosophila embryos.

2.2.12 Construction and amplification of recombinant baculovirus

Construction of recombinant baculovirus was performed as per the BacPAK (Clontech Laboratories) and Bac-to-Bac (Invitrogen) baculovirus expression system manuals. Briefly, to construct recombinant baculovirus using the BacPAK baculovirus system, 1 x 10^6 Sf9 cells were seeded per 35mm well and left to attach for 1 hour at 27°C. Growth media was removed, replaced with 96µl of transfection mixture containing BacPAK6 viral DNA, BacPAK8 pbl^{fl} plasmid DNA and Bacfectin (Clontech) and cells incubated for 5 hours at 27°C. 1.5ml Grace's medium was added and the supernatant containing recombinant virus harvested 72 hours later.

To construct recombinant virus using the Bac-to-Bac baculovirus system, electrocompetent DH10Bac *E. coli* cells were transformed with 1ng FastBac plasmid DNA (see 2.2.9 and 2.2.10). White colonies were picked 48 hours later and used to inoculate cultures from which recombinant bacmid DNA was isolated as per the Bac-to-Bac manual. Bacmid DNA was analyzed by PCR to confirm the presence of the gene of interest. To transfect insect cells with bacmid DNA, 35mm wells were seeded with 9 x 10^5 Sf9 cells and allowed to attach for 1 hour at 27°C. Growth media was removed, replaced with a transfection mixture containing 1µg bacmid DNA and Cellfectin reagent (Invitrogen) and incubated at 27°C for 5 hours. The transfection mixture was removed and 2ml Grace's

medium added to the well. The supernatant containing recombinant baculovirus was harvested 72 hours later.

To amplify baculoviral stocks, 25 ml Sf9 cultures were seeded at 2 x 10^6 cells/ml and left to attach for 1 hour at 27°C. 50µl of viral stock was added to the culture and cells monitored for signs of infection. Once infection was well established, as judged by detachment of cells from the flask and obvious viral budding (usually 48-72 hours post-infection), the supernatant containing recombinant baculovirus was harvested and stored at 4°C.

2.2.13 Over-expression and purification of recombinant proteins

Shaking High Five insect cell cultures were seeded at a density of 5x10^5 cells/ml and left to grow for 24 hours. 250µl of an amplified baculovirus preparation was then added and cultures left to grow for at least 48 hours. Over-expressed protein samples from cultured High Five insect cells were prepared at 4°C as follows. High five cells were harvested, gently pelleted by centrifuging at 1100 rpm for 5 minutes and the supernatant discarded. Cell pellets were snap frozen in liquid nitrogen and stored at -80° for later use. When the over-expressed protein was to be purified, frozen pellets were gently resuspended in 4ml lysis buffer per 1-2 x 10^7 cells and incubated on ice for 15 minutes. Complete cell lysis was promoted by sonication (Virtis408912, Virsonic) for 10 seconds at 70% maximal frequency (0.7) three times with 30 second cooling intervals between sonications to ensure the cell lysate remained chilled. Cellular lysates were then

centrifuged at 15,000rpm for 30 minutes at 4°C to pellet cellular debris. The supernatant was filtered through a 0.45μm syringe filter and loaded onto the appropriate purification column. Columns were run on an AKTA Basic or Explorer fast protein liquid chromatography (FPLC) system using the UNICORN software. Column purification or buffer exchange methods were carried out as specified by the manufacturers.

To analyze protein in the insoluble material, 0.5ml 1x sample buffer was used to resuspend a 50μl post-sonication wet cell pellet. Protease inhibitors were used at all stages of purification except in over-expression trials and EDTA was not used prior to affinity purification as it would otherwise strip Nickel ions from the column. To analyze protein samples by SDS-polyacrylamide gel electrophoresis, sample buffer was added to a 1x concentration and the protein sample boiled at 100°C for 10 minutes, briefly centrifuged and loaded directly onto a protein gel.

2.2.14 SDS-polyacrylamide gel electrophoresis

The Bio-rad Mini-Protean II gel electrophoresis system was used to cast and run protein gels. Protein samples were boiled at 100°C for 5 minutes in protein sample buffer and loaded and run on 8-12% SDS-polyacrylamide gels at 200V. Separated protein samples were transferred onto nitrocellulose membranes (Schleicher and Schuell, Germany), using a Bio-rad Transblot SD Semi-dry transfer cell according to manufacturer's guidelines. In general, a current of 0.3 mA per cm^3 of gel was applied for 60 minutes.

2.2.15 Western blotting

Nitrocellulose membranes, containing the separated proteins, were blocked in PBST with 5% Milk powder for one hour with agitation. The primary antibody was incubated with the membrane in PBST with 5% Milk powder overnight at 4°C. The membrane was washed three times with PBST for 15 minutes. An HRP-conjugated secondary antibody, diluted in PBST with 5% milk powder, was incubated with the membrane for 2 hours at room temperature and then washed three times with PBST for 15 minutes. The secondary antibodies were detected by mixing 5ml of the ECL solution A with 5ml of solution B. The membrane was incubated in this solution for one minute, excess fluid blotted and the membrane exposed to ECL film (GE Healthcare) for varying lengths of time. Film was developed manually by incubation in developer for 1 min with agitation, rinsed thoroughly in water, incubated in fixer for 1 min with agitation, again rinsed thoroughly in water and air dried.

2.2.16 Western blot stripping

To strip probed western blots for analysis with a different antibody the blot was washed in PBST to remove the chemiluminescent substrate and incubated with Restore Western Blot Stripping Buffer (Thermo Scientific) for 15 minutes at room temperature with gentle agitation. The blot was then washed, blocked and tested for sufficient removal of antibodies by ECL before it was probed with the next antibody.

2.2.17 Protein prediction/processing software

The MultiIdent and PSIpred prediction programs were accessed from the ExPASy proteomics server (http://www.expasy.ch/tools/#proteome) and used to identify predicted isoelectric points and secondary structures respectively. Clustalw alignments were performed using the EMBL-EBI clustalw algorithm (http://www.ebi.ac.uk/Tools/clustalw2/index.html).

2.2.18 Protein quantification

Protein quantitation was carried out using the Bio-Rad Protein Assay according to the manufacturers instructions. Briefly, the dye reagent was prepared by diluting 1 part dye reagent concentrate with 4 parts MilliQ water and filtering the solution through Whatman #1 filter paper. Five dilutions of an IgG protein standard at concentrations of 0.2, 0.4, 0.6, 0.8 and 1.0 mg/ml were prepared. 100µl of each standard and sample solution were added to a 15ml tube with 5ml diluted dye reagent, vortexed to mix and incubated at room temperature for 5 minutes. The absorbance at 595nm was then measured on a spectrophotometer. Each standard and protein sample was measured in triplicate and the average value taken. A standard curve was constructed using the IgG values and the concentration of the protein sample determined from this.

2.2.19 Crystallization trials

200nl of protein solution and 200nl trial buffers were mixed per well in 96 well plates using a Honey Bee 961 System (Digilab Genomic Solutions). Duplicate plates were created for each set of trial conditions and the plates were then

sealed and stored at 4°C or room temperature and periodically inspected for the formation of protein crystals.

2.2.20 Mass spectrometry

All equipment used in SDS-polyacrylamide gel electrophoresis for mass spectrometry analysis was thoroughly washed in pyroneg detergent to remove trace proteases and all solutions filtered through 0.22μm filters. A new scalpel blade was used to excise each protein band. Excised bands were transferred to autoclaved 1.5ml centrifuge tubes and stored at -20°C prior to processing. Samples were processed at the Biomolecular Resource Facility in the John Curtin School of Medical Research (The Australian National University). Protein gel bands were destained, reduced, alkylated and digested with trypsin prior to liquid chromatography separation and analysis on a 4800 MALDI TOF-TOF mass spectrometer. Mass spectrometry data were analyzed using MASCOT and the identified peptides matched to Swissprot, TREMBL or a translation of Flybase protein databases.

2.2.21 Removal of His tag from $Pbl^{N\text{-}term}$

1000 units of AcTEV protease was added to a $Pbl^{N\text{-}term}$ solution containing 58mg protein and incubated at 30°C for 5 hours and then snap frozen. The reaction was monitored every hour for complete digestion and removal of the His tag by collecting samples for SDS PAGE and coomassie staining. Upon confirming that uncut $Pbl^{N\text{-}term}$ was no longer visible, the protein solution was thawed, and buffer exchange carried out using a desalting column. The protein solution was loaded

onto a Ni-NTA Superflow column to affinity purify the cleaved His tag and AcTEV protease from recombinant $Pbl^{N\text{-}term}$.

2.2.22 Induction of λ-Red function for recombineering

A 5 ml culture of SW102 cells containing the desired BAC or *P[acman]* construct was grown overnight at 30°C and 0.5 ml used to seed 25ml LB containing appropriate antibiotics. This was grown at 30°C for 2–2.5 hours to an OD_{A600} of 0.4-0.6. This culture was divided into two flasks -one was heat shocked at 42°C for 15 minutes to induce λ-Red function (induced sample), while the other was kept at 30°C (uninduced sample). The cultures were cooled in an ice/water slurry for 5 minutes and then used to prepare eletrocompetent cells described in 2.2.9.

2.2.23 Isolation of high quality plasmid DNA

High quality plasmid DNA, for microinjection of *D. melanogaster* embryos and for dye terminator sequencing reactions, was prepared using Qiagen mini- and midi-prep kits respectively. Purification of DNA was according to manufacturers instructions, except water heated to 65°C was used to elute DNA rather than the supplied elution buffer.

2.2.24 Isolation of *D. melanogaster* genomic DNA

Single adult flies were placed in 1.5ml microcentrifuge tubes and immobilized by incubating on ice for 10 minutes. Files were then squished against the wall of the tube with a disposable pipette tip. 50μl of squishing buffer was then added and

mixed with the remains of the fly. The solution was then incubated at 37°C for 30 minutes, followed by a 5 minute incubation at 95°C to inactivate proteinase K. Fly debris was pelleted by centrifugation at 14000 rpm for 1 minute. 1µl of this preparation was used as template for PCR.

2.2.25 Isolation of Cosmid and Bacterial Artificial Chromosome (BAC) DNA

Cosmid and BAC DNA were isolated from DH10B using Qiagen Midi Kit. A 5ml overnight culture of *DH10B* was pelleted and resuspended in 300µl of buffer P1 and lysed in 300µl of buffer P2 for 5 minutes at room temperature. 300µl of buffer P3 was then added, the solution was mixed and incubated on ice for 5 minutes. The precipitate was pelleted by centrifugation at 14000 rpm for 10 minutes at 4°C and the supernatant transferred to a new tube containing 800ml of ice-cold isopropanol and mixed. DNA was pelleted by centrifugation at 14000 rpm for 10 minutes at 4°C and the supernatant discarded. The DNA pellet was washed with 70% ethanol, air-dried and allowed to dissolve in 40µl MilliQ water. Mechanical re-suspension was not performed as it would shear large BAC DNA.

2.2.26 *D. melanogaster* cultures

Flies were raised at 25°C, with 70% humidity, on F1 medium or Harvard food. Fly stocks were maintained at 18°C. Egg lays were performed at 25°C on apple juice agar plates.

2.2.27 Collection and fixation of *D. melanogaster* embryos

Embryos were collected on apple juice agar smeared with yeast paste. They were harvested and washed thoroughly in a basket using MilliQ H2O. The basket was then immersed in 50% commercial bleach (2% sodium hypochlorite) for 3 minutes to de-chorionate the embryos. The embryos were then washed thoroughly with MilliQ H_2O. To fix the embryos they were then transferred to a glass scintillation vial containing a two-phase mix of 5 ml of 4% formaldehyde in 1X PBS and 5 ml of heptane. The vial was shaken on an orbiting platform such that the interface between the liquid phases was disrupted and the embryos were bathing in an emulsion, for 20 minutes. The bottom aqueous phase was removed and replaced with 4 ml of methanol and the vial was shaken vigorously for 30 seconds to break the vitelline membrane. De-vitellinised embryos sink from the interface and are collected from the bottom phase (methanol). Embryos were rinsed thoroughly in methanol and either immuno-stained or stored at -20°C. To stain embryos with rhodamine phalloidin embryos were also fixed as described above, except that they were stored in 90% ethanol after being de-vitellinised.

2.2.28 Whole mount immuno-staining of *Drosophila* embryos

Fixed embryos were rehydrated by replacing the methanol with PBST, followed by 3 x 5 min rinses in PBST. The embryos were then incubated with gentle agitation overnight at 4°C with primary antibody diluted in PBST. The next day the antibody solution was removed and embryos were washed 4 x 15 minutes with PBST. Embryos were then incubated with secondary antibodies in PBST for

at least three hours at room temperature with gentle agitation. The embryos were again washed 4 x 15 minutes in PBST. DNA was stained with Hoechst 33258 (1μg/μl) for 10 minutes followed by 3 x 15 min washes in PBST. The embryos were then cleared in 50% glycerol in PBST and transferred to 70% glycerol in PBST. Embryos were examined using an epifluorescence microscope (Leica M165) and mounted in a ventral orientation. Mounted embryos were imaged using a Confocal microscope (Leica SP5) using a CCD camera.

2.2.29 Alkaline phosphatase staining of *Drosophila* embryos

Drosophila embryos were fixed and incubated with primary antibodies as described in 2.2.26 and 2.2.27. The embryos were repeatedly washed in PBST and then incubated with an AP-conjugated secondary antibody for at least 4 hours, before repeated washing in PBST. The embryos were then equilibrated in AP staining buffer (2 x 5 minutes), and then color developed with the addition of 3.5μl BCIP and 4.5μl NBT in 1 ml of AP buffer. Color development was monitored under a dissecting microscope and stopped by repeated washes in PBST. AP staining was routinely used to identify homozygous mutant embryos when marked balancer chromosomes were used.

2.2.30 ΦC31 mediated transformation of *Drosophila*

2.2.30.1 Micro-injection

DNA for injection was prepared using the Qiagen plasmid midi kit according to the manufacturers protocol, except that the DNA was eluted with MilliQ water. The injection mix comprised 300ng/μl plasmid DNA in 1X embryo injecting

buffer (5mM KCl, 0.1mM $NaPO_4$ pH 6.8). The injection needle was back filled using a drawn out capillary containing 2µl of the injection mix, which had been centrifuged briefly to remove any particulate matter. Embryos to be injected were collected from 30 minute lays on apple juice agar plates at 25°C, dechorionated in 50% bleach for 3 min, and rinsed thoroughly in MilliQ water. Embryos were then aligned along a strip of non-toxic rubber glue such that their posterior ends would face the needle. A drop of halocarbon oil was placed over the embryos and the slide placed on the stage of an inverted microscope. A micromanipulator was used to position the needle, with injection carried out by moving the microscope stage to bring the embryos to the needle, such that a very small amount of DNA was injected into the posterior cytoplasm. Appropriate fly stocks that contained a source of integrase and a desired landing site for ΦC31 integrase mediated integration of DNA to specific sites of the genome (Bischof et al., 2007; Venken et al., 2006) were used for micro-injection. Embryos were injected with the attB-*P[acman]* transformation vector containing the construct of interest (Venken et al., 2006).

2.2.30.2 Identification of transformants

The slides of microinjected embryos were placed in a petri dish containing moist tissue paper with a small amount of yeast paste surrounding the embryos and kept at 18°C to allow the embryos to hatch. Larvae were collected after hatching using strips of Whatman paper and placed in a fly food vial where they developed into adult flies. The flies were then crossed to w^{1118} flies to identify transformants on the basis of the mini-white$^+$ eye pigmentation phenotype indicating the presence of a transgene. Transformants were selected and

established over an appropriate balancer chromosome.

Transgenic flies expressing all the *tum-myc* constructs were obtained using a fly strain with the attP site at the cytogenetic position 22A (Figure 2.1A). Transgenic flies expressing the *pbl-GFP* and *pav* constructs were generated using a fly strain containing an attP site at the cytogenetic position 97D, which did not possess a ΦC31 integrase source. In this case, a source of integrase was provided by crossing these flies to a strain containing the *vasa*>ΦC31 integrase on chromosome IV but also having an additional attP site on the X chromosome (Figure 2.1B). Survivors from injections were crossed to w^{1118} flies and w^+ transgenic fly lines isolated, balanced and stocks established (figure 2.1A and B). To differentiate between integration on the X and on the 3rd chromosomes, individual males from established transgenic lines were crossed to w^{1118} virgins. If integration occurred on the X chromosome, the females would be w^+ while all male progeny would be w^-. If integration had occurred on III then both males and females would be w^+. Rarely a double integration event could occur such that the construct was integrated on both chromosome III and X. If this occurred, all females would be w^+ but ½ would have two copies of w^+ and ½ would have only one copy, thus giving rise to flies with two different eye colours. In this scenario ½ of the males would be w^+ and ½ of males would be w^-. None of the *pbl-GFP* or *pav* transgenic lines created appeared to have a double integration event of the construct.

2.2.31 Creation and identification of *pbl*, *pav* and *tum* recombinants

To facilitate the creation of recombinants via mitotic recombination, attP integration sites that were distal to the endogenous gene locus were chosen. Thus as the *tum* locus is situated on the right arm of the 2nd chromosome at 50C, an attP site on the left arm at 22A was used for the integration of all the *tum* expression constructs. Similarly, *pbl* and *pav* loci are situated on the left arm of the 3rd chromosome at 66A and 64A respectively, so an attP site on the right arm at 97D was selected. The mutant alleles or deficiencies used were tum^{AR2} and Df(2R)Exel7128 for *tum-myc transgenes*, pbl^{2} and pbl^{3} for *pbl-GFP* transgenes and pav^{B200} and Df(3L)Exel9000 for *pav* transgenes. Recombinants were created via mitotic recombination of a mutant allele or deficiency with its corresponding transgene (Figure 4.2A and B)

Sequencing was used to identify pbl^{2}, pbl^{3} and tum^{AR2} recombinant lines whereas further crosses were required to distinguish pav^{B200}, Df(2R)Exel7128 and Df(3L)Exel9000 recombinants.

To identify Df(2R)Exel7128 recombinants, potential recombinant lines were crossed to two tester deficiency lines, Df(2R)BSC383 and Df(2R)BSC307, that carried deletions covering part or all of the region deleted by Df(2R)Exel7128 (Figure 2.2A and see Figure 4.3A). If Df(2R)Exel7128 was present in a potential recombinant line, progeny carrying Df(2R)Exel7128 and one of the tester deficiencies would be lethal. Therefore, by looking for the

Figure 2.1 ***Crossing schemes to generate* pbl-GFP, tum-myc *and* pav *transgenic fly lines***

The crossing schemes used to create *pbl-GFP*, *tum-myc* and *pav* transgenic lines. **A.** The crossing scheme to create *tum-myc* transgenic lines is shown for *tum-myc*^{wt} but was the same for all *tum-myc* constructs. The constructs were injected into a fly line that contained the ϕC31 integrase marked by GFP on X and an attP site on II. Survivors were crossed to w^{1118} and any w^+ transgenics individually crossed to the Gla/CyO balancer line. Balanced stocks were then established from the progeny. **B.** The crossing scheme to create *pbl-GFP* and *pav* transgenic lines is shown for *pbl-GFP*^{wt} but was the same for creating all *pbl-GFP* and *pav* transgenic lines. The line containing the desired attP integration site on III was crossed to a strain containing the ϕC31 integrase on IV and an attP site on X. The *pbl-GFP* or *pav* constructs were injected into flies heterozygous for the two attP sites and the ϕC31 integrase and survivors crossed to w^{1118}. Individual w^+ transgenic flies were crossed to TM6B/TM3 and balanced stocks established from the progeny. To determine whether integration had occurred on the X or III, individual males were crossed to w^{1118}. If integration had occurred on the X, the female progeny would be w^+ whereas males would be w^-. A line in which integrations had occurred at both attP sites would result in half the females containing two copies of w^+, half the females having one w^+, half the males possessing a single w^+ and half the males being w^-. Those crosses that produced all w^+ flies contained an integration on III and the corresponding stock was used for subsequent applications. ??? denotes a potential 3rd chromosome transgenic line.

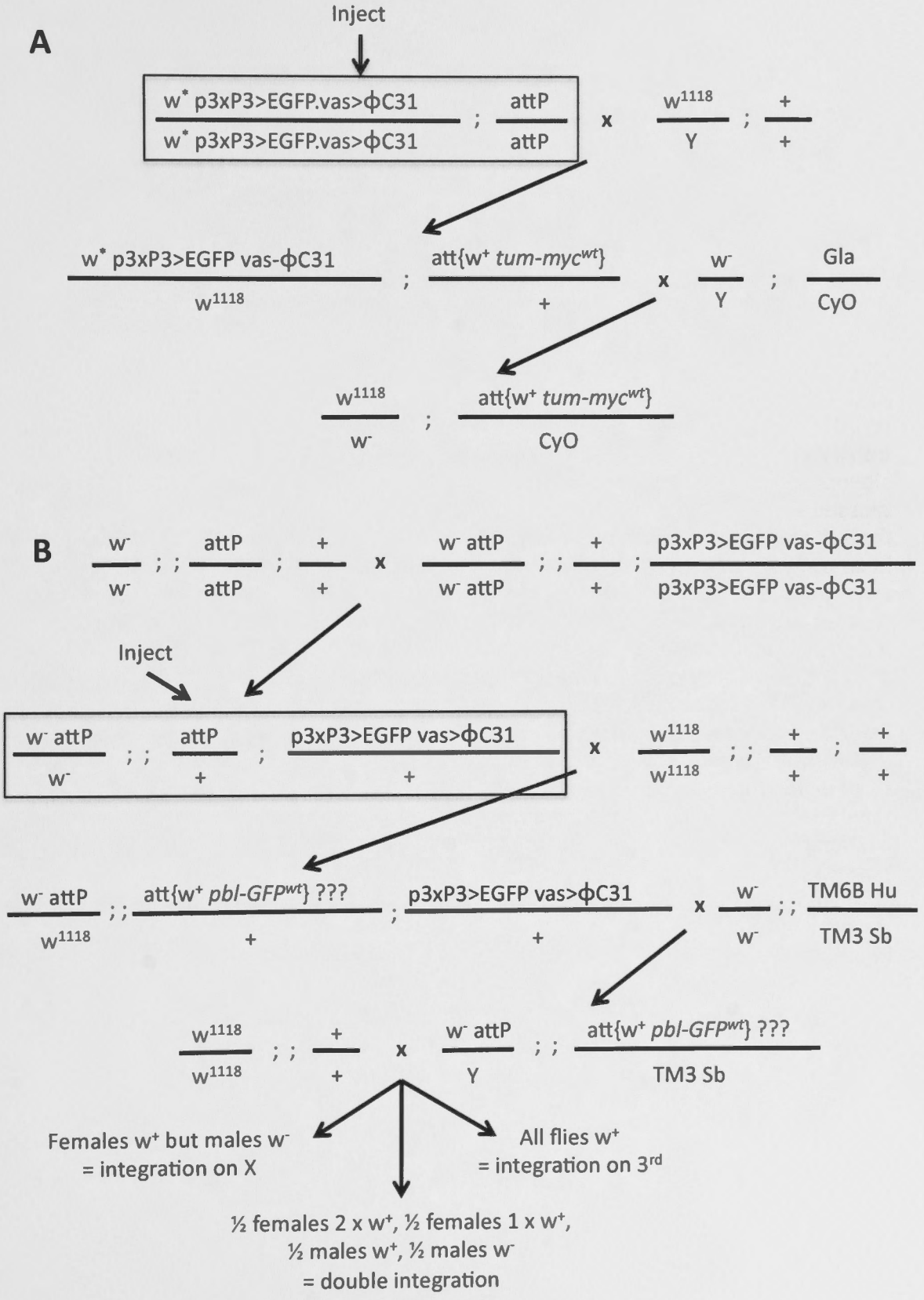
A
Inject
w* p3xP3>EGFP.vas>ϕC31 / w* p3xP3>EGFP.vas>ϕC31 ; attP / attP
x
w1118 / Y ; + / +
w* p3xP3>EGFP vas-ϕC31 / w1118 ; att{w+ tum-mycwt} / +
x
w- / Y ; Gla / CyO
w1118 / w- ; att{w+ tum-mycwt} / CyO
B
w- / w- ; ; attP / attP ; + / +
x
w- attP / w- attP ; ; + / + ; p3xP3>EGFP vas-ϕC31 / p3xP3>EGFP vas-ϕC31
Inject
w- attP / w- ; ; attP / + ; p3xP3>EGFP vas>ϕC31 / +
x
w1118 / w1118 ; ; + / + ; + / +
w- attP / w1118 ; ; att{w+ pbl-GFPwt} ??? / + ; p3xP3>EGFP vas>ϕC31 / +
x
w- / w- ; ; TM6B Hu / TM3 Sb
w1118 / w1118 ; ; + / +
x
w- attP / Y ; ; att{w+ pbl-GFPwt} ??? / TM3 Sb
Females w+ but males w-
= integration on X
All flies w+
= integration on 3rd
½ females 2 x w+, ½ females 1 x w+,
½ males w+, ½ males w-
= double integration

Figure 2.2 ***Identification of Df(2R)Exel7128 and Df(2R)Exel9000 recombinants***

A. To identify whether a potential Df(2R)Exel7128 recombinant line carries the deficiency, it was crossed to strains carrying Df(2R)BSC383 or Df(2R)BSC307 separately. If Df(2R)Exel7128 is present then unbalanced progeny will not survive. Alternatively, if the deficiency is absent then unbalanced progeny will survive. **B**. To identify whether a potential Df(2R)Exel9000 recombinant line carries the deficiency, it was crossed to strains carrying Df(2R)Exel8098 or Df(2R)BSC370 separately. If Df(2R)Exel9000 is present then unbalanced progeny will not survive. Alternatively, if the deficiency is absent then unbalanced progeny will survive.

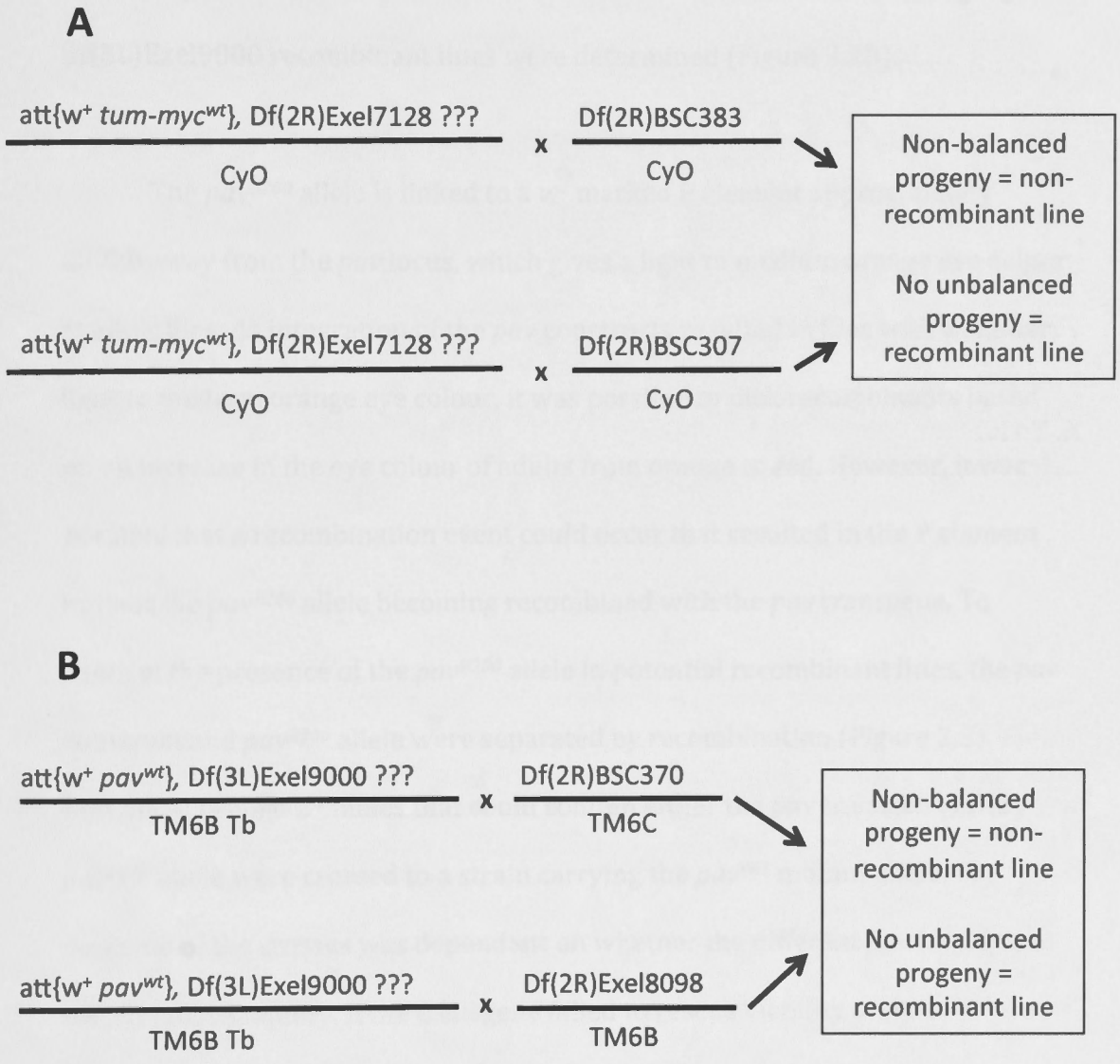
A
att{w+ tum-mycwt}, Df(2R)Exel7128 ???
CyO
x
Df(2R)BSC383
CyO
att{w+ tum-mycwt}, Df(2R)Exel7128 ???
CyO
x
Df(2R)BSC307
CyO
Non-balanced progeny = non-recombinant line
No unbalanced progeny = recombinant line
B
att{w+ pavwt}, Df(3L)Exel9000 ???
TM6B Tb
x
Df(2R)BSC370
TM6C
att{w+ pavwt}, Df(3L)Exel9000 ???
TM6B Tb
x
Df(2R)Exel8098
TM6B
Non-balanced progeny = non-recombinant line
No unbalanced progeny = recombinant line

absence of unbalanced flies in such crosses, Df(2R)Exel7128 parental recombinant lines were determined (Figure 2.2A). Similarly, two tester deficiency stocks, Df(2R)BSC370 and Df(2R)Exel8098, were used to identify Df(3L)Exel9000 recombinant lines (Figure 2.2B and see Figure 4.3B). By identifying crosses to the tester deficiencies that lacked unbalanced progeny, Df(3L)Exel9000 recombinant lines were determined (Figure 2.2B).

The pav^{B200} allele is linked to a w^+ marked P element approximately 250kb away from the *pav* locus, which gives a light to medium orange eye colour in adult flies. As integration of the *pav* constructs resulted in flies with a similar light to medium orange eye colour, it was possible to pick recombinants based on an increase in the eye colour of adults from orange to red. However, it was possible that a recombination event could occur that resulted in the P element but not the pav^{B200} allele becoming recombined with the *pav* transgene. To confirm the presence of the pav^{B200} allele in potential recombinant lines, the *pav* construct and pav^{B200} allele were separated by recombination (Figure 2.3). Individual orange w^+ males that could contain either the *pav* transgene or the pav^{B200} allele were crossed to a strain carrying the pav^{963} mutant allele. The outcome of the crosses was dependant on whether the different *pav* transgenes could rescue viability. If the transgene failed to rescue viability and pav^{B200} was present, no unbalanced progeny would survive (Figure 2.3A). Alternately, if only the w^+ marked P element had recombined with the *pav* transgene unbalanced progeny would be viable (Figure 2.3B). If the transgene could rescue viability and the pav^{B200} allele was present, unbalanced progeny from crosses containing the *pav* transgene but not pav^{B200} would survive (Figure 2.3C). However, if only

the w^+ marked P element was present then all unbalanced progeny would be viable (Figure 2.3D). The ability of the *pav* transgenes to rescue viability was assessed using previously confirmed Df(3L)Exel9000 recombinants. Using this crossing scheme, pav^{B200} recombinant lines were identified.

2.2.32 Microscopy

Drosophila embryos were sorted, and mounted by using an epifluorescence microscope (Leica M165). Fluorescence microscopy was performed on a Confocal microscope (Leica SP5) and imaged using a cooled CCD camera. Image J was used for all image preparation. *Drosophila* epidermal cells were imaged by acquiring z-stacks using a 4x optical zoom at a 512 x 512 resolution. Z-stacks to be used for binucleate cell counts were taken at a 1x optical zoom at a 1024 x 1024 resolution. Images were analyzed using Image J.

2.2.33 Regulatory considerations

All manipulations involving recombinant DNA were carried out in accordance with the regulations and approval of the Genetic Manipulation Advisory Committee and the Australian National University Council.

Figure 2.3 ***Confirming the presence of* pav^{B200} *in potential* pav *transgenic recombinant lines***

Individual orange w^+ males, which could contain either the *pav* transgene or *pav^{B200}*, were isolated from the progeny and crossed to a stock carrying the *pav^{963}* mutant allele. The outcome of the crosses was dependant on whether the different *pav* transgenes could rescue. **A** and **B**. If the transgene failed to rescue and *pav^{B200}* was present, no unbalanced progeny would survive. If only the w^+ marked P element had recombined with the *pav* transgene then unbalanced progeny would be viable. **C** and **D**. If the transgene could rescue and the *pav^{B200}* allele was present, unbalanced progeny carrying the *pav* transgene but not pav^{B200} would survive. If only the w^+ marked P element was present then all unbalanced progeny would be viable. ??? = potential recombinant.

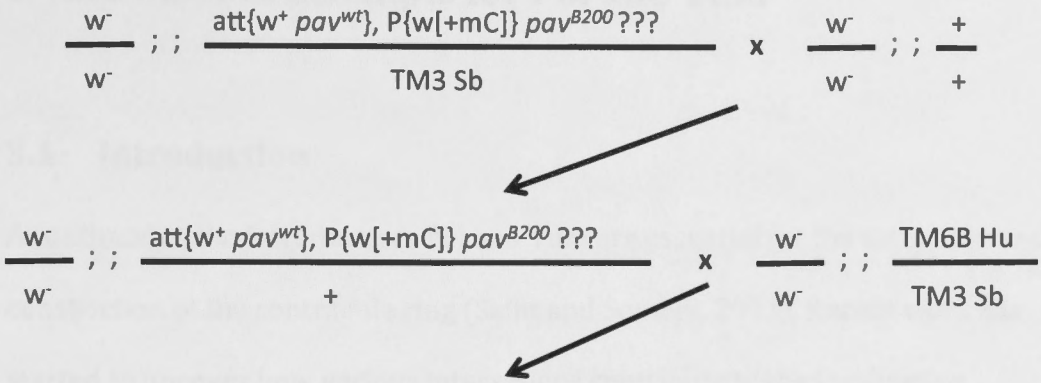

A Transgene fails to rescue

pav^{963} / TM6B x P{w[+mC]} *pav*^{B200} ??? / TM3 Sb → Unbalanced progeny **perish**

pav^{963} / TM6B x att{w⁺ *pav*^{wt}} ??? / TM3 Sb → Unbalanced progeny **perish**

B

pav^{963} / TM6B x P{w[+mC]} ??? / TM3 Sb → Unbalanced progeny **survive**

pav^{963} / TM6B x att{w⁺ *pav*^{wt}} ??? / TM3 Sb → Unbalanced progeny **perish**

C Transgene rescues

pav^{963} / TM6B x P{w[+mC]} *pav*^{B200} ??? / TM3 Sb → Unbalanced progeny **perish**

pav^{963} / TM6B x att{w⁺ *pav*^{wt}} ??? / TM3 Sb → Unbalanced progeny **survive**

D

pav^{963} / TM6B x P{w[+mC]} ??? / TM3 Sb → Unbalanced progeny **survive**

pav^{963} / TM6B x att{w⁺ *pav*^{wt}} ??? / TM3 Sb → Unbalanced progeny **survive**

Chapter 3 - The over-expression, purification and crystallization attempts for Pbl and Tum

3.1 Introduction

As outlined in the introduction, Pbl and Tum are essential for the formation and constriction of the contractile ring (Saint and Somers, 2003). Recent work has started to uncover how various interactions contribute to the localisation, assembly and constriction of the contractile ring. In *Drosophila*, Tum has been shown to interact with many key cytokinetic proteins, including Pbl, Pav and Anillin (detailed in 1.7) (Gregory et al., 2008; Saint and Somers, 2003). The regions of Tum that interact with Pbl, Pav and Anillin have been defined by yeast-two-hybrid experiments (Gregory et al., 2008; Somers and Saint, 2003). However, our attempts to specifically knock out the interaction between Tum and Pbl or Anillin, through small deletions or amino acid substitutions, without disrupting other binding partners have so far failed. This has hampered efforts to clearly define the individual roles that such interactions play in the events of cytokinesis.

One way in which protein interactions and activities are modulated in a swift and coordinated manner is through phosphorylation. The progression of mitosis is partly controlled by the action of a number of kinases. During cytokinesis Cdk1, Polo and Aurora B kinases play important roles in controlling the interactions and activities of a number of proteins (detailed in 1.9 and 1.9.1). Phospho-regulation of Pbl/Ect2 and Tum/HsCyk-4 during cytokinesis has been

shown to influence their GEF and GAP activities respectively in addition to their interaction with one another (detailed in 1.7 and 1.8).

Detailed structural information about Pbl and Tum would greatly facilitate our ability to define, and thus specifically target, residues within a protein important for an interaction and would improve out understanding of how phosphorylation events could promote or prevent particular interactions and activities. In an effort to gain such information, I attempted to over-express, purify and crystallize Pbl and Tum. The structure of the full length Pbl protein was desired as this could further illuminate how oligomeric or intra-molecular interactions occurred. Moreover, a complete structure of both Pbl and Tum might suggest the mechanism by which the two proteins interact and reveal how phosphorylation of particular residues might induce conformational changes in both the immediate and surrounding regions of the protein to mediate interactions.

3.1.1 Considerations in choosing a protein over-expression strategy

Generally, over-expression of a protein is undertaken in bacteria due to the low costs associated with growing large cultures, short generation times and short delay of expression. However, bacterial expression systems have limitations. Firstly, bacteria are unable to perform many of the post-translational modifications that occur in eukaryotic cells. This can result in the expression of a protein that may lack crucial modifications required for its native conformation

and/or activities. Secondly, many larger proteins (>60-70 kDa) are often expressed poorly or are insoluble when expressed in bacteria. Although these insoluble proteins can be purified successfully under denaturing conditions, renaturation of the protein post purification is not a trivial procedure and cannot be guaranteed to refold the protein into its native state.

By contrast, over-expressing proteins in insect cells through the use of genetically engineered baculoviruses overcomes many of the limitations encountered in bacterial expression systems. Baculovirus systems not only allow expression of large molecular weight proteins, but often these can be produced in a mainly soluble form. Moreover, since the proteins are produced in a eukaryotic cell, many of the post-translational modifications present in the endogenous protein are also incorporated into the over-expressed proteins (Murphy et al., 2004). Due to both the large sizes of Pbl and Tum, and the desire to purify these proteins in a form resembling the endogenous proteins, a baculoviral expression system was therefore employed to over-express them.

3.1.2 Baculovirus life cycle and expression system

The *Autographa californica* multiple nuclear polyhedrosis virus (AcMNPV) is the baculovirus most commonly used to express exogenous proteins. This large, enveloped, double-stranded DNA virus enters insect cells by adsorptive endocytosis and viral replication begins 0.5-6 hours post-infection. Between 6 and 12 hours post-infection, extracellular viral (EV) particles begin to bud off from an infected cell which serves to infect neighbouring cells. At around 20-48 hours post-infection, transcription of nearly all viral genes ceases except for the

polyhedrin and p10 genes, which are transcribed at a high rate. Polyhedrin is the main component of the proteinaceous viral occlusion bodies that sequester and protect virus particles from proteolytic inactivation when the infected insect cells lyse. However, expression of polyhedrin was found to be nonessential for EV-mediated infection or replication of the virus (Weyer et al., 1990). Similarly, a gene known as p10, thought to mediate nuclear membrane disintegration and play a role in occluded viral envelope formation, was also found to be dispensable for EV infection and replication (Smith et al., 1983; Vlak et al., 1988; Williams et al., 1989). Thus baculovirus expression systems have been designed where the coding sequences of the polyhedrin and p10 genes have been deleted from the viral genome and their promoters used to over-express a desired exogenous gene to produce large amounts of the target protein. In this study I make use of such a baculoviral expression system to over-express Tum and Pbl both individually and together in a eukaryotic cell environment.

3.2 Results

3.2.1 Over-expression and purification of Tum and MBPTum

In order to over-express Tum, genes encoding two recombinant proteins were constructed. The first encoded a full length protein containing a C-terminal Histidine (His) tag which would permit the over-expressed protein to be purified by affinity chromatography (referred to as Tum, Figure 3.1A). Previous attempts to over-express Tum in bacteria resulted in protein that was almost exclusively insoluble (R. Saint personal communication). Although over-expression in insect

Figure 3.1 ***Schematic diagram of the various fusion proteins over-expressed in High Five insect cells***

The domains, tags, protease cleavage sites and predicted molecular weight for each protein is indicated for Tum (**A**), MBPTum (**B**), Pbl^{fl} (**C**), $Pbl^{N\text{-}term}$ (**D**) and $Pbl^{C\text{-}term}$ (**E**).

A Tum (71kDa)

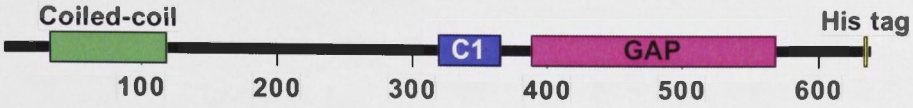

B MBPTum (117kDa)

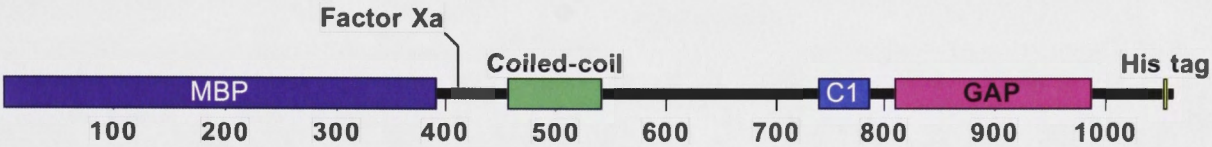

C Pbl^{fl} (97kDa)

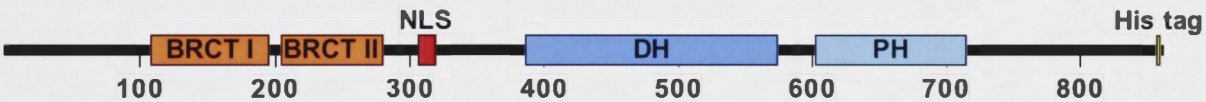

D $Pbl^{N\text{-}term}$ (43kDa)

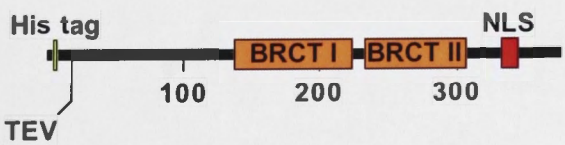

E $Pbl^{C\text{-}term}$ (60kDa)

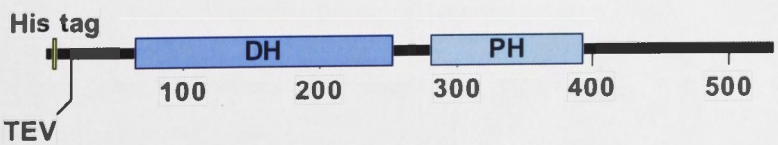

cells can often alleviate such problems, I decided to increase the likelihood of producing soluble protein through the use of a different tag. Maltose binding protein (MBP) tags have been regularly employed to improve the yield, solubility and assist in the correct folding of proteins produced in several over-expression systems (reviewed by Smyth et al., 2003). Therefore, a second recombinant protein was constructed which incorporated a MBP tag fused to the N-terminal end of Tum in addition to a C-terminal His tag (referred to as MBPTum, Figure 3.1B). The resulting MBPTum recombinant protein also contained a Factor Xa protease cleavage site between the MBP tag and Tum. Factor Xa recognises the amino acid sequence I-D/E-G-R and cleaves after the arginine residue. This recognition sequence is not found in Tum and allows removal of the MBP tag following purification. The strong p10 promoter was used to drive of expression of both recombinant proteins.

Western blot analysis was used to assess over-expression of Tum and MBPTum, as the volume of lysis buffer needed to achieve efficient cell lysis precluded the detection of the over-expressed protein in cell lysates using the traditional protein gel stain: coomassie brilliant blue (referred to subsequently as coomassie). As shown in Figure 3.2A and B while some soluble Tum protein was produced, the majority of the protein was in the insoluble fraction. By comparison, the recombinant MBP tagged Tum was not only expressed at higher levels in cell lysates but was also considerably more soluble (Figure 3.2C and D). Since harvesting cells at a later time point did not result in a significant increase in the amount of protein produced (compare 48 to 72 hrs post-infection (pi) samples in Figure 3.2A-D) cells were routinely harvested 48hrs post-infection.

The next step was to determine whether significant amounts of the expressed protein could be purified by affinity chromatography.

Affinity chromatography is an approach often used as an initial purification step due to its ability to capture and purify a high percentage of an over-expressed protein. In the case of His tagged proteins, positively charged nickel ions are immobilized on a nitrilotriacetic acid (NTA) matrix. Recombinant proteins with a string of six negatively charged Histidine residues (His tag) bind to the nickel ions as the cell lysate is passed over the matrix. Bound proteins are eluted by increasing the concentration of imidazole, a chemical that competitively binds to the nickel resulting in desorption and elution of the protein from the matrix. Since the initial expression trials indicated that the amount of soluble Tum produced was poor, subsequent purification attempts focused on the more soluble MBPTum protein.

During protein purification, efforts were made to try and minimise protein degradation by performing all experimentation at 4°C, using several potent protease inhibitors (see 2.1.13), and minimising contact time. Numerous attempts were made to purify MBPTum by affinity chromatography using an AKTA Fast Protein Liquid Chromatography (FPLC) system. However, the yields of purified protein obtained were repeatedly low despite scaling up to 500ml cultures where >$8x10^8$ cells were lysed for each purification attempt. Figure 3.2E depicts the elution fractions of one such purification attempt where although MBPTum can be detected via western blot analysis (lower panel), no significant MBPTum protein band could be identified in the corresponding coomassie

Figure 3.2 ***Representative example of over-expression trials for Tum and MBPTum and affinity purification of MBPTum***

A-D. Western blot detection of Tum and MBPTum expression in High Five insect cells harvested 48 or 72 hours post infection (pi) using rat anti-Tum antibodies. **A,B**. A small amount of Tum was detectable in the soluble cell lysate (**A**, arrowhead) with the majority of the protein being insoluble (**B**, arrowhead). **C,D**. An increase in solubility was observed with addition of the MBP tag on Tum (**C**, arrowhead) although a large portion still remained insoluble (**D**, arrowhead). **E**. Elution fractions of over-expressed MBPTum post affinity purification were analysed by SDS polyacrylamide gel electrophoresis and either stained with coomassie (upper panel), or analysed by western blotting (lower panel). Small amounts of MBPTum were only detectable through western blot analysis (arrow).

10µl of a $2x10^6$ cells/ml lysate was loaded per well for A-D. 20µl of 1ml affinity purified eluates loaded per well in E. M, protein molecular weight marker lane with sizes shown in kDa; - , uninfected High Five cells.

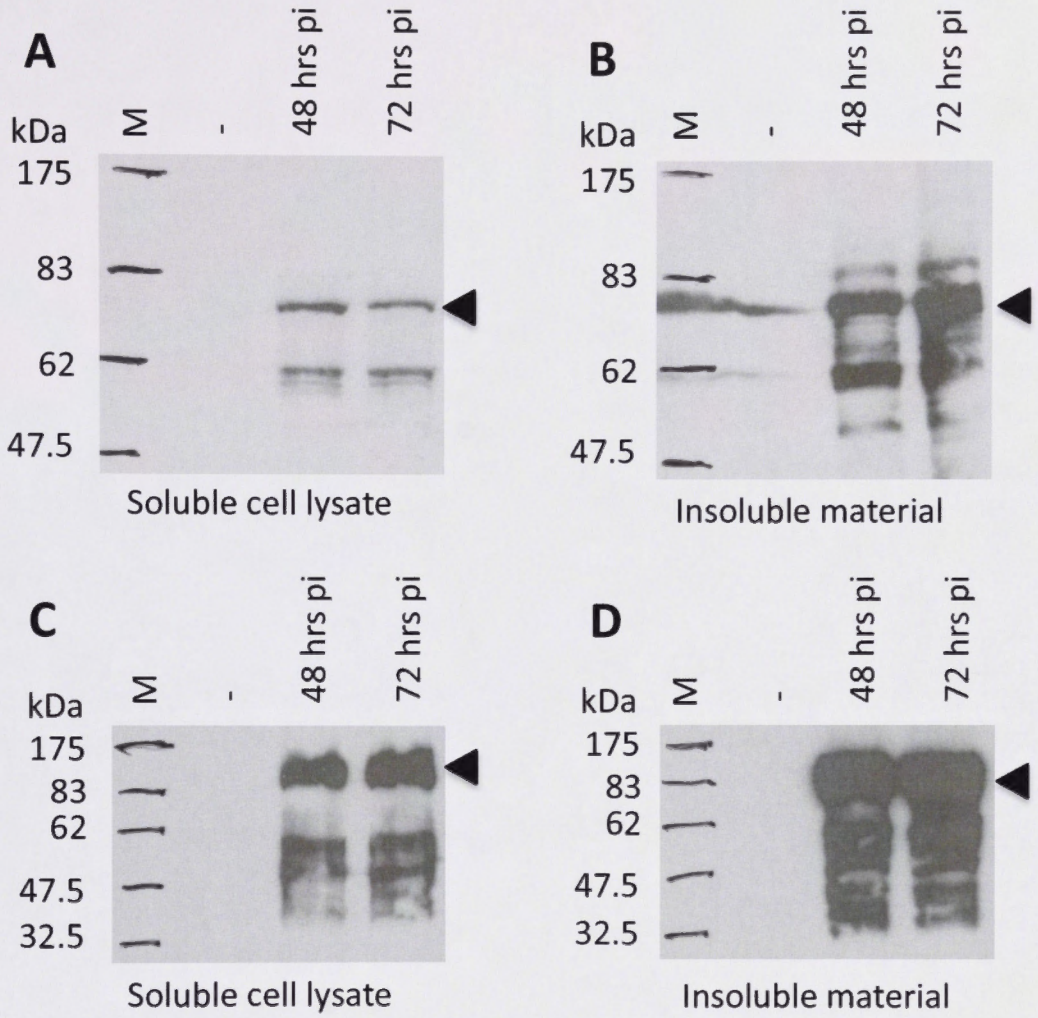
A
kDa
M
-
48 hrs pi
72 hrs pi
175
83
62
47.5
Soluble cell lysate
B
kDa
M
-
48 hrs pi
72 hrs pi
175
83
62
47.5
Insoluble material
C
kDa
M
-
48 hrs pi
72 hrs pi
175
83
62
47.5
32.5
Soluble cell lysate
D
kDa
M
-
48 hrs pi
72 hrs pi
175
83
62
47.5
32.5
Insoluble material

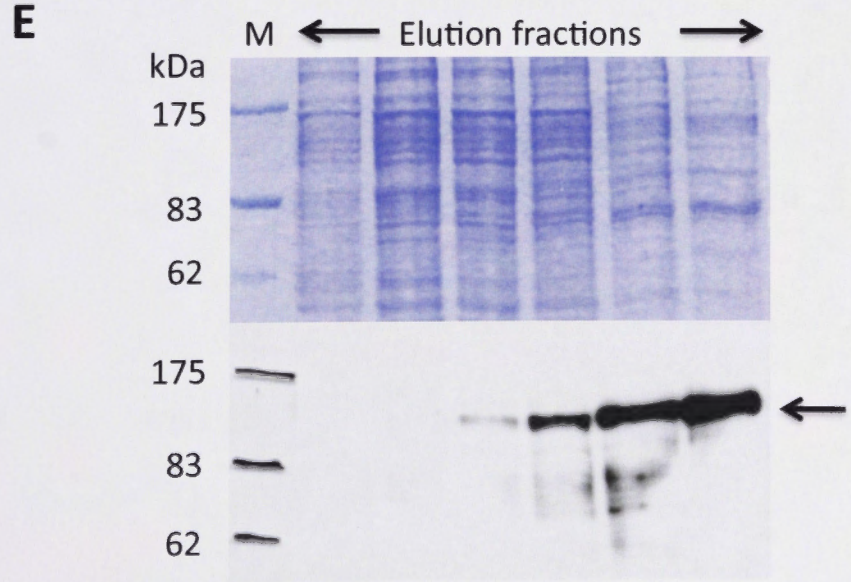
E
M
Elution fractions
kDa
175
83
62
175
83
62

stained protein gel (upper panel). Thus even though using an MBP tag improved the solubility of MBPTum, it was not possible to purify enough protein for structural studies. Therefore, purification efforts were abandoned in favour of similar efforts with Pbl, which, as will be shown in the following sections, was more amenable to over-expression and purification attempts.

3.2.2 Dual over-expression of Pbl and MBPTum

An ambitious aim in the over-expression of Tum and Pbl was to see if the proteins might purify as a complex. Since the amount of soluble MBPTum expressed was much greater than that of Tum (Figure 3.2A and C), full length *pbl* (referred to as *pbl*^{fl}) and *MBPtum* were cloned into a baculovirus expression vector that enabled co-expression of the two proteins by the polyhedrin and p10 promoters respectively. Unfortunately, while over-expression trials again detected a moderate amount of soluble and insoluble MBPTum (Figure 3.3A and C), very little Pbl^{fl} was detectable in the soluble cell lysate and was completely absent from the insoluble material (Figure 3.3B and D). Thus even if Pbl and Tum were capable of forming a complex in this over-expression system, the amount of purified protein required for structural or functional studies was not obtainable. Therefore dual over-expression attempts were abandoned.

3.2.3 Over-expression, purification and crystallization trials with Pbl^{fl}

To over-express a full length Pbl protein the coding sequence of *pbl* was fused to a sequence encoding a C-terminal His tag (encoding a protein referred to as Pbl^{fl},

see Figure 3.1C). This was cloned into a baculovirus expression vector placing *pblᶠˡ* downstream of the powerful polyhedrin promoter. Over-expression trials showed that a significant amount of Pblᶠˡ was produced in a soluble form with a minority of the protein being sequestered in the insoluble material (Figure 3.4A and B). As harvesting cells at a later time point did not increase the amount of protein produced, cells were routinely harvested 48 hours post-infection. Affinity chromatography was chosen as an initial purification strategy due to its ability to capture a high percentage of an over-expressed protein. Using this technique, an average of 6.8mg of Pblᶠˡ per $1x10^8$ cells was captured (Figure 3.4C). Although Pblᶠˡ was the dominant protein eluted from the column, to obtain a sample pure enough for crystallization trials a second purification strategy, ion exchange chromatography, was employed.

Ion exchange chromatography separates molecules according to the strength of their overall ionic interaction with a solid phase matrix. By manipulating buffer conditions, molecules of greater or lesser ionic character can be bound to or dissociated from the matrix. This is most commonly done by altering the salt concentration of the buffer passed over the matrix. The pH at which a protein has a net neutral charge is called the isoelectric point (pI). When a protein is exposed to a pH below its pI it will carry a net negative charge and bind to a cation exchanger. Conversely, a protein will carry a net positive charge when exposed to a pH above its pI and bind to an anion exchanger. Pblᶠˡ has a predicted isoelectric point of 6.9 (MultiIdent, see 2.2.17) and so can be purified by either cation or anion exchangers depending on the buffer used. Desalting columns were used to exchange the buffer of affinity purified Pblᶠˡ for an

Figure 3.3 ***Representative example of co-expression trials for MBPTum and Pbl[fl]***

Western blot analysis of co-over-expression of MBPTum and Pbl in High Five insect cells. **A,B.** Although a moderate amount of MBPTum was detected in the soluble cell lysate 72 hours post infection (pi) (A, arrowhead) the amount of Pbl[fl] expressed was small (B, arrowhead). **C,D.** MBPTum is also detected in the insoluble material (C, arrowhead) but no insoluble Pbl is evident in the insoluble material (D).

Blots **A** and **C** were probed with an antibody recognizing Tum, blots **B** and **D** were probed with an anti Pbl antibody. 10µl of a $2x10^6$ cells/ml lysate was loaded per well.
M , protein molecular weight marker lane with sizes shown in kDa;
- , uninfected High Five cells.

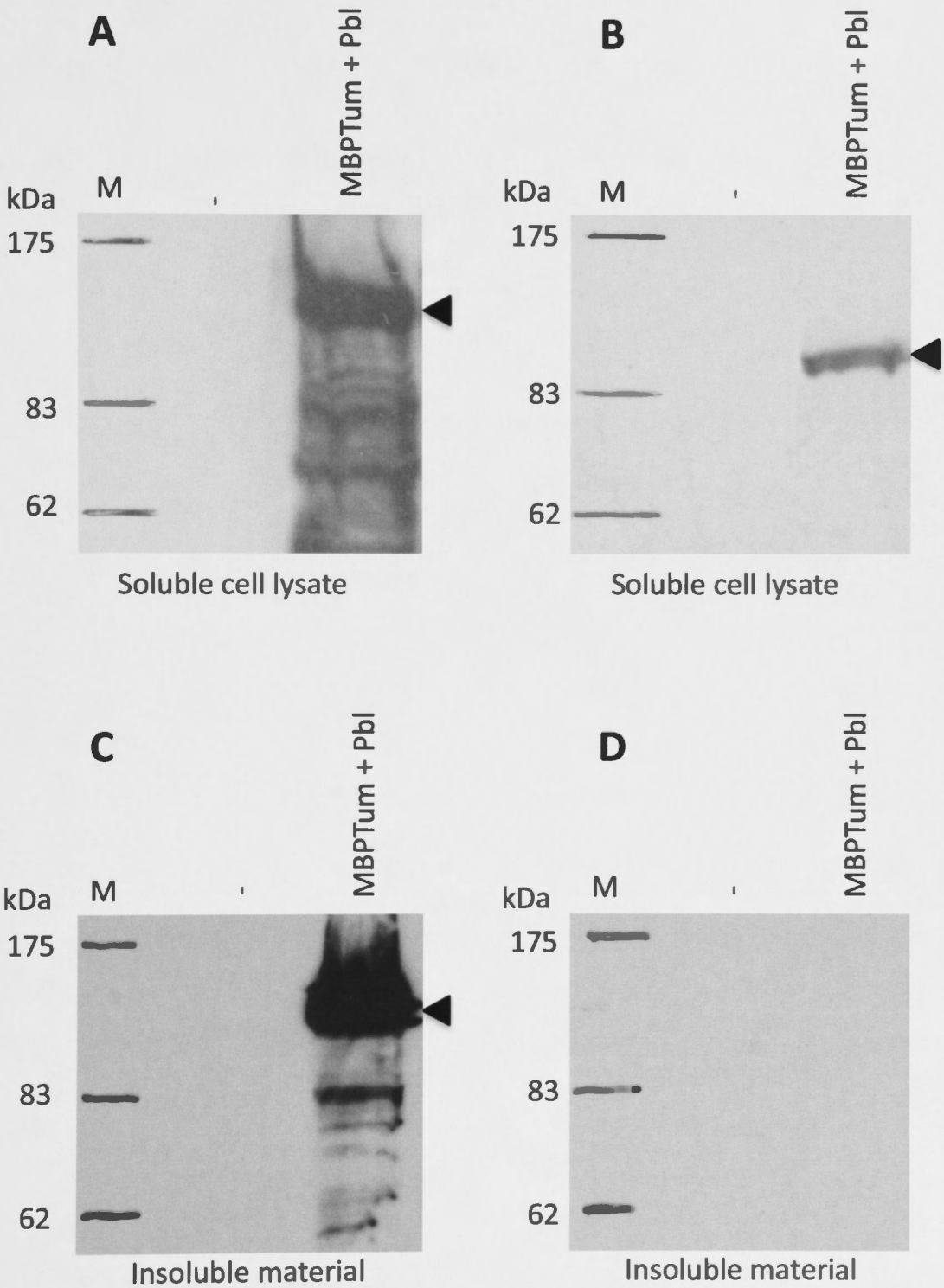
A
MBPTum + PbI
kDa
M
175
83
62
Soluble cell lysate
B
MBPTum + PbI
kDa
M
175
83
62
Soluble cell lysate
C
MBPTum + PbI
kDa
M
175
83
62
Insoluble material
D
MBPTum + PbI
kDa
M
175
83
62
Insoluble material

Figure 3.4 ***Representative example of a over-expression trial and affinity purification of Pbl^{fl}***

A and **B**. Western blot analysis of over-expression trials for Pbl^{fl} in High Five insect cells harvested 48 or 72 hours post infection (pi). A significant amount of Pbl^{fl} was detected in the soluble cell lysate (**A** arrowhead) while insoluble Pbl^{fl} made up a small fraction of the total expressed protein (**B** arrowhead). **C**. The wash and elution fractions collected post affinity purification were run on polyacrylamide gels and coomassie stained. A substantial amount of Pbl^{fl} was purified (arrow). **D**. The Pbl^{fl} sample prior to loading (pre-load) and first eluted fraction from a HiTrap Q FF anion exchanger column. Pbl^{fl} did not bind to the column and elutes in the initial wash fraction.

10µl of a 2x10^6 cells/ml lysate was loaded per well for **A** and **B**. 20µl of 1ml affinity purified eluates loaded per well in **C**. Blots were probed with an anti Pbl antibody. M , protein molecular weight marker lane with sizes shown in kDa; - , uninfected High Five cells.

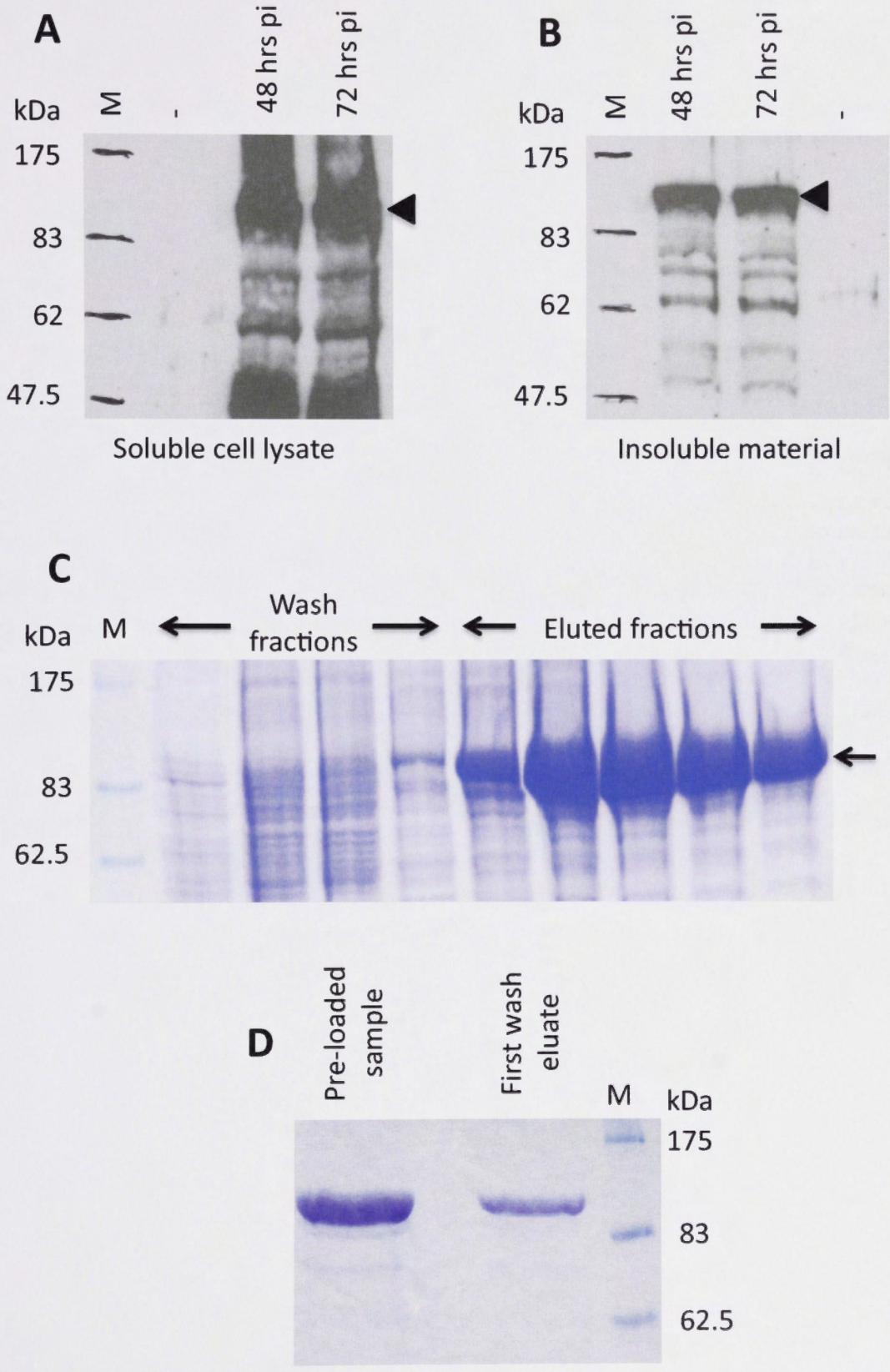
A
kDa
M
-
48 hrs pi
72 hrs pi
175
83
62
47.5
Soluble cell lysate
B
kDa
M
48 hrs pi
72 hrs pi
-
175
83
62
47.5
Insoluble material
C
kDa
M
Wash fractions
Eluted fractions
175
83
62.5
D
Pre-loaded sample
First wash eluate
M
kDa
175
83
62.5

appropriate anion exchange buffer. Thus the pH of affinity purified Pbl^{fl} samples were adjusted to 8, 8.5, 9 or 9.5 for use with a sepharose Q anion exchange resin. Using buffers with a pH above these values was avoided due to the potential deleterious effects extreme pH can have on the three dimensional structure of proteins. Unexpectedly, Pbl^{fl} did not bind to the resin as predicted, instead eluting from the column in the initial wash fractions (Figure 3.4D). No Pbl^{fl} could be detected in any elution fractions from the anion exchanger column (data not shown). Less protein appeared in the first wash compared with the pre-loaded sample due to the dilution of the protein sample following purification.

The pI of a protein can be altered by post-translational modification and/or protein-protein interactions. Although such events may have contributed to a difference between the predicted and genuine pI of Pbl^{fl}, it is strange that despite using high pH buffers, Pbl nonetheless could not be induced to bind to the column matrix. Therefore, gel filtration (i.e. size exclusion chromatography) was used as an alternative approach to further purify Pbl^{fl}.

Gel filtration uses a porous resin material to separate molecules based on their size. Large molecules are excluded from the resin pores while small molecules enter the tiny spaces, resulting in a longer path through the column and thus later elution. As previously mentioned, studies have suggested that Ect2 can oligomerise in vivo (Kim *et al.*, 2005). As it was possible that Pbl may also oligomerise, a Sephacryl S300 high resolution gel filtration column was used as it would allow the purification of Pbl^{fl} oligomers. Eluted fractions containing Pbl^{fl} from several affinity chromatography purifications were combined, concentrated

and loaded onto the S-300 column. A chromatogram of one such purification run is shown in Figure 3.5A. The initial large peak indicates that the void volume of the column has been reached. The void volume refers to the volume of buffer that needs to pass through the column in order to completely replace all the liquid within the column. Proteins that are too large to fit within the pores of the column matrix elute at this point. Thus a substantial amount of large proteins or complexes were separated from Pbl^{fl}. As seen in the Comassie stained protein gel (Figure 3.5B), the majority of Pbl^{fl} was detected in fraction A6, in addition to some lower molecular weight proteins. Western blot analysis using both a Pbl and His tag specific antibody identified these smaller molecular weight proteins as Pbl^{fl} breakdown products (Figure 3.5C and D). Thus apart from the breakdown products, the gel filtered Pbl^{fl} sample appeared to be largely free of other contaminating proteins. Although the Pbl breakdown products constitute heterogeneity in the protein sample, it was possible that these products remained part of Pbl oligomeric structures and were only being separated by the SDS gel electrophoresis process. Furthermore, intact Pbl^{fl} was by far the predominant component of the gel filtered protein sample. Therefore, it was decided to perform crystallization trials with the A6 gel filtered Pbl^{fl} protein.

Very high protein concentrations (≥10mg/ml) are required for crystallization, but many proteins will precipitate out of solution when highly concentrated. Pbl^{fl} proved amenable to concentration allowing two samples of different concentrations to be used for crystallisation trials, one concentrated to 10mg/ml the other to 26mg/ml. Trials were performed using a variety of pH, salt, polymer and neutralized organic acid mixtures (see 2.2.17). Unfortunately,

Figure 3.5 Gel filtration of affinity purified Pbl^{fl}

A. Chromatogram showing an elution profile of concentrated and affinity purified Pbl^{fl} run on a S300 gel filtration column. The magenta line represents the absorbance at 280nm measured in mAU (milli Absorbance Units, y-axis) and indicates elution of protein/s from the column. The volume of buffer (ml) passing through the column is shown on the x-axis, and the 10ml fractions collected are shown in red (A1-A12). **B**. Collected fractions were resolved on SDS polyacrylamide gels and coomassie stained. The majority of Pbl^{fl} eluted in fraction A6. The same fractions were analysed by western blotting using antibodies recognizing the His tag (**C**) and Pbl (**D**) which confirmed the presence of Pbl^{fl} and several breakdown products.

10µl of 10ml gel filtered eluates loaded per well in **B-D**. The western blot probed with the His antibody in **C** was stripped, and re-probed with an anti Pbl antibody. M , protein molecular weight marker lane with sizes shown in kDa; A4-A7, the 10ml fractions depicted in the chromatogram that were collected for further analysis.

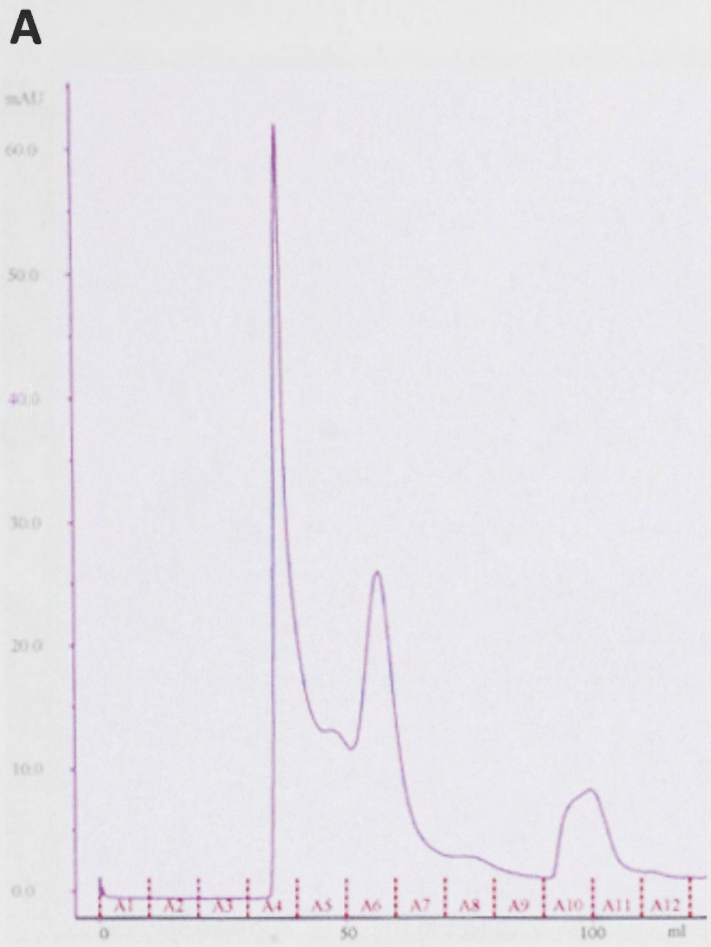
A
mAU
60.0
50.0
40.0
30.0
20.0
10.0
0.0
A1
A2
A3
A4
A5
A6
A7
A8
A9
A10
A11
A12
0
50
100
ml

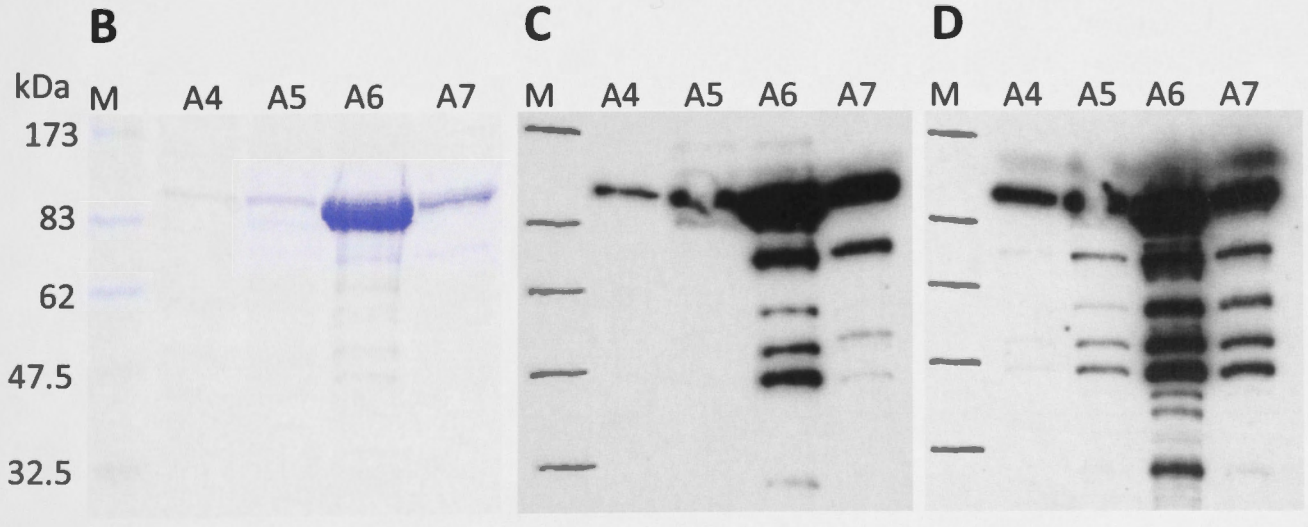
B
C
D
kDa
M
A4
A5
A6
A7
173
83
62
47.5
32.5

no crystal formation could be observed after several weeks under any of the conditions trialled. The plates were inspected periodically over the following months as crystals can form as proteins breakdown into smaller components, but no crystal formation could be detected.

In an attempt to use the over-expressed and purified Pbl^{fl} protein to identify phosphorylated residues, a mass spectrometry analysis was performed on the gel filtered sample. To this end, a protein gel was run using high concentrations of the filtered Pbl^{fl} to ensure that enough of the lower molecular weight proteins would be present to permit their analysis. Many of the bands from the corresponding coomassie stained gel were extracted and analysed by mass spectrometry (Figure 3.6 arrows). Samples were subjected to both protein identification, to identify any remaining contaminating proteins, and phosphopeptide analysis to identify phosphorylated residues of Pbl^{fl}. Regrettably, only one phosphorylated peptide was detected but the peptide sequence was unable to be matched back to its corresponding protein. Several of the small molecular weight protein bands were identified as break down products of Pbl, but interestingly a Heat shock protein 70 cognate 4 (Hsc70) and a Ras GTPase activating protein SH3 domain Binding Protein (G3BP) known as Rasputin (Rin) were also detected. This suggested a possible interaction of Hsc70 and Rin with Pbl^{fl}.

In any case, although Pbl^{fl} was the main protein within the gel filtered sample, the identification of Hsp70 and Rasputin showed that it was not devoid

of all contaminating proteins. To obtain pure Pbl protein for structural studies, a final attempt was made to over-express the individual N- and C-terminal halves.

3.2.4 Over-expression and purification of $Pbl^{N\text{-}term}$ and $Pbl^{C\text{-}term}$

As highly purified Pbl^{fl} proved difficult to obtain, an alternative, although less desirable, approach was taken. It is often possible to synthesize, purify and determine the structure of specific protein domains. Pbl exhibits a number of such domains, particularly the N-terminal BRCT domains and the C-terminal DH-PH domains. To maximise the chance of generating peptides with domain structure, the sequence of Pbl was carefully scanned for secondary structures using the PSIpred prediction program (see 2.2.17). A region predicted to have reduced secondary structure was apparent between the NLS and DH domain (see Fig. 3.1). For this reason, expression constructs encoding the protein regions N-terminal and C-terminal to this sequence were constructed. One construct encoded the sequences N-terminal to this site (amino acids 1-349), referred to as $Pbl^{N\text{-}term}$, containing the two BRCT domains and NLS, while the other construct encoded the sequences C-terminal to this site (amino acids 350-853), referred to as $Pbl^{C\text{-}term}$, containing the PH and DH domains (Figure 3.1D and E). To facilitate the purification of $Pbl^{N\text{-}term}$ and $Pbl^{C\text{-}term}$, each construct contained sequences encoding an N-terminal His tag. To ensure that the His tags did not interfere with the structure of the domains, sequences encoding a Tobacco Etch Virus (TEV) protease cleavage site was added between the His tag and the Pbl protein (Figure 3.1D and E). The TEV protease is a highly specific enzyme that recognises the amino acid sequence E-X-X-Y-X-Q-G/S, where X can be any amino acid. Cleavage occurs between the Q-G or Q-S dipeptide (Carrington and Dougherty, 1988). This

Figure 3.6 Mass spectrometry analysis of gel purified Pbl^{fl}

The A6 elution fraction of gel filtered Pbl^{fl} was subjected to SDS polyacrylamide gel electrophoresis. To ensure that there was enough of the lower molecular weight proteins for mass spectrometry analysis, 0.9mg of protein was loaded onto the gel. The protein bands present were excised and subjected to mass spectrometry analysis (arrows) to identify phosphorylated residues within Pbl and any contaminating proteins that persisted after gel purification. Bands successfully identified by mass spectrometry are labeled and include Pbl breakdown products, Hsp70 and the RasGAP SH3 binding protein Rasputin. The protein bands excised that could not be identified are shown by unlabelled arrows.

M , protein molecular weight marker lane with sizes shown in kDa.

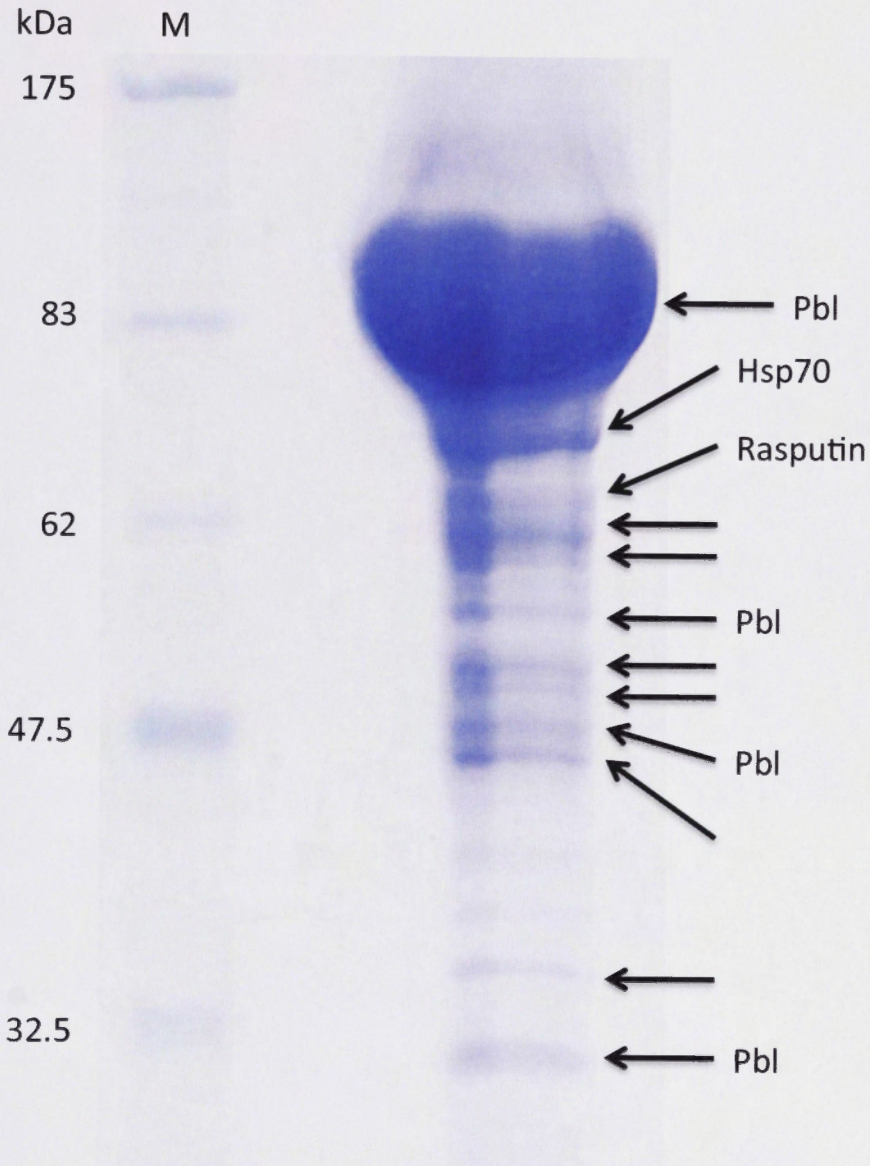
kDa
M
175
83
62
47.5
32.5
Pbl
Hsp70
Rasputin
Pbl
Pbl
Pbl

recognition sequence does not occur in either $Pbl^{N\text{-}term}$ or $Pbl^{C\text{-}term}$ enabling cleavage of the introduced site without cleavage anywhere else in the expressed proteins. A second round of His tag affinity purification after TEV cleavage should result in contaminating proteins originally co-purified with the over-expressed protein again binding to the column while the now untagged target protein passes through unhindered. Since the recombinant TEV protease contains a His tag it is removed by binding to the nickel resin. Using this strategy, the purified protein should be free of contaminating proteins.

Small scale expression of the recombinant proteins showed that significant amounts of soluble $Pbl^{N\text{-}term}$ were produced (Figure 3.7A and B). Although $Pbl^{C\text{-}term}$ was also expressed in a mainly soluble form, the total amount of protein produced was less than that of $Pbl^{N\text{-}term}$ (Figure 3.7C and D). As Tum bound to Pbl in its N-terminal region and due to the higher level of expression of $Pbl^{N\text{-}term}$ compared with $Pbl^{C\text{-}term}$, it was decided to pursue the purification of $Pbl^{N\text{-}term}$ only. For the over-expression of $Pbl^{N\text{-}term}$, insect cells were harvested 48 hours post-infection. Initial affinity chromatography purification experiments resulted in the isolation of an average of 9.7mg of $Pbl^{N\text{-}term}$ per $1x10^8$ cells (Figure 3.8A arrow). However, contaminants were still present necessitating further purification (Figure 3.8A asterisks). To further purify the protein, TEV mediated His tag removal followed by a second round of affinity purification was carried out.

$Pbl^{N\text{-}term}$ eluates from several affinity purification experiments were combined, concentrated and desalted into a suitable buffer for TEV mediated His

tag removal. The TEV protease was added to the protein solution and the reaction monitored by periodically removing samples to look for a size shift that would indicate His tag cleavage. The reaction was determined to have reached completion once the larger His tagged $Pbl^{N\text{-}term}$ species was no longer visible (Figure 3.8B). The cleaved $Pbl^{N\text{-}term}$ sample was again affinity purified and the eluted fractions resolved by SDS PAGE, coomassie staining and western blot analysis. The coomassie stain revealed that $Pbl^{N\text{-}term}$ co-purified with some large molecular weight contaminating proteins (Figure 3.8C arrow and asterisks). Western blot analysis using a His specific antibody indicated that a small amount of His tagged $Pbl^{N\text{-}term}$ also eluted in the first two fractions. These proteins are barely visible on the coomassie stained gel (Figure 3.8C arrowheads). These results were unexpected as the contaminants and any residual His tagged $Pbl^{N\text{-}term}$ should have bound to the matrix as they did in the initial affinity purification. This was not caused by column saturation as 62mg protein was loaded onto a column that had a binding capacity of at least 100mg. The inability to remove the contaminants or remaining tagged $Pbl^{N\text{-}term}$ could have been due to hydrophobic or precipitated proteins clogging the column or a lack of sufficient nickel ions to bind appropriately charged proteins in a column that had been reused multiple times. Therefore, the column was stripped, cleaned and recharged to remove all proteins and ensure that the matrix was fully charged. The $Pbl^{N\text{-}term}$ fractions collected from the previous affinity purification were concentrated and again affinity purified. However the result remained the same; a small amount of tagged $Pbl^{N\text{-}term}$ eluted in the first few fractions and the larger contaminating proteins again co-purified (data not shown). It was surprising that His tagged $Pbl^{N\text{-}term}$ was again detected in the elution fractions. However, a small amount of

Figure 3.7 ***Representative example of over-expression trials for $Pbl^{N\text{-}term}$ and $Pbl^{C\text{-}term}$***

A-D. Western blot analysis of over-expression trials for $Pbl^{N\text{-}term}$ and $Pbl^{C\text{-}term}$ in High Five insect cells harvested 48 or 72 hours post infection (pi). Significant amounts of $Pbl^{N\text{-}term}$ were detectable in the soluble cell lysate (**A** arrowhead) and to a lesser extent in the insoluble material (**B** arrowhead). A moderate amount of $Pbl^{C\text{-}term}$ is detected in the soluble cell lysate (**C** arrowhead) with slightly more being detected in the insoluble material (**D** arrowhead).

10µl of a $2x10^6$ cells/ml lysate was loaded per well. M , protein molecular weight marker lane, sizes are indicated in kDa; - , uninfected High Five cells.

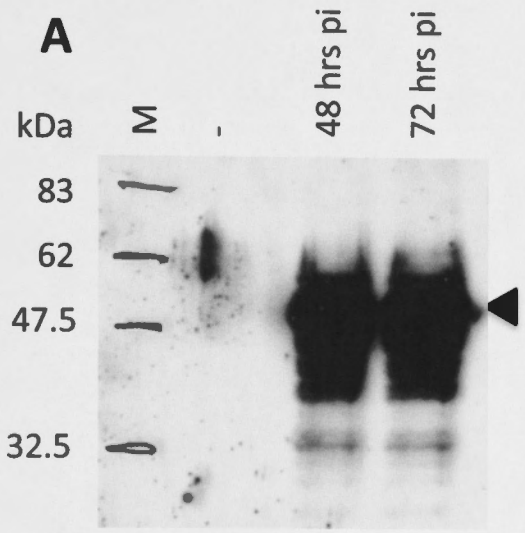

Soluble cell lysate

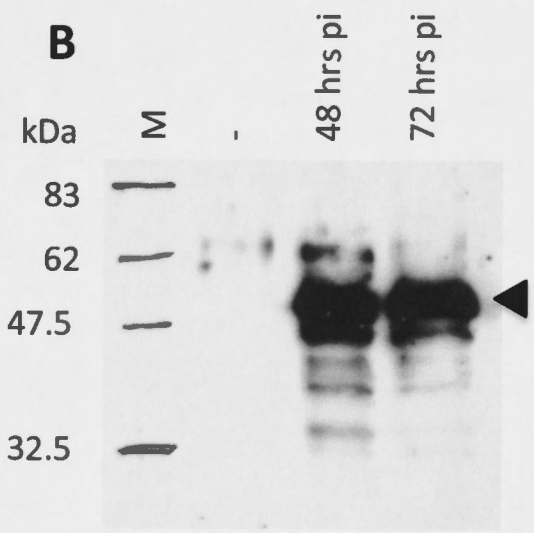

Insoluble material

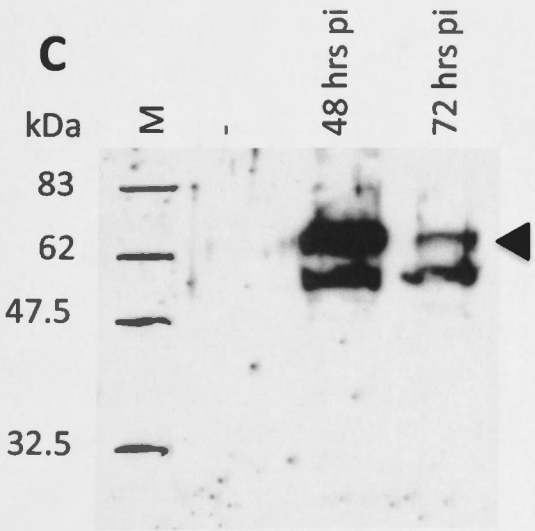

Soluble cell lysate

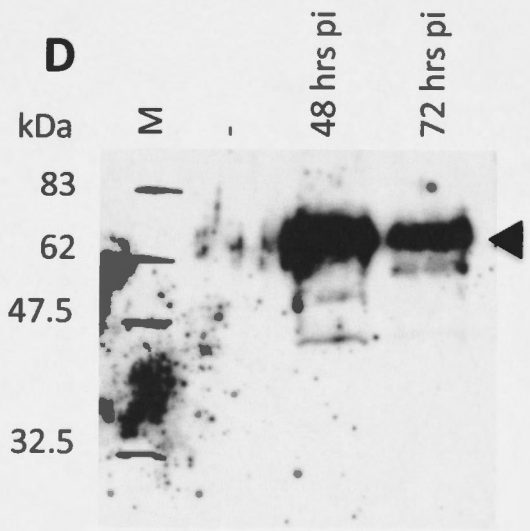

Insoluble material

Figure 3.8 ***Affinity purification of His tagged and TEV cleaved Pbl$^{N\text{-}term}$***

A. Eluted affinity purified fractions of Pbl$^{N\text{-}term}$ were subjected to SDS polyacrylamide gel electrophoresis and stained with coomassie dye. A substantial amount of Pbl$^{N\text{-}term}$ was detected in the elution fractions (arrow) although other contaminating proteins were also present. **B.** Coomassie stained SDS polyacrylamide gel of neat and diluted samples of Pbl$^{N\text{-}term}$ before and after cleavage with TEV protease to remove the His tag. Successful cleavage of the His tag is evident by a decrease in size of Pbl$^{N\text{-}term}$ (compare uncleaved with cleaved lanes). **C.** Coomassie stained SDS polyacrylamide gel (upper panel) and western blot analysis (lower panel) of affinity purified untagged Pbl$^{N\text{-}term}$. Western blots were probed with an antibody recognising the His tag. TEV cleaved Pbl$^{N\text{-}term}$ cannot bind to the affinity purification column and is eluted (arrow). Some uncleaved protein is evident in the first two elution fractions (arrowhead in the coomassie stained gel and western blot). The larger contaminating proteins also elute with Pbl$^{N\text{-}term}$ (asterisks).

10µl of 1ml affinity purified Pbl$^{N\text{-}term}$ eluates were loaded per well for **A** and 10µl of 1.5ml eluates loaded per well for **C**. 290µg and 29µg of uncleaved samples were loaded in neat and 1/10 lanes respectively and 510µg and 51µg protein of cleaved samples loaded in neat and 1/10 lanes respectively for **B**. M , protein molecular weight marker lane, sizes are indicated in kDa.

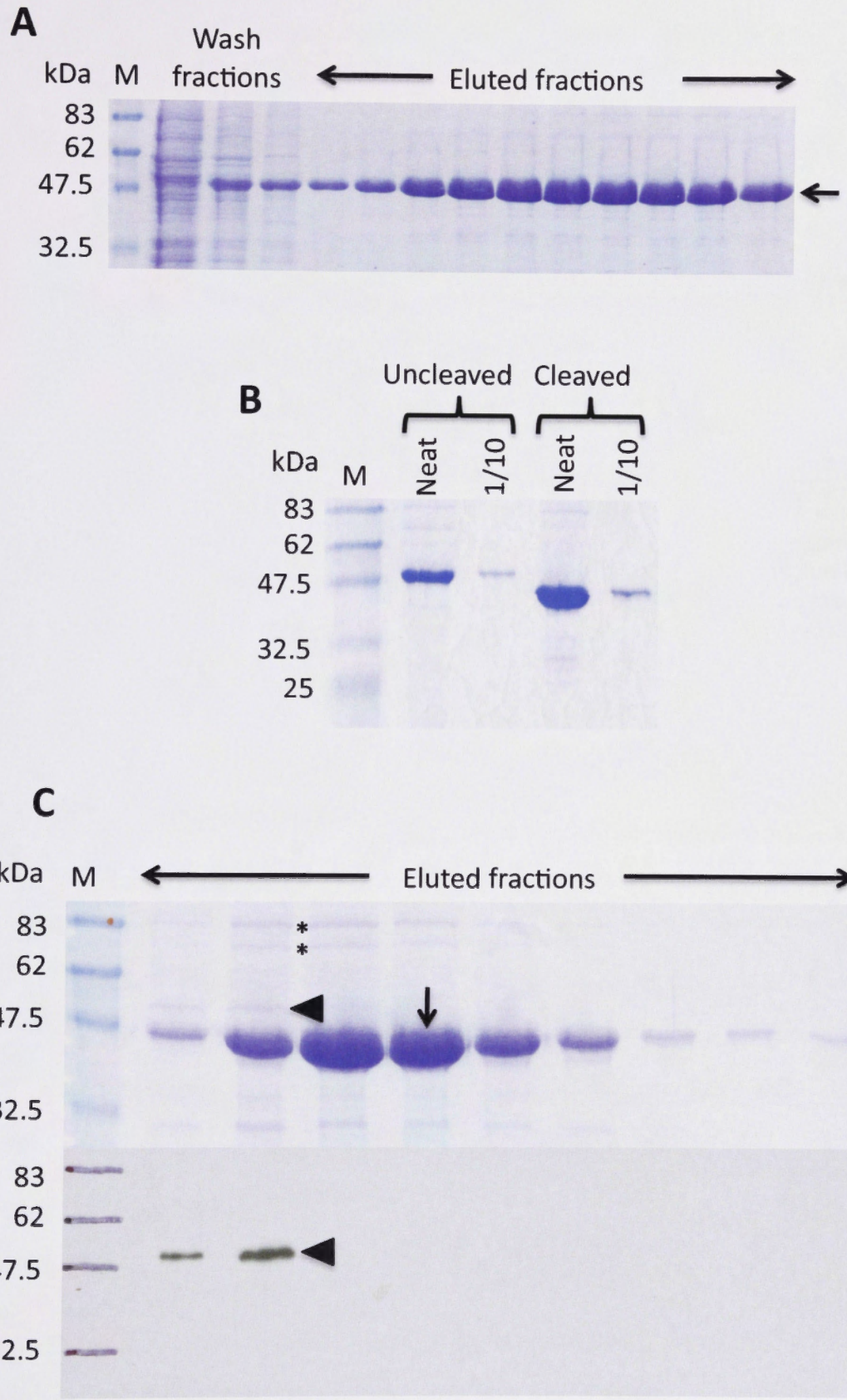
A
kDa
M
Wash fractions
Eluted fractions
83
62
47.5
32.5
B
Uncleaved
Cleaved
Neat
1/10
Neat
1/10
kDa
M
83
62
47.5
32.5
25
C
kDa
M
Eluted fractions
83
62
47.5
32.5
*
*
83
62
47.5
32.5

both Pbl^{fl} and Pbl$^{N\text{-}term}$ were often eluted in the first few washes of all the affinity purifications (see wash fractions in Figure 3.4C and 3.8A). The reason for the premature elution was probably due to the low concentration of imidazole (10mM) present in the wash buffer. This was used to inhibit non-specific binding of unwanted proteins to the column matrix but may have also prevented the binding of some Pbl$^{N\text{-}term}$. It was possible that the larger contaminating proteins co-purified because they interacted with Pbl$^{N\text{-}term}$.

As affinity purification of untagged Pbl$^{N\text{-}term}$ proved ineffective in removing all contaminating proteins gel filtration using a superdex 200 10/300 GL column was used. This column is more suitable for the separation of smaller molecular weight proteins than the S300 column used earlier, and should have separated the cleaved Pbl$^{N\text{-}term}$ from His tagged Pbl$^{N\text{-}term}$ and other contaminants based on differences in their molecular weights.

Affinity purified fractions that contained His tagged Pbl$^{N\text{-}term}$ were discarded and the rest concentrated prior to loading onto the column. The chromatogram from the resulting purification is shown in Figure 3.9A. A coomassie stain showed that Pbl$^{N\text{-}term}$ was present in all the analysed fractions (A7-B12) but was particularly prominent in the later fractions (Figure 3.9B arrow). The low molecular weight proteins were identified as Pbl$^{N\text{-}term}$ breakdown products by western blot analysis (Figure 3.9B far panel and arrowheads). As was the case with Pbl^{fl}, gel filtration failed to yield full length Pbl$^{N\text{-}term}$ free from breakdown products. Unexpectedly, the large molecular weight contaminating proteins (~70-80 kDa) were present in almost every

fraction analysed (Figure 3.9B asterisks) when, because of their size, they should have eluted in the earlier fractions. Even if the contaminants were interacting with $Pbl^{N\text{-}term}$ the increased molecular weight of such a complex (~115-125 kDa) should also have resulted in their efficient separation by size exclusion chromatography. However, the elution profile of the contaminating proteins did not fit either of these possibilities.

In an effort to identify the contaminating proteins that were persistently present after several rounds of purification, a sample from the B3 gel filtrated $Pbl^{N\text{-}term}$ was used for mass spectrometry analysis. The sample was run on a low percentage polyacrylamide gel to try and separate the larger contaminants into distinct bands. Three distinct bands were observed and excised, along with the $Pbl^{N\text{-}term}$ band, and subjected to mass spectrometry protein identification (Figure 3.10 arrows). However, the only protein identified was the $Pbl^{N\text{-}term}$ band, which was confirmed to be Pbl (Figure 3.10 labelled arrow). Regrettably, the identity of the higher molecular weight contaminants remained unknown.

Due to the inability to remove contaminating proteins and to prevent accumulation of degradation products, crystallization trials were not attempted and further efforts to purify the protein could not be conducted because of time limitations.

Figure 3.9 ***Gel filtration of concentrated TEV cleaved Pbl$^{N\text{-}term}$ and analysis of eluted fractions***

A. Chromatogram of a Pbl$^{N\text{-}term}$ sample, derived from combining and concentrating affinity purified TEV cleaved Pbl$^{N\text{-}term}$, run through a Superdex 200 10/300 GL gel filtration column. The blue line represents the absorbance at 280nm measured in mAU (y-axis) and signifies protein eluting from the column. The amount of buffer (ml) that has passed through the column is shown on the x-axis and collected fractions are labeled in red. **B.** Collected fractions post gel purification were run on SDS polyacrylamide gels and coomassie stained. Pbl$^{N\text{-}term}$ was evident in all fractions analyzed (arrow). Larger contaminating proteins are evident in most fractions (asterisks). Western blot analysis using an antibody recognising Pbl (far right) identified the lower molecular weight proteins as Pbl$^{N\text{-}term}$ breakdown products (arrowheads).

10µl of the 1ml gel filtered eluates were loaded per well in **B.** M, protein molecular weight marker lane with sizes shown in kDa. A7-B12 , the fractions depicted in the chromatogram that were collected for further analysis.

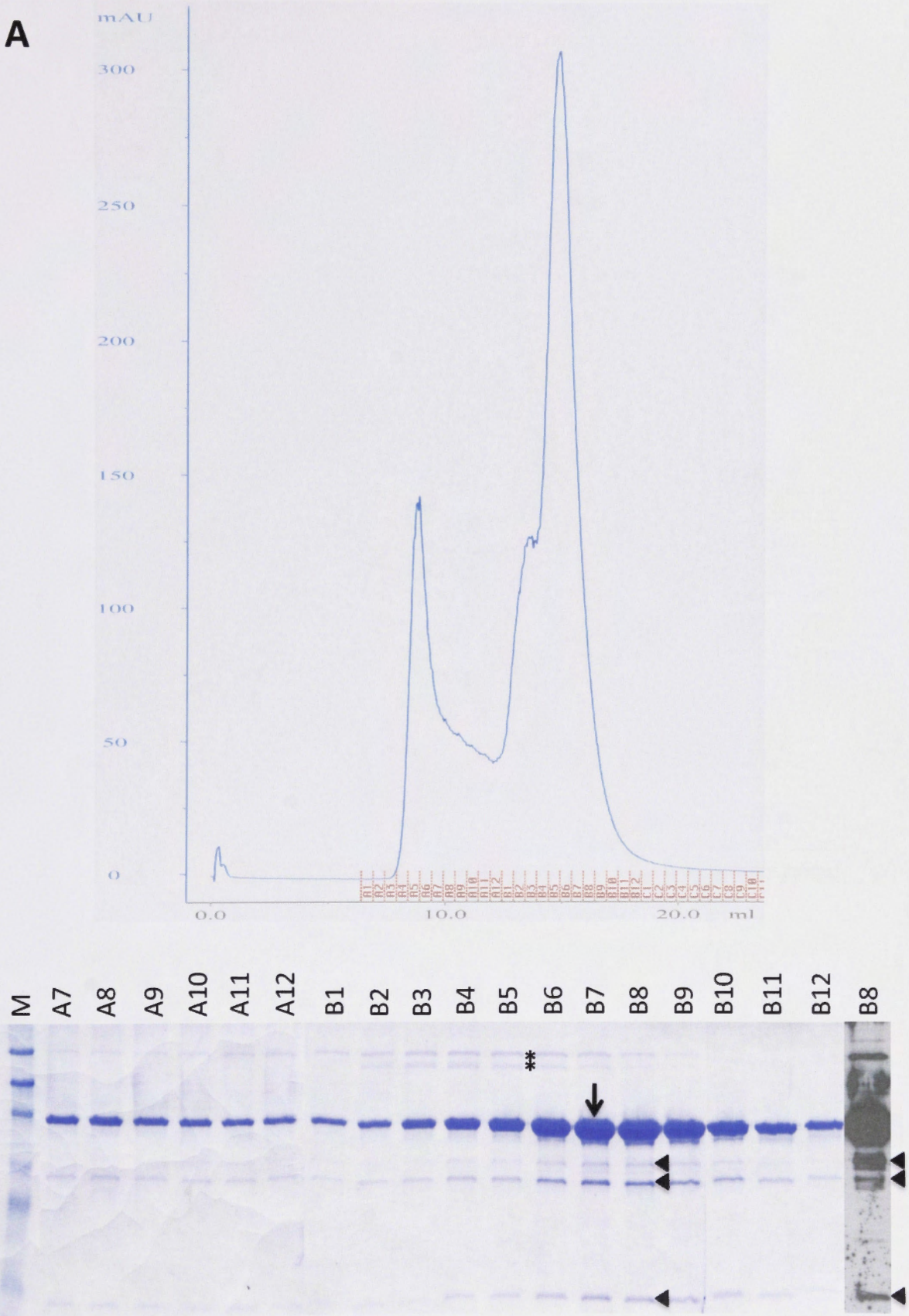
A
mAU
300
250
200
150
100
50
0
0.0
10.0
20.0
ml
B
kDa
M
A7
A8
A9
A10
A11
A12
B1
B2
B3
B4
B5
B6
B7
B8
B9
B10
B11
B12
B8
83
62
47.5
32.5
25
16.5
**

Figure 3.10 ***Mass spectrometry analysis of proteins eluted from gel filtration column.***

$Pbl^{N\text{-}term}$ and contaminating proteins co-eluting from the gel filtration column were run on an SDS polyacrylamide gel and excised for mass spectrometric analysis. $Pbl^{N\text{-}term}$ was confirmed to be Pbl (labeled) but the high molecular weight proteins were not able to be identified by mass spectrometry (unlabeled arrows).

M, protein molecular weight marker lane, sizes are indicated in kDa.
300µg of sample B3 from the gel filtration purification was loaded onto the gel.

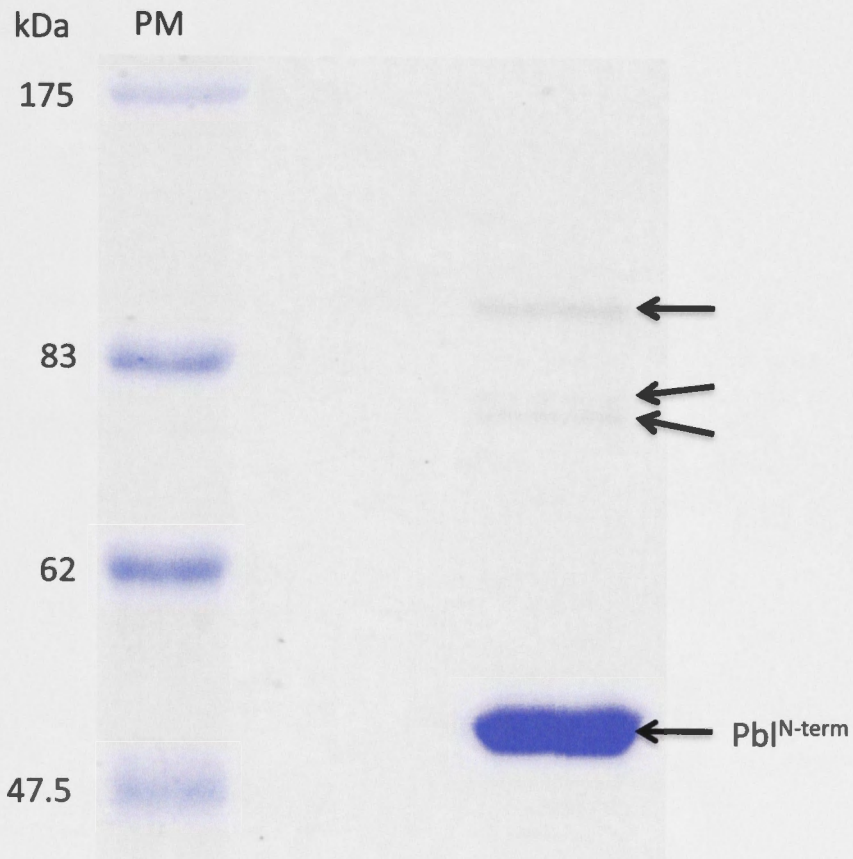
kDa
PM
175
83
62
47.5
PblN-term

3.3 Discussion

This chapter outlines the efforts undertaken to over-express and purify Pbl and Tum. Unfortunately, the majority of the Tum protein was expressed in an insoluble form. Although fusing an MBP tag to Tum resulted in an increase in the total protein expressed and the amount of the soluble form, very little MBPTum could be purified by affinity chromatography. In rare cases, the His tag of recombinant proteins can be sequestered by the tertiary structure of the protein. This possibility could be tested by purifying MBPTum under denaturing conditions to ensure that the His tag is fully accessible. However, this approach was not attempted in this study because denatured MBPTum would then have to have been refolded, which is itself a notoriously difficult process, where the refolding process would need to have been almost 100% effective for structural studies to have succeeded.

Tum may be largely insoluble due to the extensive regions of the protein that are predicted to be unstructured. Such regions can function to allow a conformation to be easily adopted upon binding to a partner. Indeed many interactions have been mapped to different regions of Tum. In the absence of these binding partners, particularly when a protein is over-expressed, there may be a propensity towards aggregation and sequestration within inclusion bodies. Although Pbl also contains regions predicted to be unstructured, the intra- and inter-molecular interactions identified for Ect2 may occur in Pbl and serve to protect Pbl from aggregating. As for $Pbl^{N\text{-}term}$ and $Pbl^{C\text{-}term}$, their small size was probably enough to promote the expression of substantial amounts of soluble protein.

Attempts to isolate a complex of Tum and Pbl through their co-expression failed to yield enough protein to warrant purification efforts. Although a moderate amount of MBPTum was expressed, very little Pbl^{fl} was produced. This poor expression was puzzling as the over-expression of Pbl^{fl}, $Pbl^{N\text{-}term}$ and $Pbl^{C\text{-}term}$ alone produced large amounts of protein. The regulatory elements, such as the promoter and poly-adenylation signal, were the same for all Pbl constructs created despite using different vectors for the expression of Pbl^{fl} alone (pBacPAK8) or with MBPTum (pFastBacDual) (see 2.2.11.1). Therefore, both constructs should have produced similar levels of Pbl^{fl}. Alternatively, there may have been transcriptional competition between the p10 and polyhedrin promoters due to their close proximity that resulted in the low expression of *pbl^{fl}* from the dual expression vector.

Formation of a stable Pbl-Tum complex may also be unlikely in this system due to a requirement for crucial phosphorylation events. Recent work has identified a Plk1 phosphorylation event required to stimulate the Ect2-HsCyk-4 interaction (Burkard et al., 2009; Wolfe et al., 2009). Indeed in the following chapter I also demonstrate a similar requirement for Polo kinase phosphorylation, an event that should be restricted to mitosis and would therefore be unlikely to occur in the baculovirus system where cells cease to proliferate within 24 hours of being infected. In light of these recent data, it is therefore unlikely that a stable Pbl-Tum complex would have formed upon co-expression of the proteins.

Over-expression of both Pbl^{fl} and $Pbl^{N\text{-}term}$ produced large amounts of soluble protein that could be captured and purified by affinity chromatography. A nickel-NTA matrix was chosen for affinity purification due to its ability to capture a high percentage of an over-expressed protein. However, as the purity rather than the yield was more problematic, perhaps a cobalt resin, which offers higher purity but lower yields, could have been used instead. Regardless of the affinity matrix used, further purification would have been required to remove the remaining contaminating proteins and this proved challenging. Ion exchange chromatography using buffers with a wide range of pH values failed to prove useful in the purification of Pbl^{fl}. As mentioned earlier, post-translational modifications and protein-protein interactions can influence the pH of a protein and may have influenced the isoelectric point of Pbl and thus its ability to bind the anion exchanger. However, the range of pH values used should have circumvented any problems caused by a variation in Pbl's isoelectric point. 2D gel electrophoresis could have been performed to identify the true pI of Pbl^{fl} allowing an appropriate column and buffer pH to be utilized for purification by ion exchange chromatography. However, 2D gel electrophoresis is performed under denaturing conditions and therefore does not indicate changes in the pI of a protein due to protein-protein interactions, such as the potential for Pbl to oligomerise.

After gel filtration, purified Pbl samples that predominantly consisted of intact Pbl^{fl} were obtained. Despite the presence of low levels of breakdown products, crystallization trials were attempted with the protein preparation. Unfortunately, protein crystal formation could not be achieved. Although protein

crystals are difficult to obtain even with the best of protein preparations, sample heterogeneity can obstruct the ordered and repetitive protein stacking required for crystal formation. Although mass spectrometry identified contaminants in the Pbl^{fl} gel filtrated sample, they were by far a minority of the total purified protein. Therefore, the heterogeneity produced by the Pbl breakdown products was more likely to be the major impediment to crystal formation. However, producing protein crystals capable of X-ray diffraction is not a trivial matter and can fail for reasons other than the protein preparation purity. It was noted recently that success rates for the crystallization of eukaryotic proteins is only 1–4% (Thornton, 2001).

As mentioned earlier, great effort was taken to try and minimise protein degradation through the use of protease inhibitors, performing experimentation at 4°C, and minimising contact time. However, breakdown products were still evident throughout the purification and were particularly prominent in the more concentrated samples. Even gel filtration, which should have separated the smaller breakdown products from the larger intact proteins, failed to yield purified protein free from degradation products for both Pbl^{fl} and $Pbl^{N\text{-}term}$. Furthermore, the identification of Hsc70 in the Pbl^{fl} sample after gel filtration suggests proper protein folding may have been an issue. Such misfolded protein would suffer from a lack of stability and be prone to degradation. This may explain why breakdown products were so difficult to eliminate and quickly accumulated in purified samples. Therefore, it appears that Pbl is an inherently unstable protein prone to degradation when over-expressed in insect cells.

The purification of $Pbl^{N\text{-}term}$ was also hindered by the presence of some unidentified higher molecular weight contaminants. These contaminants persisted through several rounds of purification; initially co-purifying with affinity purified His tagged $Pbl^{N\text{-}term}$, persisting through several subsequent affinity purifications with untagged $Pbl^{N\text{-}term}$ and then eluting in nearly all the gel filtration fractions. Affinity chromatography using native protein preparations is notorious for the co-purification of contaminants along with the desired target. This is because some proteins will possess a charge that allows them to interact with the nickel ions within the column. To prevent non-specific binding a low concentration of imidazole (10mM) was used in the wash buffer. Perhaps this was enough to permit the elution of the contaminating proteins. Alternatively, there may have been an interaction between the contaminants and $Pbl^{N\text{-}term}$. However the elution profile of the subsequent gel filtration does not fit with this hypothesis. If there was an interaction, the contaminants should have eluted with some $Pbl^{N\text{-}term}$ in a discreet number of early fractions rather than in the broad range observed. Moreover, in the absence of an interaction, the size difference between the contaminants and $Pbl^{N\text{-}term}$ should have allowed their separation. How these contaminating proteins could co-purify with $Pbl^{N\text{-}term}$ through several different purification strategies remains unclear.

Interestingly, mass spectrometry analysis of the gel purified Pbl^{fl} identified the presence of Hsc70 and Rin. Hsc70 is part of the Heat shock protein 70 family of proteins that are involved in the folding and refolding of newly synthesised proteins, the transportation of unfolded proteins, the elimination of non-functional proteins and the presentation of antigens on immune cells

(Guzhova and Margulis, 2006). If co-purification of Hsc70 with Pbl indicates a bona fide interaction, the most likely explanation would be that Hsc70 is required for folding, refolding and/or elimination of unfolded Pbl. It is possible that the over-expression of Pbl^{fl} puts a strain on the protein processing machinery of the cell, resulting in some of the produced protein being misfolded. Protein misfolding could also be exacerbated with the advancement of the baculoviral infection of the host cell resulting in the deterioration of routine cellular functions. Thus it is conceivable that Hsc70 would bind to such misfolded Pbl^{fl} proteins to prevent their irreversible aggregation, and either facilitate refolding or direct degradation of misfolded peptides.

The identification of Rin in the purification product could also suggest a potential interaction of Pbl with Rin. Rin is a RasGAP SH3 binding protein (G3BP), indicating a role in Ras family small GTPase function. There has only been a single published study of the role of Rin in *Drosophila* and its role on the development of the *Drosophila* eye, which is known to require Ras GTPase signalling for the differentiation of all photoreceptors (Pazman et al., 2000). *rin* mutants exhibit defects in photoreceptor recruitment and ommatidial polarisation in the eye. It was found that Rin genetically interacted with the Ras signalling pathway at the level of Ras or above but independent of its downstream effector Raf. The mammalian orthologues of Rin, G3BP1 and G3BP2, have also been characterized and are associated with a number of biological processes including RNA metabolism, cancer progression or maintenance, protein stability and cell differentiation. As for Rin, G3BP1 has been identified as a player in the Ras signalling pathway (Irvine et al., 2004).

Interestingly, in the *Drosophila* study, Rin was also shown to interact genetically with Rho, suggesting that Rin may act as a link between the Ras and Rho signalling pathways. This genetic evidence of a relationship between Rin and Rho signalling and the apparent co-purification of Rin with the Rho regulator, Pbl, is intriguing. It has been reported, although not yet published, that Rin is implicated in actin organization and dynamics during oogenesis (Pazman and Haynes, 2004). This is also consistent with an association between Rin and the Pbl-RhoA pathway. However there is no clear evidence for such a functional link. *rin* mutant cells are able to divide (Pazman et al., 2000), therefore Rin is not an essential component of the cytokinetic Pbl function or there is redundancy in function between Rin and one or more other proteins. The latter is unlikely as there are no paralogs of Rin in the *Drosophila* genome (data not shown).

Consistent with this, a cell division-stimulated association between Pbl and Rin is improbable as baculovirus infected insect cells cease to proliferate within 24 hours of infection. It remains possible, however, that Rin is involved in some other aspect of Pbl function, such as the cell migration activity, a possibility that could be explored by looking for genetic interactions between *rin* and *pbl* alleles.

Given the artificial nature of the expression of Pbl^{n} in the baculoviral cells, it is perhaps not surprising that the mass spectrometry analysis of Pbl^{n} did not identify any phosphopeptides. It is possible that the use of phosphatase inhibitors during purification may have prevented potential phosphatase activity

and increased the chance of identifying more phosphorylated peptides, but the in vivo relevance of such peptides identified in this artificial system would in any case have been doubtful. Phospho-proteome studies recently conducted using *Drosophila* embryo extracts and Kc167 cells have led to the identification of several phosphorylated residues in both Pbl and Tum (Bodenmiller et al., 2007; Zhai et al., 2008). However, these residues are likely to represent the phosphorylation state during interphase, and it is expected that the phosphorylation state would change considerably throughout the cell cycle. Drugs that cause the destabilization of cytoskeletal components or inhibit particular kinases are often used to stage or block mammalian cell lines at a particular phase in the cell cycle. However, these drugs fail to stage *Drosophila* cell lines (R. Saint personal communication). Several recent studies have focussed on the phosphorylation state of proteins at different stages of mitosis in mammalian cell lines (Daub et al., 2008; Dephoure et al., 2008; Malik et al., 2009; Olsen et al., 2010). Sifting through the large volume of data such phosphopeptide screens produce is likely to provide useful clues as to the phosphorylation events that play an important role during cell division.

3.4 Conclusion

High levels of expression of both Tum and Pbl were achieved in this study. However, Tum was found to accumulate in a mainly insoluble form. An alternative approach of expressing Tum fused to an MBP tag resulted in an increase in solubility, but significant amounts of MBPTum were unable to be purified by affinity chromatography. Substantial amounts of Pbl^{fl} and $Pbl^{N\text{-}term}$ were successfully expressed and purified to a high level of homogeneity,

although very low levels of contaminants and degradation products remained detectable. Attempts at crystallization of high purity, high concentration PbI^{fl} protein failed, consistent with the low success rate of such crystallization attempts.

Chapter 4 – The identification of phosphorylation events that stimulate the Pbl-Tum interaction

4.1 Introduction

In contrast to the in vitro experimentation described in the previous chapter, this chapter details an in vivo approach to probe events that stimulate the Pbl-Tum interaction during cytokinesis. Due to the prominent role many kinases play in inhibiting or stimulating interactions or activities during mitosis, I focused on potential phosphorylation events that might effect this interaction. Since two studies identified Plk1 as a key cytokinetic player in mammalian cells, I decided to target potential phosphorylation sites of the *Drosophila* orthologue Polo kinase.

For many years, the involvement of Plk1 in processes such as centrosome maturation, spindle assembly and the stabilization of kinetochore microtubules had prevented an analysis of its role during cytokinesis (Van Vugt and Medema, 2005). However, two separate studies in mammalian cell lines demonstrated that Plk1 was an essential early regulator of cytokinesis. One study used a potent and highly specific Plk1 inhibitor while the other modified the Plk1 protein so that its function could be inhibited with the use of an ATP analogue (Burkard et al., 2007; Petronczki et al., 2007). Both studies found that the equatorial localisation of Ect2 but not HsCyk-4 or MKLP1 was abolished in Plk1 inhibited cells. However, the mechanism by which Plk1 stimulated the Ect2-HsCyk-4 interaction was unclear. Plk1 phosphorylation of HsCyk-4 and/or MKLP1 may

contribute to the Ect2-HsCyk-4 interaction, which is known to be direct (Somers and Saint, 2003). Furthermore, in vitro kinase assays demonstrating that Plk1 could phosphorylate Ect2 and MKLP1 (Hara et al., 2006; Liu et al., 2004) raised the possibility that in vivo Ect2 and/or MKLP1 phosphorylation events may play a role in stimulating the Ect2-HsCyk-4 interaction.

In addition to targeting potential Polo phosphorylation sites in Pbl, Pav and Tum, I also set out to analyse the potential role of proline-directed kinases in stimulating the Pbl-Tum interaction. Proline-directed kinases such as Cdk1 phosphorylate serine or threonine residues that are preceded by a proline residue (Hall and Vulliet, 1991). Cdk1 is known to phosphorylate many targets during metaphase to restrict certain activities and interactions and thereby prevent a premature transition into anaphase. Cdk1 phosphorylation of T341 in Ect2 has been demonstrated to inhibit the Ect2-HsCyk-4 interaction, and at the same time relieve the autoinhibitory conformation of Ect2, which is suggested to promote its GEF activity (Kim et al., 2005; Niiya et al., 2006; Yüce et al., 2005). Thus Cdk1 appears to prevent the premature association of Ect2 with HsCyk4 while priming Ect2 for its subsequent activities during anaphase. Furthermore, other proline-directed kinases are known to be involved in proliferative signalling pathways. For example, the Mitogen-Activated Protein Kinases (MAPKs) are a large family of proline-directed kinases that can be activated by Rho family GTPases and are known to be involved in Rho dependent proliferative signalling pathways (Krishna and Narang, 2008). Although a cytokinetic role for MAPKs has not yet been identified, it is possible that these kinases also participate in regulating protein interactions during cytokinesis.

To identify phosphorylation events important for the Pbl-Tum interaction, I set out to identify and mutate residues that may be phosphorylated by Polo or a proline-directed kinase. Due to the close proximity of Pbl, Tum and Pav it was possible that phosphorylations of Pav might also affect the Pbl-Tum interaction. Therefore, potential phosphorylation sites on Pav were also mutated in efforts to identify the role phosphorylation events play in regulating the Pbl-Tum interaction.

4.2 Results

4.2.1 Identification of potential phosphorylation sites

A Plk1 consensus motif has been identified by mutating the residues around a known Plk1 phosphorylation site in Cdc25C. The consensus sequence D/E-X-pT/pS-Φ-X-(D/E) showed a strong preference for a hydrophobic amino acid (Φ) at the +1 position and an acidic amino acid at the -2 position relative to the phosphorylated residue (Nakajima et al., 2003). Furthermore, an acidic amino acid at the +3 position was identified as optimal for target phosphorylation. Many confirmed Plk1 phosphorylation sites match this consensus motif well, although the requirement for an acidic amino acid at the +3 position does not seem to be crucial. Proteins phosphorylated by Plk1 at sites that fit this motif include Myt1, Scc1, BubR1, Cyclin B and MKLP2 (table 4.1A) (Alexandru et al., 2001; Elowe et al., 2007; Nakajima et al., 2003; Neef et al., 2003; Yuan et al., 2002).

This consensus motif was used to identify potential Polo phosphorylation sites within Pbl, Tum and Pav. In addition, potential proline-directed phosphorylation sites were identified in Tum and Pav. We have previously created a *pbl* construct in which all the potential proline-directed phosphorylation sites were mutated (R. Saint, personal communication). However when this transgene was over-expressed in a *pbl* mutant background we could not detect any obvious cytokinesis defects. Therefore, potential proline-directed phosphorylation sites in Pbl were not targeted in this study.

The area examined in each of the proteins focused on the regions known to be involved in cytokinetic interactions (see chapter 1); namely the N-terminal ends of Pbl and Tum and the region C-terminal to the motor domain of Pav. Manual inspection of the Pbl, Tum and Pav sequences revealed the presence of several potential Polo and proline-directed phosphorylation sites (Table 4.1). In total 4-6 putative Polo and proline-directed kinase phosphorylation sites were selected for targeted mutagenesis for each protein (Figure 4.1A-C). In each case, the targeted residues were mutated into alanines.

4.2.2 Construction of Pbl, Tum and Pav vectors and the creation of transgenic *Drosophila* lines

To assess the effect that phospho specific mutations had throughout cytokinesis, a direct comparison between wild type and mutant proteins was required. Importantly, the level and developmental pattern of protein expression needs to

reflect that of the endogenous protein as closely as possible. To achieve this, a relatively new technique utilizing vectors with an amplifiable low copy number, in this case P[acman] (P/ΦC31 artificial chromosome for manipulation) was used. This technique allows the incorporation and manipulation of large pieces of genomic DNA through homologous recombination (Venken et al., 2006). The resulting vectors can then be integrated into specific sites within the *Drosophila* genome through the use of the ΦC31 integrase (Venken et al., 2006). By using the same integration site for wild type and mutant transgenes the potential complication of different expression levels due to position effects is eliminated, such that a direct comparison of the transgenes can be made and the effects of the introduced mutations assessed.

Using this system, genomic sequences encoding the individual *pbl*, *tum* or *pav* genes were recombined into the P[acman] vectors using the recombineering system (see 2.2.11.2.1). The phosphorylation site mutations were introduced by sub-cloning the region of interest into pGEM-T, introducing the desired mutations using site-directed mutagenesis (see 2.2.4 and 2.2.5) and recombining the mutated sequences into their corresponding wild type constructs to create Polo and proline-directed phosphorylation site mutant versions (see 2.2.11.2.2 and 2.2.11.2.3). To facilitate immunofluorescence detection of the localisation of the expressed proteins during cytokinesis, GFP and 5xmyc tags were fused to the 3' end of *pbl* and *tum* respectively (see 2.2.11.2.3). *pav* was left untagged as we possessed a good antibody that enabled it to be distinguished. *pbl-GFP*, *tum-myc* and *pav* constructs carrying mutations in all the Polo or proline-directed phosphorylation target sites were then constructed from their wild type

Table 4.1 ***Identification of potential phosphorylation sites in Pbl, Tum and Pav***

A. The identified Plk1 consensus sequence and the phosphorylation sites of several different proteins known to be phosphorylated by Plk1. The phosphorylation site of many Plk1 targets fit the identified consensus motif. **B.** Potential Polo and proline-directed phosphorylation sites to be targeted for site-directed mutagenesis in Pbl, Tum and Pav. The site-directed mutagenesis converted each of the targeted residues into alanines. Underlined residues indicate those that fit the Plk1 consensus motif, bolded red amino acids are potentially phosphorylated residues, the position of the phosphorylated residue within the protein sequence is indicated.

A

Plk1 phosphorylation consensus motif	
D/E - X - S/T - Φ - X - (E/D)	
Known Plk1 phosphorylation sites	
Myt1	Ser 426 – DSSLSS
	Thr 495 – EDTLDP
Cdc25c	Ser 198 – EFSLKD
Cyclin B1	Ser 133 – ETSGCA
BubR1	Ser 676 – EDSREA
MKLP2	Ser528 – EHSLQV

B

Pbl	Tum	Pav
Potential Polo phosphorylation sites		
Thr 5 – EMETIEE	Ser 59 – DKSLTK	Thr 449 – EMTQEV
Ser 10 – EQSKCE	Ser 142 – DKSYGD	Ser 583 – DRSAALE
Thr 51 – SDTGLD	Ser 157 – DLSITH	Thr 595 – ESSIDV
Ser 75 – EGASFEA	Thr 258 – ESTIES	Thr 615 – ELTFKL
Thr 196 – DATQEN	Thr 288 – EATAPP	
Potential proline-directed phosphorylation sites		
	Thr 23 – TP	Thr 458 – TP
	Thr 208 – TP	Thr 467 – TP
	Thr 278 – TP	Ser 516 – SP
	Thr 293 – TP	Thr 728 – TP
	Thr 308 – TP	Ser 836 – SP
		Ser 840 – SP

Figure 4.1 ***Location of potential phosphorylation sites targeted for mutagenesis in Pbl, Tum and Pav***

A schematic representation of Pbl, Tum and Pav showing their respective domains, interacting regions and the position of the potentially phosphorylated Polo kinase (Polo) and proline-directed kinase (Pro) residues that were targeted for mutagenesis. **A**. The residues targeted were restricted to the N-terminus of Pbl where an interaction with Tum had previously been identified. **B**. The N-terminal end of Tum was also targeted due to its interaction with Pbl **C**. Residues C-terminal to the kinesin motor domain were targeted in Pav. The residues that correspond to the *C. elegans* orthologue Zen-4 that interact with Cyk-4 are indicated. CC = coiled-coil domain, NLS = nuclear localisation signal.

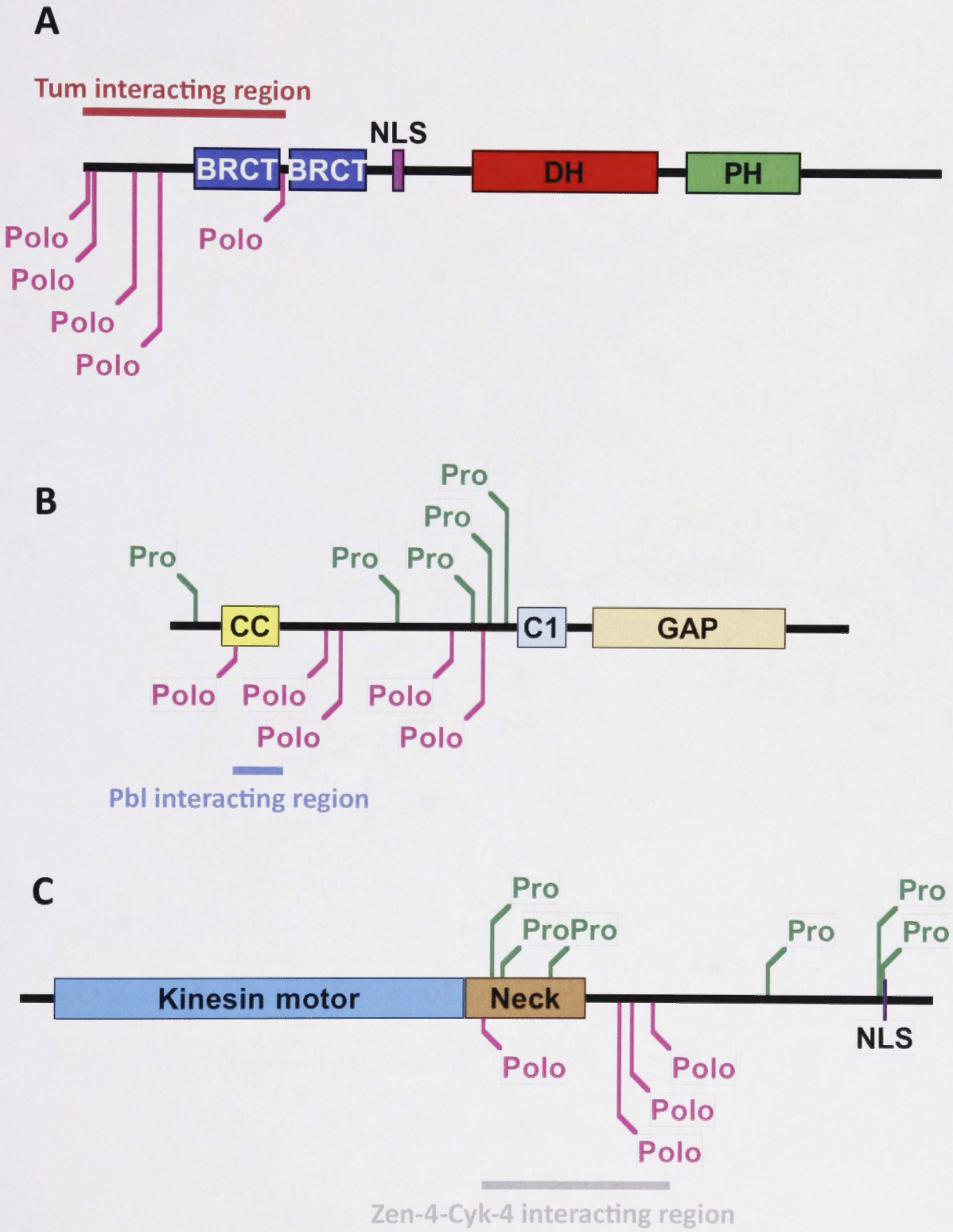
A
Tum interacting region
NLS
BRCT
BRCT
DH
PH
Polo
Polo
Polo
Polo
Polo
B
Pro
Pro
Pro
Pro
Pro
CC
C1
GAP
Polo
Polo
Polo
Polo
Polo
Pbl interacting region
C
Pro
ProPro
Pro
Pro
Pro
Kinesin motor
Neck
NLS
Polo
Polo
Polo
Polo
Zen-4-Cyk-4 interacting region

progenitors. The wild type and mutant constructs for *pbl-GFP*, *tum-myc* and *pav* were then injected into a fly strain containing an attP integration site and a germ line source of ΦC31 integrase to obtain stably integrated transgenes at a defined locus.

4.2.3 The creation of transgene and mutant allele or deficiency recombinants

In order to study the functionality of the wild type transgenes and the effect of the introduced mutations on protein function, it was necessary to express the transgenes in a mutant background where the endogenous protein is absent. To achieve this, the *pbl-GFP*, *tum-myc* and *pav* transgenes were recombined with corresponding mutant alleles or deficiencies (Figure 4.2 and detailed in 2.2.31). The *tum-myc* transgenes were recombined with the tum^{AR2} allele, which carries a nonsense mutation resulting in a truncated product of 470 amino acids and, separately, with an exelixis deficiency Df(2R)Exel7128, which covers *tum* and 15 other neighbouring transcripts (Figure 4.3A). *pbl-GFP* transgenes were recombined with the pbl^{2} or pbl^{3} alleles, which contain nonsense mutations that lead to the production of truncated proteins of 37 and 185 amino acids respectively. The *pav* transgenes were recombined with exelixis deficiency Df(3L)Exel9000, which covers *pav* and 14 flanking genes (Figure 4.3B), and the pav^{B200} allele.

Having created all the necessary stocks to analyse the *pbl-GFP*, *tum-myc* and *pav* transgenes in appropriate mutant backgrounds, the functionality of each

transgene was then determined. In brief, but discussed in more detail in the next section, this was achieved by first assessing the ability of each transgene to rescue the viability of mutant flies. Following this, the expression and localisation of the recombinant proteins throughout cytokinesis was analysed in embryonic epidermal cells using immunofluorescent staining and microscopy. Furthermore, the localisation of Anillin was used to highlight any disruption to the Pbl-Tum interaction and to help mark cytokinesis progression. Anillin suits these requirements for several reasons; its equatorial localisation requires Rho activation (Hickson and O'Farrell, 2008; Somma et al., 2002), it is an early furrow marker (Giansanti et al., 1999) and is prominent throughout constriction persisting at the midbody in telophase (Field and Alberts, 1995). Therefore, by examining the localisation of Anillin during cytokinesis any disruption to the Pbl-Tum interaction, which is required for Rho activation and furrow accumulation, could potentially be identified.

4.2.4 Analyses of cytokinesis in wild type and mutant *pbl*, *tum* and *pav* transgenic embryos

To confirm that Anillin could be successfully used to track cytokinesis progression, its localisation in wild type embryos was examined. Anillin formed a ring around the equator of the cell during anaphase (Figure 4.4 A and B arrowheads). Microtubules are spread across the breadth of anaphase cells while the DNA appears elongated due to its recent movement from the midzone of the cell. At telophase, furrow ingression compacts the microtubules while Anillin follows the inward progression of the membrane (Figure 4.4C arrowheads). At

Figure 4.2 ***Generation of mutant allele or deficiency recombinants for* pbl-GFP, tum-myc *and* pav *transgenes***

Crossing scheme to generate transgene and mutant allele or deficiency recombinants for *pbl-GFP*, *tum-myc* and *pav*. **A.** The crossing scheme shown was used to create *tum-myc^{wt}*, *tum^{AR2}* recombinants but was the same scheme used for all *tum-myc* transgenes or to create recombinants with Df(2R)Exel7128. The *tum-myc^{wt}* transgenic line was crossed to a strain containing the *tum^{AR2}* allele. Virgin females containing both the transgene and mutant allele were collected and crossed to a Gla/CyO balancer line. Individual potential recombinant males carrying the w^{+} marked *tum-myc^{wt}* transgene were again crossed to the Gla/CyO marked balancer line and balanced stocks established. **B.** The crossing scheme shown was used to create *pbl-GFP^{wt}*, *pbl^{2}* recombinants but was the same scheme used for all *pbl-GFP* and *pav* transgenes or to create recombinants with *pbl^{3}*, *pav^{B200}* or Df(3L)Exel9000. The *pbl-GFP^{wt}* transgenic line was crossed to a strain containing the *pbl^{2}* allele. Virgin females containing both the transgene and mutant allele were collected and crossed to a TM6B/TM3 balancer line. Individual potential recombinant males carrying the w^{+} marked *pbl-GFP^{wt}* transgene were crossed to a TM6B/TM3 marked balancer line and balanced stocks established. w^{-} = unknown *white* allele, w^{+} = wild type *white* allele, ??? indicates a potential recombinant.

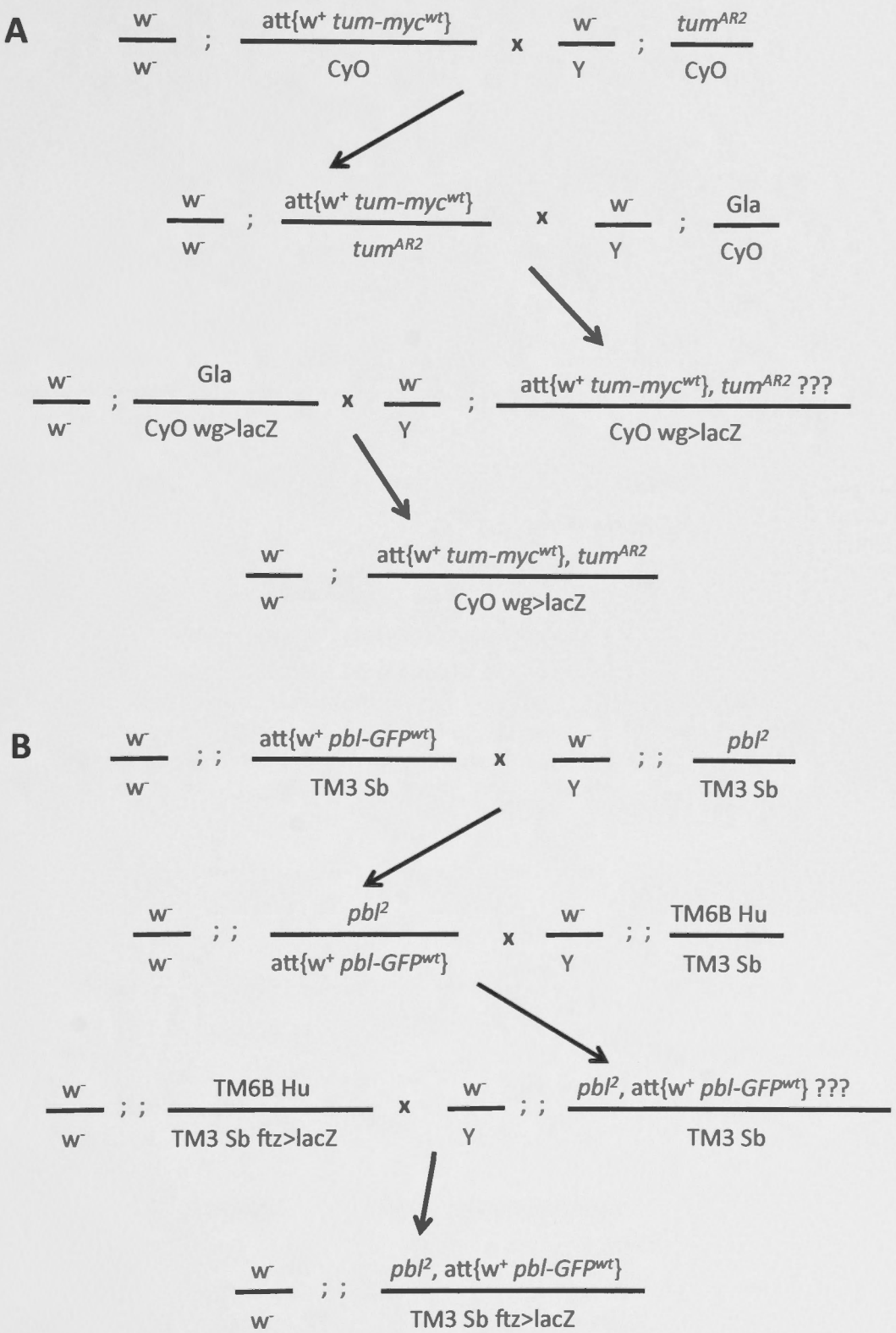
A
w-
w-
;
att{w+ tum-mycwt}
CyO
x
w-
Y
;
tumAR2
CyO
w-
w-
;
att{w+ tum-mycwt}
tumAR2
x
w-
Y
;
Gla
CyO
w-
w-
;
Gla
CyO wg>lacZ
x
w-
Y
;
att{w+ tum-mycwt}, tumAR2 ???
CyO wg>lacZ
w-
w-
;
att{w+ tum-mycwt}, tumAR2
CyO wg>lacZ
B
w-
w-
; ;
att{w+ pbl-GFPwt}
TM3 Sb
x
w-
Y
; ;
pbl2
TM3 Sb
w-
w-
; ;
pbl2
att{w+ pbl-GFPwt}
x
w-
Y
; ;
TM6B Hu
TM3 Sb
w-
w-
; ;
TM6B Hu
TM3 Sb ftz>lacZ
x
w-
Y
; ;
pbl2, att{w+ pbl-GFPwt} ???
TM3 Sb
w-
w-
; ;
pbl2, att{w+ pbl-GFPwt}
TM3 Sb ftz>lacZ

Figure 4.3 ***Deficiencies recombined with tum-myc and pav transgenes***

A. A view of the *tum* genomic region showing available deficiencies in the area. The Df(2R)Exel7128 (blue arrow) used to make recombinants deletes *tum* (red circle) and 15 other neighbouring genes. The top scaffold indicates the position on. **B.** A view of the *pav* genomic region showing available deficiencies in the area. The Df(2R)Exel9000 (blue arrow) used to make recombinants deletes *pav* (red circle) and 14 other neighboring genes. The top scaffold indicates the position on the right arm of the 2nd chromosome (**A**) or the left arm of the 3rd chromosome (**B**). Image from Gbrowse (FlyBase).

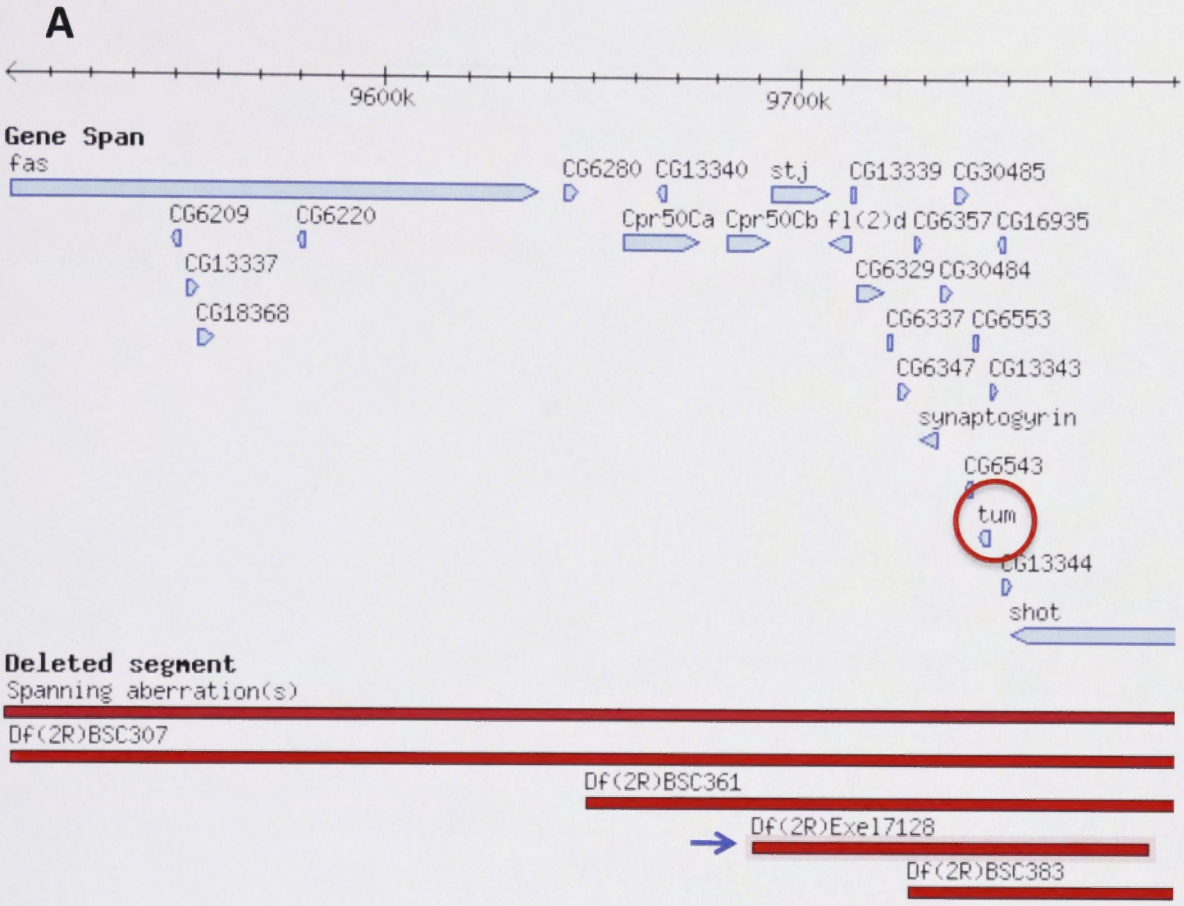
A
9600k
9700k
Gene Span
fas
CG6280
CG13340
stj
CG13339
CG30485
CG6209
CG6220
Cpr50Ca
Cpr50Cb
fl(2)d
CG6357
CG16935
CG13337
CG6329
CG30484
CG18368
CG6337
CG6553
CG6347
CG13343
synaptogyrin
CG6543
tum
CG13344
shot
Deleted segment
Spanning aberration(s)
Df(2R)BSC307
Df(2R)BSC361
Df(2R)Exel7128
Df(2R)BSC383

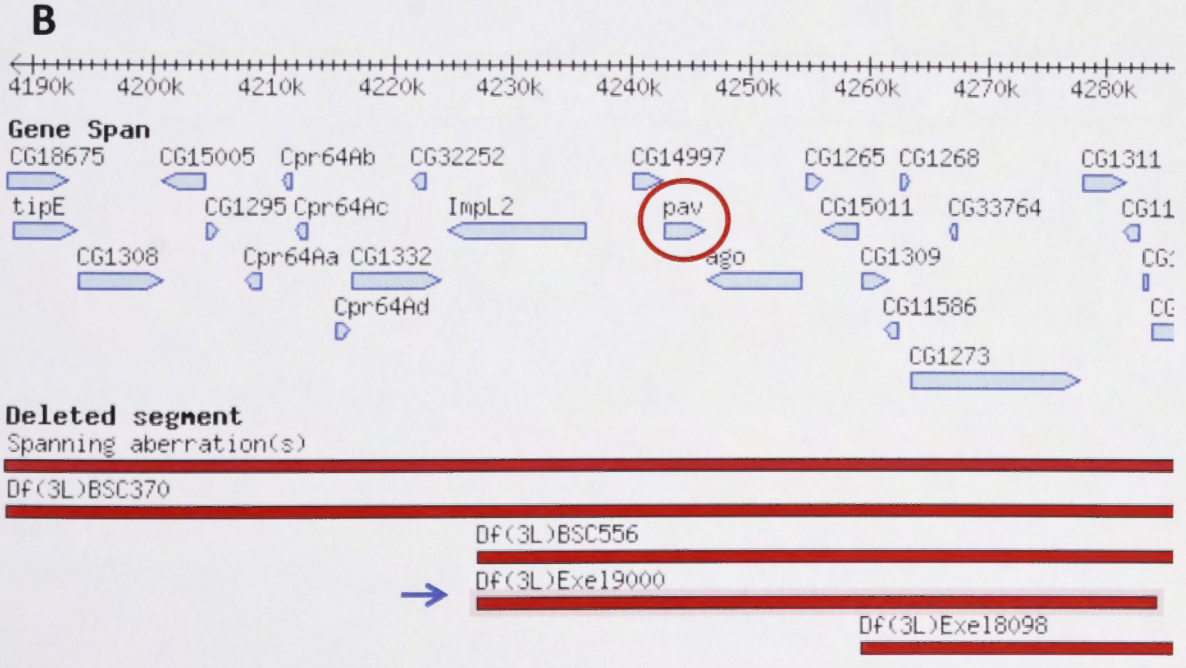
B
4190k
4200k
4210k
4220k
4230k
4240k
4250k
4260k
4270k
4280k
Gene Span
CG18675
CG15005
Cpr64Ab
CG32252
CG14997
CG1265
CG1268
CG1311
tipE
CG1295
Cpr64Ac
ImpL2
pav
CG15011
CG33764
CG1308
Cpr64Aa
CG1332
ago
CG1309
Cpr64Ad
CG11586
CG1273
Deleted segment
Spanning aberration(s)
Df(3L)BSC370
Df(3L)BSC556
Df(3L)Exel9000
Df(3L)Exel8098

Figure 4.4 ***Anillin localisation during anaphase and telophase in wild type embryos***

Late stage 9 - early stage 10 wild type embryos stained for microtubules (MT, red), Anillin (green) and DNA (blue). **A** and **B**. Anillin localised to the cleavage furrow and forms a ring at the equator of anaphase cells (arrowheads). **C**. As furrow ingression continues, Anillin staining followed the compression of the microtubules (arrowheads). At this point the DNA can be observed to round up and decondense, resulting in a blotchy staining pattern, as the nuclear envelope starts to reform. **D**. Eventually a compact microtubule dense midbody is formed where intense Anillin staining can be observed at the midbody midpoint (arrowheads). Images are maximum projections of z-series taken in 0.3μm steps. Scale bar in bottom right hand panel = 10μm.

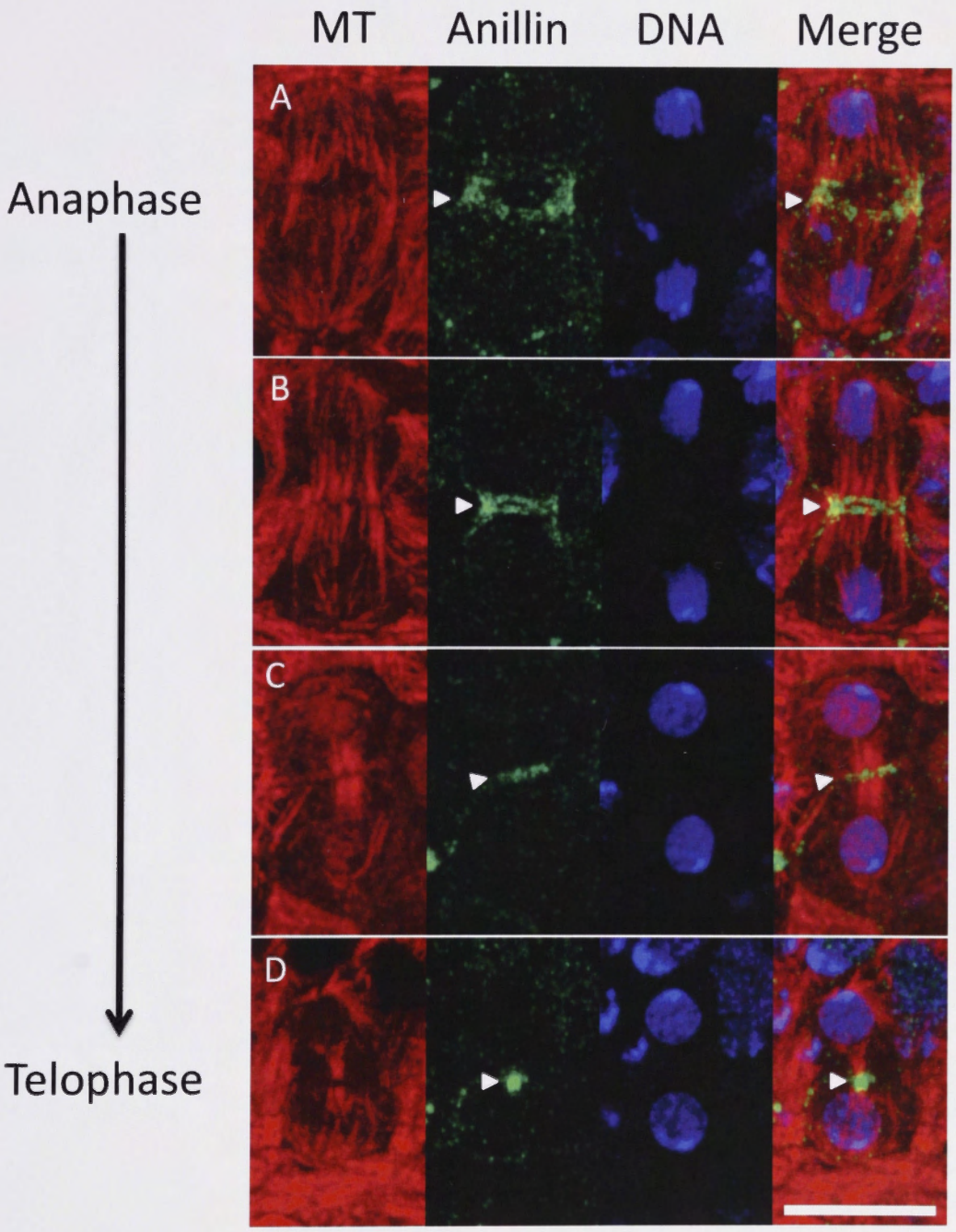
MT
Anillin
DNA
Merge
A
B
C
D
Anaphase
Telophase

this stage the DNA rounds up, decondenses and the nuclear envelope reforms resulting in a blotchy staining pattern. Eventually the microtubules are compressed into a thin bridge called the midbody where intense Anillin staining can be observed at its midpoint (Figure 4.4D arrowhead). These results demonstrate that Anillin is a useful marker for examining the progression of cytokinesis.

Although Anillin gave reproducible stains during the latter stages of cytokinesis, some staining variability was observed in the equatorial localisation of anaphase cells. This was also the case with antibodies for Pbl, Tum or Pav. In comparison, telophase cells stained much more reliably due to the concentrating effect of furrow ingression. Furthermore, the compression of the microtubules into a thick bundle provided another good marker for furrow ingression and the completion of cytokinesis. Therefore, only telophase cells were counted when assessing the ability of each transgene to rescue furrow constriction.

Unfortunately, the lack of an antibody capable of detecting Pbl via immunofluorescence precluded the ability to visualize Pbl localisation in wild type embryos and to determine whether endogenous protein persisted in *pbl* mutant embryos. *pbl* mutant embryos fail cytokinesis at the 14th division cycle, the first division after cellularisation of the syncytial blastoderm (Hime and Saint, 1992; Lehner, 1992) (Table 4.2). To examine the ability of cells to undergo cytokinesis during cycle 14, late stage 9 to early stage 10 *pbl* mutant embryos were imaged. In *pbl* mutant embryos, Anillin could not be detected at the equator of anaphase cells or in the majority of telophase cells (20/21) which also

displayed unbundled rather than compacted microtubules (Figure 4.5A and B). The single telophase cell that was able to construct robust midbody microtubules showed only weak recruitment of Anillin at the midpoint (Figure 4.5C arrowheads). Thus in the majority of cells, furrow constriction at cycle 14 failed. This is consistent with counts of binucleate cells in *pbl* mutant embryos wherein only a small percentage of cells can divide successfully (Table 4.2).

Table 4.2. Percentage of binucleate cells in *pbl*, *pav* and *tum* mutant embryos

Genotype	Percentage binucleate (mean ± std dev)	Number of cells scored (number of embryos)
pbl^{2}/pbl^{3}	95.16±2.48	442 (6)
Df(3L)Exel9000/pav^{B200}	94.70±1.29	944(6)
Df(2R)Exel7128/tum^{AR2}	81.88±2.99	1030(7)

Mid-late stage 11 *pbl* mutant embryos and mid-late stage 12 *pav* and *tum* mutant embryos were stained for lamin and F-actin, to detect the nuclear envelope and mark cell boundaries respectively, and the percentage of binucleate cells determined for each embryo. These values were used to calculate the mean and standard deviation (SD) for each genotype. As detailed below, later stages were used for *tum* and *pav* mutant embryos as cytokinesis fails at the 14th division cycle in *pbl* and the 16th division cycle in *tum* and *pav* mutant embryos.

The localisation of both Pav and Anillin in wild type and *pav* mutant embryos during cytokinesis was also examined. In wild type embryos, Pav accumulated at the centrosomes (arrows) and equator (arrowheads) of anaphase cells and was recruited to the midbody in telophase cells (Figure 4.6A and B). The maternal Pav protein persists longer than Pbl, as cytokinetic defects in *pav* mutant embryos are only observed at the 16th division cycle (Adams et al., 1998; Zavortink et al., 2005). Therefore, in order to examine cells completing

Figure 4.5 ***Anillin localisation is absent or diminished during anaphase and telophase in* pbl *mutant embryos***

Late stage 9 - early stage 10 *pbl*^{2}/*pbl*^{3} mutant embryos stained for microtubules (MT, red), Anillin (green) and DNA (blue). **A.** Anillin cannot be detected at the equator of anaphase cells. **B.** The majority of telophase cells were unable to constrict and form a midbody and failed to accumulate Anillin. **C.** A telophase cell containing robust midbody microtubules accumulated Anillin only weakly at the midpoint (arrowheads). Images are maximum projections of a z-series taken in 0.3μm steps. Scale bar in bottom right hand panel = 10μm.

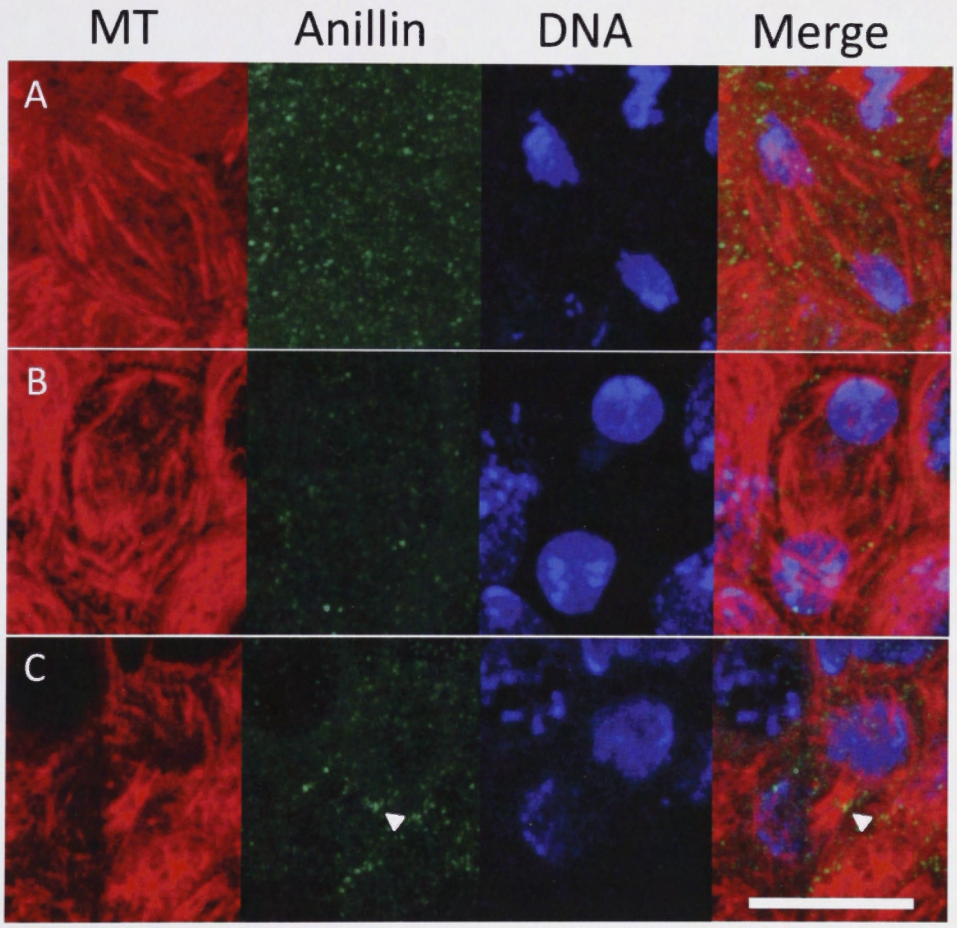
MT
Anillin
DNA
Merge
A
B
C

Figure 4.6 ***Pav is detectable in anaphase and telophase cells in wild type but not* pav *mutant embryos***

Late stage 11 - early stage 12 wild type and pav^{B200}/Df(3L)Exel9000 ($pav^{-/-}$) embryos stained for microtubules (MT, red), Pav (green) and DNA (blue). **A** and **B**. Pav accumulated at the centrosomes (arrows) and the equator of anaphase cells and became restricted to the midbody in telophase cells of wild type embryos (arrowheads). **C** and **D**. Pav cannot be detected in anaphase or telophase cells in *pav* mutant embryos. **E**. Those cells that were able to bundle some microtubules lacked Pav staining at the midpoint (arrowhead). Images are maximum projections of z-series taken in 0.3µm steps. Scale bar in bottom right hand panel = 10µm.

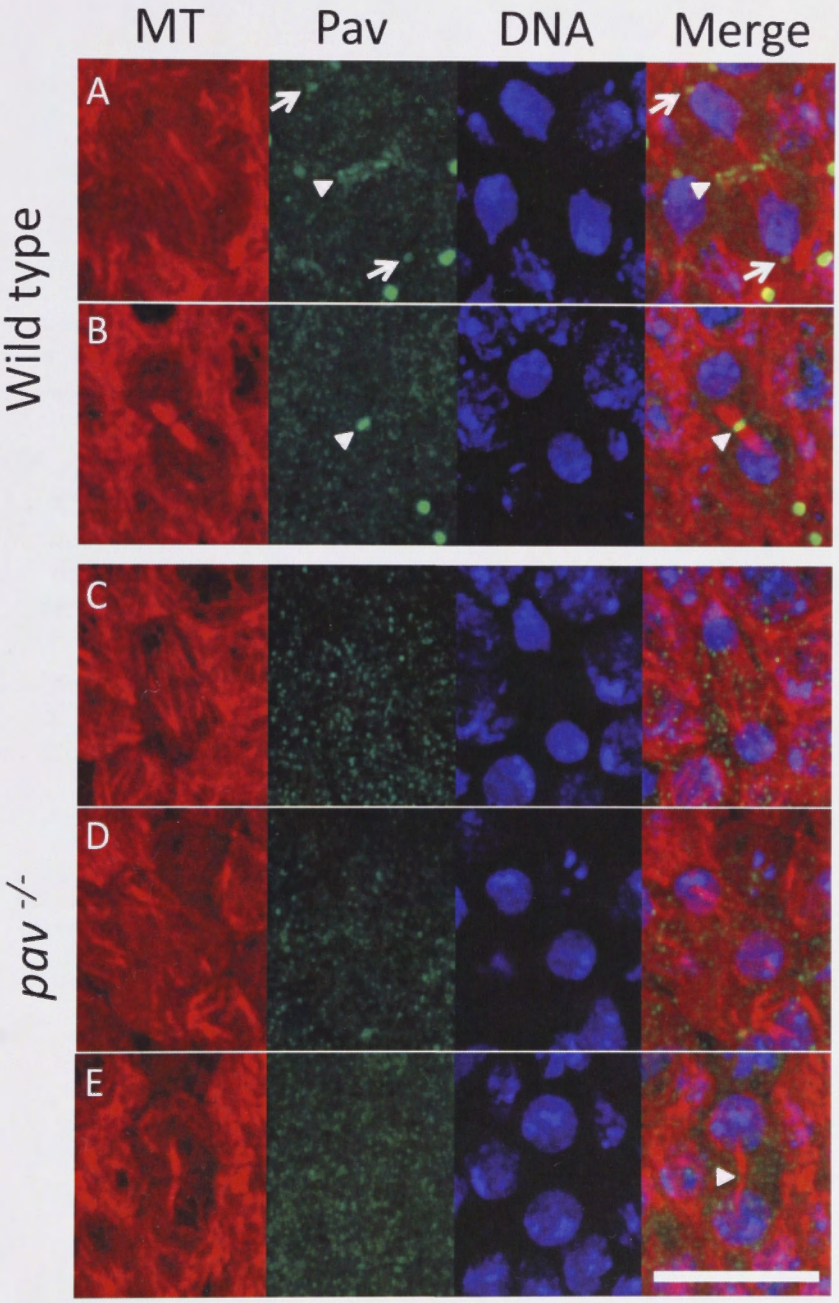
MT
Pav
DNA
Merge
A
B
C
D
E
Wild type
pav -/-

cycle 16, late stage 11 to early stage 12 *pav* mutant embryos were imaged. In *pav* mutant embryos, Pav could not be detected at the centrosomes or at the equator of anaphase or telophase cells, and the microtubules remained unbundled in most telophase cells (20/28) (Figure 4.6 C and D). Microtubule bundles could be seen in some telophase cells (8/28), but Pav was clearly absent from the midpoint of such microtubules (Figure 4.6E arrowhead). Furthermore, the microtubule bundles were thinner than the corresponding microtubules in wild type cells (compare Figure 4.6B with E) suggesting that these cells would be unlikely to complete cell division. Similarly, in *pav* mutant embryos Anillin failed to accumulate at the equator of anaphase or telophase cells (Figure 4.7A and B). A small number of telophase cells contained some bundled microtubules (2/22), but these cells failed to recruit Anillin to the midpoint (Figure 4.7C arrowheads). These cells may have been able to initiate but not complete constriction, leading to the formation of some bundled microtubules. Furthermore, the absence of Pav or Anillin at their midpoints indicated that it was unlikely that these cells would have been able to complete cytokinesis. Moreover, cell counts showed that, at mid-late stage 12, approximately 94% of cells in *pav* mutant embryos were binucleate confirming that the majority of cells were unable to divide (Table 4.2).

The localisation of Tum and Anillin was assessed in both wild type and *tum* mutant embryos. In wild type embryos, Tum localised to the equator of anaphase cells and was concentrated to the midbody of telophase cells (31/31) (Figure 4.8A and B arrowheads) By contrast, in *tum* mutant embryos Tum was not detectable at the equator of anaphase cells or telophase cells (Figure 4.7C and D). Similar to *pav* mutant embryos, some telophase cells (14/47) in *tum*

mutant embryos displayed bundled microtubules, although Tum was not detectable at the midbody (Figure 4.8E arrowhead). Furthermore, a small number of telophase cells (6/47) seemed capable of constriction as indicated by a normal robust midbody bundle of microtubules (Figure 4.8F). However, Tum was again not evident at the midpoint of these cells (Figure 4.8F arrowhead). Anaphase and telophase cells (32/38) also failed to show localisation of Anillin to the equator (Figure 4.9A and B). One anaphase cell capable of localising some Anillin to the equator was detected, but distribution across the entire breadth of an anaphase cell was never observed (Figure 4.9C arrowheads). Furthermore, equatorial Anillin localisation was also observed in a subset of telophase cells (6/38). Some telophase cells (2/38) accumulated Anillin across the entire breadth of the cell but did not show furrow constriction (Figure 4.9D arrowheads). This could have been because the accumulation of furrow components was either insufficient to stimulate furrow ingression or was not able to sustain furrowing resulting in furrow regression. Some telophase cells (4/38) resembled wild type in that they were able to assemble midbody microtubules with Anillin accumulation at the midpoint (Figure 4.9E arrowheads). Thus despite the inability to visually detect Tum at the cell equator, the presence of Anillin suggests that some Tum accumulated at the furrow to activate downstream effectors. These results indicate that *tum* mutant embryos were capable of progressing through cytokinesis more so than *pbl* or *pav* mutant embryos. This was confirmed by cell counts of *tum* mutant embryos where approximately 81% of cells were found to be binucleate compared with 95% for *pbl* and 94% for *pav* mutant embryos (Table 4.2). Thus the protein product produced from the tum^{AR2} allele appears to retain some functionality. In addition,

Figure 4.7 ***Anillin localisation is absent during anaphase and telophase in* pav *mutant embryos***

Late stage 11 - early stage 12 *pav*^{B200}/Df(3L)Exel9000 embryos stained for microtubules (MT, red), Anillin (green) and DNA (blue). **A.** Anillin cannot be detected at the equator of anaphase cells. **B.** The majority of telophase cells were unable to constrict and form a midbody and lacked detectable Anillin. **C.** Those cells that were capable of some microtubule bundling were not able to accumulate Anillin at the midpoint (arrowheads). Images are maximum projections of a z-series taken in 0.3µm steps. Scale bar in bottom right hand panel = 10µm.

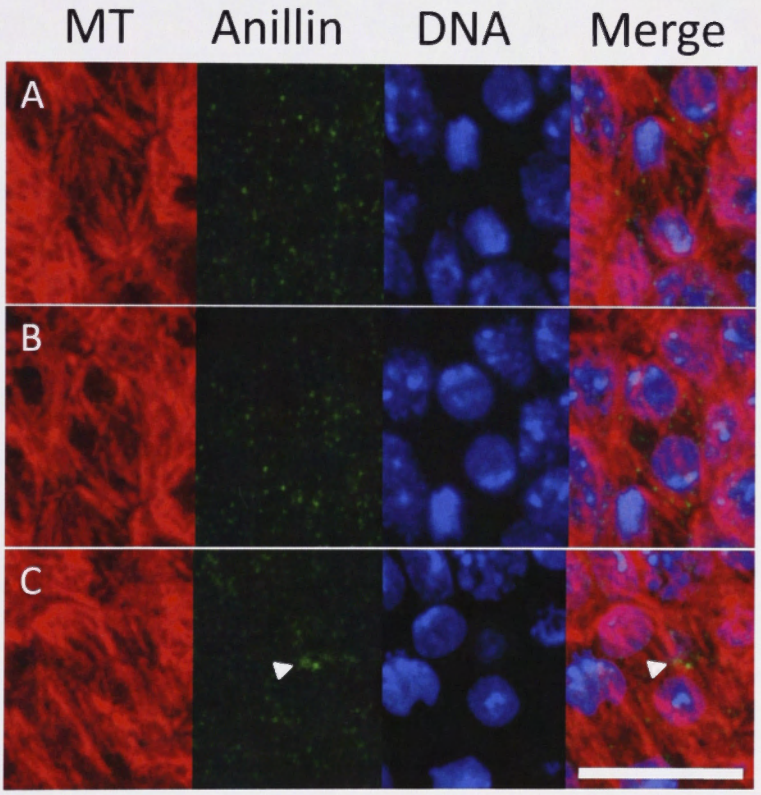
MT
Anillin
DNA
Merge
A
B
C

Figure 4.8 ***Tum is detectable in anaphase and telophase cells in wild type but not* tum *mutant embryos***

Late stage 11 - early stage 12 wild type and *tum*^{AR2}/Df(2R)Exel7128 mutant embryos (*tum*$^{-/-}$) stained for microtubules (MT, red), Tum (green) and DNA (blue). **A** and **B**. Tum accumulated at the equator of anaphase cells and the midbody of telophase cells in wild type embryos (arrowheads). **C**. Equatorial Tum accumulation could not be observed in anaphase cells of *tum* mutant embryos. **D**. The majority of telophase cells were unable to constrict and form a midbody and lacked detectable Tum. **E**. Tum was not distinguishable in those cells that exhibited some microtubule bundling (arrowhead). **F**. Tum was not able to be identified in those telophase cells that were capable of constricting, as indicated by the formation of robust midbody microtubules. Images are maximum projections of z-series taken in 0.3μm steps. Scale bar in bottom right hand panel = 10μm.

MT
Tum
DNA
Merge
A
B
C
D
E
F
Wild type
tum -/-

Figure 4.9 ***Anillin localisation is absent or reduced in anaphase and telophase cells of* tum *mutant embryos***

Late stage 11 - early stage 12 *tum*^{AR2}/Df(2R)Exel7128 mutant embryos stained for microtubules (MT, red), Anillin (green) and DNA (blue). **A.** Anillin cannot be detected in the majority of anaphase cells. **B.** The majority of telophase cells are unable to constrict to form a midbody and fail to accumulate Anillin. **C.** Some anaphase cells showed a limited capacity to recruit Anillin to the equator of the cell (arrowheads). **D.** Telophase cells that have failed to constrict but accumulated Anillin at the cleavage furrow (arrowheads) are observable. **E.** Those cells that were capable of constructing robust midbody microtubules and presumably completing cytokinesis showed reduced Anillin accumulation at the midbody midpoint. Images are maximum projections of a z-series taken in 0.3μm steps. Scale bar in bottom right hand panel = 10μm.

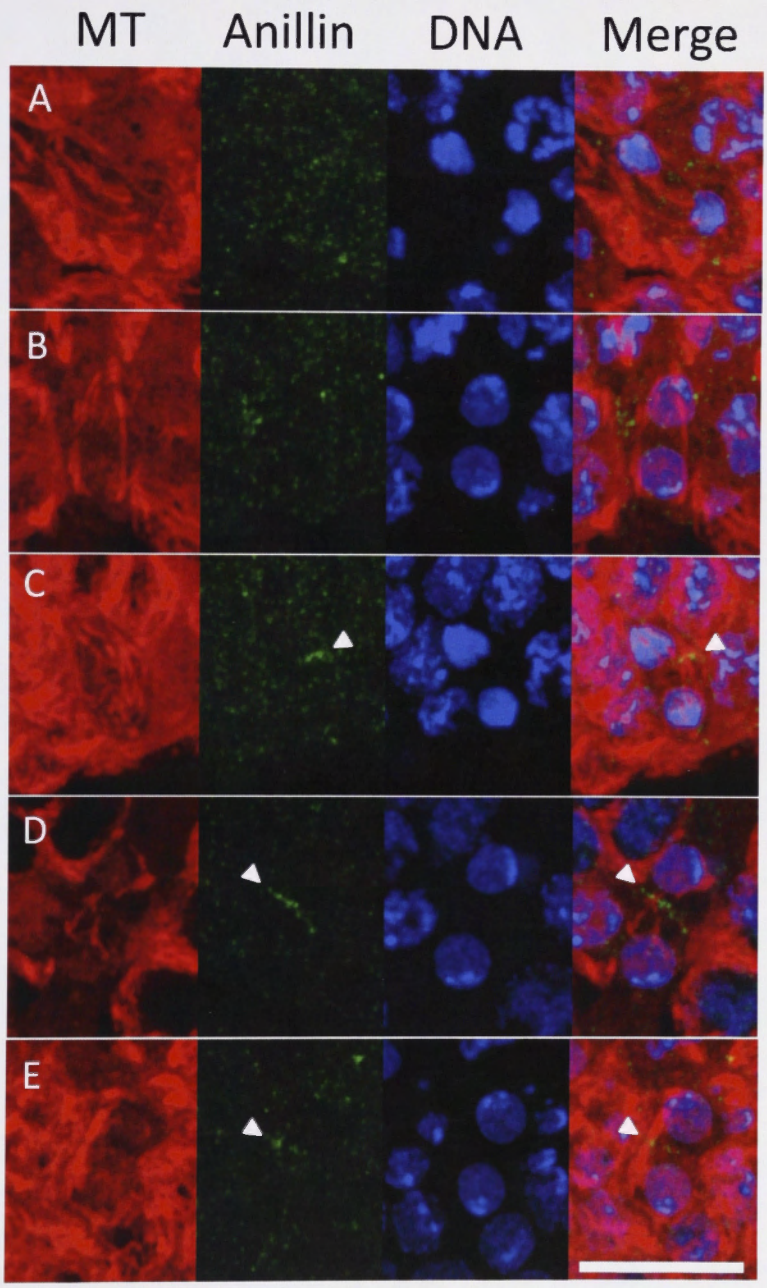
MT
Anillin
DNA
Merge
A
B
C
D
E

the persistence of maternal product may contribute to the observed level of cytokinesis rescue.

Having characterised the ability of cells carrying the *pbl*, *pav* and *tum* alleles to initiate and complete cytokinesis, the ability of each of the wild type and mutated transgenes to rescue cytokenesis was then assessed.

4.2.5 *pbl-GFP^{wt}* and *pbl-GFP^{Polo}* rescue furrow constriction in *pbl* mutant embryos in vivo

The ability of the *pbl-GFP* transgenes to rescue *pbl* mutant flies was tested by crossing flies that contained a *pbl* allele recombined with a *pbl-GFP* transgene. Wild type and mutant transgenes are hereafter distinguished by wt, Polo or Pro superscripts. While *pbl-GFP^{wt}* and *pbl-GFP^{Polo}* failed to rescue *pbl^{2}/pbl^{2}* or *pbl^{2}/pbl^{3}* flies to adulthood, both transgenes were capable of rescuing in a *pbl^{3}/pbl^{3}* mutant background when two copies of the transgene were present. However, these flies exhibited reduced viability (≈10%) compared with their heterozygous (i.e. over a balancer chromosome) counterparts. Thus although the *pbl-GFP^{wt}* and *pbl-GFP^{Polo}* transgenes could rescue *pbl* mutant flies, the reduced viability suggested that the transgenes failed to completely recapitulate endogenous *pbl* expression and/or functionality. To confirm that the *pbl-GFP^{wt}* or *pbl-GFP^{Polo}* transgenes could rescue furrow constriction, the localisation of Pbl-GFP^{wt}, Pbl-GFP^{Polo} and Anillin was assessed during the 14th division cycle. To do this, recombinant lines carrying a *pbl* allele and *pbl-GFP* transgene over a *lacZ* marked balancer were crossed together (Figure 4.10A). Embryos were collected

and stained for β–galactosidase (expressed from the *lacZ* gene on the balancer chromosome) to identify *pbl* mutant embryos homozygous for a *pbl-GFP* transgene by virtue of a lack of staining. For simplicity, embryos homozygous for the *pbl-GFP^{wt}* or *pbl-GFP^{Polo}* trangenes in a *pbl* mutant background will hereafter be referred to as *pbl-GFP^{wt}* or *pbl-GFP^{Polo}*.

Immunofluorescent staining showed that Pbl-GFP^{wt} localised to the equator of anaphase cells in *pbl* mutant embryos (Figure 4.11A arrowheads). Cytokinesis appeared to progress analogously to a wild type cell, as Pbl-GFP^{wt} was observed to follow furrow ingression, becoming enriched at the midbody, and then cycling back into the nucleus (Figure 4.11B arrowheads and arrows). Pbl-GFP^{Polo} showed a similar pattern of localisation, it was detected at the equator of anaphase cells (Figure 4.11C arrowheads), and then concentrated at the midbody and within the nuclei at telophase (Figure 4.11D arrowheads and arrows respectively).

Localisation of Anillin was used as a marker to confirm that cytokinesis was progressing normally in both *pbl-GFP^{wt}* and *pbl-GFP^{Polo}* embryos. In *pbl-GFP^{wt}* embryos, Anillin accumulated normally at the equator of anaphase cells (Figure 4.12A arrowheads). As cells progressed to telophase, intense Anillin staining could be observed at the midbody of all cells examined (24/24) (Figure 4.12B arrowheads). Faint nuclear staining was also detectable due to fluorescence from the GFP tag fused to Pbl (Figure 4.12B asterisks). *pbl-GFP^{Polo}* embryos also exhibited typical Anillin staining with the protein accumulating at the equator of anaphase cells (Figure 4.12C arrowheads). All telophase cells

Figure 4.10 ***Identification of embryos homozygous for* pbl-GFP, tum-myc *or* pav *transgenes in a mutant background***

Crossing schemes used to isolate embryos containing the transgene in a mutant background. **A.** Recombinant fly lines carrying a *pbl-GFP* transgene with the pbl^{2} or pbl^{3} mutant allele over a *lacZ* marked balancer were crossed together. To identify embryos that were homozygous for the *pbl-GFP* transgene in a mutant background a β–galactosidase stain was performed to distinguish those embryos that carried the marked balancer. **B.** Recombinant fly lines carrying a *pav* transgene with the pav^{B200} mutant allele or Exel9000 deficiency over a *lacZ* marked balancer were crossed together. To identify embryos that were homozygous for the *pav* transgene in a mutant background a β–galactosidase stain was performed to distinguish those embryos that carried the marked balancer. **C.** Recombinant fly lines carrying a *tum-myc* transgene with the tum^{AR2} mutant allele or Exel7128 deficiency over a *lacZ* marked balancer were crossed together. To identify embryos that were homozygous for the *tum-myc* transgene in a mutant background a β–galactosidase stain was performed to distinguish those embryos that carried the marked balancer.

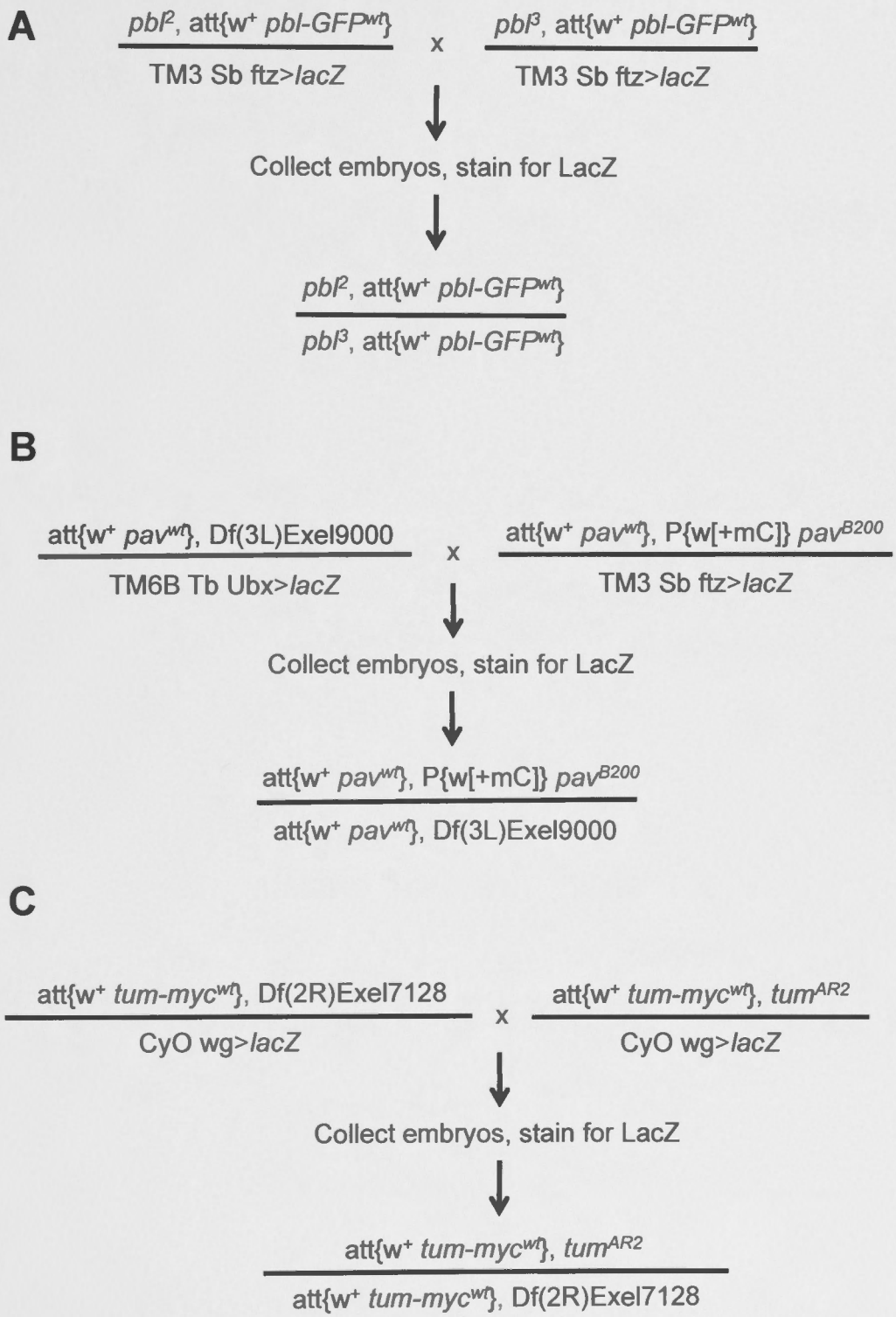
A
pbl2, att{w+ pbl-GFPwt}
TM3 Sb ftz>lacZ
x
pbl3, att{w+ pbl-GFPwt}
TM3 Sb ftz>lacZ
Collect embryos, stain for LacZ
pbl2, att{w+ pbl-GFPwt}
pbl3, att{w+ pbl-GFPwt}
B
att{w+ pavwt}, Df(3L)Exel9000
TM6B Tb Ubx>lacZ
x
att{w+ pavwt}, P{w[+mC]} pavB200
TM3 Sb ftz>lacZ
Collect embryos, stain for LacZ
att{w+ pavwt}, P{w[+mC]} pavB200
att{w+ pavwt}, Df(3L)Exel9000
C
att{w+ tum-mycwt}, Df(2R)Exel7128
CyO wg>lacZ
x
att{w+ tum-mycwt}, tumAR2
CyO wg>lacZ
Collect embryos, stain for LacZ
att{w+ tum-mycwt}, tumAR2
att{w+ tum-mycwt}, Df(2R)Exel7128

Figure 4.11 ***Pbl-GFP^{wt} and Pbl-GFP^{Polo} accumulate at the cleavage furrow during anaphase and are sequestered in the nucleus in telophase***

Late stage 9 - early stage 10 *pbl-GFP^{wt}, pbl^{2}/ pbl-GFP^{wt}, pbl^{3}* (*pbl-GFP^{wt}*) and *pbl-GFP^{Polo}, pbl^{2}/ pbl-GFP^{Polo}, pbl^{3}* (*pbl-GFP^{Polo}*) embryos stained for microtubules (MT, red), GFP (green) and DNA (blue). **A** and **C**. Pbl-GFP^{wt} and Pbl-GFP^{Polo} accumulated at the equator of anaphase cells (arrowheads). **B** and **D**. The majority of Pbl^{wt} and Pbl^{Polo} is sequestered within the nucleus at telophase (arrows) but some protein persisted at the midbody (arrowheads). Images are maximum projections of a z-series taken in 0.3μm steps. Scale bar in bottom right hand panel = 10μm.

MT
GFP
DNA
Merge
A
B
C
D
Pbl-GFPwt
Pbl-GFPPolo

Figure 4.12 ***Anillin localises normally during anaphase and telophase in* pbl-GFP^{wt} *and* pbl-GFP^{Polo} *embryos***

Late stage 9 - early stage 10 *pbl-GFP^{wt}*, *pbl^{2}/ pbl-GFP^{wt}*, *pbl^{3}* (*pbl-GFP^{wt}*) and *pbl-GFP^{Polo}*, *pbl^{2}/ pbl-GFP^{Polo}*, *pbl^{3}* (*pbl-GFP^{Polo}*) embryos stained for microtubules (MT, red), Anillin (green) and DNA (blue). **A** and **C**. Anillin accumulated at the equator of anaphase cells in *pbl-GFP^{wt}* and *pbl-GFP^{Polo}* embryos (arrowheads). **B** and **D**. At telophase Anillin became concentrated at the midbody (arrowheads). Faint outlines of the nuclei are visible in telophase cells due to fluorescence from the C-terminal GFP tag fused to Pbl^{wt} and Pbl^{Polo} (asterisks). Images are maximum projections of z-series taken in 0.3μm steps. Scale bar in bottom right hand panel = 10μm.

MT
Anillin
DNA
Merge
A
B
C
D
pbl-GFPwt
pbl-GFPPolo

examined (21/21) were capable of completing cytokinesis exhibiting robust midbody microtubules with intense Anillin staining at the midbody (Figure 4.12D arrowheads). Faint nuclear staining was again evident due to the C-terminal GFP tag (Figure 4.12D asterisks).

These results demonstrated that both *pbl-GFP^{wt}* and *pbl-GFP^{Polo}* were able to rescue furrow constriction in cells completing the 14th division cycle. As there was no detectable difference between the rescue by the two transgenes, it can be concluded that the mutations introduced into *pbl-GFP^{Polo}* did not effect the Pbl-Tum interaction or any other function of Pbl.

4.2.6 *pav^{wt}*, *pav^{Pro}* and *pav^{Polo}* rescue furrow constriction in *pav* mutant embryos in vivo

To assess the ability of the different *pav* transgenes to rescue *pav* mutant flies, each of the transgenes was crossed into a *pav* mutant background. *pav^{wt}*, *pav^{Pro}* and *pav^{Polo}* were all able to rescue viability of *pav* mutant flies with one or two copies of the transgene. To confirm that the transgenes could rescue furrow constriction, cells completing cycle 16 were imaged for Pav and Anillin. To achieve this, recombinant lines containing a *pav* transgene and *pav^{B200}* or Df(3L)Exel9000 over a *lacZ* marked balancer were crossed together (Figure 4.10B). The embryos collected from this cross were stained for β–galactosidase to identify *pav* mutant embryos homozygous for the *pav* transgene. For simplicity, embryos homozygous for the *pav^{wt}*, *pav^{Pro}* or *pav^{Polo}* trangenes in a *pav* mutant background will hereafter be referred to as *pav^{wt}*, *pav^{Pro}* or *pav^{Polo}*.

The localisation of Pav^{wt}, Pav^{Pro} and Pav^{Polo} was found to replicate endogenous Pav localisation, with each protein detected at the centrosomes (arrowheads) and equator (arrows) during anaphase (Figure 4.13A, C and E). Cytokinesis progressed to completion and each of the transgenic proteins became restricted to the midbody at telophase (Figure 4.13B, D and F arrows). Similarly, in each of the transgenic backgrounds the localisation of Anillin was normal, showing equatorial accumulation during anaphase (Figure 4.14A, C and E). All telophase cells examined in *pav^{wt}*, *pav^{Pro}* and *pav^{Polo}* embryos (37/37, 39/39 and 33/33 respectively) were capable of constriction and accumulated Anillin at the midbody (Figure 4.14B, D and F).

These data demonstrate that *pav^{wt}*, *pav^{Pro}* and *pav^{Polo}* were all able to rescue furrow constriction. Thus the mutations introduced into *pav^{Pro}* and *pav^{Polo}* did not affect the Pbl-Tum interaction or prevent any other process required for the completion of cell division.

4.2.7 *tum-myc^{wt}* and *tum-myc^{Pro}* but not *tum-myc^{Polo}* are able to rescue furrow constriction in *tum* mutant embryos in vivo

To evaluate whether *tum-myc^{wt}*, *tum-myc^{Pro}* or *tum-myc^{Polo}* could rescue *tum* mutant flies each of the transgenes were placed into a *tum* mutant background. Although none of the transgenes could rescue viability with a single copy, indicating that the transgene constructs did not completely recapitulate normal *tum* expression levels and/or function, both *tum-myc^{wt}* and *tum-myc^{Pro}* but not

Figure 4.13 **Pav^{wt}, Pav^{Pro} *and* Pav^{Polo} *localise normally during anaphase and telophase***

Late stage 11 - early stage 12 *pav^{wt}*, Df(3L)Exel9000/*pav^{wt}*, *pav^{B200}* (*pav^{wt}*), *pav^{Prot}*, Df(3L)Exel9000/*pav^{Pro}*, *pav^{B200}* (*pav^{Pro}*) and *pav^{Polo}*, Df(3L)Exel9000/*pav^{Polo}*, *pav^{B200}* (*pav^{Polo}*) embryos stained for microtubules (MT, red), Pav (green) and DNA (blue). **A**, **C** and **E**. Pav^{wt}, Pav^{Pro} and Pav^{Polo} all replicate the endogenous Pav staining pattern as they are localised to the centrosomes (arrowheads) and equator (arrows) during anaphase. **B**, **D** and **F**. At telophase Pav^{wt}, Pav^{Pro} and Pav^{Polo} are concentrated at the midbody (arrows). Images are maximum projections of z-series taken in 0.3μm steps. Scale bar in bottom right hand panel = 10μm.

MT
Pav
DNA
Merge
A
B
C
D
E
F
pavwt
pavPro
pavPolo

Figure 4.14 ***Anillin localisation is unperturbed during anaphase and telophase in* pav^{wt}, pav^{Pro} *and* pav^{Polo} *embryos***

Late stage 11 - early stage 12 *pav^{wt}*, Df(3L)Exel9000/*pav^{wt}*, *pav^{B200}* (*pav^{wt}*), *pav^{Prot}*, Df(3L)Exel9000/*pav^{Pro}*, *pav^{B200}* (*pav^{Pro}*) and *pav^{Polo}*, Df(3L)Exel9000/*pav^{Polo}*, *pav^{B200}* (*pav^{Polo}*) embryos stained for microtubules (MT, red), Anillin (green) and DNA (blue). **A**, **C** and **E**. Anillin accumulated at the equator of anaphase cells in *pav^{wt}*, *pav^{Pro}* and *pav^{Polo}* embryos (arrowheads). **B**, **D** and **F**. Anillin became concentrated at the midbody at telophase (arrowheads). Images are maximum projections of z-series taken in 0.3µm steps. Scale bar in bottom right hand panel = 10µm.

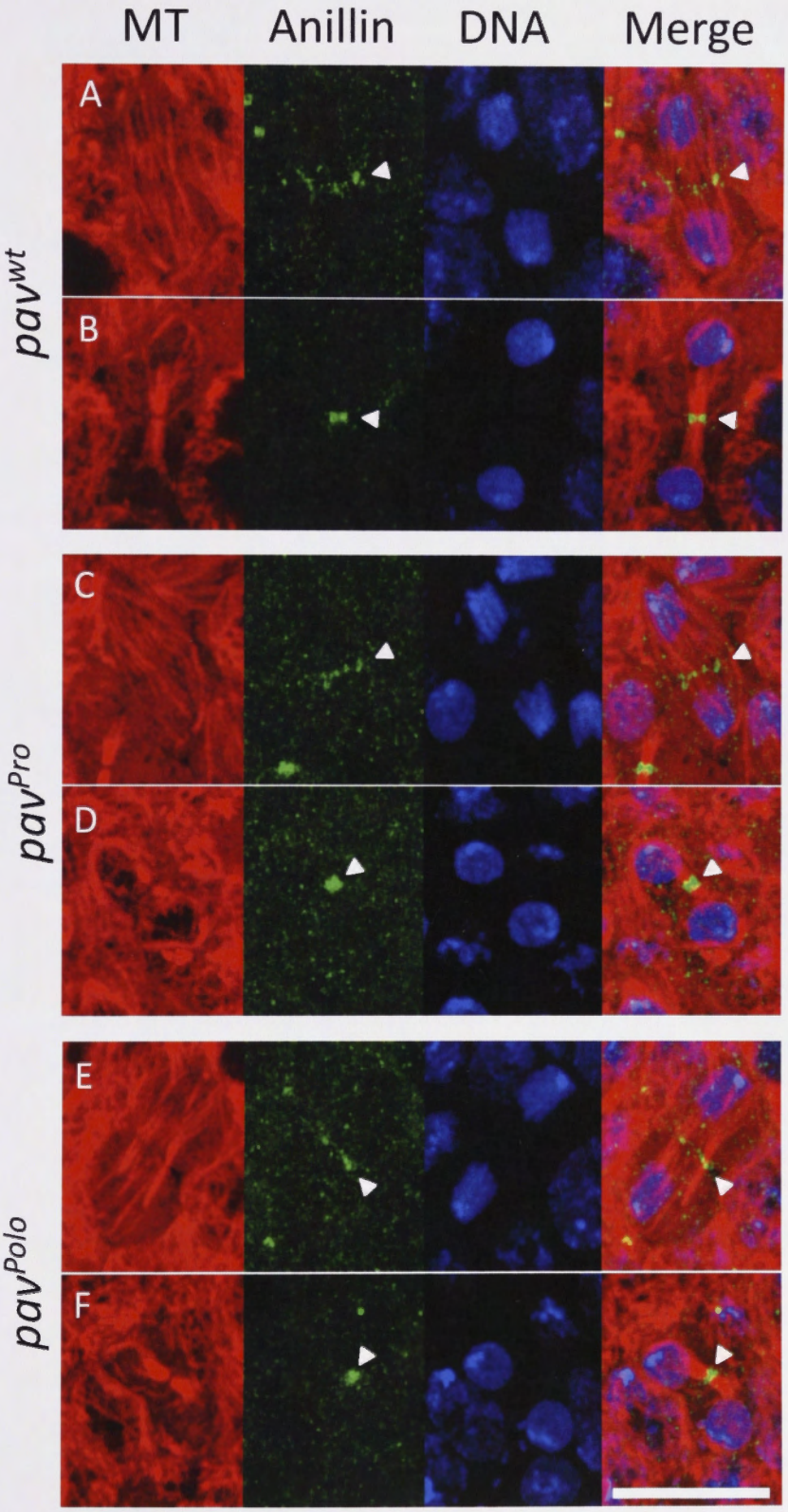
MT
Anillin
DNA
Merge
A
B
C
D
E
F
pav^wt
pav^Pro
pav^Polo

tum-myc^{Polo} could rescue viability when two copies were present. This strongly suggested that the introduced mutations in *tum-myc*^{Polo} interfered with its cytokinetic activities. To examine the effect these transgenes had on cytokinesis, cells completing cycle 16 were stained for Tum (myc tag) and Anillin. Recombinant lines containing a *tum-myc* transgene and *tum*^{AR2} or Df(2R)Exel7128 over *lacZ* marked balancers were crossed together (Figure 4.10C). Embryos were stained for β–galactosidase to identify embryos homozygous for a *tum-myc* transgene in a *tum* mutant background. For simplicity, embryos homozygous for the *tum-myc*^{wt}, *tum-myc*^{Pro} or *tum-myc*^{Polo} trangenes in a *tum* mutant background will hereafter be referred to as *tum-myc*^{wt}, *tum-myc*^{Pro} or *tum-myc*^{Polo}.

Tum-myc^{wt} and Tum-myc^{Pro} were found to recapitulate endogenous Tum localisation, accumulating at the equator of anaphase cells (Figure 4.15A and C arrowheads). Cells were capable of furrow constriction as indicated by intense Tum-myc^{wt} or Tum-myc^{Pro} staining at the midbody (Figure 4.15B and D arrowheads). Tum-myc^{Polo} also accumulated at the equator of anaphase cells (Figure 4.16A arrowheads), however cytokinesis defects were detected in these embryos. 42.9% (12/28) of telophase cells appeared capable of completing cytokinesis as indicated by the formation of robust midbody microtubules and intense accumulation of Tum-myc^{Polo} at the midbody (Figure 4.16B arrowheads). By contrast, 57.1% (16/28) of telophase cells failed furrow constriction (Figure 4.16C). These cells sometimes contained bundled microtubules, but the large unconstricted ring of Tum-myc^{Polo} at the equator clearly indicated that although Tum-myc^{Polo} is recruited to the equator in these cells, it was failing to promote

constriction at the cleavage furrow (Figure 4.16C arrowheads). The ability of Tum-myc^{Polo} to localise to the equator indicates that the introduced mutations have not completely disrupted function.

To confirm these findings, the localisation of Anillin was analysed for each *tum* transgene. Anillin was found to localise normally in *tum-myc^{wt}* and *tum-myc^{Pro}* embryos, where it accumulated at the equator of anaphase cells (Figure 4.17A and C), and 59/59 *tum-myc^{wt}* and 56/56 *tum-myc^{Pro}* telophase cells completed cytokinesis as evident from the presence of compacted microtubules with strong Anillin staining at the midbody (Figure 4.17B and D). By contrast, in *tum-myc^{Polo}* embryos Anillin could not be detected at the equator in the majority of anaphase cells (Figure 4.18A and C). At telophase 39.5% of cells (43/109) were capable of completing cytokinesis, as indicated by intense Anillin staining at the midbody, while 60.6% (66/109) showed no constriction (Figure 4.18B and D) and in these cells a faint ring of Anillin could sometimes be observed showing no signs of constriction (Figure 4.18E). These data indicate that although Anillin can be recruited to the equator of *tum-myc^{Polo}* cells, it is often absent or in insufficient quantities to promote the completion of cytokinesis.

The ability of *tum-myc^{Polo}* to rescue cytokinesis in *tum* mutant embryos was determined by comparing the number of binucleate cells between *tum-myc^{wt}* and *tum-myc^{Polo}* embryos. The absence of binucleate cells in *tum-myc^{wt}* embryos indicated that cytokinesis was completely rescued by the transgene (Table 4.3). In contrast, the *tum-myc^{Polo}* transgene was only able to partially rescue cytokinesis, with a substantial proportion of the cells in these embryos being

Figure 4.15 ***Tum-myc^{wt} and Tum-myc^{Pro} mimic endogenous Tum localisation during anaphase and telophase***

Late stage 11 - early stage 12 tum-myc^{wt}, Df(2R)Exel7128/tum-myc^{wt}, tum^{AR2} (tum-myc^{wt}) and tum-myc^{Pro}, Df(2R)Exel7128/tum-myc^{Pro}, tum^{AR2} (tum-myc^{Pro}) embryos stained for microtubules (MT, red), myc (green) and DNA (blue). **A** and **C**. Tum-myc^{wt} and Tum-myc^{Pro} mimicked the localisation of endogenous Tum as they accumulated at the equator of anaphase cells (arrowheads). **B** and **D**. At telophase Tum-myc^{wt} and Tum-myc^{Pro} became restricted to the midbody (arrowheads). Images are maximum projections of a z-series taken in 0.3μm steps. Scale bar in bottom right hand panel = 10μm.

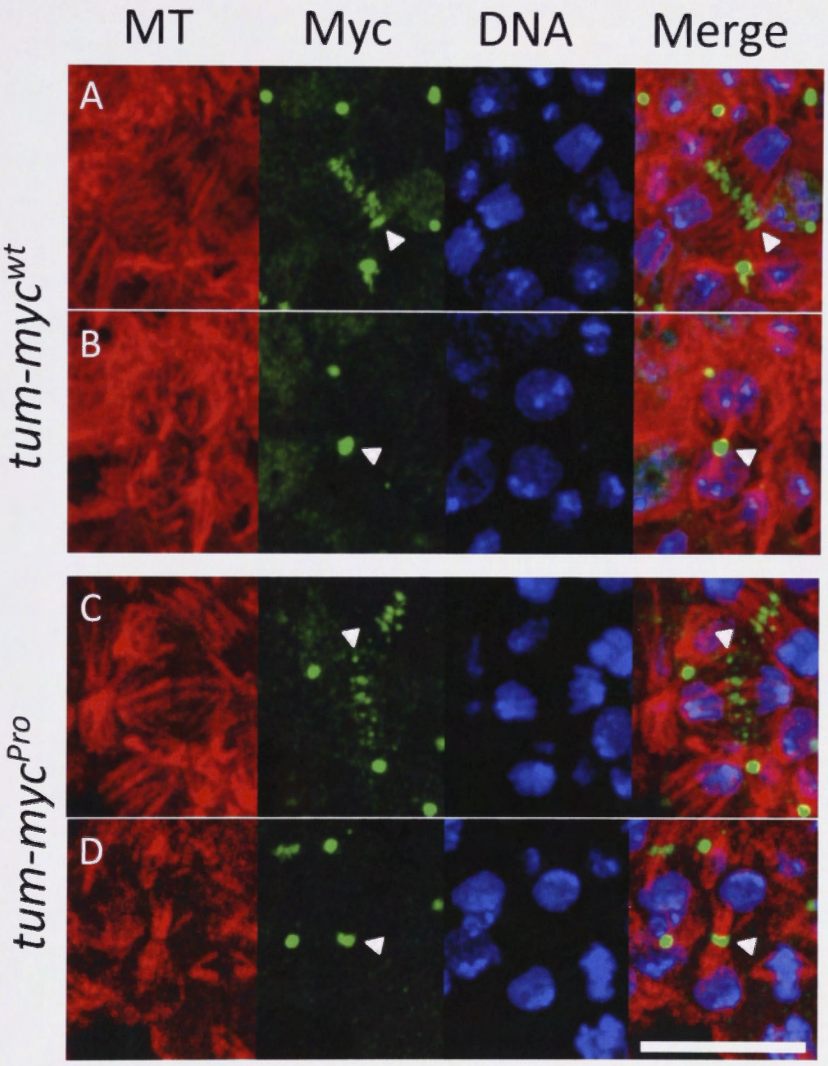
MT
Myc
DNA
Merge
A
B
C
D
tum-myc^wt
tum-myc^Pro

Figure 4.16 ***Tum-myc^{Polo} mimics endogenous Tum localisation during anaphase and telophase but many cells fail cytokinesis***

Late stage 11 - early stage 12 *tum-myc^{Polo}*, Df(2R)Exel7128/*tum-myc^{Polo}*, *tum^{AR2}* embryos stained for microtubules (MT, red), myc (green) and DNA (blue). **A.** Tum-myc^{Polo} mimicked endogenous Tum localisation during cytokinesis accumulating at the equator of anaphase cells (arrowheads). **B.** Some telophase cells completed cytokinesis as indicated by the formation of a robust midbody and strong Tum-myc^{Polo} staining at the midbody midpoint (arrowheads). **C.** However, many telophase cells failed cytokinesis despite the localisation of Tum-myc^{Polo} to the equator (arrowhead). Microtubules can be observed to traverse the equator of such cells indicating cytokinesis has failed. Images are maximum projections of a z-series taken in 0.3μm steps. Scale bar in bottom right hand panel = 10μm.

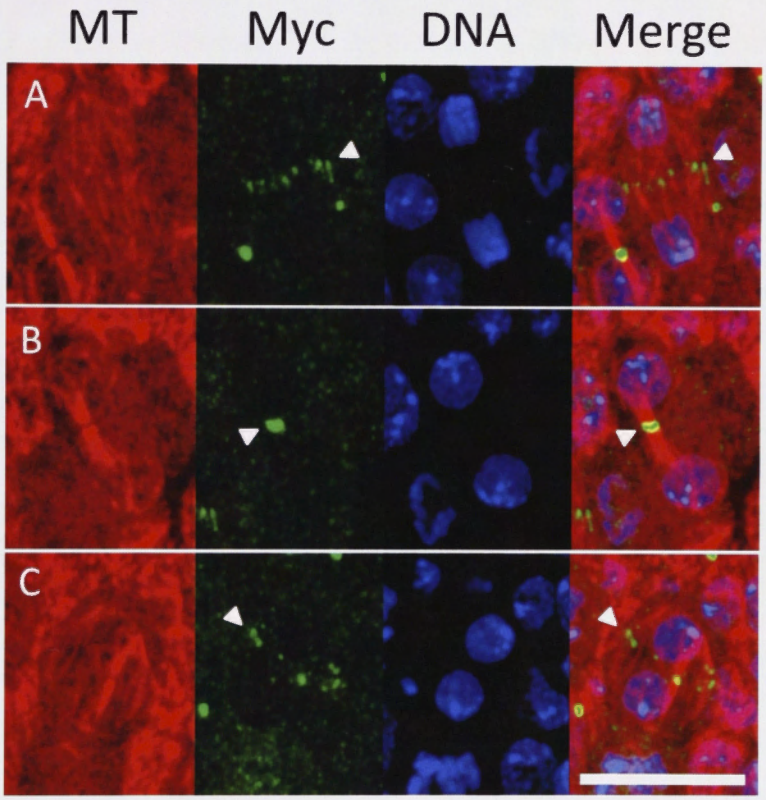
MT
Myc
DNA
Merge
A
B
C

Figure 4.17 ***Anillin localisation occurs normally during anaphase and telophase in* tum-myc^{wt} *and* tum-myc^{Pro} *embryos***

Late stage 11 - early stage 12 *tum-myc^{wt}*, Df(2R)Exel7128/*tum-myc^{wt}*, *tum^{AR2}* (*tum-myc^{wt}*) and *tum-myc^{Pro}*, Df(2R)Exel7128/*tum-myc^{Pro}*, *tum^{AR2}* (*tum-myc^{Pro}*) embryos stained for microtubules (MT, red), Anillin (green) and DNA (blue). **A** and **C**. Anillin accumulated at the equator of anaphase cells in *tum-myc^{wt}* and *tum-myc^{Pro}* embryos (arrowheads). **B** and **D**. Anillin became restricted to the midbody at telophase (arrowheads). Images are maximum projections of z-series taken in 0.3μm steps. Scale bar in bottom right hand panel = 10μm.

MT
Anillin
DNA
Merge
A
B
C
D
tum-myc^wt
tum-myc^Pro

Figure 4.18 ***Anillin localisation during anaphase and telophase is disrupted in many tum-myc^{Polo} embryos***

Late stage 11 - early stage 12 *tum-myc^{Polo}*, Df(2R)Exel7128/*tum-myc^{Polo}*, *tum^{AR2}* embryos stained for microtubules (MT, red), Anillin (green) and DNA (blue). **A.** Anillin accumulated at the equator of some anaphase cells (arrowheads). **B.** A number of telophase cells completed cytokinesis as demonstrated by their ability to construct a robust midbody and the intense Anillin staining at the midbody midpoint (arrowheads). **C.** Conversely, some anaphase cells were unable to accumulate Anillin at the equator (arrowhead). **D.** Similarly, telophase cells unable to construct midbodies or concentrate Anillin are observable. **E.** However, equatorial Anillin accumulation can be observed in some telophase cells that seemed unable to divide (arrowheads). Images are maximum projections of z-series taken in 0.3µm steps. Scale bar in bottom right hand panel = 10µm.

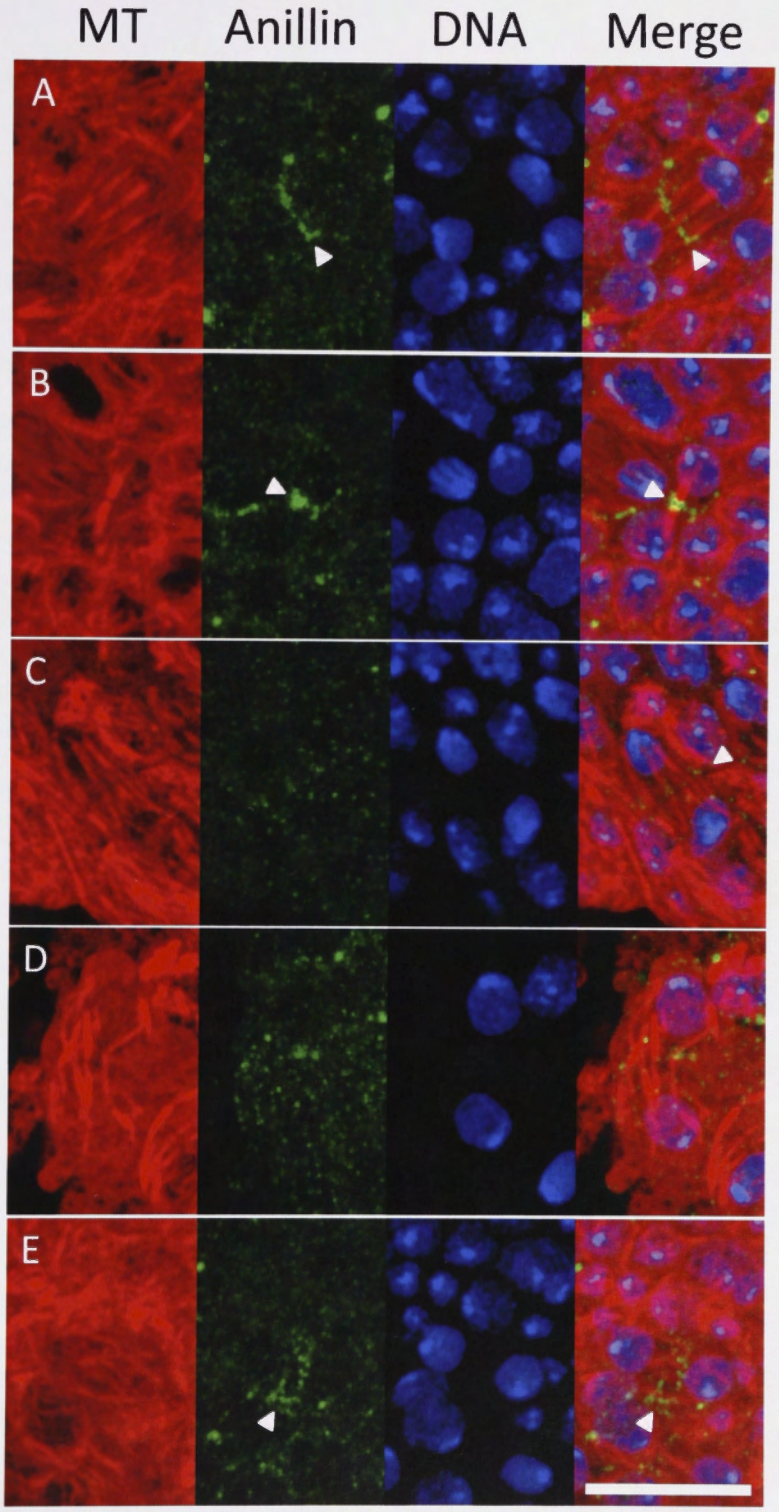
MT
Anillin
DNA
Merge
A
B
C
D
E

binucleate (≈55%) (Table 4.3). This corresponds to a percentage of cytokinesis failure of 68.7% in *tum-myc*^{Polo} compared with 90% in *tum* mutants (table 4.3).

Table 4.3. Percentage of binucleate cells in *tum*, *tum-myc*^{wt} and *tum-myc*^{Polo} mutant embryos

Genotype	Percentage binucleate (mean ± SD)	Percentage cells failing division	Number of cells scored (# embryos)
Df(2R)Exel7128/*tum*^{AR2}	81.88±2.99	90.0	1030(7)
tum-myc^{wt}, Df(2R)Exel7128/ *tum-myc*^{wt}, *tum*^{AR2}	0±0	0	1044(6)
tum-myc^{Polo}, Df(2R)Exel7128/ *tum-myc*^{Polo}, *tum*^{AR2}	54.63±6.60	68.7	1994(7)

Mid-late stage 12 *tum* mutant, *tum-myc*^{wt} and *tum-myc*^{Polo} embryos were stained for lamin and F-actin, to detect the nuclear envelope and mark cell boundaries respectively, and the percentage of binucleate cells determined for each embryo. These values were used to calculate the mean and standard deviation (SD) for each genotype. To determine the percentage of cells failing division the number of mononucleate cells was halved and combined with the total number of binucleate cells and the percentage of cells failing to divide calculated.

To determine how the mutations in the putative polo kinase motifs in the Tum-myc^{Polo} transgene were affecting cytokinesis, I looked to see if the mutations altered the ability of Tum to interact with Pbl and thereby recruit Pbl to the cleavage furrow. To do this it was necessary to generate flies expressing Tum-myc^{Polo} and Pbl-GFP^{wt} in a *pbl* and *tum* mutant background (Figure 4.19). The embryos examined lacked both *tum* and *pbl* wild type function and contained one copy of the *tum-myc*^{wt} or *tum-myc*^{Polo} and *pbl-GFP*^{wt} transgenes, and are hereafter referred to as *tum-myc*^{wt};*pbl-GFP*^{wt} or *tum-myc*^{Polo};*pbl-GFP*^{wt}. In *tum-myc*^{wt};*pbl-GFP*^{wt} embryos, Pbl-GFP^{wt} accumulated at the equator of anaphase cells (Figure 4.20A arrowheads) and followed the constricting furrow in the majority of telophase cells examined (19/26) (Figure 4.20B arrowheads).

However, 27% of cells (7/26) were unable to complete constriction as evident from the unbundled microtubules and lack of Pbl-GFP^{wt} accumulation at the equator (Figure 4.20C). By contrast, Pbl-GFP^{wt} could not be detected at the equator of anaphase cells in all the *tum-myc^{Polo};pbl-GFP^{wt}* embryos examined (Figure 4.20D). Furthermore, most telophase cells (19/22) failed to complete constriction with an absence of microtubule bundling and Pbl-GFP^{wt} accumulation at the equator (Figure 4.20E). In the three telophase cells that showed furrow constriction, only one accumulated significant levels of Pbl-GFP^{wt} (Figure 4.20F arrowheads). These results indicate that Tum-myc^{Polo} was unable to efficiently recruit and maintain Pbl-GFP^{wt} at the equator of cells initiating cytokinesis. Thus the mutations in *tum-myc^{Polo}* appear to disrupt the Pbl-Tum interaction which leads to widespread cytokinesis failure.

4.3 Discussion

In this chapter I have tested the importance of candidate phosphorylation target residues in Pbl, Pav and Tum that may facilitate the interaction between Tum and Pbl. I found that while proline-directed phosphorylation sites were not important for stimulating the Pbl-Tum interaction, Polo-sites in Tum, but not Pav or Pbl, are critical for the equatorial accumulation of Pbl, furrow constriction and the completion of cytokinesis. These results extend our understanding of the mechanisms that regulate the Pbl-Tum interaction and implicate Polo kinase as a key regulator of cytokinesis in *Drosophila*.

Tum plays a central role in cytokinesis through the formation of the central spindle and by facilitating the construction and constriction of the

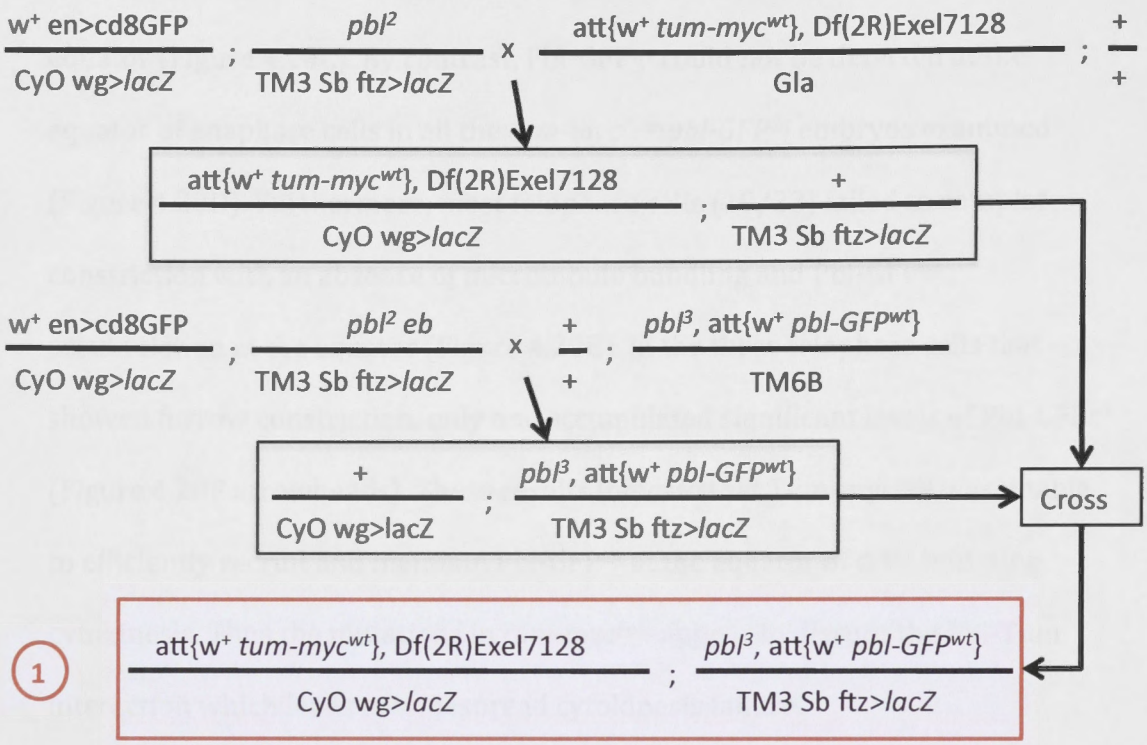
w+ en>cd8GFP
CyO wg>lacZ
pbl2
TM3 Sb ftz>lacZ
att{w+ tum-mycwt}, Df(2R)Exel7128
Gla
att{w+ tum-mycwt}, Df(2R)Exel7128
CyO wg>lacZ
TM3 Sb ftz>lacZ
w+ en>cd8GFP
CyO wg>lacZ
pbl2 eb
TM3 Sb ftz>lacZ
pbl3, att{w+ pbl-GFPwt}
TM6B
CyO wg>lacZ
pbl3, att{w+ pbl-GFPwt}
TM3 Sb ftz>lacZ
Cross
1
att{w+ tum-mycwt}, Df(2R)Exel7128
CyO wg>lacZ
pbl3, att{w+ pbl-GFPwt}
TM3 Sb ftz>lacZ

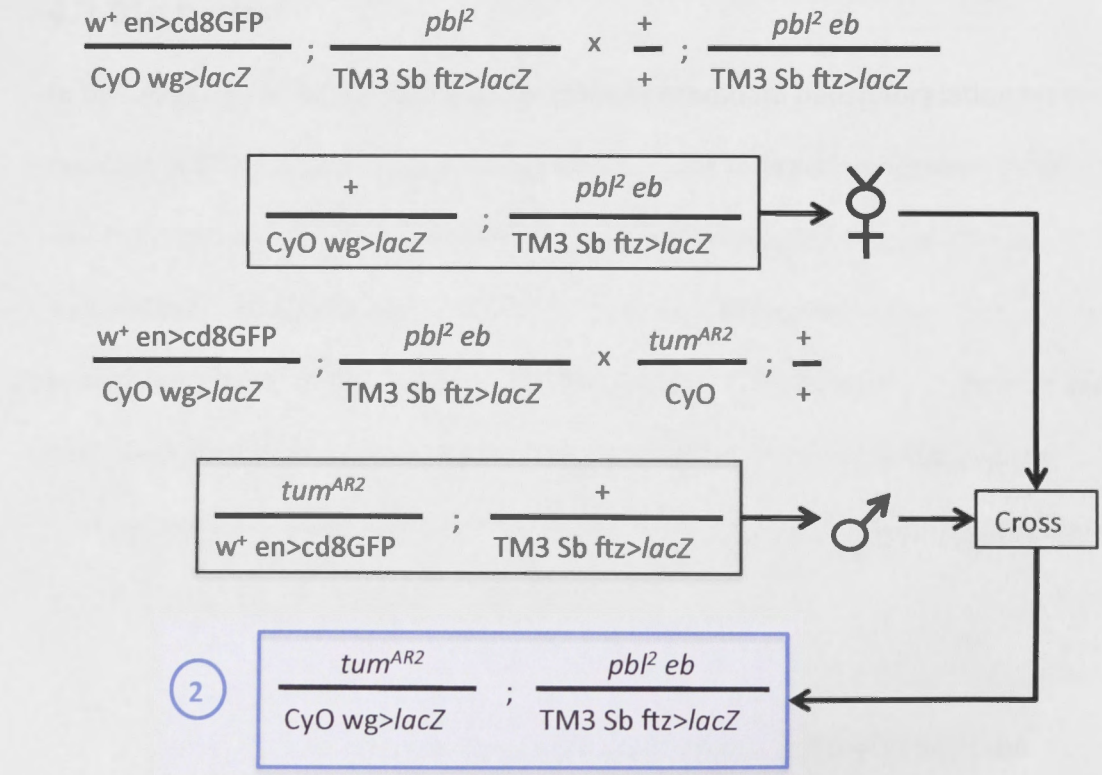
w+ en>cd8GFP
CyO wg>lacZ
pbl2
TM3 Sb ftz>lacZ
pbl2 eb
TM3 Sb ftz>lacZ
CyO wg>lacZ
pbl2 eb
TM3 Sb ftz>lacZ
w+ en>cd8GFP
CyO wg>lacZ
pbl2 eb
TM3 Sb ftz>lacZ
tumAR2
CyO
tumAR2
w+ en>cd8GFP
TM3 Sb ftz>lacZ
Cross
2
tumAR2
CyO wg>lacZ
pbl2 eb
TM3 Sb ftz>lacZ

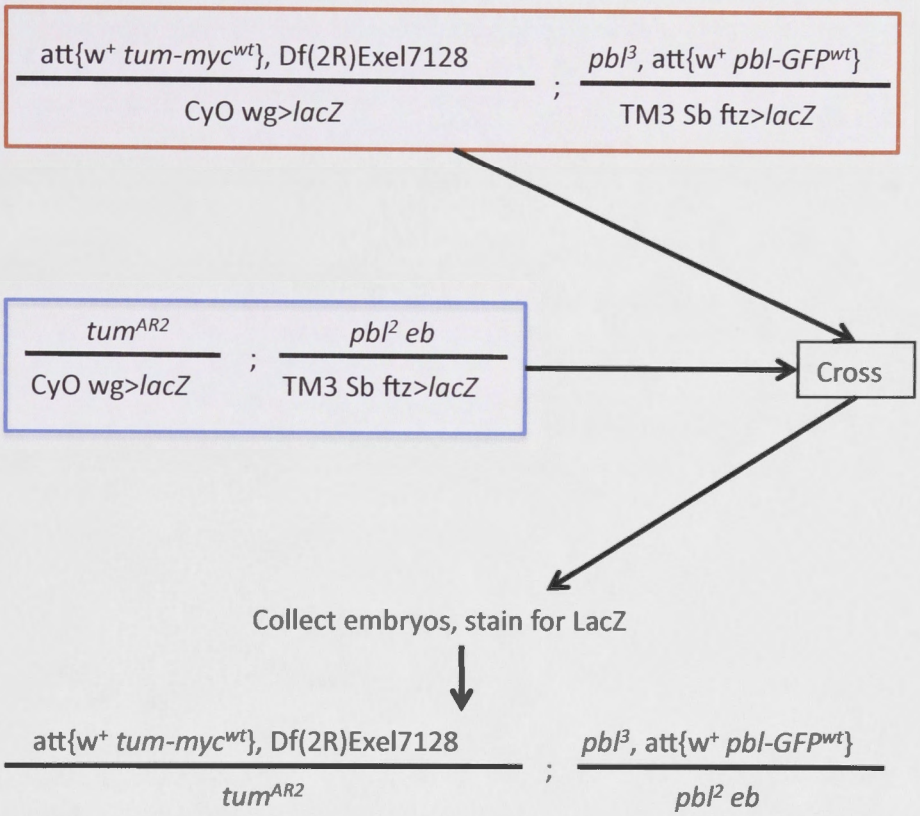

Figure 4.19 ***Creating fly lines to enable the localisation of Pbl-GFP^{wt} to be examined in Tum-myc^{wt} or Tum-myc^{Polo} mutant backgrounds***

The crossing scheme used to combine *pbl-GFP^{wt}* with *tum-myc^{wt}* or *tum-myc^{Polo}* in a *pbl* and *tum* mutant background is depicted. Two stocks were initially created; one was heterozygous for the tum-myc and pbl-GFP transgenes over *lacZ* marked balancers (upper panel, labeled (1)), while the other contained the tum^{AR2} pbl^{2} alleles over *lacZ* marked balancers (lower panel, labeled (2)). These two stocks were then crossed together, embryos collected and stained for LacZ to identify embryos of the desired genotype that were subsequently stained for immunofluorescence analysis.

Figure 4.20 ***Pbl-GFP cleavage furrow localisation is disrupted in tum-myc^{Polo};pbl-GFP^{wt} embryos***

Late stage 11 - early stage 12 *tum-myc^{wt}*, Df(2R)Exel7128/*tum-myc^{wt}*, *tum^{AR2}* ; *pbl-GFP^{wt}*, *pbl^{2}/ pbl-GFP^{wt}*, *pbl^{3}* (*tum-myc^{wt};pbl-GFP^{wt}*) and *tum-myc^{Polo}*, Df(2R)Exel7128/*tum-myc^{Polo}*, *tum^{AR2}* ; *pbl-GFP^{wt}*, *pbl^{2}/ pbl-GFP^{wt}*, *pbl^{3}* (*tum-myc^{Polo};pbl-GFP^{wt}*) embryos stained for microtubules (MT, red), GFP (green) and DNA (blue). **A.** Pbl-GFP^{wt} could be identified at the equator of anaphase cells in *tum-myc^{wt};pbl-GFP^{wt}* embryos. **B.** Most telophase cells (19/26) completed cytokinesis where robust midbody microtubules indicated furrowing had proceeded and Pbl-GFP^{wt} was detected at the midbody midpoint (arrowheads). **C.** However, some telophase cells (7/26) failed to construct a midbody or show any signs of Pbl-GFP^{wt} accumulation at the equator. **D.** Pbl-GFP^{wt} could not be detected at the equator of any anaphase cells in *tum-myc^{Polo};pbl-GFP^{wt}* embryos. **E.** The majority of telophase cells (19/22) failed to constrict, form a midbody or accumulate Pbl-GFP^{wt} at the equator. **F.** A few telophase cells (3/22) completed cytokinesis as demonstrated by their ability to form midbody microtubules although Pbl-GFP^{wt} was only faintly detectable at the midbody midpoint (arrows). Images are maximum projections of z-series taken in 0.3μm steps. Scale bar in bottom right hand panel = 10μm.

MT
GFP
DNA
Merge
A
B
C
D
E
F
tum-myc^wt;pbl-GFP^wt
tum-myc^Polo;pbl-GFP^wt

contractile ring. This makes Tum a strong candidate for being targeted and regulated by phosphorylation, particularly following studies that demonstrated a role for Plk1 in stimulating the Ect2-HsCyk-4 interaction (Burkard et al., 2007; Petronczki et al., 2007). Assessment of the ability of the *tum-myc* constructs to rescue *tum* mutant flies showed that none were able to rescue *tum* mutant flies to adulthood with a single copy of a transgene. By contrast, flies carrying a single functional copy of endogenous *tum* are viable. This suggested that the *tum-myc* transgenes failed to completely replicate endogenous *tum* expression levels or that the myc tag interferes with Tum function. Position effects due to site of integration and/or the absence of some regulatory elements in the constructs could both have affected expression levels. However, while two copies of both *tum-myc^{wt}* and *tum-myc^{Pro}* were able to rescue *tum* mutant flies to adulthood, two copies of *tum-myc^{Polo}* was unable to do so. This suggested that the mutations introduced into Tum-myc^{Polo} interfered with its cytokinetic activities. Immunofluorescence analysis showed that this was in fact the case. As expected, cytokinesis defects could not be detected in *tum-myc^{wt}* or *tum-myc^{Pro}* cells. By contrast, while all the Tum-myc recombinant proteins were capable of localising equatorially at anaphase, most *tum-myc^{Polo}* cells were unable to progress through telophase as evident from the unbundled microtubules and an unconstricted ring of Tum-myc^{Polo} at the equator. Cytokinesis failure was confirmed by the Anillin stains which showed that Anillin accumulation at the equator was highly variable; being completely absent in some cells yet present in others but unable to stimulate completion of cytokinesis. This suggested that some cells were able to accumulate enough Pbl at the equator to activate Rho, recruit Anillin and complete cytokinesis.

As fixed samples were used it was possible that the furrowing observed in some cells, which were judged to have ultimately completed cytokinesis, eventually regressed resulting in division failure. Indeed the number of cells determined to have failed cytokinesis in *tum-myc^{Polo}* embryos, as determined by an inability to compact microtubules or concentrate Tum-myc^{Polo} (57.1%) or Anillin (60.6%) at the midbody, was slightly lower than binucleate cell counts (68.7%). This suggests that furrow regression may have occurred in a small number of cells exhibiting compacted microtubules and significant Tum-myc^{Polo} or Anillin accumulation. The prevalence of furrow regression could be verified using live imaging.

Counts of binucleate cells showed that *tum-myc^{Polo}* was partially able to rescue *tum* mutant embryos. However, this rescue may have over-estimated the ability of Tum-myc^{Polo} to function. Previous work has shown that *tum^{AR2}* is a hypomorphic allele and thus produces a protein with some functionality (Zavortink et al., 2005). As centralspindlin is a heterotetramer consisting of two molecules of Pav and Tum, some complexes may have contained both Tum^{AR2} and Tum-myc^{Polo}. In this situation Tum-myc^{Polo} may have stabilized Tum^{AR2} and promoted recruitment of Tum^{AR2} to the equator. Tum^{AR2} contains the Pbl binding region, so a stabilization may lead to an increased accumulation of Pbl at the equator compared to *tum* mutant embryos. Thus the partial rescue of cell division by Tum-myc^{Polo} may have been facilitated by the synergistic effect of Tum^{AR2}. To test this, *tum-myc^{Polo}* recombinants containing a null *tum* allele could

be created, where binucleate counts should increase if *tum*^{AR2} was contributing to the degree of rescue.

Consistent with this, the immunofluorescence studies reported here show that there was a significant reduction in the accumulation of Pbl-GFP^{wt} at the equator of *tum-myc*^{Polo}*;pbl-GFP*^{wt} cells compared with *tum-myc*^{wt}*;pbl-GFP*^{wt} cells. Since Tum-myc^{Polo} is recruited to the equator in these cells, the residues mutated in Tum-myc^{Polo} are most likely to disrupt the interaction with Pbl, leading to a reduction in the accumulation of Pbl at the furrow and subsequently cytokinesis failure. Although some cells fail cytokinesis in *tum-myc*^{wt}*;pbl-GFP*^{wt} embryos, this was not unexpected as neither *tum-myc*^{wt} or *pbl-GFP*^{wt} was able to rescue the viability of *tum* or *pbl* mutant flies with a single copy of the transgene. These data indicate that *tum-myc*^{wt} and *pbl-GFP*^{wt} fail to replicate endogenous *tum* and *pbl* expression levels. Therefore, a combination of reduced levels of both Pbl and Tum may have prevented the completion of cytokinesis in some cells.

Coimmunoprecipitation experiments would have complemented the data presented here and confirmed that the mutations introduced into *tum-myc*^{Polo} disrupted the Pbl-Tum interaction in vivo. However this would be difficult to demonstrate using *Drosophila* embryo extracts. Although we have previously coimmunoprecipitated Pbl and Tum from embryo extracts (Somers and Saint, 2003), this was achieved using stage 1-5 embryos. Cellularisation has still not occurred in these early embryos and nuclear divisions occur in synchronous waves. This increases the proportion of mitotic cells and thus facilitates the detection of the Pbl-Tum interaction. Since maternally deposited Tum would

compete with Tum-myc^{wt} or Tum-myc^{Polo} for Pbl binding, coimmunoprecipitation should be performed on stage 11 or older embryos where maternal Tum has been depleted. A detailed analysis of embryos at these later stages has demonstrated that there are distinct mitotic domains within the now cellularised blastoderm that divide in a sequential pattern (Foe, 1989). Therefore, the fraction of mitotic cells in a stage 11 or older embryo would be very small. Thus it would be extremely difficult to coimmunoprecipitate Tum-myc^{wt} or Tum-myc^{Polo} and Pbl using embryonic extracts. Another possibility would be to coimmunoprecipitate Pbl from *Drosophila* cell lines transfected with either *tum-myc^{Polo}* or *tum-myc^{wt}* expression constructs. However, we are currently unable to synchronise *Drosophila* cell lines during mitosis, which poses a similar problem since the proportion of mitotic cells would be very small. Therefore immunoprecipitation experiments from *Drosophila* cultured cell lines are not feasible. One possibility would be to phosphorylate N-terminal fragments of Tum^{wt} and Tum^{Polo} in vitro using Polo kinase and test their ability to pull down N-terminal Pbl. However, this would require the construction, expression and purification of several recombinant proteins and is beyond the scope of this study.

Although it was not shown that Polo phosphorylates the targeted residues in Tum-myc^{Polo}, the sites targeted here showed high homology with the consensus phosphorylation motif. Furthermore, two recent studies in mammals identified similar Plk1 phosphorylation events that stimulate the Ect2-HsCyk-4 interaction (Burkard et al., 2009; Wolfe et al., 2009). Although the number and position of the identified phosphorylation sites differed slightly between the two

studies, three of the phosphorylation sites were common to both studies (Figure 4.21). Moreover, immunoprecipitation assays from mitotic lysates suggested that Ser157 in HsCyk-4 was the major phosphorylation site that mediated the interaction as mutation of Ser157 prevented the Ect2-HsCyk-4 interaction (Burkard et al., 2009; Wolfe et al., 2009). The phosphorylation sites near Ser157 in HsCyk-4 are not conserved in Tum (Figure 4.21). Therefore, it is highly likely that Ser157 in Tum is the only Polo kinase site that influences the Pbl-Tum interaction in *Drosophila*. Construction of a transgenic *tum* construct containing a single S157 to A mutation and immunofluorescence experiments to detect localisation of Pbl would determine if this were the case.

Immunoprecipitation assays using Plk1 mutant versions of HsCyk-4 have been shown to severely disrupt its interaction with Ect2 (Burkard et al., 2009; Wolfe et al., 2009). However, Ect2 is still detectable in many of these pull-down assays. These results may reflect a phosphorylation-independent low affinity Ect2-HsCyk-4 interaction that is not stable enough to pull-down significant amounts of protein. Consistent with this, an Ect2 pull-down assay detected HsCyk-4 in phosphatase treated mitotic lysates (Yüce et al., 2005). Furthermore, although the HsCyk-4 Plk1-target site mutant construct led to cytokinesis failure, it did provide some level of rescue to HsCyk-4 RNAi treated cells (Wolfe et al., 2009). This emulated the binucleate counts presented here where *tum-myc*^{Polo} was able to partially rescue *tum* mutant cells. Moreover, yeast two hybrid experiments have shown that Pbl and Tum are capable of interacting in the absence of Polo kinase (Somers and Saint, 2003). This evidence supports the premise that Polo phosphorylation is not absolutely required for the Pbl/Ect2-

Tum/HsCyk-4 interaction. Instead, it seems that Polo/Plk1 phosphorylation of Tum/HsCyk-4 ensures a high affinity interaction with Pbl/Ect2. In the absence of this phosphorylation event a low affinity interaction can still occur that is sometimes enough to recruit and maintain sufficient levels of Pbl/Ect2 at the furrow to permit the completion of cytokinesis.

Since previous work showed that Plk1 could phosphorylate Ect2 in vitro (Hara et al., 2006), it is possible that *Drosophila* Polo may phosphorylate Pbl in vivo and stimulate the Pbl-Tum interaction during cytokinesis. However, immunofluorescence detection showed that there was no difference in the recruitment of either Pbl-GFP^{wt} and Pbl-GFP^{Polo} to the equatorial cortex. Moreover, the localisation of Anillin was unperturbed in both *pbl-GFP^{wt}* and *pbl-GFP^{Polo}* embryos. Significantly, then, these data indicate that Polo phosphorylation of the N-terminus of Pbl does not play a role in stimulating the Pbl-Tum interaction and is not required for Pbl's cytokinetic functions.

Despite the ability of the *pbl-GFP* transgenes to rescue furrow constriction, they were only partially capable of rescuing *pbl* mutant flies to adulthood and only when in a *pbl^3/pbl^3* homozygous mutant background. The ability to rescue in this specific *pbl* mutant background was probably due to deleterious background mutations on the *pbl^3* chromosome being separated from the *pbl^3* allele when it was recombined with the *pbl-GFP* transgenes. Position effects relating to the site of integration may have altered *pbl-GFP* transgene expression preventing them from replicating the endogenous expression pattern. However, the *pav* transgenes were integrated into the same

Figure 4.21 ***Alignment of Tum orthologues indicating residues implicated in Pbl-Tum interaction***

An alignment of the amino acid sequences of Tum and its orthologues in *Homo sapiens*, *Mus musculus*, *Danio rerio*, and *Xenopus laevis*. Two mammalian studies identified several Plk1 phosphorylated residues crucial for the Ect2-HsCyk-4 interaction (indicated in red). Of these residues only S157 is conserved in *Drosophila*. The position of the sequence within each protein is indicated prior to the amino acid sequence.

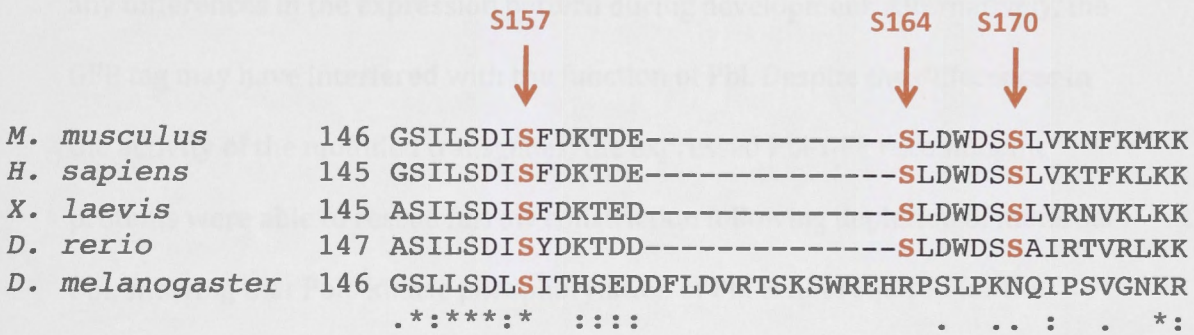
S157
S164
S170
M. musculus 146 GSILSDISFDKTDE----------SLDWDSSLVKNFKMKK
H. sapiens 145 GSILSDISFDKTDE----------SLDWDSSLVKTFKLKK
X. laevis 145 ASILSDISFDKTED----------SLDWDSSLVRNVKLKK
D. rerio 147 ASILSDISYDKTDD----------SLDWDSSAIRTVRLKK
D. melanogaster 146 GSLLSDLSITHSEDDFLDVRTSKSWREHRPSLPKNQIPSVGNKR

attP site and were capable of rescuing *pav* mutant flies to adulthood when either one or two copies of the transgene. This suggests that suppressive position effects were not responsible for the lack of *pbl-GFP* rescue. These results suggest that despite the inclusion of flanking genomic sequences (see 2.2.11.2.1), some regulatory elements were omitted from the *pbl* constructs preventing them from replicating endogenous *pbl* expression levels and/or patterns. The expression levels of *pbl* in the transgenic embryos could be determined using quantitative real time PCR and compared directly to expression levels of endogenous *pbl* at different developmental stages. In situ hybridisation could also be used to detect any differences in the expression pattern during development. Alternatively, the GFP tag may have interfered with the function of Pbl. Despite the differences in the activity of the modified transgenes, the expressed Pbl-GFP recombinant proteins were able to rescue furrow constriction following depletion of maternal Pbl, showing that Polo kinase phosphorylation of Pbl is not required for the progression of cytokinesis.

Although Pav has not been shown to be directly involved in mediating the Pbl-Tum interaction, it is essential for the localisation of Tum. Thus because the two proteins interact in the centralspindlin complex, it was possible that Pav participated in recruiting or stabilising Pbl by affecting the tertiary structure of Tum. However, each of the *pav* transgenes tested here could fully rescue the viability of *pav* mutant flies. Furthermore, the localisation of Pav^{wt}, Pav^{Pro}, Pav^{Polo} and Anillin throughout cytokinesis appeared normal confirming that the introduced mutations did not perturb the function of Pav. These results indicate that phosphorylation of Pav by Polo is not required to stimulate the Pbl-Tum

interaction or any other role of Pav during cytokinesis. Similarly, the results from the *pav*^{Pro} transgene demonstrate that proline-directed phosphorylation is not required for important cytokinetic activities. Furthermore, some of the potential phosphorylation sites targeted in Pav were within the analogous region of Zen-4 identified to interact with Cyk-4 in *C. elegans*. Therefore, as Pav and Tum are interdependent for their localisation to the equator (Zavortink et al., 2005), as are their *C. elegans* orthologues (Jantsch-Plunger et al., 2000), I conclude that neither Polo nor proline-directed phosphorylation events stimulate the Tum-Pav interaction.

4.4 Conclusion

Wild type and mutant *pbl-GFP*, *tum-myc* and *pav* transgenes were tested for their ability to rescue furrow constriction in embryos. The results show that proline-directed phosphorylation is not required to stimulate cytokinetic interactions. However, Polo phosphorylation of Tum, but not Pav or Pbl, is required for cytokinesis completion. As mutations in the Polo kinase sites of Tum (i.e. Tum-myc^{Polo}) significantly reduced recruitment of Pbl-GFP at the cleavage furrow, it is likely that disruption to cytokinesis occurs because the ability of Pbl to interact with Tum is diminished.

Chapter 5: Final discussion

The aim of the studies described in this thesis was to define molecular events that regulate the Pbl-Tum interaction and thereby control the initiation of cytokinesis. The Pbl-Tum interaction is essential for the correct equatorial localisation of Pbl and for the initiation of cytokinesis through the activation of Rho. This study used two approaches to define the mechanisms that regulate this interaction.

The first approach involved over-expression and purification of recombinant Pbl and Tum proteins in an effort to crystallize both proteins for structural studies. Significant amounts of soluble Pbl protein were produced and isolated, but it proved difficult to remove contaminating proteins and to prevent the accumulation of degradation products. Similarly, significant amounts of $Pbl^{N\text{-}term}$ were produced, isolated and purified to a high degree. However, contaminating proteins and the persistence of breakdown products precluded crystallization trials. Despite this, a nearly pure preparation of full length Pbl (Pbl^{fl}) was prepared, but failed to produce protein crystals. Initial expression of Tum produced mainly insoluble protein. Incorporation of an MBP tag improved solubility, but I was unable to isolate substantial amounts of soluble MBPTum protein.

The second approach to Pbl and Tum characterization involved targeted mutagenesis of potentially important phosphorylation sites in Pbl, Tum and Pav.

The localisation of the recombinant proteins and other cytokinesis components were then used to compare the progression of cytokinesis in wild type and mutant transgene backgrounds. The results from this work demonstrated that the Polo phosphorylation sites on Tum, but not on Pbl or Pav, were required for the recruitment of Pbl by Tum and the progression of cytokinesis. In contrast, mutations to the proline-directed phosphorylation sites of Pav or Tum had no effect.

5.1 The Pbl-Tum interaction is phospho-regulated

The ability of Pbl/Ect2 to interact with Tum/HsCyk-4 appears to be tightly regulated by a number of phosphorylation events mediated by both Cdk1 and Polo. Several studies detected changes in the phosphorylation state of Ect2 during mitosis, as indicated by shifts in the migration rate of the protein when run on protein gels and western blot analyses using antibodies that recognise specific phosphoepitopes (Hara et al., 2006; Niiya et al., 2006; Tatsumoto et al., 1999; Yüce et al., 2005; Zhao and Fang, 2005). Many of these studies observed a change in the phosphorylation state of Ect2 when cells entered anaphase. Since Cdk1 is rapidly deactivated at the metaphase to anaphase transition, the ability of Cdk1 to phosphorylate Ect2 was investigated. It was found that Cdk1 phosphorylates Ect2 at T341 which prevents a premature association with HsCyk-4 (Yüce et al., 2005) and relieves the autoinhibitory conformation of Ect2 thereby activating GEF function (Hara et al., 2006). Furthermore, Cdk1 phosphorylation of residue T412 in Ect2 enhances its ability to bind Rho (Niiya et al., 2006). However, as T412 does not reside within the GEF domain of Ect2, it is unlikely to modulate GTPase binding specificity. Rather, this phosphorylation

event is more likely to alter the conformation of Ect2, resulting in an open conformation capable of GEF activity. Therefore, Cdk1 regulates the onset of the Ect2-HsCyk-4 interaction while also contributing to GEF activation. Although these phosphorylation events have not been confirmed in *Drosophila*, prolonging Cdk1 activity into anaphase inhibits the cytokinetic functions of Pbl (Echard and O'Farrell, 2003). Therefore, Cdk1 may mediate phosphorylation that inhibits the Pbl-Tum interaction in *Drosophila* in a similar manner.

In this study, I tested the possibility that proline-directed phosphorylation events might influence the Pbl-Tum interaction. Of particular significance, I used advanced recombineering and targeted transformation to construct in vivo tests for the function of particular residues. Although such an approach involves extensive molecular manipulations and genetic crossing schemes to put the right genotypes together, it has the enormous benefit of being a true in vivo test of the modifications, as opposed to the more common in vitro biochemical or cell culture tests.

The first clear outcome to arise from these experiments is that no cytokinesis defects were observed when potential proline-directed phosphorylation sites were mutated in Tum or Pav. Furthermore, cells that over-expressed a Pbl construct in which potential proline-directed phosphorylation sites were mutated did not exhibit cytokinesis defects in *Drosophila* embryos (R. Saint and M. Murray unpublished observations). Significantly, therefore, proline-directed phosphorylation of Pbl, Tum or Pav does not appear to be required for the Pbl-Tum interaction or other cytokinesis functions. Moreover, since the

residues targeted in Pav encompass the Tum interaction region, proline-directed phosphorylation also appears not to be required to induce formation of centralspindlin. Furthermore, given that Cdk1 is itself a proline-directed kinase, these results suggest that preventing Cdk1 phosphorylation of Pbl, Tum or Pav individually is insufficient to induce premature cytokinesis. In other words, it is the culmination of many coordinated events that results in the initiation of cytokinesis. If Cdk1 does play a role in the timing of the onset of cytokinesis in *Drosophila*, preventing the phosphorylation of a single Pbl, Tum or Pav target does not appear to be sufficient to prematurely induce cytokinesis.

Polo phosphorylation of Tum, however, does appear to be important for Pbl/Tum interactions. Interestingly, early studies suggested that the Tum/HsCyk-4 protein does not require any modifications to interact with Pbl/Ect2. An N-terminal Ect2 recombinant protein was able to pull down equivalent amounts of HsCyk-4 from both metaphase and anaphase cell extracts (Yüce et al., 2005). This study suggested that at metaphase HsCyk-4 contained all the necessary modifications to interact with Ect2 and lacked any modifications that might prevent the interaction. Furthermore, N-terminal Pbl and full length Tum are able to interact in a yeast two hybrid assay (Somers and Saint, 2003). Since mitotic modifications of Tum are unlikely to occur in this system, these observations demonstrate that Pbl and Tum are able to interact in the absence of such modifications. Based on my results, however, it appears that Polo phosphorylation of Tum is important for establishing an appropriate interaction in vivo. Chapter 4 described the inability of most cells (68.7%) to complete cytokinesis in embryos expressing Tum protein mutated at the putative Polo

phosphorylation sites (*tum*^{Polo}). In these cells Tum-myc^{Polo} protein localised normally but equatorial Anillin accumulation was reduced or absent. Cytokinesis failure and defective Anillin accumulation was most likely caused by an inability to recruit significant levels of PblGFP^{wt} to the equator. Similar results have been observed in mammalian cell lines, where inhibiting Plk1 activity or mutating potential Plk1 phosphorylation sites in HsCyk-4 severely reduced its interaction and ability to localise Ect2 to the cleavage furrow. Although Plk1 may phosphorylate HsCyk-4 at several sites, S157 appears to be the major phosphorylation site that promotes the interaction with Ect2 (Burkard et al., 2009; Wolfe et al., 2009). Interestingly, sequence comparisons of various Tum orthologues showed that S157 is the only conserved Polo phosphorylation site in Tum (see Chapter 4). Therefore, although several sites were mutated in Tum, it is highly likely that Ser157 is a crucial residue that facilitates the association with Pbl. Further work to confirm this would involve mutating this residue alone and assessing the effects on cytokinesis and the localisation of Tum and Pbl. In summary, Polo regulates the Pbl-Tum interaction, most likely by phosphorylating S157 to promote a high affinity interaction.

5.2 A promiscuous Polo?

Several studies have suggested that Polo/Plk1 can bind to different components of the centralspindlin-Pbl/Ect2 complex. These associations were proposed based on the results of coimmunoprecipitation and mitotic lysate pull down assays. However, these techniques do not necessarily detect individual interactions between two protein partners, especially if the identified protein is known to be part of a larger protein complex.

An interaction between Polo and the centralspindlin-Pbl complex was first identified by the coimmunoprecipitation of Polo with Pav from *Drosophila* embryos (Adams et al., 1998). In mammals, coimmunoprecipitation also suggested Plk1 interacted with MKLP1 where a Polo-box domain (PBD) dependant binding mechanism was proposed (Liu et al., 2004). Pull down assays and coimmunoprecipitation detected a similar Plk1 PBD dependent interaction with Ect2 (Niiya et al., 2006). However, none of these studies probed for the presence of other centralspindlin-Pbl/Ect2 components. Therefore, these experiments may have isolated the entire centralspindlin-Pbl/Ect2 complex. Indeed a recent study detected the presence of both Ect2 and Plk1 from HsCyk-4 immunoprecipitates (Burkard et al., 2009) raising the possibility that previous immunoprecipitation experiments may have isolated the whole centralspindlin-Ect2-Plk1 complex rather than discrete protein pairs. Moreover, the Plk1 PBD constructs used in these studies all contained the intermediate domain, a region between the kinase and PBD domains that our lab has recently demonstrated mediates a PBD independent interaction between Polo and Tum in *Drosophila* (Ebrahimi et al., 2010). Therefore, the identified Plk1 interactions could potentially have been mediated by the intermediate domain binding Tum/ HsCyk-4 rather than the PBD domain binding Pav/MKLP1 and/or Ect2. Indeed, based on our analysis of FRET interactions in *Drosophila* brain cells, and our yeast two hybrid results, Polo interacts only with Tum, and not with Pbl or Pav (Ebrahimi et al., 2010).

Separating the PBD and intermediate domains will be necessary to categorically determine which part of Plk1 mediates the interaction in mammals. Furthermore, an in vitro interaction assay, such as yeast two hybrid analysis, would enable individual components of the centralspindlin-Ect2 complex to be tested for their ability to bind to Plk1.

5.3 Polo kinase – a master regulator of cytokinesis

One of the earliest actions of Polo in cytokinesis may be to promote the midzone accumulation of centralspindlin. While two mammalian studies suggested Plk1 activity is not required for centralspindlin localisation (Burkard et al., 2007; Petronczki et al., 2007), the Plk1 inhibitors used were added 20-30 minutes after cells were released from a metaphase arrest. Therefore, this approach may have missed an early cytokinetic role of Plk1. Interestingly, we observed that centralspindlin failed to accumulate in combined *polo/mad2* mutant cells suggesting Polo facilitates the movement of centralspindlin (Ebrahimi et al., 2010). The *mad2* mutation inactivates the spindle associated checkpoint, forcing these cells to exit mitosis rather than arresting at metaphase due to mutation of *polo*. However, anaphase spindles that failed to localise centralspindlin were observed in *polo/mad2* mutant cells (Ebrahimi et al., 2010) indicating that centralspindlin mislocalisation is not a result of a lack of spindle formation. In the work outlined in Chapter 4, normal accumulation of Pav^{Polo} was observed at the equator. However, since none of the residues targeted in Pav^{Polo} resided within the motor domain of Pav, critical residues controlling Pav^{Polo} localisation were unperturbed. Furthermore, it cannot be ruled out that Polo stimulates centralspindlin movement through an indirect mechanism, perhaps by activating

another cytokinesis kinase. Alternatively, the absence of Polo during the early stages of mitosis may disrupt signalling pathways that ultimately contribute to stimulating centralspindlin movement. Therefore, the role of Polo in facilitating centralspindlin translocation warrants further investigation.

The direct Tum-Polo interaction provides a simple mechanism by which Polo is positioned adjacent to the Tum residues that bind Pbl. This proximity would allow efficient phosphorylation of residue S157 in Tum to create a high affinity binding site for Pbl. My results show that the Pbl-Tum interaction can still occur in the absence of this phosphorylation event, but such an association is unable to recruit sufficient Pbl to the equator to promote cleavage furrow formation. It is also possible that Pbl-Tum binding promotes the Rho GEF activity of Pbl. Furthermore, the interaction with Tum may provide an additional platform from which Polo can phosphorylate and thereby modulate the activities of other cytokinetic components, although late cytokinesis targets are yet to be identified. Moreover, the Tum-Polo interaction may contribute to the equatorial accumulation of Polo, through Tum's association with Pav, similar to other known midzone directed Polo binding partners such as Feo and Sub (Cesario et al., 2006; D'avino et al., 2007). The above results indicate that Polo occupies a top hierarchical position in the signalling pathways that regulate cytokinesis.

The ability of Plk1 to phosphorylate Ect2 in vitro (Hara et al., 2006) raised the possibility that Plk1 may regulate Ect2 function during cytokinesis - possibly by priming Pbl/Ect2 for its interaction with Tum/HsCyk-4. However, the work described in this thesis shows that cytokinesis proceeds normally in *pbl-GFP^{Polo}*

cells, indicating that Polo phosphorylation of Pbl is not required to stimulate the Pbl-Tum interaction in vivo. It has been proposed that Plk1 phosphorylation of Ect2 may induce an open conformation capable of binding HsCyk-4 (Petronczki et al., 2007). This could prevent the resumption of an autoinhibitory conformation once the Cdk1 phosphorylations are removed at anaphase. However, as cell division was unperturbed in *pbl-GFP*^{Polo} embryos, such a mechanism does not appear to be critical. Rather, Tum may rapidly bind to Pbl as Cdk1 phosphorylations that inhibit their association are removed. Finally, it is possible that Polo may modulate the GEF activity of Pbl. While Pbl and Ect2 have been shown to be capable of activating a wide range of GTPases including Rho (Tatsumoto et al., 1999; van Impel et al., 2009), phosphorylation of the GEF domain may promote activity towards Rho. In order to avoid mutations that could affect GEF activity, potential Polo phosphorylation sites within the GEF domain of Pbl were not targeted in this study. Therefore, a role for Polo in regulating the GEF activity of Pbl cannot be ruled out.

In addition to the early cytokinetic functions of Polo described above, late cytokinesis roles are beginning to emerge. For example, in an experiment in which the catalytic domain of Plk1 was fused to HsCyk-4 in cells depleted of endogenous Plk1 activity (Burkard et al., 2009), cells localised Ect2 to the equator and initiated ingression, but in the majority of cells furrowing ultimately regressed leading to cytokinesis failure. Thus, Polo may be required for as yet unknown late cytokinetic events. Separating early and late cytokinetic roles may prove extremely difficult however, since the approach that has proved so successful in separating mitotic and cytokinetic roles (i.e. mitotic arrest and

acute application of chemical inhibitors), is not really practical given the speed of cytokinesis in mammalian cell culture (~15mins).

Whether Polo is continuously required throughout furrowing to ensure its targets remain phosphorylated, or whether it phosphorylates new targets as cytokinesis progresses remains unknown. Novel Plk1 target proteins could perhaps be identified by searching for sequences containing Plk1 consensus motifs in the phosphopeptides from staged mitotic mammalian cell phosphoproteome studies (Olsen et al., 2010). However, each potential target would need to be experimentally confirmed.

Undoubtedly, the critical role of Polo during cytokinesis will attract further investigation. Indeed its importance in cell division has resulted in the initiation of several clinical trials that are attempting to inhibit Plk1 activity to halt or eliminate tumours (Hofheinz et al., 2010; Sebastian et al., 2010; Soto et al., 2010).

5.4 A model for events that regulate the association, localisation and activity of Pbl, Tum and Pav

From the regulatory mechanisms and interactions outlined above, we can construct a model describing the events that influence the activities of Pbl, Tum and Pav during cytokinesis (Figure 5.1). By inference from studies with MKLP1 (Mishima et al., 2004), Cdk1 phosphorylation inhibits the motor activity of Pav to block cytokinesis during metaphase. Cdk1 also may inhibit the cytokinetic

Figure 5.1 ***Modelling the events that influence the association, localization and activities of Pbl and Tum***

During metaphase Cdk1 binds to cyclin B which results in its activation. Cdk1 phosphorylates Pbl to relieve its autoinhibitory conformation whilst also inhibiting its interaction with Tum. Cdk1 also phosphorylates Pav to inhibit its motor activity and thereby prevent accumulation at the midzone. As cells progress into anaphase, cyclin B is rapidly degraded leading to the inactivation of Cdk1. This results in the removal of inhibitory Cdk1 phosphorylations on Pbl and Pav. At the same time, Polo binds to and phosphorylates Tum creating a high affinity binding site for Pbl. Evidence also suggests that Polo stimulates the motor activity of Pav, possibly through direct phosphorylation. Together these events induce the formation of a complex comprising Pbl, Tum, Pav and Polo. Pav then transports its cargo to the cleavage furrow where the GEF activity of Pbl results in accumulation of activated Rho and the formation and constriction of the contractile ring.

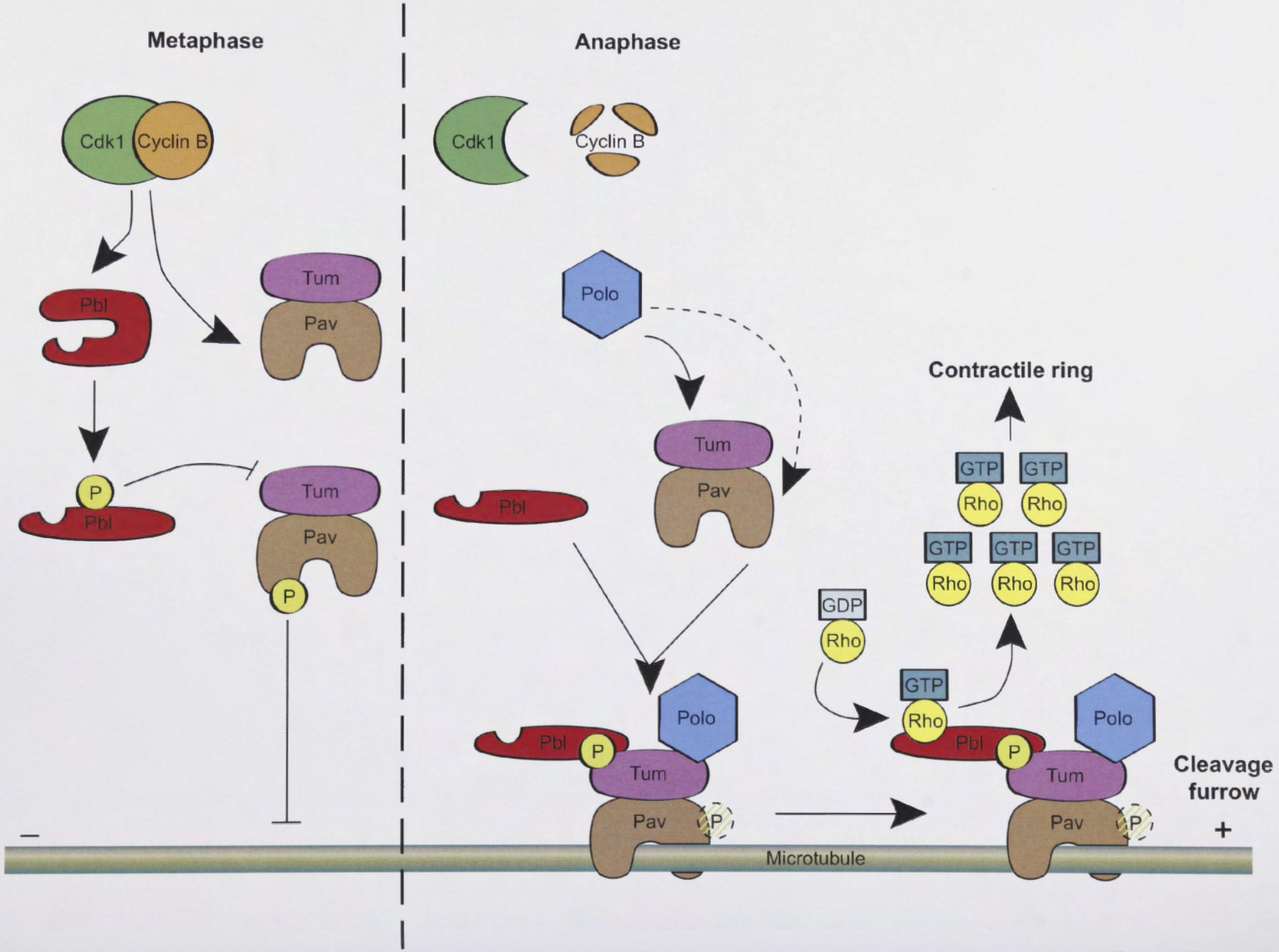
Metaphase
Anaphase
Cdk1
Cyclin B
Cdk1
Cyclin B
Pbl
Tum
Pav
Polo
P
Pbl
Tum
Pav
Tum
Pav
P
Pbl
Contractile ring
GTP
Rho
GDP
Rho
Polo
Pbl
P
Tum
Pav
P
Polo
Pbl
P
Tum
Pav
P
Cleavage furrow
–
+
Microtubule

activities of Pbl (Echard and O'Farrell, 2003), probably by preventing a premature interaction with Tum as occurs in mammals (Yüce et al., 2005). A non-phosphorylatable form of Pbl cannot induce premature cytokinesis, perhaps because of the independent effect of Cdk1 on MKLP1/Pav and other cytokinetic factors. As cells proceed into anaphase and Cdk1 is inactivated, both of these inhibitory phosphorylations are removed by an as yet unidentified phosphatase. Concurrently, Polo binds to and phosphorylates Tum, most likely on S157, to promote the Pbl-Tum interaction. Polo may also phosphorylate Pav to stimulate its motor activity and enable it to translocate the complex to the equator. Once at the equator, Pbl activates Rho to stimulate the formation and constriction of the contractile ring.

5.5 Concluding remarks

This study has investigated regulatory mechanisms that promote the association of Pbl with Tum. While production of high levels of Pbl were achieved and the protein purified to near purity, crystallization attempts were unsuccessful. However, the structure-function analysis reported in this thesis, using an elegant in vivo assay system, shows that the most likely proline-directed phosphorylations that might play a role in cytokinesis are in fact not required to induce the Pbl-Tum interaction. However, Polo is required for the Pbl-Tum interaction by phosphorylating Tum, but not Pbl or Pav. These results identify a previously uncharacterized mechanism by which the association of Pbl and Tum is regulated in *Drosophila*. As an equivalent interaction was identified from mammalian cells during the course of these studies (Burkard et al., 2009; Wolfe

et al., 2009) I conclude that this mechanism is conserved between protostomes (e.g. *Drosophila*) and deuterostomes (e.g. mammals), the two great animal lineages, indicating that it is likely to operate in a very wide range of animal species.

References

Abe, H., Obinata, T., Minamide, L. S., and Bamburg, J. R. 1996. Xenopus laevis actin-depolymerizing factor/cofilin: a phosphorylation-regulated protein essential for development. J Cell Biol *132,* 871-85.

Adam, J. C., Pringle, J. R., and Peifer, M. 2000. Evidence for functional differentiation among Drosophila septins in cytokinesis and cellularization. Mol Biol Cell *11,* 3123-35.

Adams, R. R., Tavares, A. A., Salzberg, A., Bellen, H. J., and Glover, D. M. 1998. pavarotti encodes a kinesin-like protein required to organize the central spindle and contractile ring for cytokinesis. Genes Dev *12,* 1483-94.

Adams, R. R., Wheatley, S. P., Gouldsworthy, A. M., Kandels-Lewis, S. E., Carmena, M., Smythe, C., Gerloff, D. L., and Earnshaw, W. C. 2000. INCENP binds the Aurora-related kinase AIRK2 and is required to target it to chromosomes, the central spindle and cleavage furrow. Curr Biol *10,* 1075-8.

Adelstein, R. S., and Conti, M. A. 1975. Phosphorylation of platelet myosin increases actin-activated myosin ATPase activity. Nature *256,* 597-8.

Alberts, A. S. 2001. Identification of a carboxyl-terminal diaphanous-related formin homology protein autoregulatory domain. J Biol Chem *276,* 2824-30.

Alexandru, G., Uhlmann, F., Mechtler, K., Poupart, M. A., and Nasmyth, K. 2001. Phosphorylation of the cohesin subunit Scc1 by Polo/Cdc5 kinase regulates sister chromatid separation in yeast. Cell *105,* 459-72.

Alsop, G. B., and Zhang, D. 2003. Microtubules are the only structural constituent of the spindle apparatus required for induction of cell cleavage. J Cell Biol *162,* 383-90.

Alsop, G. B., and Zhang, D. 2004. Microtubules continuously dictate distribution of actin filaments and positioning of cell cleavage in grasshopper spermatocytes. J Cell Sci *117,* 1591-602.

Anborgh, P. H., Qian, X., Papageorge, A. G., Vass, W. C., DeClue, J. E., and Lowy, D. R. 1999. Ras-specific exchange factor GRF: oligomerization through its Dbl homology domain and calcium-dependent activation of Raf. Mol Cell Biol *19,* 4611-22.

Archambault, V., and Glover, D. 2009. Polo-like kinases: conservation and divergence in their functions and regulation. Nat Rev Mol Cell Biol *10,* 265-75.

Asnes, C. F., and Schroeder, T. E. 1979. Cell cleavage. Ultrastructural evidence against equatorial stimulation by aster microtubules. Exp Cell Res *122,* 327-38.

Ausubel, F. M., Brent, R., Kingston, R. E., Moore, D. D., Seidman, J. G., Smith, J. A., and Struhl, K., 1994, Current Protocols in Molecular Biology, New York: Greene Publishig Associates and Wiley-Interscience.

Balch, W. 1990. Small GTP-binding proteins in vesicular transport. Trends Biochem Sci *15,* 473-477.

Ban, R., Irino, Y., Fukami, K., and Tanaka, H. 2004. Human mitotic spindle-associated protein PRC1 inhibits MgcRacGAP activity toward Cdc42 during the metaphase. J Biol Chem *279,* 16394-402.

Barral, Y., Mermall, V., Mooseker, M. S., and Snyder, M. 2000. Compartmentalization of the cell cortex by septins is required for maintenance of cell polarity in yeast. Mol Cell *5,* 841-51.

Baruni, J. K., Munro, E. M., and von Dassow, G. 2008. Cytokinetic furrowing in toroidal, binucleate and anucleate cells in C. elegans embryos. J Cell Sci *121,* 306-16.

Basto, R., Lau, J., Vinogradova, T., Gardiol, A., Woods, C. G., Khodjakov, A., and Raff, J. W. 2006. Flies without centrioles. Cell *125,* 1375-86.

Bement, W. M., Benink, H. A., and von Dassow, G. 2005. A microtubule-dependent zone of active RhoA during cleavage plane specification. J Cell Biol *170,* 91-101.

Bezanilla, M., Forsburg, S. L., and Pollard, T. D. 1997. Identification of a second myosin-II in Schizosaccharomyces pombe: Myp2p is conditionally required for cytokinesis. Mol Biol Cell *8,* 2693-705.

Bi, E., Maddox, P., Lew, D. J., Salmon, E. D., McMillan, J. N., Yeh, E., and Pringle, J. R. 1998. Involvement of an actomyosin contractile ring in Saccharomyces cerevisiae cytokinesis. J Cell Biol *142,* 1301-12.

Bischof, J., Maeda, R. K., Hediger, M., Karch, F., and Basler, K. 2007. An optimized transgenesis system for Drosophila using germ-line-specific phiC31 integrases. Proc Natl Acad Sci USA *104,* 3312-7.

Bodenmiller, B., Malmstrom, J., Gerrits, B., Campbell, D., Lam, H., Schmidt, A., Rinner, O., Mueller, L. N., Shannon, P. T., Pedrioli, P. G., Panse, C., Lee, H. K., Schlapbach, R., and Aebersold, R. 2007. PhosphoPep--a phosphoproteome resource for systems biology research in Drosophila Kc167 cells. Mol Syst Biol *3,* 139.

Bonaccorsi, S., Giansanti, M. G., and Gatti, M. 1998. Spindle self-organization and cytokinesis during male meiosis in asterless mutants of Drosophila melanogaster. J Cell Biol *142,* 751-61.

Bond, J., Roberts, E., Mochida, G. H., Hampshire, D. J., Scott, S., Askham, J. M., Springell, K., Mahadevan, M., Crow, Y. J., Markham, A. F., Walsh, C. A., and Woods, C. G. 2002. ASPM is a major determinant of cerebral cortical size. Nat Genet *32,* 316-20.

Bourne, H. R., Sanders, D. A., and McCormick, F. 1990. The GTPase superfamily: a conserved switch for diverse cell functions. Nature *348,* 125-32.

Braun, M., Drummond, D. R., Cross, R. A., and McAinsh, A. D. 2009. The kinesin-14 Klp2 organizes microtubules into parallel bundles by an ATP-dependent sorting mechanism. Nat Cell Biol *11,* 724-30.

Bringmann, H., and Hyman, A. A. 2005. A cytokinesis furrow is positioned by two consecutive signals. Nature *436,* 731-4.

Bucciarelli, E., Giansanti, M. G., Bonaccorsi, S., and Gatti, M. 2003. Spindle assembly and cytokinesis in the absence of chromosomes during Drosophila male meiosis. J Cell Biol *160,* 993-9.

Burkard, M. E., Maciejowski, J., Rodriguez-Bravo, V., Repka, M., Lowery, D. M., Clauser, K. R., Zhang, C., Shokat, K. M., Carr, S. A., Yaffe, M. B., and Jallepalli, P. V. 2009. Plk1 self-organization and priming phosphorylation of HsCYK-4 at the spindle midzone regulate the onset of division in human cells. PLoS Biol *7,* e1000111.

Burkard, M. E., Randall, C. L., Larochelle, S., Zhang, C., Shokat, K. M., Fisher, R. P., and Jallepalli, P. V. 2007. Chemical genetics reveals the requirement for Polo-like kinase 1 activity in positioning RhoA and triggering cytokinesis in human cells. Proc Natl Acad Sci U S A *104,* 4383-8.

Canman, J. C., Cameron, L. A., Maddox, P. S., Straight, A., Tirnauer, J. S., Mitchison, T. J., Fang, G., Kapoor, T. M., and Salmon, E. D. 2003. Determining the position of the cell division plane. Nature *424,* 1074-8.

Canman, J. C., Hoffman, D. B., and Salmon, E. D. 2000. The role of pre- and post-anaphase microtubules in the cytokinesis phase of the cell cycle. Curr Biol *10,* 611-4.

Canman, J. C., Lewellyn, L., Laband, K., Smerdon, S. J., Desai, A., Bowerman, B., and Oegema, K. 2008. Inhibition of Rac by the GAP activity of centralspindlin is essential for cytokinesis. Science *322,* 1543-6.

Cao, L. G., and Wang, Y. L. 1996. Signals from the spindle midzone are required for the stimulation of cytokinesis in cultured epithelial cells. Mol Biol Cell *7,* 225-32.

Carmena, M., Riparbelli, M. G., Minestrini, G., Tavares, A. M., Adams, R., Callaini, G., and Glover, D. M. 1998. Drosophila polo kinase is required for cytokinesis. J Cell Biol *143,* 659-71.

Carrington, J. C., and Dougherty, W. G. 1988. A viral cleavage site cassette: identification of amino acid sequences required for tobacco etch virus polyprotein processing. Proc Natl Acad Sci USA *85,* 3391-5.

Castillon, G. A., Adames, N. R., Rosello, C. H., Seidel, H. S., Longtine, M. S., Cooper, J. A., and Heil-Chapdelaine, R. A. 2003. Septins have a dual role in controlling mitotic exit in budding yeast. Curr Biol *13,* 654-8.

Castrillon, D. H., and Wasserman, S. A. 1994. Diaphanous is required for cytokinesis in Drosophila and shares domains of similarity with the products of the limb deformity gene. Development *120,* 3367-77.

Cesario, J. M., Jang, J. K., Redding, B., Shah, N., Rahman, T., and McKim, K. S. 2006. Kinesin 6 family member Subito participates in mitotic spindle assembly and interacts with mitotic regulators. J Cell Sci *119,* 4770-80.

Chalamalasetty, R. B., Hümmer, S., Nigg, E. A., and Silljé, H. H. 2006. Influence of human Ect2 depletion and overexpression on cleavage furrow formation and abscission. J Cell Sci *119,* 3008-19.

Chang, F., Drubin, D., and Nurse, P. 1997. cdc12p, a protein required for cytokinesis in fission yeast, is a component of the cell division ring and interacts with profilin. J Cell Biol *137,* 169-82.

Chen, F., Ma, L., Parrini, M. C., Mao, X., Lopez, M., Wu, C., Marks, P. W., Davidson, L., Kwiatkowski, D. J., Kirchhausen, T., Orkin, S. H., Rosen, F. S., Mayer, B. J., Kirschner, M. W., and Alt, F. W. 2000. Cdc42 is required for PIP(2)-induced actin polymerization and early development but not for cell viability. Curr Biol *10,* 758-65.

Chen, Y., Yang, Z., Meng, M., Zhao, Y., Dong, N., Yan, H., Liu, L., Ding, M., Peng, H. B., and Shao, F. 2009. Cullin mediates degradation of RhoA through evolutionarily conserved BTB adaptors to control actin cytoskeleton structure and cell movement. Mol Cell *35,* 841-55.

Chikumi, H., Barac, A., Behbahani, B., Gao, Y., Teramoto, H., Zheng, Y., and Gutkind, J. S. 2004. Homo- and hetero-oligomerization of PDZ-RhoGEF, LARG and p115RhoGEF by their C-terminal region regulates their in vivo Rho GEF activity and transforming potential. Oncogene *23,* 233-40.

Collins, R. T., and Cohen, S. M. 2005. A Genetic Screen in Drosophila for Identifying Novel Components of the Hedgehog Signaling Pathway. Genetics *170,* 173.

Cooke, C. A., Heck, M. M., and Earnshaw, W. C. 1987. The inner centromere protein (INCENP) antigens: movement from inner centromere to midbody during mitosis. J Cell Biol *105,* 2053-67.

D'avino, P., Archambault, V., Przewloka, M., Zhang, W., Lilley, K., Laue, E., and Glover, D. 2007. Recruitment of Polo kinase to the spindle midzone during cytokinesis requires the Feo/Klp3A complex. PLoS ONE *2,* e572.

D'avino, P., Takeda, T., Capalbo, L., Zhang, W., Lilley, K., Laue, E. D., and Glover, D. 2008. Interaction between Anillin and RacGAP50C connects the actomyosin contractile ring with spindle microtubules at the cell division site. J Cell Sci *121,* 1151-8.

D'Avino, P. P., Savoian, M. S., and Glover, D. M. 2004. Mutations in sticky lead to defective organization of the contractile ring during cytokinesis and are enhanced by Rho and suppressed by Rac. J Cell Biol *166,* 61-71.

Daub, H., Olsen, J. V., Bairlein, M., Gnad, F., Oppermann, F. S., Korner, R., Greff, Z., Keri, G., Stemmann, O., and Mann, M. 2008. Kinase-selective enrichment enables quantitative phosphoproteomics of the kinome across the cell cycle. Mol Cell *31,* 438-48.

De Lozanne, A., and Spudich, J. A. 1987. Disruption of the Dictyostelium myosin heavy chain gene by homologous recombination. Science *236,* 1086-91.

Dechant, R., and Glotzer, M. 2003. Centrosome separation and central spindle assembly act in redundant pathways that regulate microtubule density and trigger cleavage furrow formation. Dev Cell *4,* 333-44.

Dephoure, N., Zhou, C., Villen, J., Beausoleil, S. A., Bakalarski, C. E., Elledge, S. J., and Gygi, S. P. 2008. A quantitative atlas of mitotic phosphorylation. Proc Natl Acad Sci U S A *105,* 10762-7.

Desai, A., and Mitchison, T. J. 1997. Microtubule polymerization dynamics. Annu Rev Cell Dev Biol *13,* 83-117.

Devore, J. J., Conrad, G. W., and Rappaport, R. 1989. A model for astral stimulation of cytokinesis in animal cells. J Cell Biol *109,* 2225-32.

Di Cunto, F., Calautti, E., Hsiao, J., Ong, L., Topley, G., Turco, E., and Dotto, G. P. 1998. Citron rho-interacting kinase, a novel tissue-specific ser/thr kinase encompassing the Rho-Rac-binding protein Citron. J Biol Chem *273,* 29706-11.

do Carmo Avides, M., Tavares, A., and Glover, D. M. 2001. Polo kinase and Asp are needed to promote the mitotic organizing activity of centrosomes. Nat Cell Biol *3,* 421-4.

Douglas, M. E., Davies, T., Joseph, N., and Mishima, M. 2010. Aurora B and 14-3-3 coordinately regulate clustering of centralspindlin during cytokinesis. Curr Biol *20,* 927-33.

Drechsel, D. N., Hyman, A. A., Hall, A., and Glotzer, M. 1997. A requirement for Rho and Cdc42 during cytokinesis in Xenopus embryos. Curr Biol *7,* 12-23.

Dutartre, H., Davoust, J., Gorvel, J. P., and Chavrier, P. 1996. Cytokinesis arrest and redistribution of actin-cytoskeleton regulatory components in cells expressing the Rho GTPase CDC42Hs. J Cell Sci *109 (Pt 2),* 367-77.

Ebrahimi, S., Fraval, H., Murray, M., Saint, R., and Gregory, S. L. 2010. Polo kinase interacts with RacGAP50C and is required to localize the cytokinesis initiation complex. J Biol Chem *285,* 28667-73.

Echard, A., Hickson, G. R., Foley, E., and O'Farrell, P. H. 2004. Terminal cytokinesis events uncovered after an RNAi screen. Curr Biol *14,* 1685-93.

Echard, A., and O'Farrell, P. H. 2003. The degradation of two mitotic cyclins contributes to the timing of cytokinesis. Current Biology *13,* 373-83.

Eda, M., Yonemura, S., Kato, T., Watanabe, N., Ishizaki, T., Madaule, P., and Narumiya, S. 2001. Rho-dependent transfer of Citron-kinase to the cleavage furrow of dividing cells. J Cell Sci *114,* 3273-84.

Eisenhaure, T. M., Francis, S. A., Willison, L. D., Coughlin, S. R., and Lerner, D. J. 2003. The Rho guanine nucleotide exchange factor Lsc homo-oligomerizes and is negatively regulated through domains in its carboxyl terminus that are absent in novel splenic isoforms. J Biol Chem *278,* 30975-84.

Elia, A. E., Cantley, L. C., and Yaffe, M. B. 2003a. Proteomic screen finds pSer/pThr-binding domain localizing Plk1 to mitotic substrates. Science *299,* 1228-31.

Elia, A. E., Rellos, P., Haire, L. F., Chao, J. W., Ivins, F. J., Hoepker, K., Mohammad, D., Cantley, L. C., Smerdon, S. J., and Yaffe, M. B. 2003b. The molecular basis for phosphodependent substrate targeting and regulation of Plks by the Polo-box domain. Cell *115,* 83-95.

Elowe, S., Hummer, S., Uldschmid, A., Li, X., and Nigg, E. A. 2007. Tension-sensitive Plk1 phosphorylation on BubR1 regulates the stability of kinetochore microtubule interactions. Genes Dev *21,* 2205-19.

Field, C. M., al-Awar, O., Rosenblatt, J., Wong, M. L., Alberts, B., and Mitchison, T. J. 1996. A purified Drosophila septin complex forms filaments and exhibits GTPase activity. J Cell Biol *133,* 605-16.

Field, C. M., and Alberts, B. M. 1995. Anillin, a contractile ring protein that cycles from the nucleus to the cell cortex. J Cell Biol *131,* 165-78.

Field, C. M., and Kellogg, D. 1999. Septins: cytoskeletal polymers or signalling GTPases? Trends Cell Biol *9,* 387-94.

Fink, G., Hajdo, L., Skowronek, K. J., Reuther, C., Kasprzak, A. A., and Diez, S. 2009. The mitotic kinesin-14 Ncd drives directional microtubule-microtubule sliding. Nat Cell Biol *11,* 717-23.

Foe, V. E. 1989. Mitotic domains reveal early commitment of cells in Drosophila embryos. Development *107,* 1-22.

Foe, V. E., and von Dassow, G. 2008. Stable and dynamic microtubules coordinately shape the myosin activation zone during cytokinetic furrow formation. J Cell Biol *183,* 457-70.

Frazier, J. A., Wong, M. L., Longtine, M. S., Pringle, J. R., Mann, M., Mitchison, T. J., and Field, C. 1998. Polymerization of purified yeast septins: evidence that organized filament arrays may not be required for septin function. J Cell Biol *143,* 737-49.

Fujiwara, K., and Pollard, T. D. 1976. Fluorescent antibody localization of myosin in the cytoplasm, cleavage furrow, and mitotic spindle of human cells. J Cell Biol *71,* 848-75.

Gassmann, R., Carvalho, A., Henzing, A. J., Ruchaud, S., Hudson, D. F., Honda, R., Nigg, E. A., Gerloff, D. L., and Earnshaw, W. C. 2004. Borealin: a novel chromosomal passenger required for stability of the bipolar mitotic spindle. J Cell Biol *166,* 179-91.

Giansanti, M. G., Bonaccorsi, S., and Gatti, M. 1999. The role of anillin in meiotic cytokinesis of Drosophila males. J Cell Sci *112 (Pt 14),* 2323-34.

Giansanti, M. G., Bonaccorsi, S., Williams, B., Williams, E. V., Santolamazza, C., Goldberg, M. L., and Gatti, M. 1998. Cooperative interactions between the central spindle and the contractile ring during Drosophila cytokinesis. Genes Dev *12,* 396-410.

Glotzer, M. 2005. The molecular requirements for cytokinesis. Science *307,* 1735-9.

Goshima, G., Nedelec, F., and Vale, R. D. 2005. Mechanisms for focusing mitotic spindle poles by minus end-directed motor proteins. J Cell Biol *171,* 229-40.

Gregory, S. L., Ebrahimi, S., Milverton, J., Jones, W. M., Bejsovec, A., and Saint, R. 2008. Cell division requires a direct link between microtubule-bound RacGAP and Anillin in the contractile ring. Curr Biol *18,* 25-9.

Gruneberg, U., Neef, R., Honda, R., Nigg, E. A., and Barr, F. A. 2004. Relocation of Aurora B from centromeres to the central spindle at the metaphase to anaphase transition requires MKlp2. J Cell Biol *166,* 167-72.

Guizetti, J., and Gerlich, D. W. 2010. Cytokinetic abscission in animal cells. Semin Cell Dev Biol 11.

Gunsalus, K. C., Bonaccorsi, S., Williams, E., Verni, F., Gatti, M., and Goldberg, M. L. 1995. Mutations in twinstar, a Drosophila gene encoding a cofilin/ADF homologue, result in defects in centrosome migration and cytokinesis. J Cell Biol *131,* 1243-59.

Guse, A., Mishima, M., and Glotzer, M. 2005. Phosphorylation of ZEN-4/MKLP1 by aurora B regulates completion of cytokinesis. Curr Biol *15,* 778-86.

Guzhova, I., and Margulis, B. 2006. Hsp70 chaperone as a survival factor in cell pathology. Int Rev Cytol *254,* 101-49.

Hall, F. L., and Vulliet, P. R. 1991. Proline-directed protein phosphorylation and cell cycle regulation. Curr Opin Cell Biol *3,* 176-84.

Hames, C., Halbedel, S., Schilling, O., and Stulke, J. 2005. Multiple-mutation reaction: a method for simultaneous introduction of multiple mutations into the glpK gene of Mycoplasma pneumoniae. Appl Environ Microbiol *71,* 4097-100.

Hara, T., Abe, M., Inoue, H., Yu, L. R., Veenstra, T. D., Kang, Y. H., Lee, K. S., and Miki, T. 2006. Cytokinesis regulator ECT2 changes its conformation through phosphorylation at Thr-341 in G2/M phase. Oncogene *25,* 566-78.

Hartwell, L. H. 1971. Genetic control of the cell division cycle in yeast. IV. Genes controlling bud emergence and cytokinesis. Exp Cell Res *69,* 265-76.

Hatsumi, M., and Endow, S. A. 1992. Mutants of the microtubule motor protein, nonclaret disjunctional, affect spindle structure and chromosome movement in meiosis and mitosis. J Cell Sci *101 (Pt 3),* 547-59.

Hickson, G. R., and O'Farrell, P. H. 2008. Rho-dependent control of anillin behavior during cytokinesis. J Cell Biol *180,* 285-94.

Hime, G., and Saint, R. 1992. Zygotic expression of the pebble locus is required for cytokinesis during the postblastoderm mitoses of Drosophila. Development *114,* 165-71.

Hirose, K., Kawashima, T., Iwamoto, I., Nosaka, T., and Kitamura, T. 2001. MgcRacGAP is involved in cytokinesis through associating with mitotic spindle and midbody. J Biol Chem *276,* 5821-8.

Hofheinz, R. D., Al-Batran, S. E., Hochhaus, A., Jager, E., Reichardt, V. L., Fritsch, H., Trommeshauser, D., and Munzert, G. 2010. An open-label, phase I study of the polo-like kinase-1 inhibitor, BI 2536, in patients with advanced solid tumors. Clin Cancer Res *16,* 4666-74.

Hotulainen, P., Paunola, E., Vartiainen, M. K., and Lappalainen, P. 2005. Actin-depolymerizing factor and cofilin-1 play overlapping roles in promoting rapid F-actin depolymerization in mammalian nonmuscle cells. Mol Biol Cell *16,* 649-64.

Hutterer, A., Glotzer, M., and Mishima, M. 2009. Clustering of centralspindlin is essential for its accumulation to the central spindle and the midbody. Curr Biol *19,* 2043-9.

Ikebe, M. 1989. Phosphorylation of a second site for myosin light chain kinase on platelet myosin. Biochemistry *28,* 8750-5.

Ikebe, M., Hartshorne, D. J., and Elzinga, M. 1987. Phosphorylation of the 20,000-dalton light chain of smooth muscle myosin by the calcium-activated, phospholipid-dependent protein kinase. Phosphorylation sites and effects of phosphorylation. J Biol Chem *262,* 9569-73.

Imai, K., Kijima, T., Noda, Y., Sutoh, K., Yoda, K., and Adachi, H. 2002. A Rho GDP-dissociation inhibitor is involved in cytokinesis of Dictyostelium. Biochem Biophys Res Commun *296,* 305-12.

Imamura, H., Tanaka, K., Hihara, T., Umikawa, M., Kamei, T., Takahashi, K., Sasaki, T., and Takai, Y. 1997. Bni1p and Bnr1p: downstream targets of the Rho family small G-proteins which interact with profilin and regulate actin cytoskeleton in Saccharomyces cerevisiae. Embo J *16,* 2745-55.

Inoue, Y. H., Savoian, M. S., Suzuki, T., Máthé, E., Yamamoto, M. T., and Glover, D. 2004. Mutations in orbit/mast reveal that the central spindle is comprised of two microtubule populations, those that initiate cleavage and those that propagate furrow ingression. J Cell Biol *166,* 49-60.

Irvine, K., Stirling, R., Hume, D., and Kennedy, D. 2004. Rasputin, more promiscuous than ever: a review of G3BP. Int. J. Dev. Biol. *48,* 1065-77.

Jantsch-Plunger, V., Gönczy, P., Romano, A., Schnabel, H., Hamill, D., Schnabel, R., Hyman, A. A., and Glotzer, M. 2000. CYK-4: A Rho family gtpase activating protein (GAP) required for central spindle formation and cytokinesis. J Cell Biol *149,* 1391-404.

Jiang, W., Jimenez, G., Wells, N. J., Hope, T. J., Wahl, G. M., Hunter, T., and Fukunaga, R. 1998. PRC1: a human mitotic spindle-associated CDK substrate protein required for cytokinesis. Mol Cell *2,* 877-85.

Jones, W. M., and Bejsovec, A. 2005. RacGap50C negatively regulates wingless pathway activity during Drosophila embryonic development. Genetics *169,* 2075-86.

Kaitna, S., Mendoza, M., Jantsch-Plunger, V., and Glotzer, M. 2000. Incenp and an aurora-like kinase form a complex essential for chromosome segregation and efficient completion of cytokinesis. Curr Biol *10,* 1172-81.

Kamasaki, T., Osumi, M., and Mabuchi, I. 2007. Three-dimensional arrangement of F-actin in the contractile ring of fission yeast. J Cell Biol *178,* 765-71.

Kamijo, K., Ohara, N., Abe, M., Uchimura, T., Hosoya, H., Lee, J. S., and Miki, T. 2006. Dissecting the role of Rho-mediated signaling in contractile ring formation. Mol Biol Cell *17,* 43-55.

Kanada, M., Nagasaki, A., and Uyeda, T. Q. 2009. Stabilization of anaphase midzone microtubules is regulated by Rho during cytokinesis in human fibrosarcoma cells. Experimental Cell Research

Kang, F., Purich, D. L., and Southwick, F. S. 1999. Profilin promotes barbed-end actin filament assembly without lowering the critical concentration. J Biol Chem *274,* 36963-72.

Karess, R. E., Chang, X. J., Edwards, K. A., Kulkarni, S., Aguilera, I., and Kiehart, D. P. 1991. The regulatory light chain of nonmuscle myosin is encoded by spaghetti-squash, a gene required for cytokinesis in Drosophila. Cell *65,* 1177-89.

Kim, J. E., Billadeau, D. D., and Chen, J. 2005. The tandem BRCT domains of Ect2 are required for both negative and positive regulation of Ect2 in cytokinesis. J Biol Chem *280,* 5733-9.

Kimble, M., and Church, K. 1983. Meiosis and early cleavage in Drosophila melanogaster eggs: effects of the claret-non-disjunctional mutation. J Cell Sci *62,* 301-18.

Kimura, K., Ito, M., Amano, M., Chihara, K., Fukata, Y., Nakafuku, M., Yamamori, B., Feng, J., Nakano, T., Okawa, K., Iwamatsu, A., and Kaibuchi, K. 1996. Regulation of myosin phosphatase by Rho and Rho-associated kinase (Rho-kinase). Science *273,* 245-8.

Kinoshita, M. 2003. Assembly of mammalian septins. J Biochem *134,* 491-6.

Kinoshita, M., Field, C. M., Coughlin, M. L., Straight, A. F., and Mitchison, T. J. 2002. Self- and actin-templated assembly of Mammalian septins. Dev Cell *3,* 791-802.

Kinoshita, M., Kumar, S., Mizoguchi, A., Ide, C., Kinoshita, A., Haraguchi, T., Hiraoka, Y., and Noda, M. 1997. Nedd5, a mammalian septin, is a novel

cytoskeletal component interacting with actin-based structures. Genes Dev *11,* 1535-47.

Kishi, K., Sasaki, T., Kuroda, S., Itoh, T., and Takai, Y. 1993. Regulation of cytoplasmic division of Xenopus embryo by rho p21 and its inhibitory GDP/GTP exchange protein (rho GDI). J Cell Biol *120,* 1187-95.

Knecht, D. A., and Loomis, W. F. 1987. Antisense RNA inactivation of myosin heavy chain gene expression in Dictyostelium discoideum. Science *236,* 1081-6.

Kosako, H., Goto, H., Yanagida, M., Matsuzawa, K., Fujita, M., Tomono, Y., Okigaki, T., Odai, H., Kaibuchi, K., and Inagaki, M. 1999. Specific accumulation of Rho-associated kinase at the cleavage furrow during cytokinesis: cleavage furrow-specific phosphorylation of intermediate filaments. Oncogene *18,* 2783-8.

Kosako, H., Yoshida, T., Matsumura, F., Ishizaki, T., Narumiya, S., and Inagaki, M. 2000. Rho-kinase/ROCK is involved in cytokinesis through the phosphorylation of myosin light chain and not ezrin/radixin/moesin proteins at the cleavage furrow. Oncogene *19,* 6059-64.

Kozma, R., Ahmed, S., Best, A., and Lim, L. 1995. The Ras-related protein Cdc42Hs and bradykinin promote formation of peripheral actin microspikes and filopodia in Swiss 3T3 fibroblasts. Mol Cell Biol *15,* 1942-52.

Krishna, M., and Narang, H. 2008. The complexity of mitogen-activated protein kinases (MAPKs) made simple. Cell. Mol. Life Sci. *65,* 3525-44.

Kuriyama, R., Gustus, C., Terada, Y., Uetake, Y., and Matuliene, J. 2002. CHO1, a mammalian kinesin-like protein, interacts with F-actin and is involved in the terminal phase of cytokinesis. J Cell Biol *156,* 783-90.

Lee, K. S., Yuan, Y. L., Kuriyama, R., and Erikson, R. L. 1995. Plk is an M-phase-specific protein kinase and interacts with a kinesin-like protein, CHO1/MKLP-1. Mol Cell Biol *15,* 7143-51.

Lehner, C. F. 1992. The pebble gene is required for cytokinesis in Drosophila. J Cell Sci *103 (Pt 4),* 1021-30.

Lenzen, C., Cool, R. H., Prinz, H., Kuhlmann, J., and Wittinghofer, A. 1998. Kinetic analysis by fluorescence of the interaction between Ras and the catalytic domain of the guanine nucleotide exchange factor Cdc25Mm. Biochemistry *37,* 7420-30.

Liu, X., Zhou, T., Kuriyama, R., and Erikson, R. L. 2004. Molecular interactions of Polo-like-kinase 1 with the mitotic kinesin-like protein CHO1/MKLP-1. J Cell Sci *117,* 3233-46.

Logarinho, E., and Sunkel, C. E. 1998. The Drosophila POLO kinase localises to multiple compartments of the mitotic apparatus and is required for the phosphorylation of MPM2 reactive epitopes. J Cell Sci *111 (Pt 19),* 2897-909.

Loiodice, I., Staub, J., Setty, T. G., Nguyen, N. P., Paoletti, A., and Tran, P. T. 2005. Ase1p organizes antiparallel microtubule arrays during interphase and mitosis in fission yeast. Mol Biol Cell *16,* 1756-68.

Lowy, D. R., and Willumsen, B. M. 1993. Function and regulation of ras. Annu Rev Biochem *62,* 851-91.

Mabuchi, I., Hamaguchi, Y., Fujimoto, H., Morii, N., Mishima, M., and Narumiya, S. 1993. A rho-like protein is involved in the organisation of the contractile ring in dividing sand dollar eggs. Zygote *1,* 325-31.

Mabuchi, I., and Okuno, M. 1977. The effect of myosin antibody on the division of starfish blastomeres. J Cell Biol *74,* 251-63.

Madaule, P., Eda, M., Watanabe, N., Fujisawa, K., Matsuoka, T., Bito, H., Ishizaki, T., and Narumiya, S. 1998. Role of citron kinase as a target of the small GTPase Rho in cytokinesis. Nature *394,* 491-4.

Malik, R., Lenobel, R., Santamaria, A., Ries, A., Nigg, E. A., and Korner, R. 2009. Quantitative analysis of the human spindle phosphoproteome at distinct mitotic stages. J Proteome Res *8,* 4553-63.

Mastronarde, D. N., McDonald, K. L., Ding, R., and McIntosh, J. R. 1993. Interpolar spindle microtubules in PTK cells. J Cell Biol *123,* 1475-89.

Matsui, T., Amano, M., Yamamoto, T., Chihara, K., Nakafuku, M., Ito, M., Nakano, T., Okawa, K., Iwamatsu, A., and Kaibuchi, K. 1996. Rho-associated kinase, a novel serine/threonine kinase, as a putative target for small GTP binding protein Rho. Embo J *15,* 2208-16.

Matthies, H. J., McDonald, H. B., Goldstein, L. S., and Theurkauf, W. E. 1996. Anastral meiotic spindle morphogenesis: role of the non-claret disjunctional kinesin-like protein. J Cell Biol *134,* 455-64.

Matuliene, J., and Kuriyama, R. 2002. Kinesin-like protein CHO1 is required for the formation of midbody matrix and the completion of cytokinesis in mammalian cells. Mol Biol Cell *13,* 1832-45.

Miller, A., and Bement, W. 2009. Regulation of cytokinesis by Rho GTPase flux. Nat Cell Biol *11,* 71-7.

Miller, K. G., Field, C. M., and Alberts, B. M. 1989. Actin-binding proteins from Drosophila embryos: a complex network of interacting proteins detected by F-actin affinity chromatography. J Cell Biol *109,* 2963-75.

Minoshima, Y., Kawashima, T., Hirose, K., Tonozuka, Y., Kawajiri, A., Bao, Y. C., Deng, X., Tatsuka, M., Narumiya, S., May, W. S., Jr., Nosaka, T., Semba, K., Inoue, T., Satoh, T., Inagaki, M., and Kitamura, T. 2003. Phosphorylation by aurora B converts MgcRacGAP to a RhoGAP during cytokinesis. Dev Cell *4,* 549-60.

Mishima, M., and Glotzer, M. 2003. Cytokinesis: a logical GAP. Curr Biol *13,* R589-91.

Mishima, M., Kaitna, S., and Glotzer, M. 2002. Central spindle assembly and cytokinesis require a kinesin-like protein/RhoGAP complex with microtubule bundling activity. Dev Cell *2,* 41-54.

Mishima, M., Pavicic, V., Grüneberg, U., Nigg, E. A., and Glotzer, M. 2004. Cell cycle regulation of central spindle assembly. Nature *430,* 908-13.

Mizuno, T., Tsutsui, K., and Nishida, Y. 2002. Drosophila myosin phosphatase and its role in dorsal closure. Development *129,* 1215-23.

Moffat, J., and Andrews, B. 2003. Ac'septin' a signal: kinase regulation by septins. Dev Cell *5,* 528-30.

Mollinari, C., Kleman, J. P., Jiang, W., Schoehn, G., Hunter, T., and Margolis, R. L. 2002. PRC1 is a microtubule binding and bundling protein essential to maintain the mitotic spindle midzone. J Cell Biol *157,* 1175-86.

Moore, M. S., and Blobel, G. 1993. The GTP-binding protein Ran/TC4 is required for protein import into the nucleus. Nature *365,* 661-3.

Morita, K., Hirono, K., and Han, M. 2005. The Caenorhabditis elegans ect-2 RhoGEF gene regulates cytokinesis and migration of epidermal P cells. EMBO Rep *6,* 1163-8.

Mountain, V., Simerly, C., Howard, L., Ando, A., Schatten, G., and Compton, D. A. 1999. The kinesin-related protein, HSET, opposes the activity of Eg5 and cross-links microtubules in the mammalian mitotic spindle. J Cell Biol *147,* 351-66.

Murphy, C. I., Piwnica-Worms, H., Grünwald, S., Romanow, W. G., Francis, N., and Fan, H. Y. 2004. Overview of the baculovirus expression system. Current protocols in molecular biology / edited by Frederick M Ausubel [et al] *Chapter 16,* Unit 16.9.

Murthy, K., and Wadsworth, P. 2005. Myosin-II-dependent localization and dynamics of F-actin during cytokinesis. Curr Biol *15,* 724-31.

Murthy, K., and Wadsworth, P. 2008. Dual role for microtubules in regulating cortical contractility during cytokinesis. J Cell Sci *121,* 2350-9.

Naim, V., Imarisio, S., Di Cunto, F., Gatti, M., and Bonaccorsi, S. 2004. Drosophila citron kinase is required for the final steps of cytokinesis. Mol Biol Cell *15,* 5053-63.

Nakajima, H., Toyoshima-Morimoto, F., Taniguchi, E., and Nishida, E. 2003. Identification of a consensus motif for Plk (Polo-like kinase) phosphorylation reveals Myt1 as a Plk1 substrate. J Biol Chem *278,* 25277-80.

Nakano, K., and Mabuchi, I. 2006. Actin-depolymerizing protein Adf1 is required for formation and maintenance of the contractile ring during cytokinesis in fission yeast. Mol Biol Cell *17,* 1933-45.

Narumiya, S., and Yasuda, S. 2006. Rho GTPases in animal cell mitosis. Curr Opin Cell Biol *18,* 199-205.

Neef, R., Gruneberg, U., Kopajtich, R., Li, X., Nigg, E. A., Sillje, H., and Barr, F. A. 2007. Choice of Plk1 docking partners during mitosis and cytokinesis is controlled by the activation state of Cdk1. Nat Cell Biol *9,* 436-44.

Neef, R., Klein, U. R., Kopajtich, R., and Barr, F. A. 2006. Cooperation between mitotic kinesins controls the late stages of cytokinesis. Curr Biol *16,* 301-7.

Neef, R., Preisinger, C., Sutcliffe, J., Kopajtich, R., Nigg, E. A., Mayer, T. U., and Barr, F. A. 2003. Phosphorylation of mitotic kinesin-like protein 2 by polo-like kinase 1 is required for cytokinesis. J Cell Biol *162,* 863-75.

Neufeld, T. P., and Rubin, G. M. 1994. The Drosophila peanut gene is required for cytokinesis and encodes a protein similar to yeast putative bud neck filament proteins. Cell *77,* 371-9.

Niiya, F., Tatsumoto, T., Lee, K. S., and Miki, T. 2006. Phosphorylation of the cytokinesis regulator ECT2 at G2/M phase stimulates association of the mitotic kinase Plk1 and accumulation of GTP-bound RhoA. Oncogene *25,* 827-37.

Niiya, F., Xie, X., Lee, K. S., Inoue, H., and Miki, T. 2005. Inhibition of cyclin-dependent kinase 1 induces cytokinesis without chromosome segregation in an ECT2 and MgcRacGAP-dependent manner. J Biol Chem *280,* 36502-9.

Nishikawa, M., Sellers, J. R., Adelstein, R. S., and Hidaka, H. 1984. Protein kinase C modulates in vitro phosphorylation of the smooth muscle heavy meromyosin by myosin light chain kinase. J Biol Chem *259,* 8808-14.

Nishimura, Y., and Yonemura, S. 2006. Centralspindlin regulates ECT2 and RhoA accumulation at the equatorial cortex during cytokinesis. J Cell Sci *119,* 104-14.

Nobes, C. D., and Hall, A. 1995. Rho, rac, and cdc42 GTPases regulate the assembly of multimolecular focal complexes associated with actin stress fibers, lamellipodia, and filopodia. Cell *81,* 53-62.

O'Connell, C. B., Wheatley, S. P., Ahmed, S., and Wang, Y. L. 1999. The small GTP-binding protein rho regulates cortical activities in cultured cells during division. J Cell Biol *144,* 305-13.

Oceguera-Yanez, F., Kimura, K., Yasuda, S., Higashida, C., Kitamura, T., Hiraoka, Y., Haraguchi, T., and Narumiya, S. 2005. Ect2 and MgcRacGAP regulate the activation and function of Cdc42 in mitosis. J Cell Biol *168,* 221-32.

Odell, G. M., and Foe, V. E. 2008. An agent-based model contrasts opposite effects of dynamic and stable microtubules on cleavage furrow positioning. J Cell Biol *183,* 471-83.

Olsen, J. V., Vermeulen, M., Santamaria, A., Kumar, C., Miller, M. L., Jensen, L. J., Gnad, F., Cox, J., Jensen, T. S., Nigg, E. A., Brunak, S., and Mann, M. 2010. Quantitative phosphoproteomics reveals widespread full phosphorylation site occupancy during mitosis. Sci Signal *3,* ra3.

Ong, S., Foote, C., and Tan, C. 2010. Mutations of DMYPT cause over constriction of contractile rings and ring canals during Drosophila germline cyst formation. Dev Biol 11.

Ono, K., Parast, M., Alberico, C., Benian, G. M., and Ono, S. 2003. Specific requirement for two ADF/cofilin isoforms in distinct actin-dependent processes in Caenorhabditis elegans. J Cell Sci *116,* 2073-85.

Pavicic-Kaltenbrunner, V., Mishima, M., and Glotzer, M. 2007. Cooperative assembly of CYK-4/MgcRacGAP and ZEN-4/MKLP1 to form the centralspindlin complex. Mol Biol Cell *18,* 4992-5003.

Pazman, C., and Haynes, S. 2004. The Drosophila rasputin is required for dynamic actin rearrangements during oogenesis. A Dros Res Conf *45,* 221B.

Pazman, C., Mayes, C. A., Fanto, M., Haynes, S. R., and Mlodzik, M. 2000. Rasputin, the Drosophila homologue of the RasGAP SH3 binding protein, functions in ras- and Rho-mediated signaling. Development *127,* 1715-25.

Pelham, R. J., and Chang, F. 2002. Actin dynamics in the contractile ring during cytokinesis in fission yeast. Nature *419,* 82-6.

Peng, J., Wallar, B. J., Flanders, A., Swiatek, P. J., and Alberts, A. S. 2003. Disruption of the Diaphanous-related formin Drf1 gene encoding mDia1 reveals a role for Drf3 as an effector for Cdc42. Curr Biol *13,* 534-45.

Pengelley, S. C., Chapman, D. C., Mark Abbott, W., Lin, H. H., Huang, W., Dalton, K., and Jones, I. M. 2006. A suite of parallel vectors for baculovirus expression. Protein Expr Purif *48,* 173-81.

Petronczki, M., Glotzer, M., Kraut, N., and Peters, J. M. 2007. Polo-like kinase 1 triggers the initiation of cytokinesis in human cells by promoting recruitment of the RhoGEF Ect2 to the central spindle. Dev Cell *12,* 713-25.

Piekny, A., Werner, M., and Glotzer, M. 2005. Cytokinesis: welcome to the Rho zone. Trends Cell Biol *15,* 651-8.

Piekny, A. J., and Glotzer, M. 2008. Anillin is a scaffold protein that links RhoA, actin, and myosin during cytokinesis. Curr Biol *18,* 30-6.

Piekny, A. J., and Mains, P. E. 2002. Rho-binding kinase (LET-502) and myosin phosphatase (MEL-11) regulate cytokinesis in the early Caenorhabditis elegans embryo. J Cell Sci *115,* 2271-82.

Pollard, T. D. 2009. Mechanics of cytokinesis in eukaryotes. Curr Opin Cell Biol *22,* 50-6.

Poperechnaya, A., Varlamova, O., Lin, P. J., Stull, J. T., and Bresnick, A. R. 2000. Localization and activity of myosin light chain kinase isoforms during the cell cycle. J Cell Biol *151,* 697-708.

Prokopenko, S. N., Brumby, A., O'Keefe, L., Prior, L., He, Y., Saint, R., and Bellen, H. J. 1999. A putative exchange factor for Rho1 GTPase is required for initiation of cytokinesis in Drosophila. Genes & Development *13,* 2301-14.

Raich, W. B., Moran, A. N., Rothman, J. H., and Hardin, J. 1998. Cytokinesis and midzone microtubule organization in Caenorhabditis elegans require the kinesin-like protein ZEN-4. Mol Biol Cell *9,* 2037-49.

Rappaport, R. 1961. Experiments concerning the cleavage stimulus in sand dollar eggs. J Exp Zool *148,* 81-9.

Rappaport, R. 1968. Geometrical relations of the cleavage stimulus in flattened, perforated sea urchin eggs. Embryologia (Nagoya) *10,* 89-104.

Rappaport, R. 1985. Repeated furrow formation from a single mitotic apparatus in cylindrical sand dollar eggs. J Exp Zool *234,* 167-71.

Rappaport, R. 1996. Cytokinesis in animal cells. Cambridge University Press

Rappaport, R., and Rappaport, B. 1983. Cytokinesis: Effects of blocks between the mitotic apparatus and the surface on furrow establishment in flattened echinoderm eggs. Journal of Experimental Zoology *227,* 213-227.

Ridley, A. J., and Hall, A. 1992. The small GTP-binding protein rho regulates the assembly of focal adhesions and actin stress fibers in response to growth factors. Cell *70,* 389-99.

Ridley, A. J., Paterson, H. F., Johnston, C. L., Diekmann, D., and Hall, A. 1992. The small GTP-binding protein rac regulates growth factor-induced membrane ruffling. Cell *70,* 401-10.

Rieder, C. L., Khodjakov, A., Paliulis, L. V., Fortier, T. M., Cole, R. W., and Sluder, G. 1997. Mitosis in vertebrate somatic cells with two spindles: implications for the metaphase/anaphase transition checkpoint and cleavage. Proc Natl Acad Sci U S A *94,* 5107-12.

Rivero, F., Illenberger, D., Somesh, B. P., Dislich, H., Adam, N., and Meyer, A. K. 2002. Defects in cytokinesis, actin reorganization and the contractile vacuole in cells deficient in RhoGDI. Embo J *21,* 4539-49.

Rosa, J., Canovas, P., Islam, A., Altieri, D. C., and Doxsey, S. J. 2006. Survivin modulates microtubule dynamics and nucleation throughout the cell cycle. Mol Biol Cell *17,* 1483-93.

Royou, A., Sullivan, W., and Karess, R. 2002. Cortical recruitment of nonmuscle myosin II in early syncytial Drosophila embryos: its role in nuclear axial expansion and its regulation by Cdc2 activity. J Cell Biol *158,* 127-37.

Saint, R., and Somers, W. G. 2003. Animal cell division: a fellowship of the double ring? J Cell Sci *116,* 4277-81.

Saito, S., Liu, X. F., Kamijo, K., Raziuddin, R., Tatsumoto, T., Okamoto, I., Chen, X., Lee, C. C., Lorenzi, M. V., Ohara, N., and Miki, T. 2004. Deregulation and mislocalization of the cytokinesis regulator ECT2 activate the Rho signaling pathways leading to malignant transformation. J Biol Chem *279,* 7169-79.

Salmon, E. D., Leslie, R. J., Saxton, W. M., Karow, M. L., and McIntosh, J. R. 1984. Spindle microtubule dynamics in sea urchin embryos: analysis using a fluorescein-labeled tubulin and measurements of fluorescence redistribution after laser photobleaching. J Cell Biol *99,* 2165-74.

Salzberg, A., D'Evelyn, D., Schulze, K. L., Lee, J. K., Strumpf, D., Tsai, L., and Bellen, H. J. 1994. Mutations affecting the pattern of the PNS in Drosophila reveal novel aspects of neuronal development. Neuron *13,* 269-87.

Sambrook, J., Fritsch, E. F., and Maniatis, T., 1989, Molecular Cloning: A Laboratory Manual, Plainview, New York: Cold Spring Harbor Laboratory Press.

Sampath, S. C., Ohi, R., Leismann, O., Salic, A., Pozniakovski, A., and Funabiki, H. 2004. The chromosomal passenger complex is required for chromatin-induced microtubule stabilization and spindle assembly. Cell *118,* 187-202.

Sanders, L. C., Matsumura, F., Bokoch, G. M., and de Lanerolle, P. 1999. Inhibition of myosin light chain kinase by p21-activated kinase. Science *283,* 2083-5.

Sanger, J. M., Dome, J. S., and Sanger, J. W. 1998. Unusual cleavage furrows in vertebrate tissue culture cells: insights into the mechanisms of cytokinesis. Cell Motil Cytoskeleton *39,* 95-106.

Sanger, J. M., and Sanger, J. W. 1980. Banding and polarity of actin filaments in interphase and cleaving cells. J Cell Biol *86,* 568-75.

Santamaria, D., Barriere, C., Cerqueira, A., Hunt, S., Tardy, C., Newton, K., Caceres, J. F., Dubus, P., Malumbres, M., and Barbacid, M. 2007. Cdk1 is sufficient to drive the mammalian cell cycle. Nature *448,* 811-5.

Satterwhite, L. L., Lohka, M. J., Wilson, K. L., Scherson, T. Y., Cisek, L. J., Corden, J. L., and Pollard, T. D. 1992. Phosphorylation of myosin-II regulatory light chain by cyclin-p34cdc2: a mechanism for the timing of cytokinesis. J Cell Biol *118,* 595-605.

Saunders, W. S., and Hoyt, M. A. 1992. Kinesin-related proteins required for structural integrity of the mitotic spindle. Cell *70,* 451-8.

Savoian, M. S., Earnshaw, W. C., Khodjakov, A., and Rieder, C. L. 1999. Cleavage furrows formed between centrosomes lacking an intervening spindle and chromosomes contain microtubule bundles, INCENP, and CHO1 but not CENP-E. Mol Biol Cell *10,* 297-311.

Saxton, W. M., and McIntosh, J. R. 1987. Interzone microtubule behavior in late anaphase and telophase spindles. J Cell Biol *105,* 875-86.

Saxton, W. M., Stemple, D. L., Leslie, R. J., Salmon, E. D., Zavortink, M., and McIntosh, J. R. 1984. Tubulin dynamics in cultured mammalian cells. J Cell Biol *99,* 2175-86.

Scholey, J. M., Taylor, K. A., and Kendrick-Jones, J. 1980. Regulation of non-muscle myosin assembly by calmodulin-dependent light chain kinase. Nature *287,* 233-5.

Schroeder, T. E. 1972. The contractile ring. II. Determining its brief existence, volumetric changes, and vital role in cleaving Arbacia eggs. J Cell Biol *53,* 419-34.

Schroeder, T. E. 1973. Actin in dividing cells: contractile ring filaments bind heavy meromyosin. Proc Natl Acad Sci U S A *70,* 1688-92.

Schuyler, S. C., Liu, J. Y., and Pellman, D. 2003. The molecular function of Ase1p: evidence for a MAP-dependent midzone-specific spindle matrix. Microtubule-associated proteins. J Cell Biol *160,* 517-28.

Sebastian, M., Reck, M., Waller, C. F., Kortsik, C., Frickhofen, N., Schuler, M., Fritsch, H., Gaschler-Markefski, B., Hanft, G., Munzert, G., and von Pawel, J. 2010. The efficacy and safety of BI 2536, a novel Plk-1 inhibitor, in patients with stage IIIB/IV non-small cell lung cancer who had relapsed after, or failed, chemotherapy: results from an open-label, randomized phase II clinical trial. J Thorac Oncol *5,* 1060-7.

Segbert, C., Barkus, R., Powers, J., Strome, S., Saxton, W. M., and Bossinger, O. 2003. KLP-18, a Klp2 kinesin, is required for assembly of acentrosomal meiotic spindles in Caenorhabditis elegans. Mol Biol Cell *14,* 4458-69.

Severson, A. F., Baillie, D. L., and Bowerman, B. 2002. A Formin Homology protein and a profilin are required for cytokinesis and Arp2/3-independent assembly of cortical microfilaments in C. elegans. Curr Biol *12,* 2066-75.

Shandala, T., Gregory, S. L., Dalton, H. E., Smallhorn, M., and Saint, R. 2004. Citron Kinase is an essential effector of the Pbl-activated Rho signalling pathway in Drosophila melanogaster. Development *131,* 5053.

Shannon, K. B., Canman, J. C., Ben Moree, C., Tirnauer, J. S., and Salmon, E. D. 2005. Taxol-stabilized microtubules can position the cytokinetic furrow in mammalian cells. Mol Biol Cell *16,* 4423-36.

Shelden, E., and Wadsworth, P. 1990. Interzonal microtubules are dynamic during spindle elongation. J Cell Sci *97 (Pt 2),* 273-81.

Smith, G. E., Fraser, M. J., and Summers, M. D. 1983. Molecular Engineering of the Autographa californica Nuclear Polyhedrosis Virus Genome: Deletion Mutations Within the Polyhedrin Gene. J Virol *46,* 584-593.

Smyth, D. R., Mrozkiewicz, M. K., McGrath, W. J., Listwan, P., and Kobe, B. 2003. Crystal structures of fusion proteins with large-affinity tags. Protein Sci *12,* 1313-22.

Solomon, M. J., Glotzer, M., Lee, T. H., Philippe, M., and Kirschner, M. W. 1990. Cyclin activation of p34cdc2. Cell *63,* 1013-24.

Somers, W. G., and Saint, R. 2003. A RhoGEF and Rho family GTPase-activating protein complex links the contractile ring to cortical microtubules at the onset of cytokinesis. Dev Cell *4,* 29-39.

Somlyo, A. P., and Somlyo, A. V. 1994. Signal transduction and regulation in smooth muscle. Nature *372,* 231-6.

Somma, M. P., Fasulo, B., Cenci, G., Cundari, E., and Gatti, M. 2002. Molecular dissection of cytokinesis by RNA interference in Drosophila cultured cells. Mol Biol Cell *13,* 2448-60.

Sommi, P., Ananthakrishnan, R., Cheerambathur, D. K., Kwon, M., Morales-Mulia, S., Brust-Mascher, I., and Mogilner, A. 2010. A mitotic kinesin-6, Pav-KLP, mediates interdependent cortical reorganization and spindle dynamics in Drosophila embryos. J Cell Sci *123,* 1862-72.

Soto, E., Staab, A., Tillmann, C., Trommeshauser, D., Fritsch, H., Munzert, G., and Troconiz, I. F. 2010. Semi-mechanistic population pharmacokinetic/pharmacodynamic model for neutropenia following therapy with the Plk-1 inhibitor BI 2536 and its application in clinical development. Cancer Chemother Pharmacol *66,* 785-95.

Steigemann, P., and Gerlich, D. W. 2009. Cytokinetic abscission: cellular dynamics at the midbody. Trends Cell Biol *19,* 606-16.

Straight, A. F., Cheung, A., Limouze, J., Chen, I., Westwood, N. J., Sellers, J. R., and Mitchison, T. J. 2003. Dissecting temporal and spatial control of cytokinesis with a myosin II Inhibitor. Science *299,* 1743-7.

Straight, A. F., Field, C. M., and Mitchison, T. J. 2005. Anillin binds nonmuscle myosin II and regulates the contractile ring. Mol Biol Cell *16,* 193-201.

Suetsugu, S., Miki, H., and Takenawa, T. 1999. Distinct roles of profilin in cell morphological changes: microspikes, membrane ruffles, stress fibers, and cytokinesis. FEBS Lett *457,* 470-4.

Sunkel, C. E., and Glover, D. M. 1988. polo, a mitotic mutant of Drosophila displaying abnormal spindle poles. J Cell Sci *89 (Pt 1),* 25-38.

Surka, M. C., Tsang, C. W., and Trimble, W. S. 2002. The mammalian septin MSF localizes with microtubules and is required for completion of cytokinesis. Mol Biol Cell *13,* 3532-45.

Swan, K. A., Severson, A. F., Carter, J. C., Martin, P. R., Schnabel, H., Schnabel, R., and Bowerman, B. 1998. cyk-1: a C. elegans FH gene required for a late step in embryonic cytokinesis. J Cell Sci *111 (Pt 14),* 2017-27.

Takizawa, P. A., DeRisi, J. L., Wilhelm, J. E., and Vale, R. D. 2000. Plasma membrane compartmentalization in yeast by messenger RNA transport and a septin diffusion barrier. Science *290,* 341-4.

Tan, C., Stronach, B., and Perrimon, N. 2003. Roles of myosin phosphatase during Drosophila development. Development *130,* 671-81.

Tanaka, K., Okubo, Y., and Abe, H. 2005. Involvement of slingshot in the Rho-mediated dephosphorylation of ADF/cofilin during Xenopus cleavage. Zoolog Sci *22,* 971-84.

Tatsumoto, T., Xie, X., Blumenthal, R., Okamoto, I., and Miki, T. 1999. Human ECT2 is an exchange factor for Rho GTPases, phosphorylated in G2/M phases, and involved in cytokinesis. J Cell Biol *147,* 921-8.

Terada, Y., Tatsuka, M., Suzuki, F., Yasuda, Y., Fujita, S., and Otsu, M. 1998. AIM-1: a mammalian midbody-associated protein required for cytokinesis. Embo J *17,* 667-76.

Thornton, J. 2001. Structural genomics takes off. Trends Biochem Sci *26,* 88-9.

Tolliday, N., VerPlank, L., and Li, R. 2002. Rho1 directs formin-mediated actin ring assembly during budding yeast cytokinesis. Curr Biol *12,* 1864-70.

Tominaga, T., Sahai, E., Chardin, P., McCormick, F., Courtneidge, S. A., and Alberts, A. S. 2000. Diaphanous-related formins bridge Rho GTPase and Src tyrosine kinase signaling. Mol Cell *5,* 13-25.

Totsukawa, G., Yamakita, Y., Yamashiro, S., Hosoya, H., Hartshorne, D. J., and Matsumura, F. 1999. Activation of myosin phosphatase targeting subunit by mitosis-specific phosphorylation. J Cell Biol *144,* 735-44.

Toure, A., Dorseuil, O., Morin, L., Timmons, P., Jegou, B., Reibel, L., and Gacon, G. 1998. MgcRacGAP, a new human GTPase-activating protein for Rac and Cdc42 similar to Drosophila rotundRacGAP gene product, is expressed in male germ cells. J Biol Chem *273,* 6019-23.

Touré, A., Mzali, R., Liot, C., Seguin, L., Morin, L., Crouin, C., Chen-Yang, I., Tsay, Y. G., Dorseuil, O., Gacon, G., and Bertoglio, J. 2008. Phosphoregulation of MgcRacGAP in mitosis involves Aurora B and Cdk1 protein kinases and the PP2A phosphatase. FEBS Lett *582,* 1182-8.

Trimble, W. S. 1999. Septins: a highly conserved family of membrane-associated GTPases with functions in cell division and beyond. J Membr Biol *169,* 75-81.

Uren, A. G., Wong, L., Pakusch, M., Fowler, K. J., Burrows, F. J., Vaux, D. L., and Choo, K. H. 2000. Survivin and the inner centromere protein INCENP

show similar cell-cycle localization and gene knockout phenotype. Curr Biol *10,* 1319-28.

van Impel, A., Schumacher, S., Draga, M., Herz, H. M., Grosshans, J., and Muller, H. A. 2009. Regulation of the Rac GTPase pathway by the multifunctional Rho GEF Pebble is essential for mesoderm migration in the Drosophila gastrula. Development *136,* 813-22.

Van Vugt, M., and Medema, R. 2005. Getting in and out of mitosis with Polo-like kinase-1. Oncogene *24,* 2844-59.

Velasco, G., Armstrong, C., Morrice, N., Frame, S., and Cohen, P. 2002. Phosphorylation of the regulatory subunit of smooth muscle protein phosphatase 1M at Thr850 induces its dissociation from myosin. FEBS Lett *527,* 101-4.

Venken, K. J., He, Y., Hoskins, R. A., and Bellen, H. J. 2006. P[acman]: a BAC transgenic platform for targeted insertion of large DNA fragments in D. melanogaster. Science *314,* 1747-51.

Verbrugghe, K. J., and White, J. G. 2007. Cortical centralspindlin and G alpha have parallel roles in furrow initiation in early C. elegans embryos. J Cell Sci *120,* 1772-8.

Vernì, F., Somma, M. P., Gunsalus, K. C., Bonaccorsi, S., Belloni, G., Goldberg, M. L., and Gatti, M. 2004. Feo, the Drosophila homolog of PRC1, is required for central-spindle formation and cytokinesis. Current Biology *14,* 1569-75.

Vlak, J. M., Klinkenberg, F. A., Zaal, K. J., Usmany, M., Klinge-Roode, E. C., Geervliet, J. B., Roosien, J., and van Lent, J. W. 1988. Functional studies on the p10 gene of Autographa californica nuclear polyhedrosis virus using a recombinant expressing a p10-beta-galactosidase fusion gene. J Gen Virol *69 (Pt 4),* 765-76.

Wakefield, J. G., Bonaccorsi, S., and Gatti, M. 2001. The drosophila protein asp is involved in microtubule organization during spindle formation and cytokinesis. J Cell Biol *153,* 637-48.

Walczak, C. E., Verma, S., and Mitchison, T. J. 1997. XCTK2: a kinesin-related protein that promotes mitotic spindle assembly in Xenopus laevis egg extracts. J Cell Biol *136,* 859-70.

Warming, S., Costantino, N., Court, D. L., Jenkins, N. A., and Copeland, N. G. 2005. Simple and highly efficient BAC recombineering using galK selection. Nucleic Acids Res *33,* e36.

Weyer, U., Knight, S., and Possee, R. D. 1990. Analysis of very late gene expression by Autographa californica nuclear polyhedrosis virus and the further

development of multiple expression vectors. J Gen Virol *71 (Pt 7),* 1525-34.

Wheatley, S. P., Carvalho, A., Vagnarelli, P., and Earnshaw, W. C. 2001. INCENP is required for proper targeting of Survivin to the centromeres and the anaphase spindle during mitosis. Curr Biol *11,* 886-90.

Wheatley, S. P., Hinchcliffe, E. H., Glotzer, M., Hyman, A. A., Sluder, G., and Wang, Y. 1997. CDK1 inactivation regulates anaphase spindle dynamics and cytokinesis in vivo. J Cell Biol *138,* 385-93.

White, J. G., and Borisy, G. G. 1983. On the mechanisms of cytokinesis in animal cells. J Theor Biol *101,* 289-316.

Whitehead, I. P., Campbell, S., Rossman, K. L., and Der, C. J. 1997. Dbl family proteins. Biochim Biophys Acta *1332,* F1-23.

Williams, G. V., Rohel, D. Z., Kuzio, J., and Faulkner, P. 1989. A cytopathological investigation of Autographa californica nuclear polyhedrosis virus p10 gene function using insertion/deletion mutants. J Gen Virol *70 (Pt 1),* 187-202.

Wolfe, B. A., Takaki, T., Petronczki, M., and Glotzer, M. 2009. Polo-like kinase 1 directs assembly of the HsCyk-4 RhoGAP/Ect2 RhoGEF complex to initiate cleavage furrow formation. PLoS Biol *7,* e1000110.

Yamashita, A., Sato, M., Fujita, A., Yamamoto, M., and Toda, T. 2005. The roles of fission yeast ase1 in mitotic cell division, meiotic nuclear oscillation, and cytokinesis checkpoint signaling. Mol Biol Cell *16,* 1378-95.

Yasuda, S., Oceguera-Yanez, F., Kato, T., Okamoto, M., Yonemura, S., Terada, Y., Ishizaki, T., and Narumiya, S. 2004. Cdc42 and mDia3 regulate microtubule attachment to kinetochores. Nature *428,* 767-71.

Yoshigaki, T. 2003. Theoretical evidence that more microtubules reach the cortex at the pole than at the equator during anaphase in sea urchin eggs. Acta Biotheor *51,* 43-53.

Yoshizaki, H., Ohba, Y., Kurokawa, K., Itoh, R. E., Nakamura, T., Mochizuki, N., Nagashima, K., and Matsuda, M. 2003. Activity of Rho-family GTPases during cell division as visualized with FRET-based probes. J Cell Biol *162,* 223-32.

Yuan, J., Eckerdt, F., Bereiter-Hahn, J., Kurunci-Csacsko, E., Kaufmann, M., and Strebhardt, K. 2002. Cooperative phosphorylation including the activity of polo-like kinase 1 regulates the subcellular localization of cyclin B1. Oncogene *21,* 8282-92.

Yüce, O., Piekny, A., and Glotzer, M. 2005. An ECT2-centralspindlin complex regulates the localization and function of RhoA. J Cell Biol *170,* 571-82.

Yumura, S. 2001. Myosin II dynamics and cortical flow during contractile ring formation in Dictyostelium cells. J Cell Biol *154,* 137-46.

Zavortink, M., Contreras, N., Addy, T., Bejsovec, A., and Saint, R. 2005. Tum/RacGAP50C provides a critical link between anaphase microtubules and the assembly of the contractile ring in Drosophila melanogaster. J Cell Sci *118,* 5381-92.

Zhai, B., Villen, J., Beausoleil, S. A., Mintseris, J., and Gygi, S. P. 2008. Phosphoproteome analysis of Drosophila melanogaster embryos. J Proteome Res *7,* 1675-82.

Zhao, W. M., and Fang, G. 2005a. Anillin is a substrate of anaphase-promoting complex/cyclosome (APC/C) that controls spatial contractility of myosin during late cytokinesis. J Biol Chem *280,* 33516-24.

Zhao, W. M., and Fang, G. 2005b. MgcRacGAP controls the assembly of the contractile ring and the initiation of cytokinesis. Proc Natl Acad Sci USA *102,* 13158-63.

Zhu, C., and Jiang, W. 2005. Cell cycle-dependent translocation of PRC1 on the spindle by Kif4 is essential for midzone formation and cytokinesis. Proc Natl Acad Sci U S A *102,* 343-8.

Zhu, C., Lau, E., Schwarzenbacher, R., Bossy-Wetzel, E., and Jiang, W. 2006. Spatiotemporal control of spindle midzone formation by PRC1 in human cells. Proc Natl Acad Sci U S A *103,* 6196-201.

Zhu, K., Debreceni, B., Bi, F., and Zheng, Y. 2001. Oligomerization of DH domain is essential for Dbl-induced transformation. Mol Cell Biol *21,* 425-37.